Design and Development of Some Naphthalimide Luminogens: Studying Supramolecular Interactions, Photophysical Properties and Applications

A thesis submitted by

Kavita

Roll No. 186122014

to

Indian Institute of Technology Guwahati

for the award of the degree of

Doctor of Philosophy

Department of Chemistry
Indian Institute of Technology Guwahati
Guwahati - 781039
India

May-2024

INDIAN INSTITUTE OF TECHNOLOGY GUWAHATI
Department of Chemistry

STATEMENT

I do hereby declare that the work contained in the thesis entitled **"Design and Development of Some Naphthalimide Luminogens: Studying Supramolecular Interactions, Photophysical Properties and Applications."** is the result of investigations carried out by me in the Department of Chemistry, Indian Institute of Technology Guwahati, Guwahati, Assam India under the supervision of Prof. Parameswar Krishnan Iyer, Professor, Department of Chemistry, Indian Institute of Technology Guwahati, Guwahati, Assam, India. This work has not been submitted elsewhere for the award of any degree.

Kavitaa

May 2024 **Kavita**

IIT Guwahati

INDIAN INSTITUTE OF TECHNOLOGY GUWAHATI
Department of Chemistry

CERTIFICATE

This is to certify that the work contained in the thesis entitled **"Design and Development of Some Naphthalimide Luminogens: Studying Supramolecular Interactions, Photophysical Properties and Applications."** by **Kavita**, a Ph.D. student of Department of Chemistry, Indian Institute of Technology Guwahati, for the award of degree of Doctor of Philosophy has been carried out under my supervision and this work has not been submitted elsewhere for any degree.

May, 2024
Guwahati

Prof. Parameswar Krishnan Iyer
Thesis Supervisor
Department of Chemistry
Indian Institute of Technology Guwahati
Guwahati – 781039
Assam, India.

Dedicated to My late Brother Kapil

Table of Contents

Table of Contents

The content of this synopsis report entitled.

"Design and development of some naphthalimide luminogens: Studying supramolecular interactions, photophysical properties and applications" is divided into five chapters. *Chapter 1* gives brief introduction about the respective research area where the scope and significance of the subsequent chapters are discussed. *Chapter 2* describes the unique aggregation pattern in naphthalimide luminogen NMICY (J*-Aggregation) which is applied for selective detection of adulterated melamine in milk and milk powder samples in sustainable aqueous media. *Chapter 3* discussed the supramolecular interactions of naphthalimide luminogen ODNI and BrODNI and their impact on room temperature phosphorescence application. *Chapter 4* highlights the development of series of six naphthalimide luminogens and reports intermolecular interactions and detailed analysis of their aggregation pattern and their self-assembling behavior. These luminogens were used for the detection of NS1 protein of Japanese Encephalitis virus. *Chapter 5* discuss the polymorphism property of two naphthalimide compounds NPH and NPMe and analysis of their supramolecular interactions.

Chapter 1: Introduction

Supramolecular chemistry, pioneered by Pederson, Lehn, and Cahn has progressed greatly in the last few decades.[1] Supramolecular self-assembly is used as a tool to develop functional nano-architectures from organic small molecules which finds application in a wide range of areas such as sensing, energy storage, catalysis, bio-medicine, bio-mimicking, image-guided therapy such as PDT, PTT, and chemotherapy.[2] Weak intermolecular interactions play important role in developing supramolecular self-assembled constructive architectures,[3] which is widely explored for polymers and seldom studied for small molecules.[4] To construct supramolecular self-assembly in nanomaterials, the bottom-up method and organization of colloids are used by the researchers.[5] Functional nanoarchitectures can be promising in sensing due to their unique properties.[6] Supramolecular self-assembly is a wide and emerging area of research. In recent years studies have been reported by researchers on tuneable photophysical properties by aggregation in pure organic luminogens.[7] The aggregation pattern of organic molecules greatly tunes the photophysical properties by tuning the intermolecular interaction which consequently changes the molecular orbital distribution.[8] Supramolecular interactions involve various weak intermolecular interactions. In the crystal, all the weak intermolecular interactions can be tuned to construct the overall molecular framework. Weak supramolecular interactions in crystal and self-assemblies greatly tune the aggregation pattern which consequently varied the photophysical properties.[9] Thus these weak supramolecular

interactions can play a vital role in the development of new pure organic luminogens for the application of organic room temperature phosphorescence, aggregation-induced emission, sensing, functional nanomaterials, supramolecular self-assemblies, and organic electronics. **(Figure 1)**.

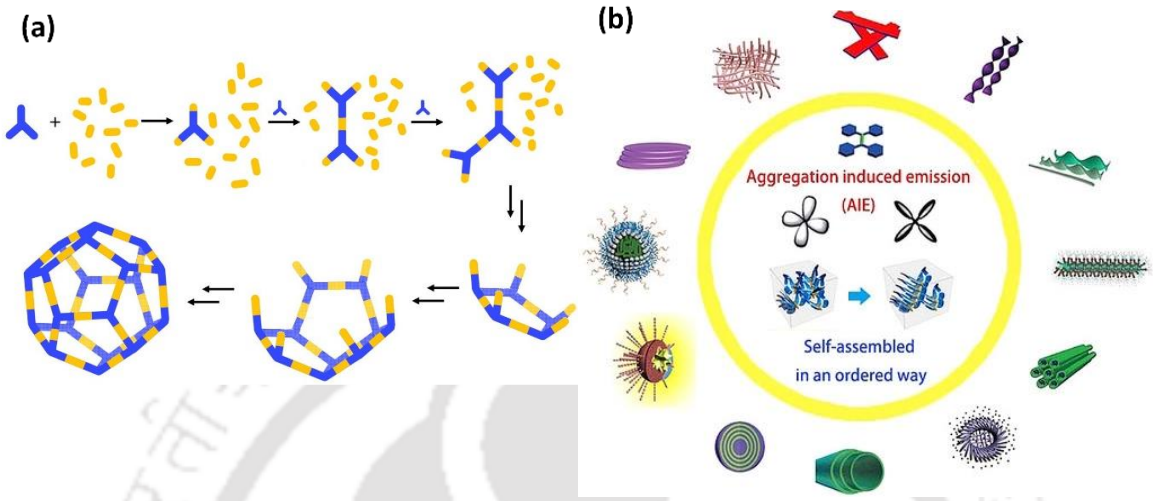

Figure 1. (a) Growth of dodecahedral assembly.[10] (b) Functional supramolecular self-assembly tetraphenyl ethylene in aggregation induced emission.[11]

Chapter 2: Molecular Engineering of Naphthalimide Methylcyclohexane Luminogen: Unraveling J*-Aggregation Pattern and Sensing Melamine in Aqueous Media

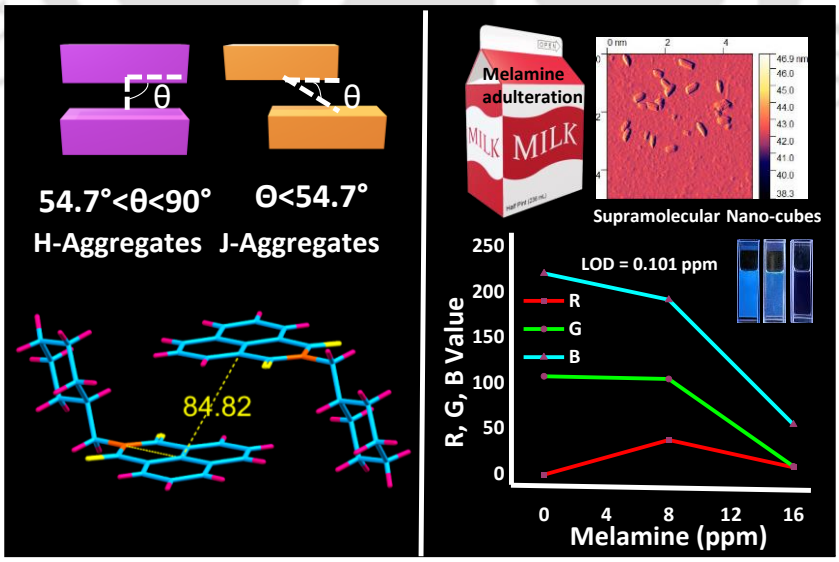

Chapter 2 discusses the role of substituted cyclohexane in naphthalimide luminogen. Since cyclohexane is an integral part of natural products and their conformational isomers they have great importance in medicine, biology, and supramolecular chemistry. In this work, molecular

conformation directed aggregation induced emission (AIE) luminogen NMICY (naphthalimide methylcyclohexane) was prepared, and its pure equatorial conformer was isolated and characterized via single crystal X-ray diffraction (SC-XRD) analysis. In NMICY, the methyl-cyclohexane substituent adopted the most stable chair conformation which remarkably prevented the intermolecular π-π interaction among the naphthalimide cores. A large bathochromic shift of ~80 nm along with a large stroke shift of ~100 nm in NMICYs condensed state was observed and potentially transformed the aggregation-caused quenching (ACQ) 1,8-naphthalic anhydride (NA) molecule into aggregation induced emission (AIE) luminogen (NMICY) due to the likely restriction in intramolecular motion (RIM) assisted by the methyl-cyclohexane attaining a stable chair configuration. The condensed state structure property in aqueous media and supramolecular self-assembly behavior of NMICY were optimized, and a facile strategy for melamine detection in milk and aqueous milk powder is reported with a limit of detection (LOD) value of 0.184 ppm (milk) and 0.101 ppm (milk powder) achieved via the rare acceptor-excited photoinduced electron transfer (a-PET) sensing mechanism.

Thus, the design, development and application of conformation directed AIE luminogen having cyclohexane appended to NMICY is reported. A pure equatorial CI of this flexible molecule was isolated via crystallization at RT and a unique J* aggregation (ideal J aggregation) pattern was identified. An understanding of the crucial role of methyl cyclohexyl on the self-assembly and condensed state fluorescence properties, thermodynamically favorable conformation, changes in bond angles, and design strategy for conformationally flexible luminescent material has been investigated systematically. Further, pure CI could be isolated via crystallization and provided guidelines to design new CI-based luminescent materials for application in active drug conformer, image-guided drug delivery, supramolecular assembly, and natural product synthesis. The NMICY was applied for the detection of melamine in aqueous milk solution and milk powder samples with LOD values of 0.101 ppm (milk powder) and 0.184 ppm (milk) via the rare a-PET mechanism. Additionally, a smartphone-based sensing analysis of melamine in milk samples was also developed which will permit its utility even by a non-expert at any location. Through this work, we report the first conformation directed AIE luminogen NMICY with a unique J* aggregation pattern, a simple design strategy to develop conformationally flexible luminescent material, detailed molecular properties study of the pure equatorial conformational isomer through crystallization, and the most efficient method to detect melamine in milk and milk powder samples in aqueous media.

Chapter 3: Mechanistic Insights on the Impact of Long Alkyl Chain and Bromine Substitution on the Molecular Packing and Phosphorescence Behavior in Naphthalimides

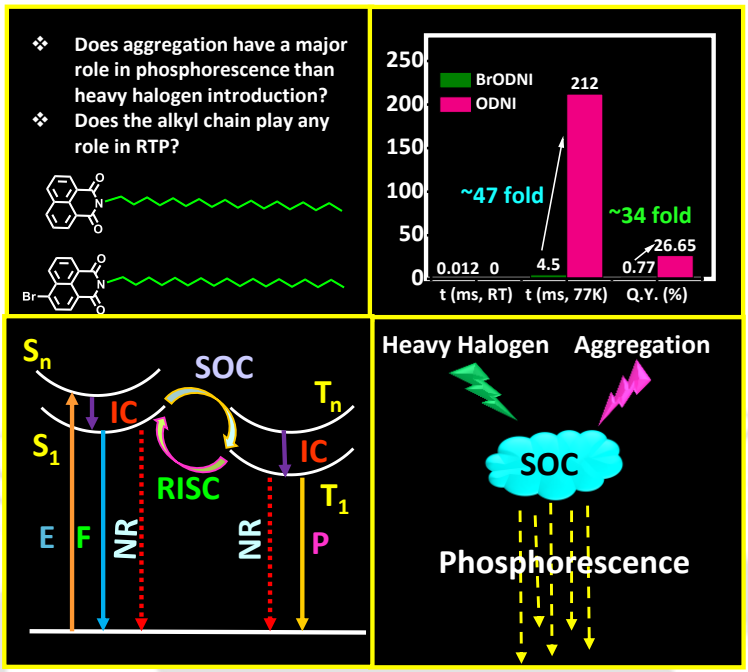

In the Chapter 3, the electron-deficient naphthalimide core which is explored for its potential application in the field of organic electronics, fluorescent sensors, laser dyes, and bioimaging is compared for the influence of functional group substitution. Recently many new naphthalimide room temperature phosphorescence luminogens are reported by tuning the head anhydride position or 4th position of the aromatic ring. It is supposed that the alkyl chains have no role in tuning room temperature phosphorescence (RTP) properties[12] and introducing a heavy halogen atom enhances the spin-orbit coupling which facilitates phosphorescence lifetime and quantum yield. Our group's previous work suggests that tuning alkyl chain length can reduce π-π interaction between two naphthalimide cores and simultaneously enhance aggregation-induced emission properties.[13] In this chapter we further explore the alkyl chain engineering role in RTP property and find that alkyl chain length plays prominent role in establishing intermolecular interactions between two core groups and which also in tuning the RTP. Also, it has been explored that introducing heavy halogen atom as bromine in naphthalimide core can enhance the spin-orbit coupling and further facilitates intersystem crossing.[14] We have introduced bromine as a heavy halogen atom in the naphthalimide core and studied phosphorescence properties at room temperature and also at 77 K. Thus, we report that only halogen substitution cannot facilitate phosphorescence in naphthalimide core

intermolecular interaction, but dipole-dipole interactions also play a key role. We further explored the introduction of the halogen atom in fluorescent luminogens AIE property and supramolecular self-assembly. We find that substituting bromine can introduce bathochromic shifts and provide micelle with similar self-assembly to the molecule.

In order to increase phosphorescence, heavy halogen atoms like bromine can enhance triplet excitons, however excess heavy atom effect (HAE) might be detrimental because of the inherent struggle between phosphorescence lifetime and quantum yield. When halogen atoms are introduced, the synergistic effect of HAE and halogen bonding, which is essential for balancing heavy atom effect (HAE) enables the alteration of RTP properties. Strong coupling has already been successfully used to produce triplet exciton with H aggregation. H-aggregates in ODNI have a strong coupling effect that has stabilized the triplet excitons, and excess non-radiative decay could be minimized at 77 K. As a result, ODNI displayed a 48-fold longer phosphorescence lifetime than BrODNI (211 ms), even though pure H-aggregation cannot be claimed for this material due to photophysical measurements showing a bathochromic shift in PL with increasing polarity.

In summary, we have studied AIE, self-assembly, and phosphorescence study of ODNI and BrODNI and we concluded that by introducing bromine in ODNI its aggregation pattern and self-assembly varied, due to which all the photophysical properties of BrODNI changed. The introduction of bromine has introduced probable dipole-dipole interchromophore interaction which changes their aggregation pattern. We have also studied the phosphorescence properties of both ODNI and BrODNI. It is observed that only the introduction of bromine which increases spin-orbit coupling of an overall molecule is not responsible for increased phosphorescence but supramolecular interactions and consequently aggregation patterns play a more important role.

Chapter 4: Beyond H- and J- Aggregation in Naphthalimide Luminogens

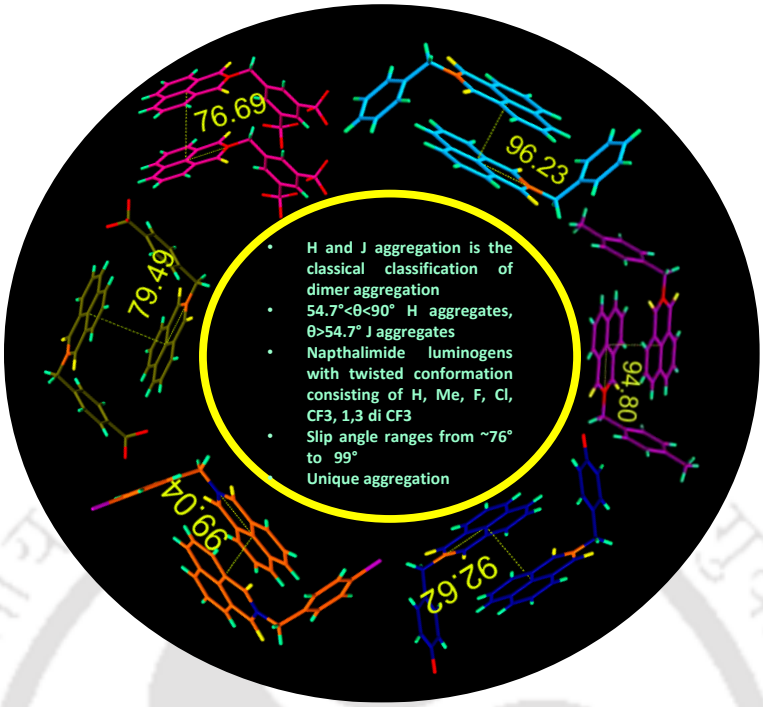

Chapter 4 described the design and development of a series of naphtalimide luminogens by varying substituent at the head position of 1, 8-Naphthalic anhydride. We have synthesized NPH, NPMe, NPF, NPCl, NMPCF_3, and 1, 3 m-NPCF_3. In this series, there are two set of molecules, one with a positive inductive effect with hydrogen and methyl and the other sets with a negative inductive effect with fluorine, chlorine and CF_3. The substituent of all these molecules has increasing electronegativity from methyl, hydrogen, chlorine, fluorine, CF_3, and 1, 3 m-CF_3. The different functional groups have greatly tuned the photo-physical properties, supramolecular interaction, and supramolecular self-assemblies. We have studied their photophysical properties in liquid, solid (powder), and crystalline states. It is also observed that tuning of the functional group has introduced variation in intermolecular interaction in their crystalline state and consequently aggregation patterns varied greatly. The present work has great importance in studying the effect of functional group tuning in naphthalimide luminogen molecules. Supramolecular interactions are key in regulating the aggregation and emission properties of organic luminogens. In particular, "H-aggregation" and "J-aggregation" are two commonly observed supramolecular interactions. Several optoelectronic applications, such as organic light-emitting diodes (OLEDs), sensors, and bioimaging, are significantly impacted by supramolecular aggregation in organic luminogens. A vital aspect in developing effective and high-performance organic optoelectronic devices is designing luminogens that can display

controlled aggregation behavior. Our study unveils that by tuning functional group, the aggregation pattern and their luminescence properties can be greatly tuned.

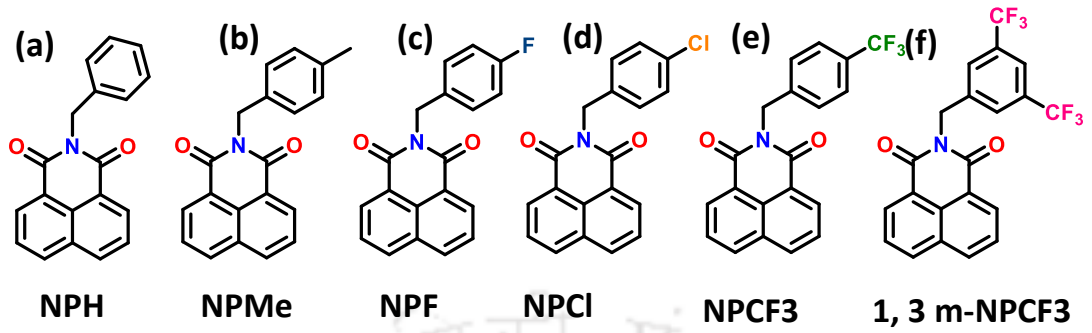

Figure 5. Naphthalimide luminogens (a)NPH (b) NPMe (c) NPF (d) NPCl (e) $NPCF_3$ (f) 1,3 m-$NPCF_3$

Japanese encephalitis (JE) is a resurging zoonotic disease, leading to high childhood mortality. It is a significant cause of endemic encephalitis in over 24 countries in the Western Pacific and Southeast Asia, resulting in 50,000 to 67,900 cases and 10,000 to 20,000 deaths annually, with a 30% fatality rate among affected individuals. This disease poses a major public health concern, affecting nearly half of the global population residing in endemic areas. The worldwide burden of JE is estimated to be 709,000 disability-adjusted life years (DALYs), leading to substantial economic losses due to the significant psychiatric and neurological complications that affect 30 to 50% of survivors.

In this study, we purified viral protein NS1 and allowed it to interact with naphthalimide luminogens. Notably, this research marks the first-time reporting of the interactions and their impact on the photoluminescence (PL) intensity of naphthalimide luminogens. The results revealed significant observations, shedding light on the unique nature of this interaction between the protein and the luminogens. Further biological significance of the interaction is an area of active investigation.

Chapter 5: Molecular Packing Dictates Optical Destiny: Polymorphism and Mechanoluminescence in Naphthaliimide Luminogens.

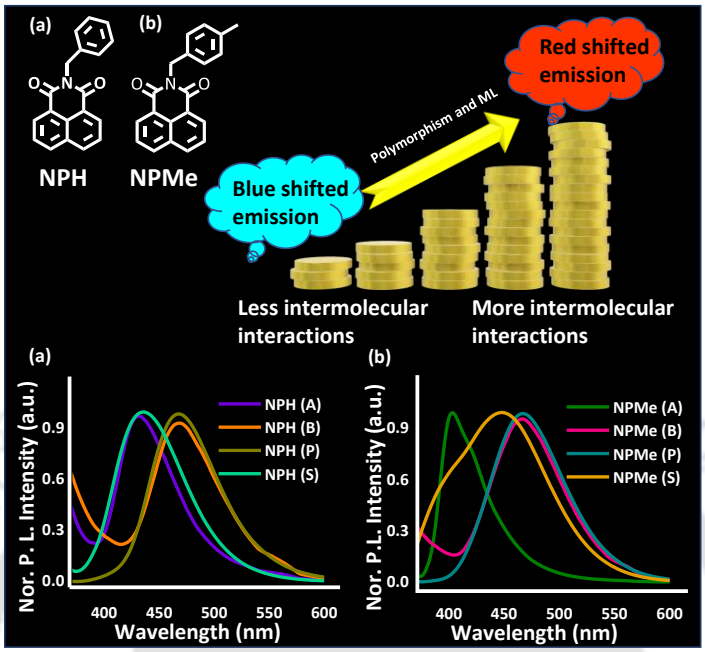

The chapter 5 discusses polymorphism as a very practical method to adjust the emission properties of organic solids based on one component, especially in the context of the demanding and time-consuming production of optoelectronic materials. Smart luminescent materials exhibit dramatic alteration in their luminescence characteristics in response to external stimuli like light, electricity, temperature, pressure, and solvent. These materials show great potential for use in sensors, information storage, encryption, and photoelectric devices. Among these, mechanoluminescence (ML) materials, which can spontaneously generate light in response to mechanical stress, are quite fascinating due to their distinct advantages of real-time detection and environmentally benign excitation mode. We have studied polymorphs and mechanoluminscence in two naphthalimide compounds NPH and NPMe. Both exhibited two types of polymorph NPHA, NPHB, NPMeA and NPMeB. Among them the "B" set of crystals which has been grown in chloroform with slow evaporation method has exhibited Red shifted emission compared to "A" set of crystals which were grown in MeOH with fast evaporation. Whicle grinding crystals of "A" set they exhibits Mechano-luminescence and showed similar emission like "B" sets of crystals. We have studied phophysical properties of NPHA, NPHB, NPMeA and NPMeB in their crystal form and also powder and aggregated state (f_w = 99.9%)

and unveils the factors which governs the polymorphism, mechano-luminescence of NPH and NPMe crystals, powder and aggregated state.

Conclusion and thesis overview

In conclusion, we have design and developed various sets of simple and novel pure organic naphthalimide luminogens and analysed their supramolecular interactions in detail. The presented thesis embarks on a comprehensive exploration of pure naphthalimide organic luminogens, delving into their design, development, and intricate supramolecular interactions. The overarching objective was to unravel various facets of supramolecular chemistry, ranging from sensing to luminescence applications, including fluorescence, phosphorescence, viral detection, and tuneable solid-state luminescence. Through a series of meticulously designed research endeavours, the thesis investigates the potential of novel luminogens across diverse applications, elucidating their underlying mechanisms and implications.

References:

1. a) Pedersen, C. J. The Discovery of Crown Ethers (Noble Lecture). *Angew. Chem. Int. Ed.* **1988**, *27* (8), 1021–1027. https://doi.org/10.1002/anie.198810211.

b) Lehn, J.-M. Supramolecular Chemistry—Scope and Perspectives Molecules, Supermolecules, and Molecular Devices(Nobel Lecture). *Angew. Chem. Int. Ed.* **1988**, *27* (1), 89–112. https://doi.org/10.1002/anie.198800891.

c) Cram, D. J. The Design of Molecular Hosts, Guests, and Their Complexes (Nobel Lecture). *Angew. Chem. Int. Ed.* **1988**, *27* (8), 1009–1020. https://doi.org/10.1002/anie.198810093.

2. Li, J.; Wang, J.; Li, H.; Song, N.; Wang, D.; Tang, B. Z. Supramolecular Materials Based on AIE Luminogens (AIEgens): Construction and Applications. *Chem. Soc. Rev.* **2020**, *49* (4), 1144–1172. https://doi.org/10.1039/c9cs00495e.

3. Song, N.; Zhang, Z.; Liu, P.; Yang, Y.-W.; Wang, L.; Wang, D.; Tang, B. Z. Nanomaterials with Supramolecular Assembly Based on AIE Luminogens for Theranostic Applications. *Adv. Mater.* **2020**, *32* (49), e2004208. https://doi.org/10.1002/adma.202004208.

4. Nai, J.; Guan, B. Y.; Yu, L.; Lou, X. W. D. Oriented Assembly of Anisotropic Nanoparticles into Frame-like Superstructures. *Sci. Adv.* **2017**, *3* (8), e1700732. https://doi.org/10.1126/sciadv.1700732.

5. Jones, M. R.; Seeman, N. C.; Mirkin, C. A. Programmable Materials and the Nature of the DNA Bond. *Science* **2015**, *347* (6224), 1260901–1260901. https://doi.org/10.1126/science.1260901.

6. Sagara, Y.; Traeger, H.; Li, J.; Okado, Y.; Schrettl, S.; Tamaoki, N.; Weder, C. Mechanically Responsive Luminescent Polymers Based on Supramolecular Cyclophane Mechanophores. *J. Am. Chem. Soc.* **2021**, *143* (14), 5519–5525. https://doi.org/10.1021/jacs.1c01328.

7. Li, Z.; Mukhopadhyay, S.; Jang, S.-H.; Brédas, J.-L.; Jen, A. K.-Y. Supramolecular Assembly of Complementary Cyanine Salt J-Aggregates. *J. Am. Chem. Soc.* **2015**, *137* (37), 11920–11923. https://doi.org/10.1021/jacs.5b08072.

8. Feng, H.-T.; Li, Y.; Duan, X.; Wang, X.; Qi, C.; Lam, J. W. Y.; Ding, D.; Tang, B. Z. Substitution Activated Precise Phototheranostics through Supramolecular Assembly of AIEgen and Calixarene. *J. Am. Chem. Soc.* **2020**, *142* (37), 15966–15974. https://doi.org/10.1021/jacs.0c06872.

9. Meher, N.; Iyer, P. K. Functional Group Engineering in Naphthalimides: A Conceptual Insight to Fine-Tune the Supramolecular Self-Assembly and Condensed State Luminescence. *Nanoscale* **2019**, *11* (28), 13233–13242. https://doi.org/10.1039/c9nr04593g

10. Davis, A. V.; Yeh, R. M.; Raymond, K. N. Supramolecular Assembly Dynamics. *Proc. Natl. Acad. Sci. U. S. A.* **2002**, *99* (8), 4793–4796. https://doi.org/10.1073/pnas.052018299.

11. Wu, T.; Huang, J.; Yan, Y. Self-Assembly of Aggregation-Induced-Emission Molecules. *Chem. Asian J.* **2019**, *14* (6), 730–750. https://doi.org/10.1002/asia.201801884.

12. Goudappagouda, A.; Manthanath, V. C.; Wakchaure, K. C.; Ranjeesh, T.; Das, K.; Vanka, T.; Nakanishi, S. S. *Angew. Chem. Int. Ed* **2018**, *58*.

13. Meher, N.; Iyer, P. Spontaneously Self-Assembled Naphthalimide Nanosheets: Aggregation-Induced Emission and Unveiling a-PET for Sensitive Detection of Organic Volatile Contaminants in Water. *Angew. Chem. Int. Ed* **2018**, *57*, 1–6.

14. Chen, X.; Xu, C.; Wang, T.; Zhou, C.; Du, J.; Wang, Z.; Xu, H.; Xie, T.; Bi, G.; Jiang, J.; Zhang, X.; Demas, J. N.; Trindle, C. O.; Luo, Y.; Zhang, G. Versatile Room-Temperature-Phosphorescent Materials Prepared from N-Substituted Naphthalimides: Emission Enhancement and Chemical Conjugation. *Angew. Chem. Int. Ed* **2016**, *55* (34), 9872–9876. https://doi.org/10.1002/anie.201601252.

15. Meher, N.; Iyer, P. K. Pendant Chain Engineering to Fine-Tune the Nanomorphologies and Solid-State Luminescence of Naphthalimide AIEEgens: Application to Phenolic Nitro-Explosive Detection in Water. *Nanoscale* **2017**, *9* (22), 7674–7685. https://doi.org/10.1039/c7nr02174g.

Chapter 1

Introduction

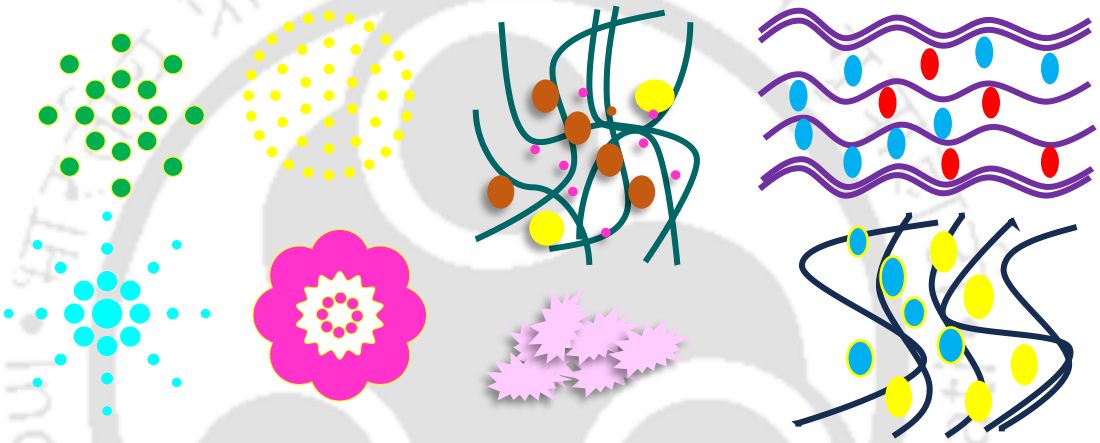

Supramolecular interactions in various state of matter.

1.1. Beyond the Molecules: Supramolecular Chemistry

Assembly is a common process in daily life that involves arranging systems, people, and objects to accomplish tasks or produce desired results. The idea of assembly permeates all facets of our lives. It serves as the foundation for advancement and creativity, from the complex assembly of molecules that form the base of life to the planned assembly of components in technologies and infrastructure.[1] **(Figure 1.1)** The fascinating field of supramolecular chemistry studies the complex assemblages and interactions created by non-covalent bonds at the intersection of chemistry, physics, and other sciences.[2] Supramolecular chemistry explores the dynamic and reversible nature of interactions, in contrast to conventional covalent chemistry, and reveals a world in which molecules can self-organize into intricate designs with emergent features.[3] This field presents new possibilities for the development of drug delivery systems, catalysts, and functional materials.[4] Its foundation is based on molecular recognition,[5] host-guest chemistry,[6] and self-assembly[7] principles. Through this thesis, we will investigate the basic ideas, cutting-edge techniques, and wide range of applications in the fascinating field of supramolecular chemistry. **(Figure 1.2)** Supramolecular chemistry, commonly referred as "chemistry beyond the molecule," focuses on the research of molecular recognition and high-order assemblages produced by noncovalent interactions.[8] Supramolecular chemistry, pioneered by Charles J. Pederson, Jean-Marie Lehn, and Donald J. Cram, has been greatly developed in the last few decades.[9] Cram, Lehn, and Pedersen shared the 1987 Nobel Prize in Chemistry, which was given in recognition of the "development and use of molecules with structure-specific reactions with high selectivity''[10] This established supramolecular chemistry as a recognized branch of chemistry. Supramolecular systems can demonstrate stimuli-responsive behaviour because they are constructed from components connected by noncovalent interactions.[11]

1.2. Supramolecular Interactions and Organic Luminogens

Supramolecular interactions are captivating phenomena within the realm of Chemistry. Unlike traditional covalent bond chemistry which involves electron sharing supramolecular interactions involve reversible weak non-covalent interactions, bonds and forces that include hydrogen bonding, π-π stacking, Van der Waals contacts, electrostatic interactions, and hydrophobic effects.[12] These interactions play a crucial role in shaping the spatial arrangement of chemical system from discrete molecules. It stimulates them to self-assemble into more

substantial, well-defined structures, like helices, crystalline arrays, and molecular cages.[13] A prevalent interaction observed in supramolecular assemblies involves the alignment of aromatic rings. π-π stacking impacts the electronic transition leading to enhanced luminescence in organic luminogens. Similarly hydrophobic interactions drive the aggregation of luminogens in solid state, resulting the distinct luminescence. These effects are particularly relevant in self-assembled structures. Intermolecular hydrogen bonds influence energy level and molecular packing. In organic luminogens hydrogen bonds can modulate molecular emission wavelength and quantum yield. Charge on neighbouring molecules significantly impact the luminescence. Electrostatic interactions between luminophores and counteraction play crucial role in destemming photophysical properties. Also, by encapsulating luminophores within host molecule, the emission properties can be tailored. Host guest complex exhibits altered photophysical behaviour, making them intriguing candidate for luminescent material. Considering supramolecular interactions can control the characteristics and functions of materials at the nanoscale, it is critical to comprehend and make use of them in materials research.[14] Through the utilization of these interplays, with customized characteristics like stimuli responsiveness, self-healing abilities, and hierarchical structures, opening doors for developments in sensing, tuneable luminescence, polymorphism and selective drug-protein interaction.[15] The aggregation-induced enhancement of fluorescence intensity is a crucial phenomenon in wide range of applications, particularly in the field of sensing. By leveraging supramolecular interactions precise control over the assembly of luminogens is achieved, resulting in tuneable luminescence properties such as emission wavelength and intensity.[16] This tuneability plays a crucial role in the design of highly sensitive sensing platforms, where changes in fluorescence can be exploited for analyte detection. In the realm of biotechnology, supramolecular interactions are leveraged for targeted viral protein detection.[17] By designing ligands or receptors with specific affinity towards viral protein, organic luminogens can serve as fluorescent probes for virus detection. The selective detection of viral protein triggers changes in fluorescence intensity or spectral properties, enabling rapid and specific detection without the need for complex instrumentation.[18] Furthermore, these interactions significantly influence the polymorphic behaviour of organic luminogens, affecting their crystallization and packing arrangements and consequently optical characteristics.[19] Understanding and harnessing these intricate interactions not only advances materials science but also holds great promise for biotechnological applications.

Thus, the foundation for creating next-generation materials with improved performance and flexibility is provided by supramolecular interactions.[20] Organic luminogens are now utilized in diverse applications because of their wide structural choices and easy synthesis and scale-up possibility, photostability, and tuneable optical characteristics.[21]

Figure 1.1: Schematic illustration of assembly and interaction in different fields.

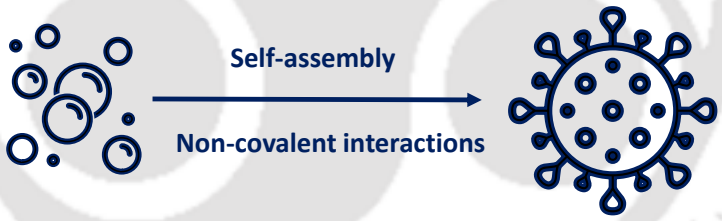

Figure 1.2: Schematic illustration of supramolecular assembly.

1.3. Type of Aggregation and its impact on Luminescence.

For several reasons, it is essential to investigate supramolecular interactions and aggregation patterns in organic luminogens.[22] By comprehending the supramolecular interactions between these molecules, their assembly can be manipulated, which in turn affects their optical characteristics.[23] Designing luminogens with desirable emission wavelengths, quantum yields, and aggregation-induced emission enhancement (AIEE) effects becomes achievable with this understanding of aggregation in organic luminogens which can elucidate their luminescent characteristics in solid form.[23] The emission properties of these molecules might vary between solution and solid states due to changes in molecular arrangement and interactions caused by

aggregation.[24] The molecular structure of luminogens to reduce unwanted quenching effects and increase their emission efficiency in solid-state devices can be altered by investigating how aggregation impacts luminescence.[25] Furthermore, the self-assembly of organic luminogens into nanostructures and hierarchical architectures is mediated in a significant way by supramolecular interactions.[26] These nanostructures are interesting prospects because of their specific optical and electrical properties that set them apart from individual molecules. the shape and characteristics of nanostructures can be tuned by regulating supramolecular interactions.[27] Studying supramolecular interactions and aggregation patterns in organic luminogens is crucial for enhancing our basic comprehension of these materials and harnessing their complete.[28] Proficiency in organic luminogens with improved stability, performance, and versatility by utilizing the concepts of supramolecular chemistry.

Aggregation of single molecules that can form an organized mesoscopic entity where all integrated molecules behave as one due to coherent electronic coupling between molecular electronic excitations. By enabling the efficient transfer of energy from light-harvesting antennas to photosynthetic reaction centres, such coherent coupling phenomena play a crucial role in biological photosynthetic systems.[29]

There are many different intermolecular interactions in organic aggregates, such as electrostatic, dispersion, exchange (repulsion), induction (polarization), dipole-dipole, ion-dipole, hydrogen bonding, and halogen bonding, among others. These interactions can alter excited-state energy dissipation pathways, which is difficult and system-dependent, as well as the geometric and electrical structures of molecules.[30] Scheibe[31] and Jelley[32] independently proposed the traditional J aggregation with strong excitonic coupling, which has a larger transition dipole moment due to in-phase quantum superposition, and it was long thought to be the primary factor enhancing solid-phase luminescence. The plausible intermolecular quantum phase led by aggregation will be hampered by the flexible intramolecular motions in these AIEgens, which are typically much weaker than the intramolecular electron-vibration coupling, and thus it cannot adequately explain the phenomena of the majority of newly synthesized AIEgens.[33] As a result, numerous explanations for AIE phenomena for various organic systems have been put forth. These explanations include restrictions on intramolecular rotation (RIR), restrictions on intermolecular motion (RIM), and blocking of nonradiative decay channels, restrictions on the E/Z isomerization process, restrictions on the excited-state intramolecular proton transfer, restrictions on access to the dark state via isomerization, and restricted access

to conical intersection crystalline-inducing processes.[34] The microscopic AIE mechanism, the related relationship between photophysical property and mechanism, and general principles of aggregation behavior modulation, however, have not yet been given a clear and complete image.[35]

Mechanism insights: Dark n-π* to bright π-π* due to Aggregation

Terephthalic acid (TPA), a typical aromatic diacid, was found to exhibit a peculiar characteristic of intense fluorescence, delayed fluorescence, and phosphorescence during crystallization, in contrast to extremely weak visible light in solution and amorphous phases.[36] They compare the geometrical and electronic structures of the low-lying excited states of the isolated and crystalline TPA at hybrid CASPT2/ANO-RCC-VDZP/AMBER level by integrating the MOLCAS and TINKER package in order to determine the morphology dependency of luminescence properties. **(Figure 1.3a)** Electrostatic interaction with the surrounding molecules in the crystal can significantly increase the energy of the excited state with the n-π* transition and slightly decrease the energy of the excited state with the π-π* transition. The n-orbital is sensitive to electrostatic forces because the charge concentrates on the oxygen, causing a separation of charge, but the π orbital is insensitive since the charge is distributed uniformly. Thus, during crystallization, the ^{1}(n-π*) state is raised to the second-lowest excited state S_2 (5.05 eV) from the first-lowest excited state S_1 (4.81 eV) in the gas phase. These results confirm that, according to Kasha's rule, crystallization causes the S_1 state in TPA to change from a dark ^{1}(n-π*) to a bright ^{1}(π-π*), recovering the strong emission. Aggregation substantially increases the transition dipole moment of S_1, which is essential for fluorescence or phosphorescence. More intriguingly, the electrostatic interaction not only contributes to a faster radiative decay by altering the energy order of the low-lying excited state, but it also introduces a slower nonradiative decay by reducing the electron-vibration coupling between S_1 and S_0 during crystallization. Strong fluorescence and phosphorescence are produced upon crystallization because of the enhancement of the radiative decay rate and the reduction of the nonradiative decay rate combined, which justifies the mechanism underlying the experimentally observed occurrence of two-fold emission caused by crystallization.

Crystallization-induced reversal from dark (n+σ)-π* to bright state (π-π)*

A novel squaraine derivative, CIEE-SQ, demonstrates increasingly intense light emission when transitioning from a crystal to a cocrystal with CIEE-SQ: CHCl3 = 1:1, compared to its minimal emission in solution. This phenomenon is uncommon among previous reported squaraine derivatives. **(Figure 1.3b)** In conclusion, crystallization or cocrystallization causes the transition from the dark $^1(n+\pi^*)$ state to the bright $^1(\pi+\pi^*)$ state, which produces a noticeably fast radiative decay rate and simultaneously suppresses the nonradiative decay rate, enhancing fluorescence.[37] **(Figure 1.4)** More significantly, a novel type of AIEgens lacking the traditional conjugation property has been used for high-performance solid-phase luminescence, which motivates researchers to create superior solid-phase fluorophores by excited-state manipulation.

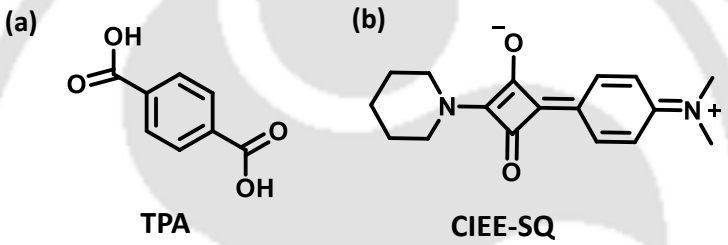

Figure 1.3. The Chemical structure of (a) TPA (b) CIEE-SQ

Aggregation structures and molecular stacking models can have a significant impact on the photoluminescent properties of organic π-conjugated materials in the solid state. Earlier in 1963, Kasha and colleagues published the theoretical foundation for molecular exciton theory, which holds that interactions between molecular transition dipoles in aggregates reflect the emission properties. This work was a pioneer in the field.[38] Cofacial, parallel transition dipoles (H-aggregate) typically show quenched fluorescence and blue shift absorption. Due to the significant π–π overlap, the H-aggregate is advantageous for charge transfer even if it is unfavorable to fluorescence. Molecules can form stacked J-aggregates with prominent fluorescence by slipping along the directions of transition dipoles based on the cofacial packings. Later, using the exciton-vibrational coupling theory as a basis, Spano and colleagues methodically[39] examined the absorption and emission spectrum characteristics of H-aggregates and J-aggregates. Cornil[47] and associates suggested in 1998 that lowering exciton interactions is an effective strategy to prevent solid-state luminescence quenching. However, when cofacial stacking occurs, X-aggregates can show intense fluorescence. The rapid advancement of X-ray

diffraction technology may also provide an accurate means of analysing the refined molecular structures and packing patterns within the aggregates. Various aggregation structures and aggregation dependent luminescent properties are introduced which is based on organic luminescent crystals. The experimental instances of controlling the properties of solid-state emissions through manipulation of the aggregation structures are then compiled. The polymorphic and stimulus-induced luminescence properties (stress, heat, light, etc.) are introduced for single-component materials. Cocrystals and acid protonated crystals are summed up as reasonable methods of eliciting unique luminous features for multicomponent materials. Designing attractive organic luminous materials can greatly benefit from a thorough understanding of the related internal mechanisms, particularly the connection between the aggregation structure and luminescent characteristic.[40]

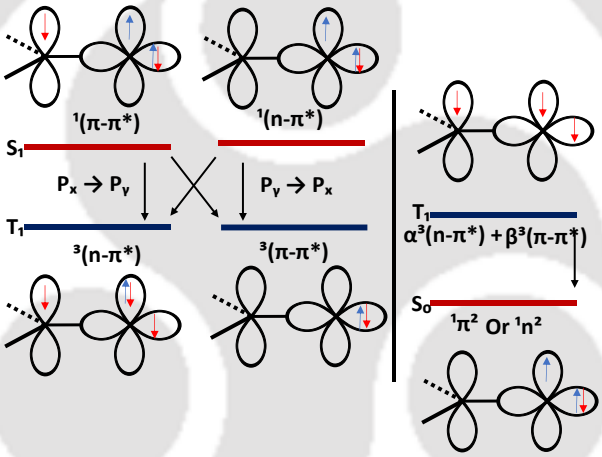

Figure 1.4. Schematic illustration of El-Sayed's rule for Intersystem Crossing (ISC) and its application in regulating the phosphorescence decay rate through the molecular-orbital hybridization of the lowest triplet states.

Types of Aggregates and related mechanisms are following.

1.3.1. H-Aggregates

Cofacial, parallel molecule stacking with a slip angle greater than 54.7° is present in H-aggregate. The prefix "H" originates from the German word "Häufung," which means stacking or piling.[41] In 2005, Gierschner and colleagues published a study on the optical features of distyrylbenzene (DSB) and fluorinated distyrylbenzene (F12DSB) crystals related to their aggregation. DSB crystals exhibit H-aggregation with herringbone topologies in their molecular organization.[42] **(Figure 1.5a, 1.5b)** The molecular transition dipoles in H-aggregates

are arranged "side-by-side," wherein the upper excited state of the two split energy levels produced by dipole interactions is optically permitted and the lower excited state is optically forbidden. The optical characteristics are affected by two important factors: When comparing the optical allowed higher excited states to the solution, (a) the main absorption peak is typically blue shifted ("H" for hypsochromic); (b) the optical forbidden lower excited states, which correspond to the emitting state, cause a low radiative decay rate, and suppressed fluorescence to be seen in H-aggregates. The cofacial π–π interactions can enhance charge carrier mobility and promote charge transport, even if fluorescence is inhibited in H-aggregates. The absorption spectra of H-aggregates usually show a redshift, or bathochromic shift, in comparison to the molecule's monomeric form. Strong molecular interaction between neighbouring molecules causes this shift, which in turn causes the HOMO-LUMO (Highest Occupied Molecular Orbital - Lowest Unoccupied Molecular Orbital) energy gap to narrow. As so, longer wavelengths of light are absorbed by the H-aggregate. H-aggregates can have different emission characteristics. They may display increased fluorescence or decreased emission intensity because of exciton coupling in certain situations, or they may exhibit redshifted emission in comparison to the monomeric form in others. The expanded π-conjugation and larger transition dipole moments of H-aggregates result in improved absorption of light in the longer wavelength band (red to near-infrared). In H-aggregates, fluorescence is reduced, but cofacial π–π interactions can enhance charge transport and boost charge carrier mobility, Poly(3-hexylthiophene), a common ingredient in organic solar cells, has been discovered to create H-aggregate π-stacks in the spin-coated films.[43] **(Figure 1.5c)** Excitons, which are bonded pairs of electrons and holes, are dispersed among multiple nearby molecules in H-aggregates. Improved absorption and emission intensity are the outcome of this delocalization, which also causes a notable increase in oscillator strength. H-aggregates' optical characteristics can be influenced by the aggregate's size. Larger aggregates may indicate a decrease in the degree of spectral shift, whereas smaller aggregates may display greater severity redshifts. Temperature and solvent conditions have an impact on the development and stability of H-aggregates. Polar solvents or high temperatures may interrupt the aggregation and cause a shift back to the monomeric state. In certain instances, the phenomenon of strong H-aggregation might result in the quenching of emission, hence diminishing the efficacy of the luminogen. Currently, efforts are being made to control and modify the H-aggregation process to customize the photophysical properties of organic luminogens for specific applications. This

process encompasses the optimization of molecular architectures, selection of suitable solvents, and meticulous control of conditions throughout the device fabrication procedure.[44]

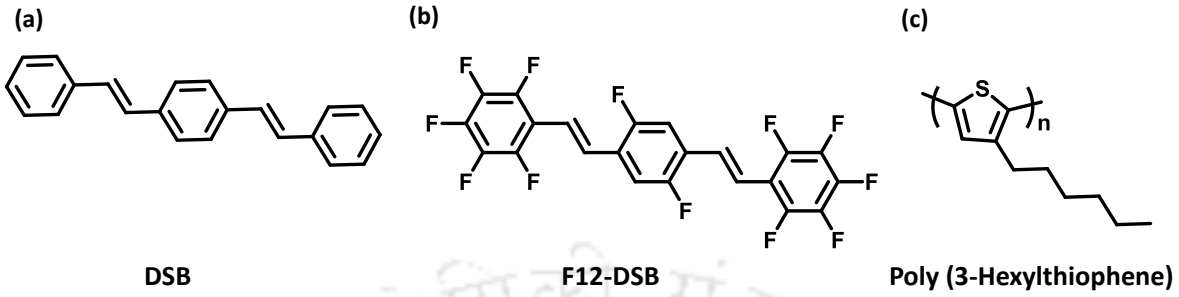

Figure 1.5 Chemical structure of (a) DSB (b) F12-DSB (c) Poly (3-Hexylthiophene)

1.3.2. J-Aggregates

The alteration in slip angle within the cofacial stacking arrangement has the potential to induce a transition from H-aggregates to staggered stacked J-aggregates, denoted as "J" in reference to Jelley.[45] The interactions between molecules in J-aggregates, known as "head-to-tail" interactions, result in the splitting of energy levels in the excited states. This splitting causes the lower excited state to be optically allowed, suggesting it can be observed by optical techniques, while the higher excited state is optically prohibited, meaning it cannot be observed through optical techniques. The absorption spectrum of H-aggregates typically exhibits a significant blue shift, whereas a comparatively modest red shift is observed in J aggregates. In In 2001, Feast and colleagues described a molecule called 4,4′-bis(2,3,4,5,6-pentafluorostyryl)stilbene that can create a "brickwall" motif J-aggregate through self-assembly using aryl-fluoroaryl interactions.[46] **(Figure 1.6a)** Additionally, J-aggregates demonstrate high radiative decay rates and fluorescence. In addition to possessing excellent solid-state luminescence efficiency, J-aggregates have the capacity to demonstrate favourable electrical characteristics. The slip angle in J-aggregates ranges from 0° to 54.7°, allowing for partial π-π overlap between neighbouring molecules. This overlap has the potential to enhance the transfer of charges between these molecules. The integration of highly emissive fluorescence and efficient charge transport features has the potential to enhance the capabilities of J-aggregates for utilization in sophisticated optoelectronic devices. efficiencies due to the correlation between the allowed lower excited states and the emission states. In addition to possessing excellent solid-state luminescence efficiency, J-aggregates have the capacity to demonstrate favourable electrical characteristics. The slip angle in J-aggregates ranges from 0°

to 54.7°, resulting in a partial π–π overlap between neighbouring molecules. This overlap has the potential to enhance the transfer of charges between these molecules. The integration of highly emissive fluorescence and efficient charge transport features has the potential to enhance the capabilities of J-aggregates for utilization in sophisticated optoelectronic devices. Liu and colleagues have shown that the organic π conjugated molecule 2,6-diphenylanthracene (DPA) exhibits high mobility and intense emission.[47]**(Figure 1.6b)**

J-aggregates refer to molecular aggregates that are created through the stacking of chromophores, which are molecules capable of absorbing light, in a well-organized, one-dimensional manner. This stacking often occurs in a head-to-tail configuration. This configuration facilitates robust exciton interaction between neighbouring chromophores. J-aggregates demonstrate a phenomenon known as a redshift, often referred to as a bathochromic shift, in their absorption spectra when compared to the monomeric state of the chromophore. The observed redshift is attributed to a significant interaction between chromophores, leading to a reduction in the energy difference between the highest occupied molecular orbital (HOMO) and the lowest unoccupied molecular orbital (LUMO). Consequently, J-aggregates exhibit a higher propensity for light absorption at extended wavelengths. J-aggregates frequently demonstrate modified emission characteristics in comparison to their monomeric counterparts. The fluorescence shown by these entities can be either amplified or suppressed, contingent upon the level of exciton coupling and the particular chromophore under consideration. The formation of J-aggregates is influenced by various circumstances. Liu and colleagues have described a significant instance of a high mobility organic laser semiconductor, 2,7-diphenyl-9H-fluorene (LD-1), crucial for the advancements in J-aggregate single crystals.[48] **(Figure 1.6c)** The formation of J-aggregates is favoured by higher concentrations of chromophores. The selection of a solvent has the potential to impact the phenomenon of J-aggregation. The development of J-aggregates can be potentially disrupted by the presence of polar solvents, whilst nonpolar solvents have the potential to enhance J-aggregate production. The phenomenon of temperature has a significant impact on the process of aggregation, as lower temperatures tend to facilitate the development of J-aggregates. J-aggregates possess considerable utility across diverse disciplines: Organic photovoltaic devices frequently employ J-aggregates to augment light absorption and boost the efficiency of charge generation. Sensors: The utilization of J-aggregates is observed in sensing applications, wherein alterations in their optical characteristics might serve as indicators for analytes or environmental circumstances. Photonic devices, including lasers, optical filters, and waveguides, find

application in various photonic systems. J-aggregates are significant in natural photosynthetic systems due to their ability to efficiently capture and transport energy. researchers endeavour to regulate and modulate J-aggregation to enhance the characteristics of organic luminogens for targeted applications. This process may entail altering the molecular composition, manipulating the concentration, and regulating the surrounding environmental parameters. Furthermore, their nonlinear optical properties make them suitable candidate for switching and signal processing. In the realm of biomedical imaging, J aggregates find the utility as contrast agent for fluorescent imaging and as photosensitizers for photodynamic therapy, capitalizing their efficient light absorption and emission properties. Overall, the unique optical characteristics of J aggregates render them indispensable for a diverse array of technological and biomedical application. A comprehensive comprehension and effective utilization of J-aggregation is of paramount importance in enhancing the efficacy of organic luminogens across a wide range of optoelectronic and photonic applications.

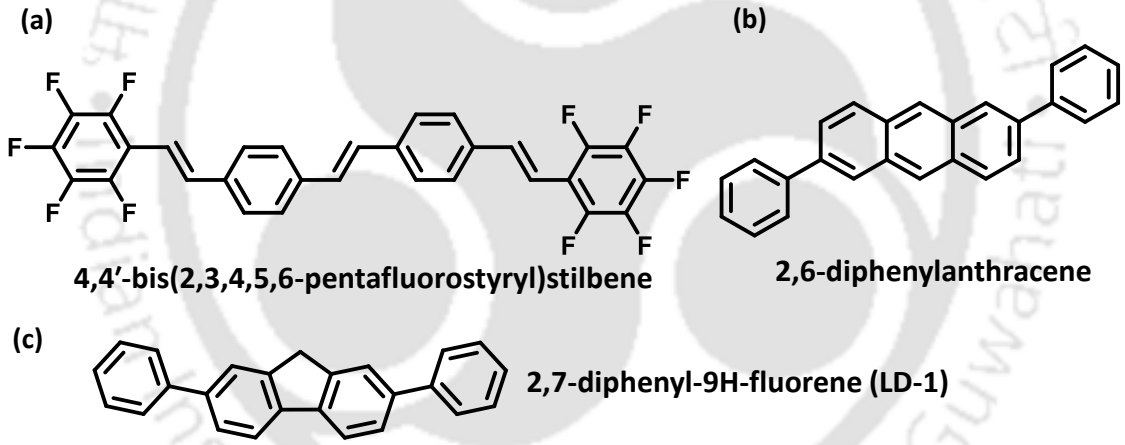

Figure 1.6. Chemical structure of (a) 4,4′-bis(2,3,4,5,6-pentafluorostyryl)stilbene (b) 2,6-diphenylanthracene (DPA) (c) 2,7-diphenyl-9H-fluorene (LD-1)

1.3.3. X-Aggregates

In 1998, Cornil and colleagues[49] selected stilbene as a case study and made a theoretical calculation to anticipate that the cross-dipole mode would serve as a highly efficient luminescence model. Unexpectedly, the process of X-aggregation in crystals has been demonstrated to be a unique approach for enhancing luminosity. Theoretical study has demonstrated that in X-aggregation, the rotational movement of neighbouring transition dipoles can effectively decrease the energy level difference between the two lowest excited states. Additionally, this arrangement allows optical transitions from both excited states to the

ground state. Specifically, the optical splitting reduces significantly as the rotation angle reaches 90 degrees, and the spectral characteristics of the X-aggregates could resemble those of monomers. The intriguing X-aggregation phenomenon was initially documented in the research conducted by Bartholomew et al. in 2000,[50] focusing on the crystal packing patterns of distyrylbenzene derivatives. They studied range of disterylbenzene and among them the benzene rings of adjacent molecules in the 1,4-bis(2,2 diphenylethenyl)benzene **(Figure 1.7a)** crystal is arranged in an edge-to-face stacking mode, suggesting that the C-H π interactions serve a part in producing a cross-stacking mode. Subsequently, Xie and colleagues[51] showed that the crystal of 2,5-diphenyl-1,4-distyrylbenzene (DPDSB), **(Figure 1.7b)** which is arranged in a cross-dipole stacking mode, had a significant increase in fluorescence efficiency. The crystal structure investigation indicated the absence of face-to-face π–π interactions between neighbouring molecules due to the significant distance (4.1 Å) between the core rings. Each cross-stacking dimer consisted of two crystallo-graphically independent conformational molecules. These molecules functioned as both proton donors and acceptors, resulting in the production of two distinct forms of C–H···π hydrogen bonds. Zhang and colleagues[52] demonstrated the ability to alter the arrangement of molecules in a twisted butterfly-shaped compound called 9,10-bis (2,2-diphenyl vinyl)anthracene (BDPVA). **(Figure 1.7c)** This compound showed a high level of fluorescence efficiency due to its unique cross-dipole stacking mode. To gain a deeper comprehension of the correlation between the photoluminescent characteristics of organic molecular aggregates and their stacking structures in crystals, Ma and colleagues[53] have introduced an exemplary framework utilizing polymorphisms of 9,10-bis-(2,2-di(4-fluorophenyl)vinyl)anthracene (BDFVA). **(Figure 1.7d)** This model aims to elucidate the optical properties associated with X-aggregation and J-aggregation. In comparison to J-aggregation, X-aggregation exhibits a higher number of contacts, which leads to a greater reduction in the fluorescence quenching effect. Furthermore, in X-aggregate, all the divided states consist of energy levels that permit optical transitions, given to their little energy separation. **(Figure 1.8)**

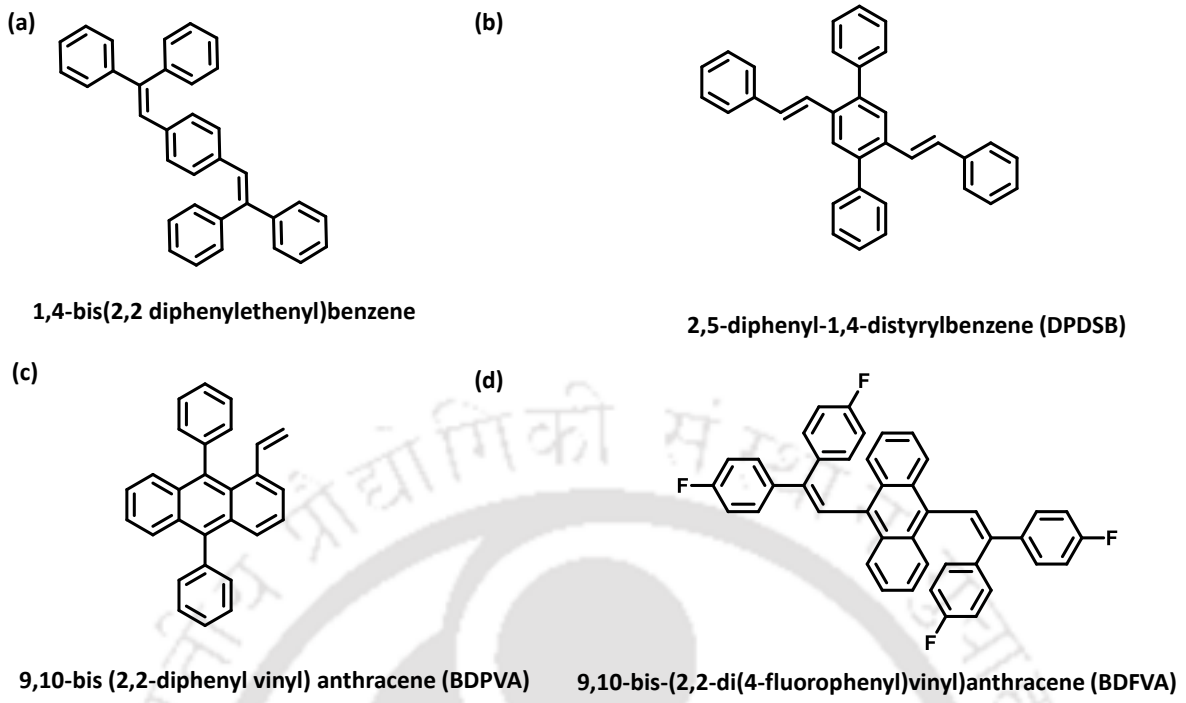

Figure 1.7. Chemical structure of (a) 1,4-bis(2,2 diphenylethenyl)benzene (b) 2,5-diphenyl-1,4-distyrylbenzene (DPDSB) (c) 9,10-bis (2,2-diphenyl vinyl) anthracene (BDPVA) (d) 9,10-bis-(2,2-di(4-fluorophenyl)vinyl)anthracene (BDFVA).

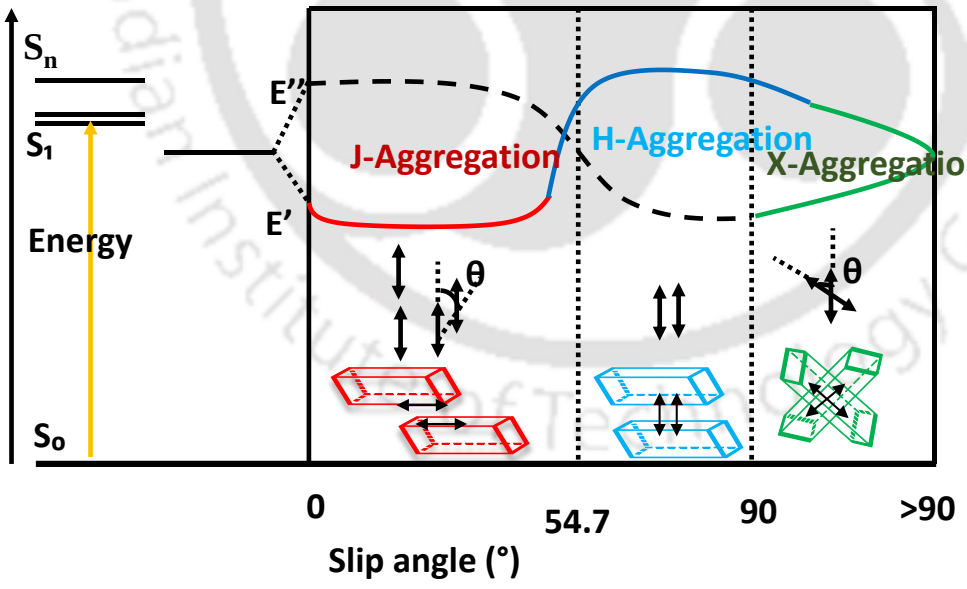

Figure 1.8. Energy splitting diagram displaying excited states for molecular aggregates in J-aggregate, H-aggregate, and X-aggregate.

1.4. Supramolecular Assembly and Luminescence

1.4.1. Fluorescent Supramolecular Assembly

Supramolecular interactions are weak interactions like non-covalent interactions, hydrogen bonding, π-π interactions, metal-ligand coordination, electrostatic interactions. These interactions are utilised to construct fluorescent supramolecular self-assemblies. Fluorescent self-assemblies are organized structures which are developed by supramolecular interactions of self-assembled nanoparticles or fluorescent molecules. Individual fluorophores' fluorescence characteristics can be altered or regulated through combining them with larger supramolecular structures like host-guest complexes or self-assembled nanomaterials. These assemblies' supramolecular interaction can facilitate energy transfer procedures, provide distinctive microenvironments, or bring about cooperative effects, altering the fluorescence emission characteristics in comparison to isolated fluorophores. Self-assembly: Supramolecular assemblies originate while molecular or nanoparticle parts spontaneously coalesce into larger structures because of non-covalent interactions. The assemblies can be dynamic and responsive to external stimuli given that these interactions might be reversible.[54] ***Fluorescent components:*** The supramolecular assembly's distinct components have fluorescence characteristics. These components can be inorganic nanoparticles with size-dependent fluorescence, like quantum dots, or organic molecules with conjugated systems, such aromatic dyes, or fluorophores.[55] ***Aggregated structure:*** Supramolecular assemblies can adopt various hierarchical structures, including nanofibers, nanotubes, micelles, vesicles, or larger aggregates. The specific structure formed depends on the nature of the building blocks and the assembly conditions. Energy transfer: In certain instances, the assembling of fluorescent components results in energy transfer processes, such as aggregation-induced emission (AIE) or fluorescence resonance energy transfer (FRET). In comparison to the individual components, energy transfer can lead to enhanced or altered fluorescence properties, enabling applications like sensing or light-emitting devices. Stimuli responsive: Supramolecular assemblies can also function in a stimuli-responsive manner, changing their structure or fluorescence characteristics in response to external stimuli including temperature, pH, light, or the presence of analytes. This aspect makes them advantageous for uses in optoelectronics, medication delivery, and chemical sensing.[56] ***Functional application:*** Fluorescent supramolecular ensembles have uses in many various domains. Due to their controlled release characteristics, they can be employed as carriers for drug delivery systems,

active materials in optoelectronic devices like organic light-emitting diodes (OLEDs), and probes for sensing and imaging applications. In general, fluorescent supramolecular assemblies provide a flexible design framework for functional materials with unique fluorescence properties and response characteristics. The development of these assemblies has the potential to revolutionize disciplines including materials science, nanotechnology, and biomedical research.[57] **(Figure 1.9, 1.10)**

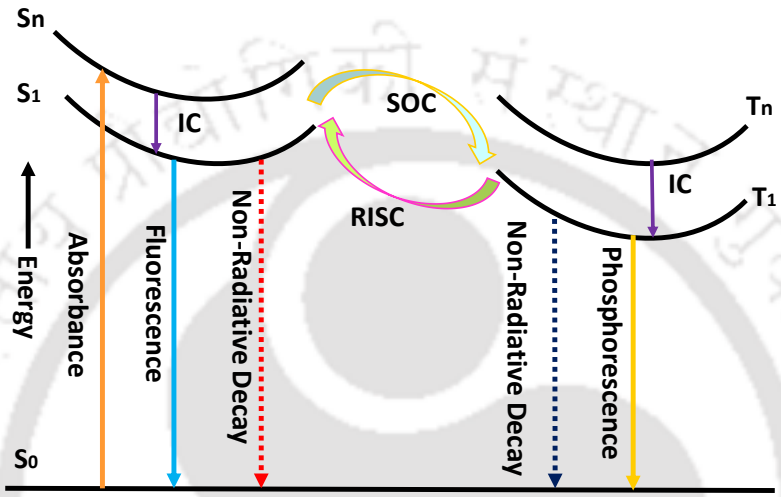

Figure 1.9. The Jablonski diagram demonstrates various photophysical relaxation processes, with a focus on intersystem crossover (ISC) between singlet and triplet states, which is essential for the phosphorescence of organic luminophores.

1.4.2. Phosphorescence Supramolecular assembly

Purely organic room-temperature phosphorescence (RTP), which possesses a triplet state, a longer lifetime, and a greater Stokes shift, has recently attracted growing study attention in recent years. which are frequently employed in molecular switches, organic light-emitting diodes (OLED), chemical sensors, and bioimaging. Organic RTP (ORTP), in contrast to inorganic or metal-based phosphorescent materials, provides an array of advantages, including simple and ecologically friendly synthesis and processing. Due to the disadvantages of weak spin-orbit coupling and a large energy gap between the singlet and triplet states (S1 and T1) of pure organic phosphorescent molecules, various design principles have been developed to increase spin-orbit coupling efficiency and prevent quenching of the triplet excited state by suppressing triplet exciton deactivation. It has been demonstrated that intersystem crossing (ISC) is promoted by adding a heteroatom or a carbonyl group to an organic molecule. In addition, nonradiative transitions have been minimized or the triplet state energy has been

stabilized using the polymer matrix, crystallization, halogen binding, H-aggregation, and host-guest interactions.[58] Three important molecular design aspects need be considered in order to develop ultralong and tuneable ORTP: 1) Incorporating halogens, carbonyls, and heteroatoms (O, N, S, P, etc.) to increase the spin-orbit coupling (SOC) or reducing the energy gap between the singlet and triplet states can boost intersystem crossing (ISC). 2) Numerous intra- and intermolecular contacts should be utilized to restrict molecular motion and squelch the non-radiative decay of triplet excitons. 3) A flexible conformation must be established to give the system the ability to control morphology at the supramolecular level. The structure and performance of these organic RTP materials depend significantly on supramolecular interactions. Researchers may foster long-lived excited states and improve phosphorescence effectiveness by carefully regulating molecular structure and arrangement.[59] Some key aspects of Supramolecular interactions in RTP is following: ***Molecular design:*** In order to promote intersystem crossing and long-lived triplet excited states, organic RTP materials are often constructed with heavy atom-containing compounds, such as transition metal complexes or heterocyclic aromatic systems. Achieving RTP behavior additionally involves the introduction of functional groups that encourage supramolecular interactions.[60] ***Host Guest System:*** To organize molecules into structures that facilitate effective phosphorescence, supramolecular host-guest interactions are frequently used. Guest molecules can be efficiently confined by host molecules that have cavities or pockets, obstructing non-radiative decay paths and limiting guest molecule motion Confinement increases the probability of radiative degeneration and induces RTP.[61] ***Aggregation Induced Emission (AIE):*** When certain luminophores aggregate, a phenomenon known as AIE occurs, where the intensity of the emission increases. By encouraging molecule packing and lowering non-radiative decay, AIE can be used in organic RTP materials to promote supramolecular interactions. Several techniques, such as crystallization, nanoparticle formation, or thin film deposition, can be used to attain this aggregation.[62] ***Energy level engineering:*** Through supramolecular interactions, the energy levels of the molecular orbitals of RTP materials can be altered. Researchers can modify the energy gaps between the singlet and triplet states, favouring the population and emission of the long-lived triplet excited states responsible for phosphorescence, by varying the strength and arrangement of the intermolecular interactions. Organic materials' capacity to produce long-lasting phosphorescence at ambient temperature opens new avenues for creating effective and adaptable luminescent systems. The goal of ongoing research in this area is to increase the

phosphorescence effectiveness and broaden the scope of applications for these materials.[63] **(Figure 1.9, 1.10)**

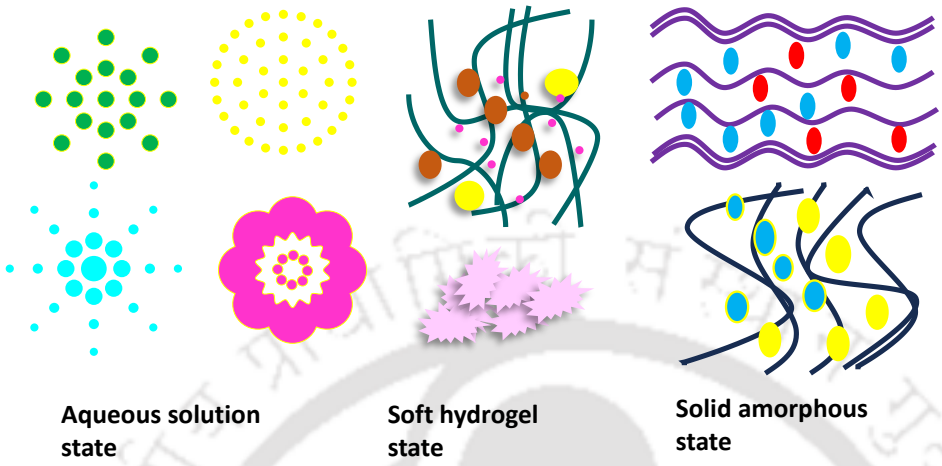

Figure 1.10. Schematic representation of phosphorescence supramolecular assembly and their applications.

1.4.3. Supramolecular interaction and aggregation induced emission:

When some organic luminogens aggregate or are in the solid form as opposed to their dispersed or diluted solution condition, an interesting phenomenon known as "aggregation-induced emission" (AIE) occurs which is discovered by Tang et al in 2001.[64] The suppression of nonradiative decay pathways and increased radiative emission have been suggested to be the basic mechanisms of AIE, which are related to the restriction of intramolecular movements (RIM) upon aggregation.[65] The aggregation of organic luminogens is facilitated by supramolecular interactions, which is essential to the AIE process. These interactions can be categorized into numerous categories, such as: ***1. π-π interactions:*** In organic compounds, interactions between aromatic systems are known as " π-π stacking." The π conjugated structures in AIE luminogens promote effective aggregation and AIE by facilitating strong intermolecular interactions. The intermolecular electronic interaction is enhanced by the close proximity of the conjugated systems in the aggregated state, boosting the emission intensity. ***2. Hydrogen bonding:*** The aggregated structures of AIE luminogens can be stabilized by hydrogen bonding interactions between hydrogen bond donor (HBD) and acceptor (HBA) groups. The development of hydrogen bonds between nearby molecules reduces their mobility, enhancing fluorescence. Common HBDs include hydroxyl (-OH) and amino (-NH2) groups, but HBAs can also include carbonyl (-C=O) or nitro groups (-NO2). ***3. π- cation interaction:***

The development of aggregation-induced emission in several AIE luminogens is significantly aided by π-cation interactions. These interactions take place between cationic species like metal ions or ammonium ions and electron-rich π systems. AIE behavior is facilitated by the electrostatic interaction between the positively charged cations and the π electron cloud of the luminogens, which fosters aggregation and limits intramolecular rotation. ***4. Charge transfer interactions:*** The exchange of electrons or electron density between molecules is referred to as charge-transfer interactions. Charge-transfer complexes can develop between the donor and acceptor moieties in AIE luminogens. These complexes' emergence stabilizes the aggregated state resulting in potent emission. In AIE luminogens, examples of donor-acceptor systems include electron-rich aromatic systems (donor) and electron-deficient groups (acceptor), such as nitro (-NO_2) or cyano (-CN). ***5. Van der Waals interactions:*** The aggregation of AIE luminogens is further influenced by Van der Waals forces, such as the London dispersion forces and the interactions between dipoles. These negligible intermolecular interactions exist amongst all molecules and are crucial for the formation of the aggregates. AIE behavior is the outcome of these interactions, which, despite being weak individually, have a cumulative effect that encourages aggregation. Overall, the interactions between supramolecular particles in AIE luminogens result in the development of highly organized aggregates or nanostructures. As a result of these supramolecular assemblies' limitations on intramolecular movements, suppression of nonradiative pathways, and facilitation of radiative decay, the emission intensity and AIE features are improved.[66] **(Figure 1.11)**

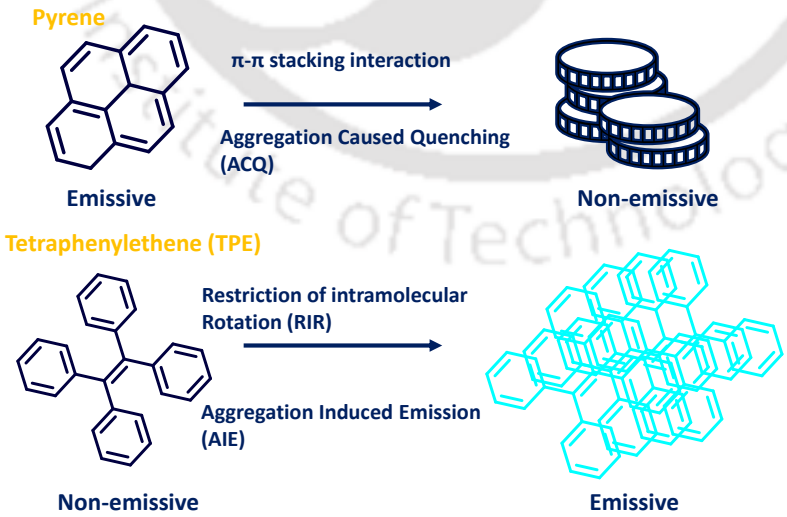

Figure 1.11. Schematic illustration of ACQ (aggregation caused quenching) phenomena in Perylene and AIE (aggregation induced emission) phenomenon in Tetraphenylethene (TPE)

1.5. Supramolecular assembly

Supramolecular assemblies are intermediated with noncovalent interaction are ideal candidate to use as chemo sensors due to their ease of formation and adaptive nature. Supramolecular can form highly ordered structure without time and energy consuming covalent bond formation and consist of relatively weaker non-covalent intermolecular interactions that underlie the supramolecular assemblies which make them adaptable in nature.[67] These assemblies can modify their configuration in response to several external stimuli and introduction of analyte, such configurational change can lead to cause optical response such as fluorescence and absorption shift. Due to the labile intermolecular connections, supramolecular assemblies also exhibit high levels of reversibility, which allows the supramolecular host to reorganize to its initial configuration if the external stimulus is eliminated. In all components of the sensor system, including interactions between the sensor and the fluorophore, analyte, and fluorophore, supramolecular luminescence sensors frequently rely on noncovalent supramolecular interactions. The following noncovalent interactions between the analyte and the chemo sensor are frequently observed: electrostatic interactions, intermolecular hydrogen bonds, hydrophobic association, cation- and anion-interactions, and other aromatic interactions, such as π-π stacking and edge-face interactions. Luminescent supramolecular detection methods frequently rely on an analyte's propensity to alter a sensor molecule's fluorescence or phosphorescent emission through the exchange of energy. Forster resonance energy transfer (FRET), photoinduced electron transfer (PET), and electron exchange (EE) are a few of the possible processes by which this energy transfer might take place. Multiple mechanism can also occur simultaneously.[68] Each mechanistic inquiry should clearly take the possibility of numerous coexisting processes into consideration. The differences in the electron transfers between the interacting molecules' lowest unoccupied molecular orbital (LUMO) and highest occupied molecular orbital (HOMO) are used to characterize the transfers. PET is only possible with closer contact with the donor and acceptor (within 2Å) so that their electron clouds could collapse and fluorescence quenching could be possible. In PET a complex between electron Donor and Acceptor (Dp*.Ap-) is formed. This complex can return to the ground state without emission of photon or exciplex emission can be observed then an extra electron on the acceptor is returned to the donor. The direction of electron transfer is determined by the oxidation and reduction potential of the donor and acceptor.[69]

1.6. Significance and Innovation

a. **Fundamental understanding:** The complexities of supramolecular interactions and aggregation patterns in organic luminogens to enhance our fundamental understanding of these materials was explored. This comprehension is essential for clarifying the fundamental principles that control their behaviour on a molecular scale, establishing the foundation for future research efforts.

b. **Rational design:** Organic luminogens with precise optical properties can be developed through instructed and focused method in the presented thesis. Furthermore, pure organic luminogens can be regulated by tuning their aggregation patterns and molecular packing with the knowledge of supramolecular interactions to get the desired emission wavelength, quantum yield and AIE properties. This rational design method helps create materials that have improved performance and functionality.

c. **Innovative material design:** Reported research could stimulate the development of innovative materials with uses in multiple fields. Enhanced comprehension of AIE mechanisms can result in the development of more effective light-emitting devices for displays, lighting, and signage. Understanding how nanostructures arise could lead to the creation of sophisticated materials used in energy harvesting, photonics, and medicinal applications.

d. **Methodological advancements:** Presented research findings could lead to the creation of new techniques and approaches for managing supramolecular interactions and aggregation patterns in organic luminogens. These improvements may allow for the creation of materials with customized properties and functions, creating new opportunities for investigation and innovation in the industry.

e. **Societal impact:** Scientific advancements could tackle important societal issues and promote technical innovation. Functional materials derived from supramolecular chemistry have potential in sustainable energy, healthcare, and environmental monitoring, offering significant societal benefits.

In conclusion, research outcomes increase scientific understanding and have real-world ramifications that may spur the creation of novel materials with a wide range of uses and social effects.

1.7. Objective and Conclusion of this thesis work

The primary focus of the presented thesis work was to design and develop novel pure organic luminogens and dive deep into the supramolecular interactions involved to explore various dynamics of supramolecular chemistry for the vast range of application in sensing, luminescence (fluorescence and phosphorescence), viral detection and tuneable solid-state luminescence. Various novel pure organic luminogens have been synthesized and successfully implemented for melamine detection of milk samples in aqueous media, organic room temperature phosphorescence, Japanese Influenzas responsible NS1 protein viral detection, mechano-luminescence, and polymorphism. The key objective for each work is following.

- The primary objective of first research work was to create and analyse the pure equatorial form of naphthalimide methylcyclohexane (NMICY) luminogen and study its supramolecular self-assembly and aggregation-induced emission capabilities. The work aims to investigate how the molecular conformation of NMICY affects its aggregation behaviour and optical properties, focusing on its potential use as a sensing platform for detecting melamine in milk and milk powder solutions. The study effectively created and identified the unadulterated equatorial form of NMICY and explained its supramolecular self-assembly properties. The research confirmed a unique J*-aggregation pattern that was mostly seen in NMICY. This pattern resulted in emission qualities about 450 nm in both crystal and aggregated forms. The study showed the creation of cube-shaped 2D-nanoarchitecture in water, as well as distinctive optical characteristics when in a clustered form. The improved structure-property connection enabled the creation of an efficient sensing technique to detect melamine in milk and milk powder solutions, attaining a low limit of detection (LOD) value. A smartphone-based sensing technology was created to provide a portable and straightforward approach for detecting melamine. The research enhances comprehension of supramolecular self-assembly and aggregation-induced emission processes and provides a practical application in chemical sensing.
- Second research aimed to study how the addition of heavy halogen atoms affects the organic room temperature phosphorescence (RTP) features of luminogens and to compare the impact of alkyl chain changes on RTP. The work attempted to clarify how heavy halogen atoms enhance spin-orbit coupling (SOC) and intersystem crossover (ISC) processes, which are important for obtaining efficient room temperature

phosphorescence (RTP). The research aimed to investigate how changes in alkyl chain structure affect the RTP properties of luminogens to understand the fundamental mechanisms controlling RTP. The research results provided valuable information on how the addition of heavy halogen atoms can improve the RTP characteristics of luminogens. The study showed that heavy halogen atoms can significantly affect phosphorescence lifetime. BrODNI had a much shorter lifetime than ODNI, as evidenced by the design and development of these two luminogens. Heavy halogen atoms are important for promoting efficient RTP by improving SOC and ISC processes. The study analysed the crystal structure of ODNI and conducted theoretical calculations for both ODNI and BrODNI to gain a better understanding of how alkyl chain structure and heavy halogen atoms affect RTP behaviour. The research enhances knowledge about RTP materials and provides vital insights for designing effective RTP luminogens for sustainable energy applications in the future.

- Third research report aims to study the supramolecular interactions of naphthalimide luminogens and characterize their aggregation patterns by single crystal X-ray diffraction (XRD). The study attempts to reveal unique aggregation characteristics that defy traditional classification as either H or J aggregates through a thorough investigation. The research aims to further comprehension of the distinctive assembly patterns displayed by these luminogens, illuminating their structural complexities. This study offers vital insights into the supramolecular behaviour of naphthalimide luminogens and their prospective applications in targeted interactions with viral proteins. The work reveals unique aggregation behaviours with slip angles exceeding 90 degrees by analysing aggregation patterns by single crystal X-ray diffraction (XRD). This research challenges traditional classifications and enhances our comprehension of the distinct assembly patterns displayed by naphthalimide luminogens. The project also involves studying the connections between naphthalimide luminogens and the NS1 protein, a vital component in the Japanese Encephalitis virus. The results show that a particular luminogen, (1,3 m-NPCF$_3$), displays remarkable luminescence dampening when interacting with the NS1 protein, indicating a possible approach for creating new methods to fight the Japanese Encephalitis virus. This research report provides vital insights that can guide future improvements in materials science and antiviral research by highlighting the significance of comprehending supramolecular behaviour in creating functional materials for various purposes.

- Fourth research report aims to study the polymorphic behaviour and mechanoluminescent features of naphthalimide luminogens NPH and NPMe. The work attempts to reveal the relationship between the molecular packing of luminogens and their optical features through a detailed examination of their single crystal X-ray diffraction (XRD) patterns. The research aims to clarify how molecular packing and fluorescence interact to understand mechanoluminescent behaviour and discover ways to customize these materials. This research study explores the polymorphic behaviour and mechanoluminescent features of naphthalimide luminogens NPH and NPMe. The work demonstrates a direct link between molecular arrangement and optical properties by analysing single crystal X-ray diffraction (XRD) patterns. The close arrangement of molecules, defined by complex intermolecular connections, leads to a shift towards longer wavelengths in the spectrum and a high level of fluorescence efficiency for NPHB and NPMeB. Loose molecular packing and reduced intermolecular contacts result in a blue-shifted spectrum, causing decreased fluorescence and quantum yield for NPHA and NPMeA. The results highlight the crucial influence of molecular arrangement on the optical characteristics of NPH and NPMe luminogens. The understanding of this interaction allows for customized control of these materials, with possible uses in optoelectronics and other areas. This research provides vital insights into the underlying understanding of molecular packing and fluorescence behaviour, which can be applied to design and manufacture useful materials with specific features.

1.8. References

1. Stupp, S. I.; Palmer, L. C. Supramolecular Chemistry and Self-Assembly in Organic Materials Design. *Chem. Mater.* **2014**, *26* (1), 507–518. https://doi.org/10.1021/cm403028b.
2. Cheng, H.; Liu, R.; Zhang, R.; Huang, L.; Yuan, Q. Recent Advances in Supramolecular Self-Assembly Derived Materials for High-Performance Supercapacitors. *Nanoscale Adv.* **2023**, *5* (9), 2394–2412. https://doi.org/10.1039/d3na00067b.
3. Xu, Z.; Peng, S.; Wang, Y.-Y.; Zhang, J.-K.; Lazar, A. I.; Guo, D.-S. Broad-spectrum Tunable Photoluminescent Nanomaterials Constructed from a Modular Light-harvesting Platform Based on Macrocyclic Amphiphiles. *Adv. Mater.* **2016**, *28* (35), 7666–7671. https://doi.org/10.1002/adma.201601719.
4. Wu, H.; Chen, Z.; Chi, W.; Bindra, A. K.; Gu, L.; Qian, C.; Wu, B.; Yue, B.; Liu, G.; Yang, G.; Zhu, L.; Zhao, Y. Structural Engineering of Luminogens with High Emission Efficiency Both in Solution and in the Solid State. *Angew. Chem. Int. Ed* **2019**, *58* (33), 11419–11423. https://doi.org/10.1002/anie.201906507.
5. Wang, H.; Zheng, X. Theoretical Study of Macrocyclic Host Molecules: From Supramolecular Recognition to Self-Assembly. *Phys. Chem. Chem. Phys.* **2022**, *24* (32), 19011–19028. https://doi.org/10.1039/d2cp02152h.
6. Park, J.; Park, J.; Lee, J.; Lim, C.; Lee, D. W. Size Compatibility and Concentration Dependent Supramolecular Host–Guest Interactions at Interfaces. *Nat. Commun.* **2022**, *13* (1). https://doi.org/10.1038/s41467-021-27659-w.
7. Busseron, E.; Ruff, Y.; Moulin, E.; Giuseppone, N. Supramolecular Self-Assemblies as Functional Nanomaterials. *Nanoscale* **2013**, *5* (16), 7098. https://doi.org/10.1039/c3nr02176a.
8. Lehn, J.-M. Supramolecular Chemistry: Where from? Where To? *Chem. Soc. Rev.* **2017**, *46* (9), 2378–2379. https://doi.org/10.1039/c7cs00115k.
9. Kolesnichenko, I. V.; Anslyn, E. V. Practical Applications of Supramolecular Chemistry. *Chem. Soc. Rev.* **2017**, *46* (9), 2385–2390. https://doi.org/10.1039/c7cs00078b.
10. Huang, F.; Anslyn, E. V. Introduction: Supramolecular Chemistry. *Chem. Rev.* **2015**, *115* (15), 6999–7000. https://doi.org/10.1021/acs.chemrev.5b00352.

11. Woods, J. F.; Gallego, L.; Pfister, P.; Maaloum, M.; Vargas Jentzsch, A.; Rickhaus, M. Shape-Assisted Self-Assembly. *Nat. Commun.* **2022**, *13* (1). https://doi.org/10.1038/s41467-022-31482-2.
12. Yang, Y.-D.; Ji, X.; Lu, Z.-H.; Yang, J.; Gao, C.; Zhang, H.; Tang, B. Z.; Sessler, J. L.; Gong, H.-Y. Time-Dependent Solid-State Molecular Motion and Colour Tuning of Host-Guest Systems by Organic Solvents. *Nat. Commun.* **2020**, *11* (1). https://doi.org/10.1038/s41467-019-13844-5.
13. Ham, R.; Nielsen, C. J.; Pullen, S.; Reek, J. N. H. Supramolecular Coordination Cages for Artificial Photosynthesis and Synthetic Photocatalysis. *Chem. Rev.* **2023**, *123* (9), 5225–5261. https://doi.org/10.1021/acs.chemrev.2c00759.
14. Sinawang, G.; Osaki, M.; Takashima, Y.; Yamaguchi, H.; Harada, A. Supramolecular Self-Healing Materials from Non-Covalent Cross-Linking Host–Guest Interactions. *Chem. Commun.* **2020**, *56* (32), 4381–4395. https://doi.org/10.1039/d0cc00672f.
15. Grabicki, N.; Dumele, O.; Sai, H.; Powers-Riggs, N. E.; Phelan, B. T.; Sangji, M. H.; Chapman, C. T.; Passarelli, J. V.; Dannenhoffer, A. J.; Wasielewski, M. R.; Stupp, S. I. Polymorphism and Optoelectronic Properties in Crystalline Supramolecular Polymers. *Chem. Mater.* **2021**, *33* (2), 706–718. https://doi.org/10.1021/acs.chemmater.0c04123.
16. Xu, L.; Wang, Z.; Wang, R.; Wang, L.; He, X.; Jiang, H.; Tang, H.; Cao, D.; Tang, B. Z. A Conjugated Polymeric Supramolecular Network with Aggregation-induced Emission Enhancement: An Efficient Light-harvesting System with an Ultrahigh Antenna Effect. *Angew. Chem. Int. Ed* **2020**, *132* (25), 9994–9999. https://doi.org/10.1002/ange.201907678.
17. Wang, Y.; Wu, H.; Hu, W.; Stoddart, J. F. Color-tunable Supramolecular Luminescent Materials. *Adv. Mater.* **2022**, *34* (22). https://doi.org/10.1002/adma.202105405.
18. He, X.-P.; Tian, H. Lightening up Membrane Receptors with Fluorescent Molecular Probes and Supramolecular Materials. *Chem* **2018**, *4* (2), 246–268. https://doi.org/10.1016/j.chempr.2017.11.006.
19. Gao, C.; Chen, G. Exploring and Controlling the Polymorphism in Supramolecular Assemblies of Carbohydrates and Proteins. *Acc. Chem. Res.* **2020**, *53* (4), 740–751. https://doi.org/10.1021/acs.accounts.9b00552.

20. Lim, S.; Kuang, Y.; Ardoña, H. A. M. Evolution of Supramolecular Systems towards Next-Generation Biosensors. *Front. Chem.* **2021**, *9*. https://doi.org/10.3389/fchem.2021.723111.
21. Ramamurthy, V.; Sivaguru, J. Supramolecular Photochemistry as a Potential Synthetic Tool: Photocycloaddition. *Chem. Rev.* **2016**, *116* (17), 9914–9993. https://doi.org/10.1021/acs.chemrev.6b00040.
22. Lou, X.-Y.; Yang, Y.-W. Aggregation-induced Emission Systems Involving Supramolecular Assembly. *Aggregate* **2020**, *1* (1), 19–30. https://doi.org/10.1002/agt2.1.
23. Takahashi, M.; Sakai, K.-I.; Sambe, K.; Akutagawa, T. Supramolecular Complexation and Collective Optical Properties Induced by Linking Two Methyl Salicylates via a σ-Bridge. *J. Phys. Chem. B* **2022**, *126* (16), 3116–3124. https://doi.org/10.1021/acs.jpcb.2c00842.
24. Lou, X.-Y.; Yang, Y.-W. Manipulating Aggregation-induced Emission with Supramolecular Macrocycles. *Adv. Opt. Mater.* **2018**, *6* (22). https://doi.org/10.1002/adom.201800668.
25. Sangji, M. H.; Sai, H.; Chin, S. M.; Lee, S. R.; R Sasselli, I.; Palmer, L. C.; Stupp, S. I. Supramolecular Interactions and Morphology of Self-Assembling Peptide Amphiphile Nanostructures. *Nano Lett.* **2021**, *21* (14), 6146–6155. https://doi.org/10.1021/acs.nanolett.1c01737.
26. Dharmarajan, N. P.; Vidyasagar, D.; Yang, J.-H.; Talapaneni, S. N.; Lee, J.; Ramadass, K.; Singh, G.; Fawaz, M.; Kumar, P.; Vinu, A. Bio-inspired Supramolecular Self-assembled Carbon Nitride Nanostructures for Photocatalytic Water Splitting. *Adv. Mater.* **2024**, *36* (2). https://doi.org/10.1002/adma.202306895.
27. Wei, X.; Lv, Y.; Shen, H.; Li, H.; Kang, X.; Yu, H.; Zhu, M. Secondary Ligand Engineering of Nanoclusters: Effects on Molecular Structures, Supramolecular Aggregates, and Optical Properties. *Aggregate* **2023**, *4* (1). https://doi.org/10.1002/agt2.246.
28. Tang, Q.; Han, Y.; Chen, L.; Qi, Q.; Yu, J.; Yu, S.-B.; Yang, B.; Wang, H.-Y.; Zhang, J.; Xie, S.-H.; Tian, F.; Xie, Z.; Jiang, H.; Ke, Y.; Yang, G.; Li, Z.-T.; Tian, J. Bioinspired Self-assembly of Metalloporphyrins and Polyelectrolytes into Hierarchical Supramolecular Nanostructures for Enhanced Photocatalytic H_2 Production in Water. *Angew. Chem. Int. Ed* **2024**, *136* (8). https://doi.org/10.1002/ange.202315599

29. Wu, J.-R.; Wu, G.; Li, D.; Yang, Y.-W. Macrocycle-based Crystalline Supramolecular Assemblies Built with Intermolecular Charge-transfer Interactions. *Angew. Chem. Int. Ed* **2023**, *135* (14). https://doi.org/10.1002/ange.202218142.
30. Scheibe, G. Über Die Veränderlichkeit Der Absorptionsspektren in Lösungen Und Die Nebenvalenzen Als Ihre Ursache. *Angew. Chem. Int. Ed* **1937**, *50* (11), 212–219. https://doi.org/10.1002/ange.19370501103.
31. Jelley, E. E. Molecular, Nematic and Crystal States of I: I-Diethyl--Cyanine Chloride. *Nature* **1937**, *139* (3519), 631–631. https://doi.org/10.1038/139631b0.
32. Sanz-Velasco, A.; Amargós-Reyes, O.; Kähäri, A.; Lipinski, S.; Cavinato, L. M.; Costa, R. D.; Kostiainen, M. A.; Anaya-Plaza, E. Controlling Aggregation-Induced Emission by Supramolecular Interactions and Colloidal Stability in Ionic Emitters for Light-Emitting Electrochemical Cells. *Chem. Sci.* **2024**, *15* (8), 2755–2762. https://doi.org/10.1039/d3sc05941c.
33. Li, J.; Wang, J.; Li, H.; Song, N.; Wang, D.; Tang, B. Z. Supramolecular Materials Based on AIE Luminogens (AIEgens): Construction and Applications. *Chem. Soc. Rev.* **2020**, *49* (4), 1144–1172. https://doi.org/10.1039/c9cs00495e.
34. Zhou, P.; Han, K. ESIPT-based AIE Luminogens: Design Strategies, Applications, and Mechanisms. *Aggregate* **2022**, *3* (5). https://doi.org/10.1002/agt2.160.
35. Barman, D.; Narang, K.; Parui, R.; Zehra, N.; Khatun, M. N.; Adil, L. R.; Iyer, P. K. Review on Recent Trends and Prospects in Π-conjugated Luminescent Aggregates for Biomedical Applications. *Aggregate* **2022**, *3* (5). https://doi.org/10.1002/agt2.172.
36. Gong, Y.; Zhao, L.; Peng, Q.; Fan, D.; Yuan, W. Z.; Zhang, Y.; Tang, B. Z. Crystallization-Induced Dual Emission from Metal- and Heavy Atom-Free Aromatic Acids and Esters. *Chem. Sci.* **2015**, *6* (8), 4438–4444. https://doi.org/10.1039/c5sc00253b.
37. Yang, S.; Yin, P.-A.; Li, L.; Peng, Q.; Gu, X.; Gao, G.; You, J.; Tang, B. Z. Crystallization-induced Reversal from Dark to Bright Excited States for Construction of Solid-emission-tunable Squaraines. *Angew. Chem. Int. Ed* **2020**, *59* (25), 10136–10142. https://doi.org/10.1002/anie.201914437.
38. Kasha, M. Energy Transfer Mechanisms and the Molecular Exciton Model for Molecular Aggregates. *Radiat. Res.* **1963**, *20* (1), 55. https://doi.org/10.2307/3571331.

39. Hestand, N. J.; Spano, F. C. Expanded Theory of H- and J-Molecular Aggregates: The Effects of Vibronic Coupling and Intermolecular Charge Transfer. *Chem. Rev.* **2018**, *118* (15), 7069–7163. https://doi.org/10.1021/acs.chemrev.7b00581.
40. Peng, Q.; Ma, H.; Shuai, Z. Theory of Long-Lived Room-Temperature Phosphorescence in Organic Aggregates. *Acc. Chem. Res.* **2021**, *54* (4), 940–949. https://doi.org/10.1021/acs.accounts.0c00556.
41. Li, H.; Lv, L.; Yuan, K.; Pan, S.; Li, Z. Understanding H-Aggregates Crystallization Induced Emissive Behavior: Insights from Theory. *Sci. Rep.* **2023**, *13* (1). https://doi.org/10.1038/s41598-023-39605-5.
42. Gierschner, J.; Ehni, M.; Egelhaaf, H.-J.; Milián Medina, B.; Beljonne, D.; Benmansour, H.; Bazan, G. C. Solid-State Optical Properties of Linear Polyconjugated Molecules: π-Stack Contra Herringbone. *J. Chem. Phys.* **2005**, *123* (14). https://doi.org/10.1063/1.2062028.
43. Panzer, F.; Bässler, H.; Lohwasser, R.; Thelakkat, M.; Köhler, A. The Impact of Polydispersity and Molecular Weight on the Order–Disorder Transition in Poly(3-Hexylthiophene). *J. Phys. Chem. Lett.* **2014**, *5* (15), 2742–2747. https://doi.org/10.1021/jz5009938.
44. Zhang, G.; Cheng, X.; Wang, Y.; Zhang, W. Supramolecular Chiral Polymeric Aggregates: Construction and Applications. *Aggregate* **2023**, *4* (1). https://doi.org/10.1002/agt2.262.
45. Jelley, E. E. Spectral Absorption and Fluorescence of Dyes in the Molecular State. *Nature* **1936**, *138* (3502), 1009–1010. https://doi.org/10.1038/1381009a0.
46. Feast, W. J.; Lövenich, P. W.; Puschmann, H.; Taliani, C. Synthesis and Structure of 4,4′-Bis(2,3,4,5,6-Pentafluorostyryl)Stilbene, a Self-Assembling J Aggregate Based on Aryl–Fluoroaryl Interactions. *Chem. Commun.* **2001**, No. 5, 505–506. https://doi.org/10.1039/b100002k.
47. Liu, J.; Zhang, H.; Dong, H.; Meng, L.; Jiang, L.; Jiang, L.; Wang, Y.; Yu, J.; Sun, Y.; Hu, W.; Heeger, A. J. High Mobility Emissive Organic Semiconductor. *Nat. Commun.* **2015**, *6* (1). https://doi.org/10.1038/ncomms10032.
48. Liu, J.; Zhang, H.; Dong, H.; Meng, L.; Jiang, L.; Jiang, L.; Wang, Y.; Yu, J.; Sun, Y.; Hu, W.; Heeger, A. J. High Mobility Emissive Organic Semiconductor. *Nat. Commun.* **2015**, *6* (1). https://doi.org/10.1038/ncomms10032.

49. Cornil, J.; dos Santos, D. A.; Crispin, X.; Silbey, R.; Brédas, J. L. Influence of Interchain Interactions on the Absorption and Luminescence of Conjugated Oligomers and Polymers: A Quantum-Chemical Characterization. *J. Am. Chem. Soc.* **1998**, *120* (6), 1289–1299. https://doi.org/10.1021/ja973761j.
50. Bartholomew, G. P.; Bazan, G. C.; Bu, X.; Lachicotte, R. J. Packing Modes of Distyrylbenzene Derivatives. *Chem. Mater.* **2000**, *12* (5), 1422–1430. https://doi.org/10.1021/cm991194o.
51. Xie, Z.; Yang, B.; Li, F.; Cheng, G.; Liu, L.; Yang, G.; Xu, H.; Ye, L.; Hanif, M.; Liu, S.; Ma, D.; Ma, Y. Cross Dipole Stacking in the Crystal of Distyrylbenzene Derivative: The Approach toward High Solid-State Luminescence Efficiency. *J. Am. Chem. Soc.* **2005**, *127* (41), 14152–14153. https://doi.org/10.1021/ja054661d.
52. Zhang, J.; Xu, B.; Chen, J.; Ma, S.; Dong, Y.; Wang, L.; Li, B.; Ye, L.; Tian, W. An Organic Luminescent Molecule: What Will Happen When the "Butterflies" Come Together? *Adv. Mater.* **2014**, *26* (5), 739–745. https://doi.org/10.1002/adma.201303639.
53. Zeng, R.; Zhang, L.; Xue, Y.; Ke, B.; Zhao, Z.; Huang, D.; Wei, Q.; Zhou, W.; Zou, B. Highly Efficient Blue Emission from Self-Trapped Excitons in Stable Sb^{3+}-Doped $Cs_2NaInCl_6$ Double Perovskites. *J. Phys. Chem. Lett.* **2020**, *11* (6), 2053–2061. https://doi.org/10.1021/acs.jpclett.0c00330.
54. Chen, Y.; Lam, J. W. Y.; Kwok, R. T. K.; Liu, B.; Tang, B. Z. Aggregation-Induced Emission: Fundamental Understanding and Future Developments. *Mater. Horiz.* **2019**, *6* (3), 428–433. https://doi.org/10.1039/c8mh01331d.
55. Zhang, J.; Qiu, H.; He, T.; Li, Y.; Yin, S. Fluorescent Supramolecular Polymers Formed by Crown Ether-Based Host-Guest Interaction. *Front. Chem.* **2020**, *8*. https://doi.org/10.3389/fchem.2020.00560.
56. Chen, X.-M.; Hou, X.-F.; Bisoyi, H. K.; Feng, W.-J.; Cao, Q.; Huang, S.; Yang, H.; Chen, D.; Li, Q. Light-Fueled Transient Supramolecular Assemblies in Water as Fluorescence Modulators. *Nat. Commun.* **2021**, *12* (1). https://doi.org/10.1038/s41467-021-25299-8.
57. Li, X.; Hu, W.; Wang, Y.; Quan, Y.; Cheng, Y. Strong CPL of Achiral AIE-Active Dyes Induced by Supramolecular Self-Assembly in Chiral Nematic Liquid Crystals (AIE-N*-LCs). *Chem. Commun.* **2019**, *55* (35), 5179–5182. https://doi.org/10.1039/c9cc01678c.

58. Kenry; Chen, C.; Liu, B. Enhancing the Performance of Pure Organic Room-Temperature Phosphorescent Luminophores. *Nat. Commun.* **2019**, *10* (1). https://doi.org/10.1038/s41467-019-10033-2.
59. Dai, X.-Y.; Huo, M.; Liu, Y. Phosphorescence Resonance Energy Transfer from Purely Organic Supramolecular Assembly. *Nat. Rev. Chem.* **2023**, *7* (12), 854–874. https://doi.org/10.1038/s41570-023-00555-1.
60. Zhou, W.-L.; Lin, W.; Chen, Y.; Liu, Y. Supramolecular Assembly Confined Purely Organic Room Temperature Phosphorescence and Its Biological Imaging. *Chem. Sci.* **2022**, *13* (27), 7976–7989. https://doi.org/10.1039/d2sc01770a.
61. Zhou, W.-L.; Lin, W.; Chen, Y.; Dai, X.-Y.; Liu, Z.; Liu, Y. Multivalent Supramolecular Assembly with Ultralong Organic Room Temperature Phosphorescence, High Transfer Efficiency and Ultrahigh Antenna Effect in Water. *Chem. Sci.* **2022**, *13* (2), 573–579. https://doi.org/10.1039/d1sc05861d.
62. Guo, W.-J.; Peng, T.; Zhu, W.; Ma, S.; Wang, G.; Li, Y.; Liu, B.; Peng, H.-Q. Visualization of Supramolecular Assembly by Aggregation-induced Emission. *Aggregate* **2023**, *4* (2). https://doi.org/10.1002/agt2.297.
63. Ma, X.-K.; Liu, Y. Supramolecular Purely Organic Room-Temperature Phosphorescence. *Acc. Chem. Res.* **2021**, *54* (17), 3403–3414. https://doi.org/10.1021/acs.accounts.1c00336.
64. Hong, Y.; Lam, J. W. Y.; Tang, B. Z. Aggregation-Induced Emission: Phenomenon, Mechanism and Applications. *Chem. Commun.* **2009**, No. 29, 4332. https://doi.org/10.1039/b904665h.
65. Hong, Y.; Lam, J. W. Y.; Tang, B. Z. Aggregation-Induced Emission: Phenomenon, Mechanism and Applications. *Chem. Commun.* **2009**, No. 29, 4332. https://doi.org/10.1039/b904665h.
66. Hong, Y.; Lam, J. W. Y.; Tang, B. Z. Aggregation-Induced Emission: Phenomenon, Mechanism and Applications. *Chem. Commun.* **2009**, No. 29, 4332. https://doi.org/10.1039/b904665h.
67. Menger, F. M. Supramolecular Chemistry and Self-Assembly. *Proc. Natl. Acad. Sci. U. S. A.* **2002**, *99* (8), 4818–4822. https://doi.org/10.1073/pnas.062524299.
68. Sierra, A. F.; Aragay, G.; Peñuelas-Haro, G.; Ballester, P. Supramolecular Fluorescence Sensing of L-Proline and l-Pipecolic Acid. *Org. Chem. Front.* **2021**, *8* (11), 2402–2412. https://doi.org/10.1039/d1qo00517k.

69. Wang, Q.; Li, Z.; Tao, D.-D.; Zhang, Q.; Zhang, P.; Guo, D.-P.; Jiang, Y.-B. Supramolecular Aggregates as Sensory Ensembles. *Chem. Commun.* **2016**, *52* (88), 12929–12939. https://doi.org/10.1039/c6cc06075g.

Chapter 2

Molecular Engineering of Naphthalimde Methylcyclohexane Luminogen: Unravelling J*-Aggregation Pattern and Sensing Melamine in Aqueous Media

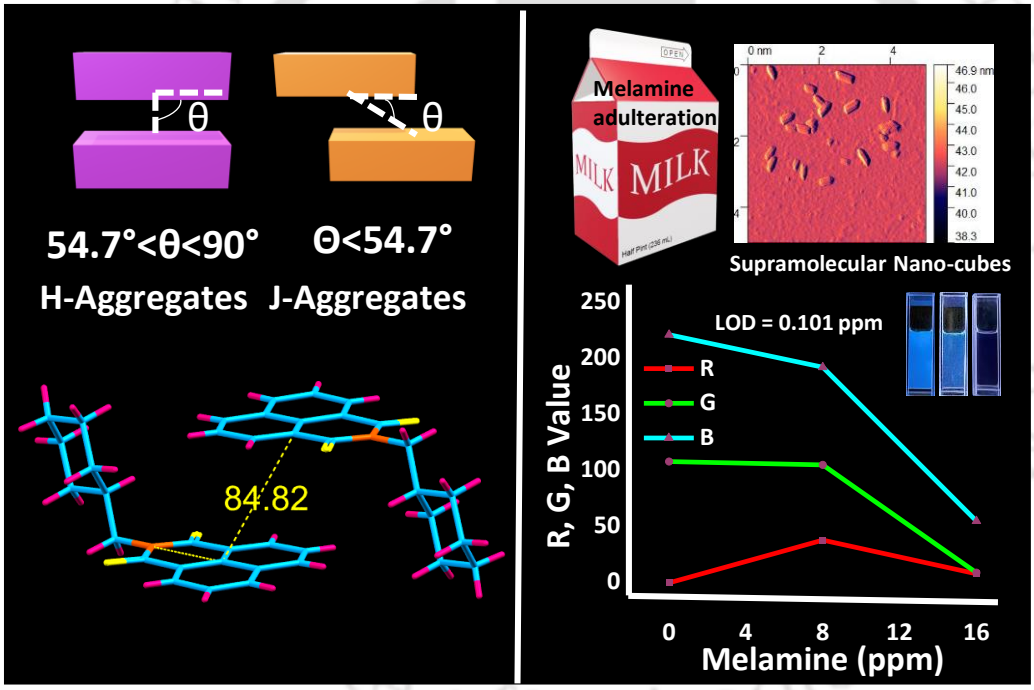

Narang, K.; Iyer, P. K. Molecular Engineering of Naphthalimde Methylcyclohexane Luminogen: Unravelling J*-Aggregation Pattern and Sensing Melamine in Aqueous Media *CCS Chem* **2024**, *6*(4), 923-931.

Abstract

Molecular conformation directed aggregation induced emission (AIE) luminogen NMICY (naphthalimide methylcyclohexane) was prepared, and its pure equatorial conformer was isolated and characterized via single crystal X-ray diffraction (SC-XRD) analysis. In NMICY, the methyl-cyclohexane substituent adapted the most stable chair conformation which completely prevented the notorious intermolecular π-π interaction among the naphthalimide cores in the aggregated state. On careful analysis of the aggregation, it was observed that an unusual J* aggregation pattern was determined for NMICY that exhibited ~450 nm emission in crystal state and in the aggregated state (λ_{max} = 455 nm, ϕ_{PL} = 23.22%, f_w = 99.9% in water or water-DMF mixture). NMICY forms self-assembled cube shaped 2D-nano-architectures as characterized by FESEM and AFM as well as confirmed via DLS (Z_{avg} = 143 nm, ~20 nm height), and displayed unique optical properties in aggregated state. The aggregated state structure-property relationship in aqueous media, and supramolecular self-assembly behaviour of NMICY, were optimized and a facile strategy for melamine detection in milk and aqueous solution of milk powder is reported with a limit of detection (LOD) value of 0.184 ppm (milk) and 0.101 ppm (milk powder), achieved via the rare acceptor-excited photoinduced electron transfer (a-PET) sensing mechanism. Further, smartphone-based portable simplified sensing analysis broadened the melamine detection process.

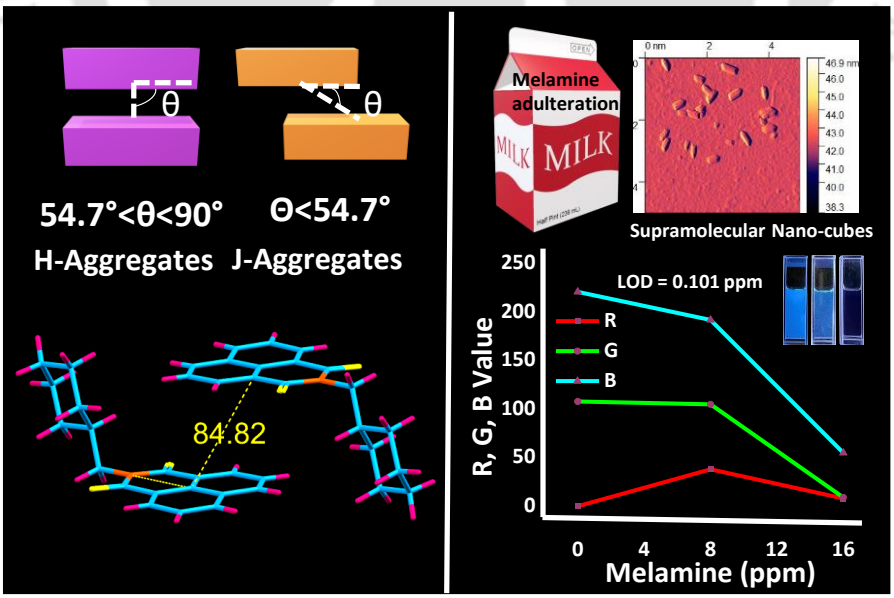

Figure 2.1 Proposed table of content of the present work.

2.1 Introduction

Organic luminescent materials have played significant roles in the advancement of interdisciplinary science and technology over the years.[1] It has been extensively used in recent decades in organic lasers, chemical and biological sensors, solid state emission and flexible screens.[2] In traditional fluorophores, the aggregation-caused quenching (ACQ) effect[3] has led to a complete or partial quenching of fluorescence in their aggregated and solid-state due to the strong π-π interaction among their planar aromatic cores.[4,5] This mandates inserting aromatic rotor groups to prevent the π-π stacking.[6] Using this approach and by analyzing the mechanism as well as the molecular aggregation properties,[7] the design and development of AIE probes has progressed well.[8] For organic conjugated materials, aggregated structure and molecular stacking models can have significant impact on PL properties which is closely related to transition dipole interaction of nearby molecules.[9] Kasha described weakening of the transition dipole interaction by reducing the co-facial interaction and increasing the slipping of molecules from H- to J-aggregate (≥ 54.7° = J-aggregation, ≤ = 54.7° = H-aggregation) which could enhance the emissive properties.[10] Jelley[11] and Scheibe's[12] discovery of a typical J-aggregate serves as the paradigm for all subsequent research. Indeed, the definition of the term "J-aggregate" has evolved all throughout history.[13] On the basis of recent developments and theoretical understanding of intermolecular interactions between slip-stacked dyes, Wurthner et al. suggested to distinguish between classical J-aggregates with predominance of long-range Coulomb coupling and charge transfer (CT) mediated or coupled J-aggregates, whose red shifts are primarily controlled by short range orbital interactions.[14] Thus, it can be deceptive to categorize a J-aggregate solely on the basis of the observed red-shift and slip angle.[15] The traditional J-aggregate's strong excitonic coupling for enhancement of solid-state luminescence cannot explain the newly synthesized AIEgen and their emission phenomenon.[16] In organic aggregates intermolecular interactions are diverse including hydrogen bonding, π-π, cation or anion-π, dipole-dipole etc. and these interactions can be altered by aggregation, flexible molecular conformation and influence of the excited state energy dissipation pathways and the molecule's electrical and geometric structures.[17,18] This opens a potentially wide and new technique for creating highly luminescent class of materials and revealing additional phenomenon about molecular excitons and aggregation patterns.[19]

Naphthalimide core, due to its structural tunability is finding applications as AIE luminogens in sensing,[20,21] bioimaging[22] and supramolecular chemistry.[23] Herein, a design strategy to prepare AIE luminogen (NMICY) from ACQ molecule 1,8-Naphthalic anhydride (NA) by inserting methylcyclohexane substituent tactically was applied, which modulated and impacted its photo-physical properties **(Scheme 2.1)**. The methylene single bond in NMICY permits the cyclohexane ring to rotate freely and adopt chair conformation in the aggregated state, thus providing it with a rare conformational flexibility and preventing intermolecular π-π aggregation of the parent cores and introduced the uncommon J*-aggregation. Further, we have isolated and studied the equatorial conformational isomers (CI) of this NMICY AIE luminogen at room temperature (RT) and analyzed its molecular and aggregated state properties carefully. To our knowledge, this study represents the first instance of a conformation directed ACQ to AIE conversion in an organic molecule. By optimizing the supramolecular self-assembling nature of NMICY, a bathochromic shift of ~80 nm and a large stroke shift of ~100 nm (f_w = 99.9%, f_w = water fraction) was observed in aqueous media which was optimized for the detection of melamine in milk and aqueous milk powder samples with very low limit of detection (LOD), high specificity, and selectivity **(Figure 2.1)**.

2.2 Experimental

2.2.1 Materials and measurements: All starting material reagents, i.e. 1,8-naphthalic anhydride, cyclohexane amine was purchased from Sigma Aldrich (India) and were reagent grade. Milk and milk powder were purchased from local dairy and used for the experiment on the same date of purchase.

NMR Measurements: A Bruker Avance 600 MHz Fourier transformation spectrometer was used to record the proton NMR spectrum at 600 MHz and the ^{13}C NMR spectrum at 200 MHz. All Proton and ^{13}C spectra solutions were obtained using the residual solvent signal as an internal reference. The chemical shifts are reported in parts per million (ppm) with respect to TMS. The short notations used are s for singlet, d for doublet, t for triplet, q for quartet, and m for multiplet.

Matrix-Assisted Laser Desorption Ionization: MALDI was performed on Bruckner model auto-flex speeds using a MALDI TOF system spectrometer.

Optical Measurements: Solution state studies: Electronic absorption spectra of luminophores in solution state were recorded on a Perkin-Elmer Model Lambda-750 spectrophotometer. PL emission spectra were recorded on the Horiba Fluromax-4

spectrofluorometer. Optical measurements were performed using 4 mm quartz cuvettes at 298 K. Crystal state studies: Electronic absorption spectra were recorded on a Perkin Elmer Model Lambda-750 spectrophotometer. Emission spectra were recorded on the FLS1000 spectrometer, an Edinburg instrument.

Lifetime and measurements: Fluorescence lifetime experiments were performed on the Horiba Delta Flex time-correlated single photon counting (TCSPC) instrument. A 373 nm Laser diode with a pulse repetition rate of 1 MHz was used as the light source. All the images were taken on an Apple iPhone 12.

2.2.2 Synthetic procedure

2.2.2a Synthesis of 2-(cyclohexylmethyl)-1H-benzo(de)-isoquionoline-1,3-2H-(dione) (NMICY):

1,8-Naphthalic anhydride (0.5 g) was taken in a 50 mL round bottom flask, and 10 mL of pure ethanol was added to it. The reaction mixture is kept for stirring. While stirring, cyclohexane-methylamine (600 µL) was added drop by drop. After the addition of cyclohexane-methylamine, the reaction set-up is kept in reflux condition for 8 hours. The completion of the reaction was monitored by TLC. After completion of the reaction, the white, hazy crude was filtered through Whatman filter paper. The crude was further purified using 5% chloroform/hexane through column chromatography. NMICY was obtained (500 mg, 95% yield), and a white solid was obtained and further characterized by ^{1}H NMR, ^{13}C NMR, HRMS, MALDI, and SCXRD.

^{1}H NMR (600 MHz, $CDCl_3$, δ ppm) 8.63 (d, 2H), 8.24 (d, 2H), 7.78 (t, 3H), 4.09 (d, 2H), 1.92 (s, 1H), 1.74 (d, 4H), 1.26 (s, 1H), 1.20(d, 2H), 1.15 (m, 3H)

^{13}C NMR: (150 MHz, $CDCl_3$, ppm) 164.62, 133.90, 131.56, 131.34, 128.19, 126.97, 122.66, 46.16, 36.74, 30.98, 26.38, 25.91) HRMS (+ESI) calculated for $C_{19}H_{19}NO_2$ = 293.14 $[M]^+$, Found 294.15 $[M+1]^+$

2.2.2b Synthesis of 2-(hexyl)-1H-benzo(de)-isoquionoline-1,3-2H-(dione), NMIH: 1,8-Naphthalic anhydride (0.5 g) was taken in a 50 mL round bottom flask, and 10 mL of pure ethanol was added to it. The reaction mixture is kept for stirring. While stirring, hexylamine (600 µL) was added drop by drop. After the addition of cyclohexane-hexylamine, the reaction set-up is kept in reflux condition for 12 hours. The completion of the reaction was monitored by TLC. After completion of the reaction, the white, hazy crude was filtered through Whatman filter paper. The crude was further purified using 5% chloroform/hexane through column chromatography. Solid white powder of NMICY was obtained (500 mg,

95% yield), and further characterized by ^{1}H NMR, ^{13}C NMR, HRMS, MALDI, and SCXRD.

^{1}H NMR (600 MHz, $CDCl_3$) δ 8.61, 8.60, 8.22, 8.20, 7.77, 7.76, 7.74, 7.28, 4.20, 4.19, 4.17, 1.74, 1.69, 1.45, 1.35, 1.35, 0.90.

^{13}C NMR (151 MHz, $CDCl_3$) δ 164.19, 133.81, 131.58, 131.15, 128.15, 126.91, 122.78, 77.25, 77.04, 76.82, 40.51, 31.57, 28.09, 26.82, 22.58, 14.06· HRMS (+ESI) calculated for C18H19NO2 = 281.36 $[M]^+$, Found 282.14 $[M+1]^+$

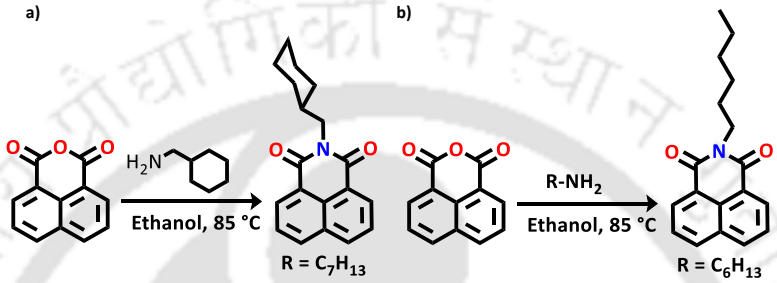

Scheme 2.1: Synthesis of Naphthalimide luminogens (a) NMICY, Ethanol, 85°C, 12 h; (b) NMICY, Ethanol, 85°C, 12 h.

2.2.3 Pre-treatment of melamine in milk powder and melamine in milk samples before sensing analysis: The milk powder and milk were purchased from local supermarkets and dairy respectively and used on the same date for analysis. 0.5 g of milk powder was taken in 50 mL of Eppendorf, followed by 4.5 mL of de-ionized water, 0.5 mL of acetic acid, and 0.5 mL of acetonitrile. For melamine in the milk sample, 3.5 mL of de-ionized water was taken followed by 0.5 mL of raw milk, 0.5 mL of acetic acid, and 0.5 mL of acetonitrile in 50 mL Eppendorf. After this, both samples were kept stirring for 10 minutes. Then, both samples were kept in centrifuges for 30 minutes at 7000 rpm. The solid parts were separated from the liquid. Liquid samples were further passed through a 100 mm mass filter.

2.2.4 Spiking of melamine in milk and milk powder filtrate: Melamine was separately dissolved in deionized water (DI water) (Melamine Solubility = 25 mg/mL; Melamine from Sigma Aldrich, CAS no. 108-78-1), and a 10 mM stock solution was prepared. After milk and milk powder pre-treatment, the filtrate volume was adjusted by 1 mL with the addition of sodium bicarbonate, and the filtrate, was neutralized (pH 7.0). Melamine (10 mM) was added to milk and milk powder filtrate and different concentration

samples (1 mM, 0.1 mM, 0.01 mM, and 0.001 mM) were prepared, which were finally used for the sensing analysis.

2.2.5 Reason to follow sample pre-treatment: Milk and milk powder have a significant amount of casein, protein, vitamins, carbohydrates, fibre, and essential metals, which need to be separated before sensing as they could cause major interference and cause many photophysical phenomena. Without sample pre-treatment, all these biological molecules could have interacted with the analyte, and the quenching mechanism would not be honestly described.

2.2.6 Theoretical calculations: To assess the interface between NMICY and melamine and amino acids used in the selectivity study, electronic properties have been calculated using DFT. The ground-state structure optimization and excited-state electronic properties, along with the HOMO/LUMO energy of NMICY, melamine and all amino acids used in the selectivity study, were calculated in the Gaussian 16 package. B3LYP hybrid functional and 6-31-G basis sets were used during the entire calculation.[24,25]

2.2.7 Procedure to perform smartphone-based sensing analysis: To perform a smartphone-based melamine sensing experiment, a small, closed chamber (10 cm/5 cm/20 cm) with a sample cuvette chamber, a phone holder, and a portable UV light source holder was built in-house. Inside this chamber, the sample in the cuvette was placed and after turning the UV-light ON, different concentrations of NMICY blank (f_w = 99.9%) and different concentrations of melamine in the milk sample, 6 ppm, 15 ppm (prepared with the same method mentioned in section 2.2.3) were taken. Later, these images were analysed by the colour picker software on the iPhone 12. The R/G/B values of these samples were: NMICY blank (f_w = 99.9%) was 0/108/221; NMICY (f_w = 99.9%) with 6 ppm of melamine in milk powder sample was 38/105/192; and 8/9/57 for NMICY (f_w = 99.9%) with 15 ppm of melamine in milk powder sample. This way, a gradual decrease in the R/G/B value of NMICY (f_w = 99.9%) was distinctly observed.[26]

2.2.8 Calculation of detection Limit: For calculation of detection limit, different concentration of melamine in milk powder solution and different concentration of melamine in milk solution was introduced to different samples of fluorophore NMICY (20 μM) suspension in water. Fluorescence spectra were recorded for each sample separately by 340 nm excitation wavelength. The Stern-Volmer Quenching constant (K_{sv}) was

calculated by plotting I0/I versus melamine in milk powder solution and melamine in milk concentration separately. By linear fitting, the curve shows correlation coefficient (R2) was calculated to be close to 1. The detection limit for melamine in milk powder solution and milk was calculated by plotting the change in the PL (Fluorescence) intensity versus concentrations of melamine in milk powder solution and melamine in milk concentrations. The limit of detection (LOD) was calculated using the equation 3σ/K, where σ signifies the standard deviation of fluorescence intensity in the absence of quencher (melamine in milk powder solution and melamine in milk) and K illustrates the slope of the linear plot.[27]

2.2.9 A. Sensitivity study: Procedure; To study the sensitivity of the NMICY towards melamine in milk and milk powder aqueous solution (adulterated with 15 ppm of melamine) and all other possible interference present in milk and milk powder such as amino acids (Glycine, Valine, Phenylalanine, L-Cysteine, Alanine, Arginine, Leucine, Threonine, Methionine, Isoleucine), urea, essential metals Ca^{2+}, Na^{+}, K^{+}, Mg^{2+}, all the mentioned interference introduced separately in 20 µM NMICY in f_w = 99.9%.For each measurement, the fluorescence intensity was measured before and after the introduction of milk and milk powder aqueous solutions (adulterated with 15 ppm of melamine), amino acids (Glycine, Valine, Phenylalanine, L-Cysteine, Alanine, Arginine, Leucine, Threonine, Methionine and Isoleucine), Urea, and essential metals Ca^{2+}, Na^{+}, K^{+}, and Mg^{2+} (15 ppm each) and plotted in a bar diagram to study the sensitivity. It has been found that fluorescence quenching was higher for milk powder than for milk (which is adulterated with 15 ppm melamine).

B. Selectivity study: To clarify the NMICY's selectivity towards an aqueous solution of milk and milk powder (adulterated with 15 ppm of melamine) and all other potential interference found in milk and milk powder, including urea, essential metals Ca^{2+}, Na^{+}, K^{+}, and Mg^{2+}, and amino acids (Glycine, Valine, Phenylalanine, L-Cysteine, Alanine, Arginine, Leucine, Threonine, Methionine, and Isoleucine). The fluorescence intensity was measured both before and after the addition of essential metals Ca^{2+}, Na^{+}, K^{+}, and Mg^{2+} (15 ppm each), urea, milk and milk powder aqueous solutions (adulterated with 15 ppm of melamine), and amino acids (Glycine, Valine, Phenylalanine, L-Cysteine, Alanine, Arginine, Leucine, Threonine, Methionine, and Isoleucine). The results were plotted in a bar diagram to study the selectivity. The results indicate that milk powder exhibited the

most fluorescence quenching, whereas milk (adulterated with 15 ppm melamine) showed the lowest. No significant alterations were seen for the other analytes.

2.3 LOD and Stern Volmer Calculations.

2.3.1 Calculation of Stern-Volmer quenching constant:

The fluorescence response of NMICY was calculated by linear fitting of the fluorescence quenching of NMICY data by adding melamine (in milk and milk powder) into the Stern-Volmer equation:

$$I_0/I = 1 + K_{sv}[Q] \quad (1)$$

I_0 = Initial fluorescence intensity of the probe (NMICY) before the addition of analyte(melamine).

I = Fluorescence intensity of the probe (NMICY) after the addition of an analyte (melamine).

Q = molar concentration of the analyte (NMICY).

K_{sv} = Stern-Volmer quenching constant.

2.3.2 Calculation of Limit of Detection:

The sensitivity of NMICY for the detection of melamine in milk and milk powder solutions was evaluated by fluorescence intensity titration at 0 to 5 ppm melamine. The Limit of Detection was calculated by following equation: -

$$\text{Limit of Detection (LOD)} = 3\sigma/K \quad (2)$$

σ = the standard deviation of the initial fluorescence intensity in the absence of an analyte (melamine).

K = slope of the linear calibration plot determined by plotting the change in the emission intensity of the probe vs. analyte concentration.

2.3.3 Quantum Yield Calculations:

Photoluminescence Quantum Yield (ϕ_{PL}) of NMICY and NMIH aggregated state (f_w = 99.9%, f_w = water fraction) by taking quinine sulphate as standard (ϕ_{PL}= 54.6% in 0.1 M H_2SO_4) by using the following calculations:

$$\phi_{PL} = \phi_r (A_r F_s / A_s F_r) (\eta_s^2 / \eta_r^2)$$

Where the quantum yield is denoted by ϕ, and s and r stand for sample and reference, the letters A signifies absorbance, F denotes relative integrated fluorescence intensity, and the η represent medium's refractive index.

2.4 Result and Discussion

2.4.1 Photo-physical properties

In the ground state, **NMICY** (DMF, f_w = 0%) exhibited characteristics of carbonyl peaks having absorption at 342 nm and 353 nm, broadening of absorption maxima, and a raised baseline in f_w = 99.9%, depicting the probable aggregation of **NMICY (Figure 2.2a, 2.2b)**. The fluorescence of NMICY, studied in the solution state (DMF) showed weak emission, which enhanced with increasing f_w, and the highest emission intensity was recorded at f_w = 99.9%, λ_{max} = 455 nm, attributed to the AIE property and confirming the directed aggregation of NMICY in water. Thus, **NMICY**, which exhibited emission maxima at 375 nm in its monomeric state (DMF, f_w = 0%), was red shifted by 80 nm (from $\lambda_{max.}$ = 455 nm) in f_w = 99.9%, representing the **NMICY** aggregated state emission with a large stroke shift of ~100 nm. Such unusual photophysical properties with high fluorescence intensity make NMICY an excellent candidate for sensing applications. The remarkable shift between f_w = 95% and f_w = 99.9% indicates the slip stacked J-aggregation **(Figure 2.2b, 2.2c, 2.2d)**. Further, on strategically introducing methylcyclohexane in the NA core, a highly emissive NMICY luminogen was obtained both in the aggregated (f_w = 99.9%, $\lambda_{max.}$ = 455 nm) **(Figure 2.2c)** and crystal ($\lambda_{max.}$ = 450 nm) states **(Figure 2.3a)**. The resemblance of NMICY in these two condensed states signifies comparable molecular arrangements in both states, confirming that the emission intensity of napthalimide luminogens depends on their aggregation pattern and intermolecular interactions. The **NMIH** molecule showed nearly identical optical properties to that of **NMICY** due to their comparable electronic contributions **(Figure 2.3b**, **Figure 2.4)** of their individual components, however, the emission intensity of **NMICY** was higher than that of **NMIH** in the aggregated state (**NMICY** ϕ_{PL} = 23.22%, f_w = 99.9%, and **NMICY** ϕ_{PL} = 19.67%, f_w = 99.9%) **(Figure 2.3a, 2.3b, 2.3c and 2.3d)**, clearly confirming that the cyclohexane chair conformation influences the photophysical and AIE behavior of **NMICY**. Further, SC-XRD provided clear insights into the effect of the cyclohexane chair conformation of **NMICY** on its aggregation behaviour.

Conformational isomers (CIs) are molecules made up of the same atoms but with dissimilar arrangements.[28] Typically, a cyclohexane molecule with a single bond can exist in various conformations, such as chair, half chair, boat, and twisted boat, among which the chair form has the lowest energy and thus the most probable conformation to be found at RT. The chair conformation of cyclohexane is free from torsion strain, angle strain, and steric strain, and the C-C-C bond angle is almost 109.4°. Cyclohexane chair conformation exists in axial and equatorial conformations and is interconvertible at RT through ring flip (energy barrier ~10 kcal mol^{-1}). Mono-substituted cyclohexane, such as methyl-cyclohexane, exists in 95% equatorial conformation and 5% axial conformation at RT. In cyclohexane, the increasing substitution thermodynamically Favors the equatorial conformer, as observed in several natural products like epoxides, neurotransmitters, and drugs.[29] Separation and identification of CIs at RT and gaining vital structural insights are crucial as they have enormous application potential in molecular biology, supramolecular chemistry, and medicine.[30]

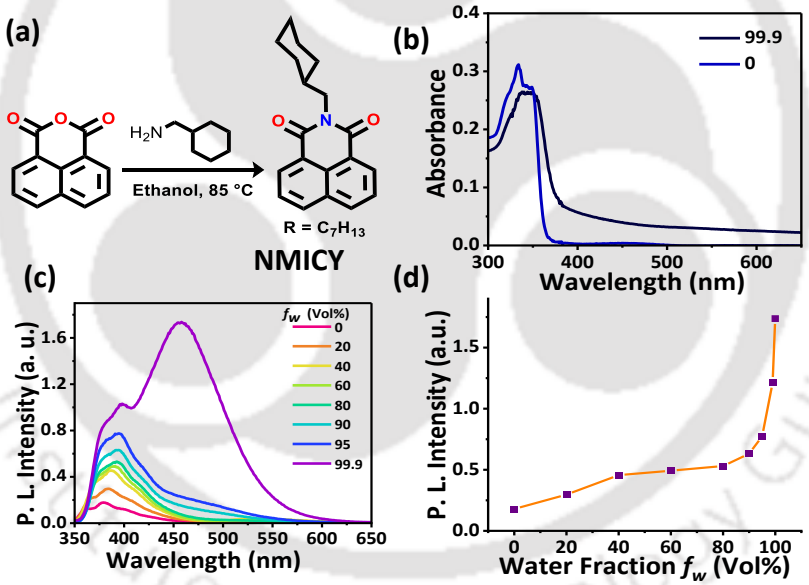

Figure 2.2 a) Synthetic strategy for the synthesis of NMICY b) Absorption spectra of NMICY (20 µM) in f_w = 99.9% and f_w = 0%. (f_w = water fraction) c) The fluorescence emission spectra of NMICY at different water fractions in DMF (20 µM, 25°C, $\lambda_{ex.}$ = 340 nm) d) plot of $\lambda_{em.max.}$ vs. water fraction.

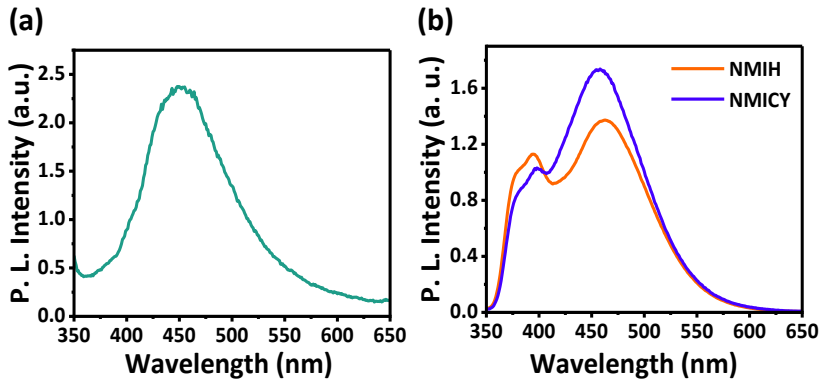

Figure 2.3 (a) PL emission of NMICY crystals (λ_{max} = 450 nm). (b) Emission comparison of NMICY and NMIH in aggregated state. (20 µM, f_w = 99.9%)

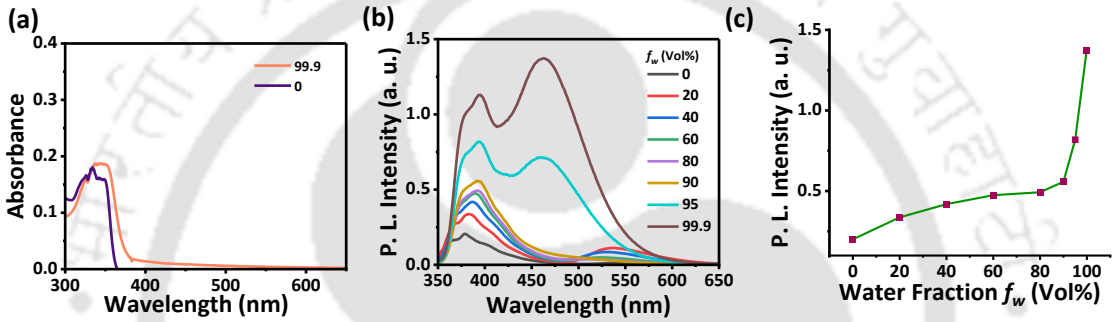

Figure 2.4 (a) Absorbance spectra of NMIH in f_w = 0% (violet) and f_w = 99.9% (peach). (b) The fluorescence emission spectra of NMIH in different water fractions in DMF (c) Respective plot of emission maxima vs. water fraction.

2.4.2 SC-XRD studies

By careful structural analysis of the SC-XRD data of NMICY, it was observed that the cyclohexane in NMICY, due to the methylene single bond bridge, turned it into a conformationally flexible luminogen and adapted the lowest energy chair conformation. It was noted that only the equatorial CI of NMICY (concerning cyclohexane) was found in the overall SC-XRD structure at RT, and despite the low energy barrier of ~10 kcal mol^{-1}, the axial CI of NMICY was not found at all **(Figure 2.5a)**. This shows that careful crystallization could be a way to isolate CIs. This method could be a big step forward in the field of drug design and natural product synthesis, since most drugs and natural product have cyclohexane as a part of their structure and CIs are common.[31] C'-C'-C' bond angles for cyclohexane equatorial chair conformation are between 111.02° and 111.72° **(Figure 2.5b)** which is close to the reported mono-substituted cyclohexane (C-C-C Bond). Except for the equatorial position, the C'1-C'2-C'6 was found at 109.65°, which is closer to the

ideal sp^3 carbon bond angle. This confirms that higher substitution in cyclohexane could also lead to the removal of angle strain in cyclohexane **(Figure 2.5a)**.

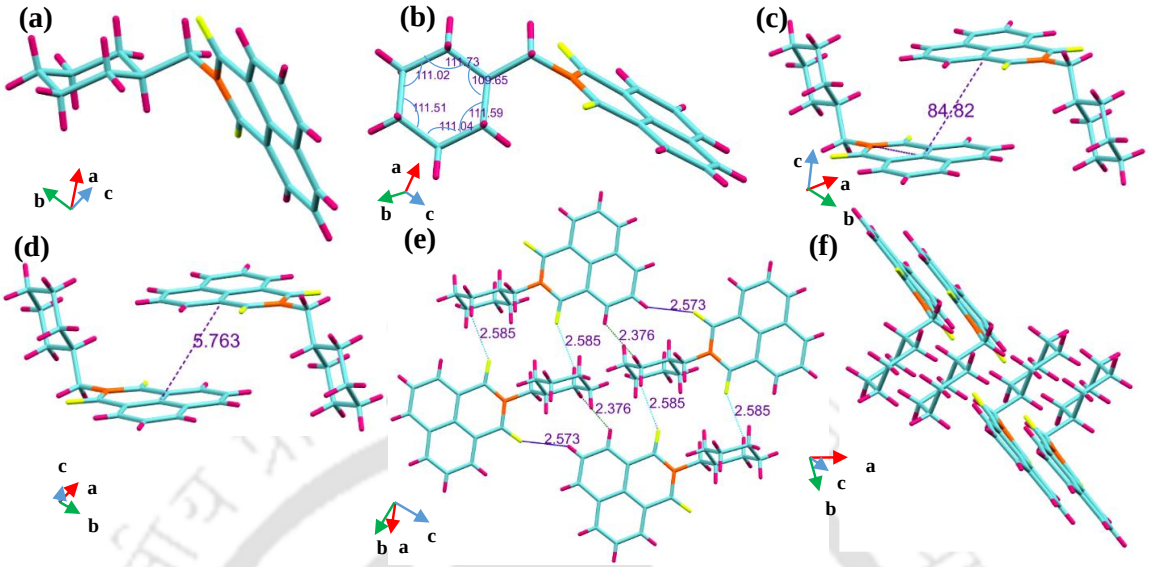

Figure 2.5 (a) Equatorial conformation of cyclohexane in NMICY. (b) All C'-C'-C' bond angle in cyclohexane of NMICY (111.02° to 111.72°) (c) The slip angle between two chromophores is 84.82°. d) The distance between two chromophores is 5.763 Å e) Strong intermolecular interaction between in-plane chromophores f) NMICY consist of two types of molecular configurations of the cyclohexane substituent, one above the plane and the other below the plane.

The C'1(CY)-C(Me)-N(NMI) bond angle was 113.82°, due to which the overall structure of NMICY was twisted **(Figure 2.5b)** and the methyl NMI adopted the equatorial position of cyclohexane. Thus, the probability to acquire an equatorial position is enhanced by functionalization, and hence in NMICY only equatorial conformation existed and a pure isomer of conformationally flexible luminescent NMICY could be isolated via crystallization. The NMICY crystal structure represents a one-unit cell having two molecules oriented in a head-to-tail fashion, but the slip angle between these two molecules is 84.82° (≥ 54.7° = J-aggregation, ≤ 54.7° = H-aggregation), which makes its aggregation pattern very interesting **(Figure 2.5c)**, while the distance between two head-to-tail chromophores was 5.763 Å. No π-π interaction existed between the two NMICY molecules in the crystal lattice (accepted limit of π-π interaction = 4 Å) due to the twisted structure of NMICY via the methylene single bond, cyclohexane chair conformation, and hydrophobic forces between the two cyclohexane chairs, which prevented the notorious aromatic core interaction and stacking, converting the ACQ NA molecule into a bright AIE luminogen, signifying that NMICY has facilitated a unique conformation directed AIE phenomenon.

(Figure 2.5d) The overall structure of NMICY has a very unique slip-stacked intermolecular interaction pattern. In-plane NMICY molecules were connected through very strong intermolecular interactions. One NMICY has two types of C=O…H-C bonds, 2.585 Å and 2.573 Å. The other interactions C(2)-H of cyclohexane and C-H of NMICY are even stronger (2.373 Å). These intermolecular interactions facilitate sheet-like patterns **(Figure 2.5e)**. Cyclohexane equatorial chair CI in the NMICY sheet structure has two types of configurations, one above the sheet and the other below the sheet **(Figure 2.5f)** which could be the possible reason for sheet-like crystals and supramolecular assembly of NMICY in the aggregated state.

The photo-physical properties and SC-XRD analysis of NMICY indicate that any Kasha[9] molecular exciton model could not be applied to explain the aggregation pattern of NMICY. In general, H-aggregates have low fluorescence and a large, blue-shifted absorption, while J-aggregates have high fluorescence and a bathochromic shift in absorption. H-aggregates are detrimental to fluorescence while also enhancing the charge transport by large π-π overlap, and on by avoiding this overlap, the charge transport drastically decreases. As mentioned, due to the chair conformation of NMICY having a twisted structure and the slip angle between two chromophores being 84.82° **(Figure 2.6a)**, there is negligible π-π interaction between the two cores. **(Figure 2.6b)**. In NMICY, the head-to-tail orientation **(Figure 2.5c)**, high-intensity fluorescence **(Figure 2.6a inset)**, and only slight bathochromic shift in absorbance shift **(Figure 2.5b)** support the J-aggregation pattern, yet unlike other traditional molecules, the slip angle observed here was 84.82°, which supports the H-aggregation pattern. Therefore, NMICY can be described as having an uncommon but ideal J* aggregation pattern because two chromophores in a one-unit cell of NMICY have zero π-π overlap, so we can discard Frenkel Charge Transfer Mixing ($t_e = t_h = 0$)[9]. Moreover, NMICY slip angle (84.82°) does not correspond to Kasha's conventional classification of H and J aggregates (≥ 54.7° = J aggregation, ≤ 54.7° = H aggregation) because Kasha's categorization accounts for Frenkel charge transfer mixing between chromophores. NMICY aggregated state emission is purely generated by short contact intermolecular interactions, facilitating high-intensity fluorescence in NMICY. J*-aggregation observed here unveils a new photo-physical concept of complex exitonic behavior in luminogens with complete avoidance of π-π interaction between two chromophores, which is a crucial milestone for the fundamental research of luminescence in fluorophores.[32] The thermodynamic effect of the chair conformation of methyl-

cyclohexane is difficult to analyze directly since other conformers (boat, half boat, etc.) are not separable at RT, but it has introduced a unique aggregation pattern in NMICY that directed the AIE and high fluorescence in the aggregated state.

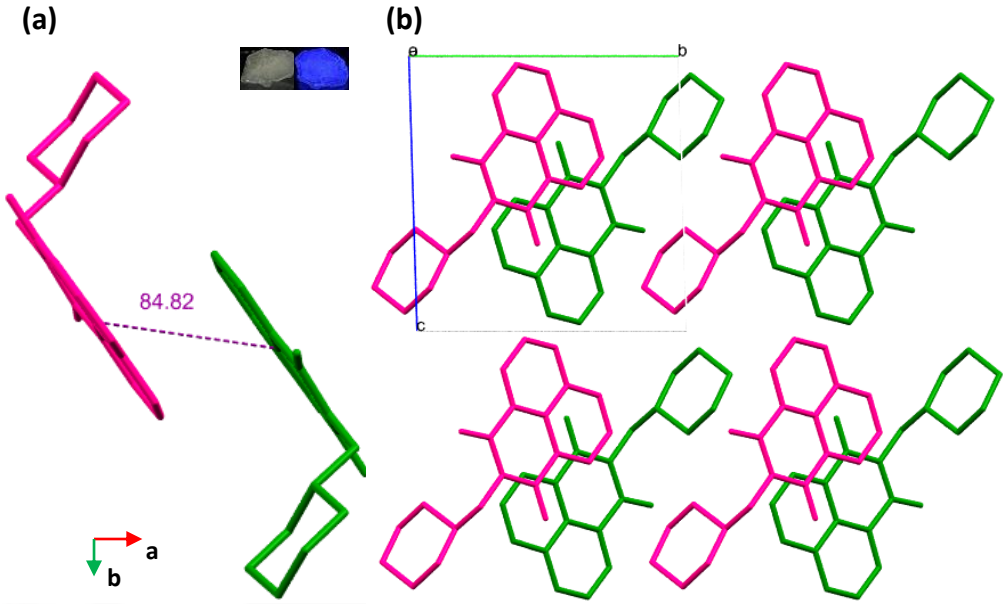

Figure 2.6 (a) The slip angle between two NMICY chromophores is 84.82° along the c axis (inset: NMICY image in daylight (UV OFF) and UV ON condition). (b) The NMICY aggregation pattern along the b-axis, demonstrates negligible π-π interaction between NMICY cores.

2.4.3 Self-assembly properties

Supramolecular self-assembly-based sensors have huge significance in environmental monitoring, disease recognition, biochemical assays, and volatile organic compound detection.[33] Thus, the morphology of self-assembled NMICY (aggregated state, f_w = 99.9%) was carefully studied via field emission electron microscopy (FESEM) and atomic force microscopy (AFM) to understand its likely changes post-sensing studies. 20 µL NMICY (stock solution 1 mM in DMF) was added dropwise in 1 mL DI water followed by vigorous stirring. Trace amounts of DMF was removed via dialysis. FESEM and AFM samples were prepared following the same conditions **(Section 2.2.8, 2.2.9)**. In FESEM analysis, cube-shaped self-assembled nano-architectures with variable size were observed **(Figure 2.7a, 2.7b)**, and similarly, AFM topography and height profile studies reveal these to be cube shaped 2D nano-architectures having an average height of 20 nm. **(Figure 2.7c, 2.7e)**. The Size distribution of this nanocubes self-assembly it was also studied via dynamic light

scattering (DLS), which revealed them to have a hydrodynamic diameter ranging between 80 nm and 210 nm. (Z_{avg} = 143 nm) **(Figure 2.7d)**. This 2D-nano-cube shaped self-assembled NMICY (f_w = 99.9%) luminogen was utilized for the selective detection of melamine in the aqueous solution of milk powder and milk due to its high ratio of charge to surface area and unique optical properties.

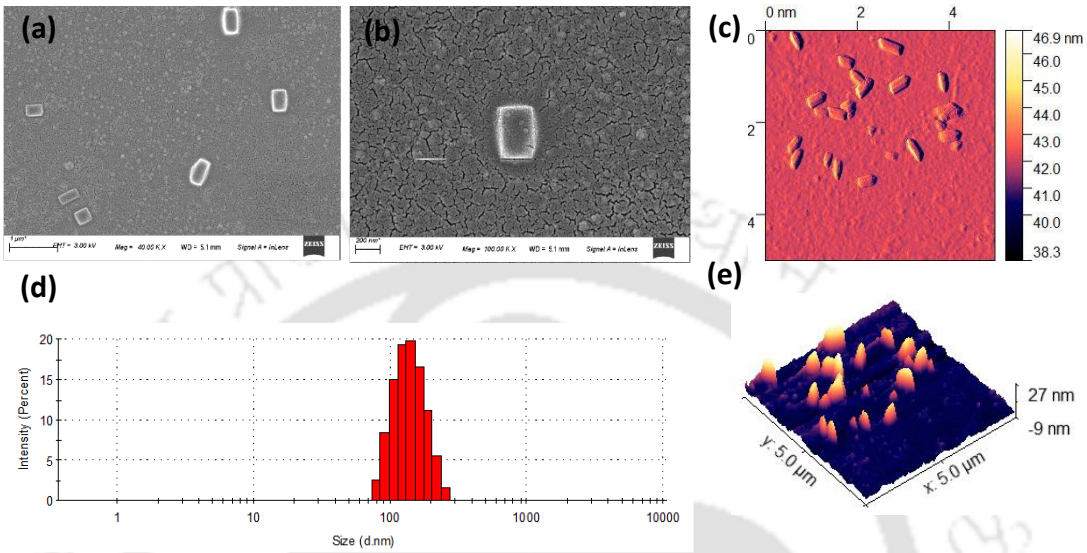

Figure 2.7 Morphology and aggregation study: (a), (b), FESEM images, (c) topography (5 µm × 5 µm) and (e) 3D (5 µm × 5 µm) AFM images of supramolecular self-assembled cube-shaped nanoarchitecture of NMICY. (d) DLS study: size distribution profile of NMICY (20 µM in f_w = 99.9%).

2.4.4 Melamine detection

Melamine is a small organic molecule primarily used in polymer resins, adhesives, plastics, flame retardants, and the coating industry.[34] Melamine, due to its high nitrogen content, is adulterated with milk, milk products, and other protein sources.[35] High concentrations of melamine in the human body can cause stomach aches, vomiting, and nausea in mild cases and forms insoluble melamine cyanurate, which leads to kidney failure, urinary system damage, and infant deaths in acute cases.[36] Hence, a sensitive, selective, rapid, and reliable method of melamine detection in real samples will be of practical significance. A few melamine detection methods based on electrochemistry,[37] Raman spectrometry,[38] optical sensors,[39] quantum dots,[40] colorimetric assay,[41] electroluminescence,[42] Au nanoparticles[43] and Ag nanoclusters[44] have been reported **(Table A2.1)** conjugated polymers and small molecules having strong absorption and emission properties and being easily tunable for targeted biosensors make them strong candidates as biosensors.[45-47] However, most of the reported methods are restricted by poor selectivity, analyte interference, instrument

availability, and many stringent experimental conditions such as pH, temperature, water-solubility, ionic strength, etc.[48]

Before performing the sensing experiments, both milk and milk powder solutions were carefully processed through the standard sample pre-treatment process,[34,49] and then spiked with known quantities of melamine (pre-treatment to avoid interference of biological components such as protein, carbohydrates, amino acid, and essential metals etc. **(Section 2.2, 2.3)**. After that, 0 to 15 ppm melamine (spiked in both milk and milk powder sample) was gradually added to NMICY in water (20 µM, f_w = 99.9%). After the addition of melamine (15 ppm, spiked in both milk and milk powder) to NMICY (20 µM, f_w = 99.9%), huge quenching in fluorescence intensity occurred (~85% for milk, ~90% for milk powder) **(Figures 2.8a 2.8b, A2.2.1, A2.2.2)** Nevertheless, quenching was more efficient for melamine in the milk powder solution. The K_{sv}, and LOD values of 0.101 ppm (milk powder) and 0.184 ppm (milk) for the above studies are listed in **Table A2.2 (Figures A2.2.3 to A2.2.6)** Melamine exhibited dissimilar quenching efficiency towards milk and milk powder, and due to the commercial processing, that the milk powder undergoes, the biological interference is nullified compared to that in raw milk.

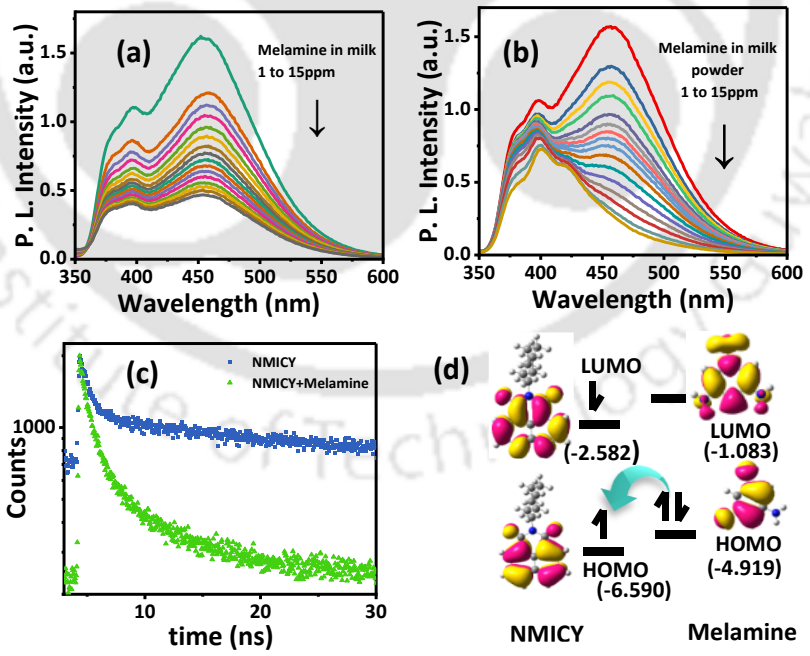

Figure 2.8 Melamine Sensing: a) Fluorescence response of NMICY (20 µM, 99.9% f_w) with the addition of melamine in milk powder (1 to 15 ppm). b) Fluorescence response of NMICY (20 µM, 99.9% f_w) with the addition of melamine in milk (1 to 15 ppm). c) Time-resolved photoluminescence spectra of NMICY (20 µM, 99.9% f_w) before (green) and after

(pink) the addition of melamine in milk powder. (λ_{max} = 455 nm) d) Sensing mechanism: The acceptor transfers electron from HOMO of melamine to HOMO of NMICY (a-PET) via photo-induced process.

2.4.5 Melamine detection mechanism

Melamine with three -NH_2 groups has a strong interaction possibility with NMICY via hydrogen bonding. When melamine (Solubility = 25 mg/mL, Melamine-Sigma Aldrich, CAS no. 108-78-1) [present in milk and milk powder samples (pH 7.0)], was added to the NMICY (f_w = 99.9%) solution, the disruption of the aggregation pattern of the NMICY assembly occurred due to multiple intermolecular interactions with the analyte and its fluorescence intensity drastically quenched **(Figures 2.8a, 2.8b)**. After the addition of melamine to NMICY, the self-assembled cube-shaped 2D nanoarchitectures was not visible, as confirmed via FESEM and AFM characterizations **(Figure 2.9a, 2.9b, 2.9c, 2.9e)**. The hydrodynamic diameter also increased ($Z_{avg.}$ = 223 nm) as observed in DLS **(Figure 2.9d)**.

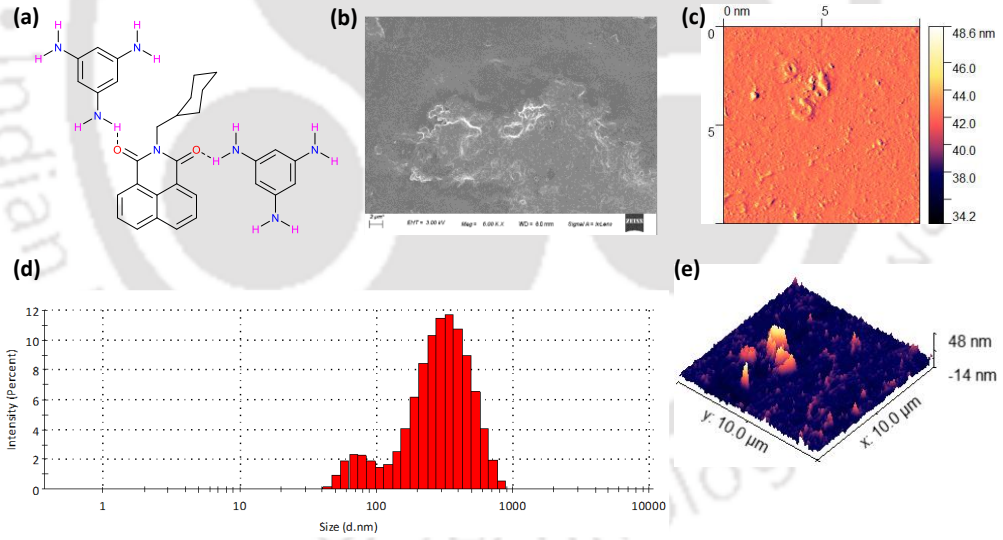

Figure 2.9 a. schematic diagram of NMICY and melamine possible interaction. b. FESEM image of NMICY after the introduction of melamine in milk powder sample. c. topography (5 µm × 5 µm) and e. 3D (5 µm × 5 µm) AFM images of supramolecular self-assembled cube-shaped Nano-architecture of NMICY after the introduction of melamine in milk powder sample. d. DLS study: size distribution profile of NMICY (20 µM in f_w = 99.9%) after the introduction of melamine in milk powder sample. The hydrodynamic diameter ranges between 60 nm to 900 nm ($Z_{avg.}$ = 225 nm). Higher intensity observed between 400 nm to 800 nm.

2.4.6 Theoretical optimization of NMICY and Melamine interaction

NMICY and Melamine Interaction: The computational analysis reveals that the highest occupied molecular orbital (HOMO) predominantly localizes within the melamine molecule, while the lowest unoccupied molecular orbital (LUMO) is primarily situated in NMICY. This distribution suggests a favourable electronic configuration for electron transfer from the HOMO of melamine to the HOMO of NMICY, supporting an excited state proton transfer (ESPT) mechanism, also known as a-PET, for melamine detection in NMICY. Theoretical optimization further substantiates the proposed interaction between NMICY and melamine, illustrating an in-plane parallel arrangement as depicted in Figure 2.9. This conformational alignment underscores the favourable spatial orientation for efficient interaction and signal transduction between NMICY and melamine molecules.

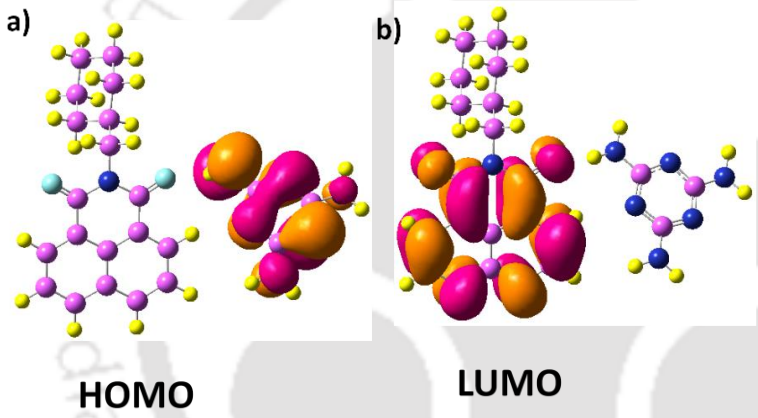

Figure 2.10 Theoretical optimization of NMICY and Melamine interaction in the Gaussian 09 package. (B3LYP hybrid functional and 6-31-G basis sets).

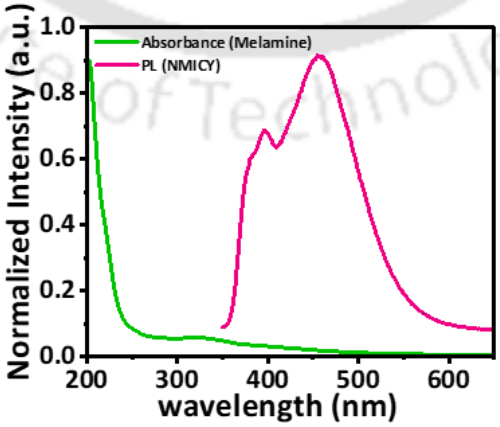

Figure 2.11 Normalized spectra of melamine absorbance (20 μM, in water) and photoluminescence (PL) spectra of NMICY (20 μM, f_w = 99.9%).

2.4.7 Sensitivity and Selectivity study

The sensitivity and selectivity of NMICY for melamine detection over other analytes with similar structures, such as amino acids, Ca, Mg, Glucose, etc., which are likely present in milk, were also evaluated **(Section 2.2.9 A and 2.2.9 B)**. In the sensitivity studies, the fluorescence response was recorded before and after the addition of various analytes in NMICT along with melamine-spiked milk and milk powder samples. None of the other analytes except melamine spiked milk and milk powder samples showed an observable fluorescence change **(Figure 2.4a)** in NMICY. Furthermore, in their selectivity studies, the fluorescence response ratio, I0/I-1 was also plotted, and it was clearly observed that the fluorescence intensity ratio was very low for other analytes. **(Figure 2.4b)** Thus, NMICY demonstrated excellent selectivity and sensitivity towards melamine over all other competing analytes which could likely be present in the detection system.

Additionally, a simple smartphone-based portable sensor protocol was designed to simplify and enhance the applicability of actual milk sample analysis by non-experts.[50,51] In this standard experiment, a setup with having a small, closed sample chamber (10 cm/5 cm/20 cm) with portable UV light, and a phone holder was built. Inside this chamber, after switching on the UV light, images of standard NMICY (20 µM, f_w = 99.9%), and after adding different concentrations of melamine adulterated milk powder sample (6 ppm, 15 ppm) were taken, and the images were analyzed by the color picker software in the iPhone 12. These images distinctly show a gradual decrease in the R/G/B value of NMICY (20 µM, f_w = 99.9%) after adding melamine of different concentrations due to the turn-off fluorescence via the a-PET mechanism **(Figure 2.4c, Section 2.2.9A and 2.2.9B)**, which otherwise are is not easily distinguished by the naked eye. This simple smartphone-based device's sensing analysis of melamine in milk provides a direct and rapid application of for determining adulteration, thus demonstrating that even non-experts can check the purity of milk and detect adulterated melamine in milk at any location accurately.

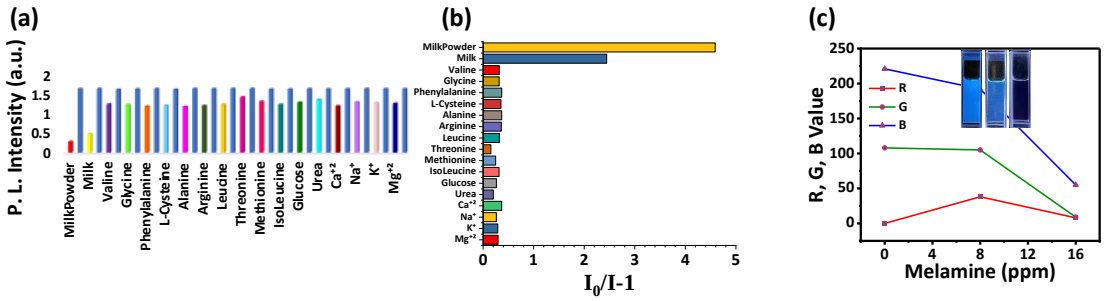

Figure 2.12 Sensitivity and selectivity study: a. Fluorescence response of NMICY (20 µM, f_w = 99.9%) before (blue) and after the addition of melamine in milk powder(red) Melamine in Milk (yellow), Valine (purple), Glycine (light green), Phenylalanine (orange), L-cysteine (light blue), Alanine (magenta), Arginine (dark green), Leucine (yellow), Threonine (purple), Methionine (pink), Isoleucine (tea-blue), Glucose (green), Urea (very light blue), Ca (maroon), Na(violet), K (pink), Mg (royal blue). b. Selectivity study: Bar diagram depicting the effect on the fluorescence intensity of NMICY (20 µM) in the presence of various interfering analytes. c. Smartphone-based Melamine sensing analysis: R (Red), G (Green), B (Blue value) of NMICY (f_w = 99.9%) blank, NMICY (f_w = 99.9%) with 6 ppm melamine in milk powder sample and NMICY (f_w = 99.9%) with 15 ppm melamine in milk powder sample derived from color picker is plotted against Melamine concentration. Inset NMICY (f_w = 99.9%) blank, NMICY (f_w = 99.9%) with 6 ppm melamine in milk powder sample, and NMICY (f_w = 99.9%) with 15 ppm melamine in milk powder (left to right)

2.5 Conclusion

In summary, this work reports the design and synthesis of conformation directed AIE luminogen with methylcyclohexane appended to NMICY, followed by fabrication of a prototype portable device for melamine sensing. Unlike traditional luminogens, this newly synthesized AIE luminogen could not be classified by the well-studied H- and J-aggregates based on its slip angle and red-shifted absorption. However, due to the presence of the methyl-cyclohexane molecule and its crucial role for in forming thermodynamically favorable equatorial chair conformation, the π-π interactions in NMICY were completely evaded, a pure equatorial CI of this flexible molecule was isolated via crystallization at RT, and an uncommon J*-aggregation (ideal J aggregation) pattern was clearly identified. This NMICY luminogen was applied for the detection of melamine in milk and the aqueous solution of milk powder samples with LOD values of 0.101 ppm (milk powder) and 0.184

ppm (milk) via the rare a-PET mechanism. Additionally, a smartphone-based sensing prototype device for the analysis of melamine in milk samples was also developed, which permits its utility even by a non-expert at any location. Through this work, we report the first conformation-directed AIE luminogen NMICY with a unique J* aggregation pattern, a simple design strategy to develop a conformationally flexible luminescent probe and detailed molecular properties of its pure equatorial conformational isomer through crystallization, and the first optical device-based method to detect melamine in milk and the aqueous solution of milk powder.

Furthermore, the elucidation of the unique J* aggregation pattern in NMICY represents a significant advancement in understanding the photophysical behaviour of conformation directed AIE luminogens. This finding underscores the importance of conformational flexibility and its impact on aggregate morphology and optical properties. The successful application of NMICY for melamine detection in milk and milk powder solutions through the rare a-PET mechanism highlights its potential for practical analytical applications. The development of a smartphone-based sensing prototype device further enhances the accessibility and usability of this detection method, offering a convenient and rapid means for melamine detection, even in resource-limited setting. Overall, this study not only contributes to the fundamental understanding of AIE luminogens but also demonstrates their utility in real world applications, paving the way for future advancement in luminescent probe design and optical device based analytical methods.

References

1. Mei, J.; Leung, N. L. C.; Kwok, R. T. K.; Lam, J. W. Y.; Tang, B. Z. Aggregation-Induced Emission: Together We Shine, United We Soar! *Chem. Rev.* **2015**, *115* (21), 11718–11940. https://doi.org/10.1021/acs.chemrev.5b00263.
2. Hong, Y.; Lam, J. W. Y.; Tang, B. Z. Aggregation-Induced Emission. *Chem. Soc. Rev.* **2011**, *40* (11), 5361–5388. https://doi.org/10.1039/c1cs15113d.
3. O'Reilly, J. E. Fluorescence Experiments with Quinine. *J. Chem. Educ.* **1975**, *52* (9), 610. https://doi.org/10.1021/ed052p610.
4. Huang, Y.; Xing, J.; Gong, Q.; Chen, L.-C.; Liu, G.; Yao, C.; Wang, Z.; Zhang, H.-L.; Chen, Z.; Zhang, Q. Reducing Aggregation Caused Quenching Effect through Co-Assembly of PAH Chromophores and Molecular Barriers. *Nat. Commun.* **2019**, *10* (1), 169. https://doi.org/10.1038/s41467-018-08092-y.
5. Chen, Y.; Lam, J. W. Y.; Kwok, R. T. K.; Liu, B.; Tang, B. Z. Aggregation-Induced Emission: Fundamental Understanding and Future Developments. *Mater. Horiz.* **2019**, *6* (3), 428–433. https://doi.org/10.1039/c8mh01331d.
6. Barman, D.; Narang, K.; Parui, R.; Zehra, N.; Khatun, M. N.; Adil, L. R.; Iyer, P. K. Review on Recent Trends and Prospects in Π-conjugated Luminescent Aggregates for Biomedical Applications. *Aggregate* **2022**, *3* (5). https://doi.org/10.1002/agt2.172.
7. Gopikrishna, P.; Meher, N.; Iyer, P. K. Functional 1,8-Naphthalimide AIE/AIEEgens: Recent Advances and Prospects. *ACS Appl. Mater. Interfaces* **2018**, *10* (15), 12081–12111. https://doi.org/10.1021/acsami.7b14473.
8. Leung, N. L. C.; Xie, N.; Yuan, W.; Liu, Y.; Wu, Q.; Peng, Q.; Miao, Q.; Lam, J. W. Y.; Tang, B. Z. Restriction of Intramolecular Motions: The General Mechanism behind Aggregation-Induced Emission. *Chemistry* **2014**, *20* (47), 15349–15353. https://doi.org/10.1002/chem.201403811.
9. Hestand, N. J.; Spano, F. C. Expanded Theory of H- and J-Molecular Aggregates: The Effects of Vibronic Coupling and Intermolecular Charge Transfer. *Chem. Rev.* **2018**, *118* (15), 7069–7163. https://doi.org/10.1021/acs.chemrev.7b00581.
10. Kasha, M.; Rawls, H. R.; Ashraf El-Bayoumi, M. The Exciton Model in Molecular Spectroscopy. *Pure Appl. Chem.* **1965**, *11* (3–4), 371–392. https://doi.org/10.1351/pac196511030371.
11. Jelley, E. E. Spectral Absorption and Fluorescence of Dyes in the Molecular State.

Nature **1936**, *138* (3502), 1009–1010. https://doi.org/10.1038/1381009a0.

12. Möbius, D. Scheibe Aggregates. *Adv. Mater.* **1995**, *7* (5), 437–444. https://doi.org/10.1002/adma.19950070503.
13. Würthner, F.; Saha-Möller, C. R.; Fimmel, B.; Ogi, S.; Leowanawat, P.; Schmidt, D. Perylene Bisimide Dye Assemblies as Archetype Functional Supramolecular Materials. *Chem. Rev.* **2016**, *116* (3), 962–1052. https://doi.org/10.1021/acs.chemrev.5b00188.
14. Kim, J. H.; Schembri, T.; Bialas, D.; Stolte, M.; Würthner, F. Slip-Stacked J-Aggregate Materials for Organic Solar Cells and Photodetectors. *Adv. Mater.* **2022**, *34* (22), e2104678. https://doi.org/10.1002/adma.202104678.
15. Guerrini, M.; Cocchi, C.; Calzolari, A.; Varsano, D.; Corni, S. Interplay between Intra- and Intermolecular Charge Transfer in the Optical Excitations of J-Aggregates. *J. Phys. Chem. C Nanomater. Interfaces* **2019**, *123* (11), 6831–6838. https://doi.org/10.1021/acs.jpcc.8b11709.
16. Peng, Q.; Shuai, Z. Molecular Mechanism of Aggregation-induced Emission. *Aggregate* **2021**, *2* (5). https://doi.org/10.1002/agt2.91 .
17. Emamian, S.; Lu, T.; Kruse, H.; Emamian, H. Exploring Nature and Predicting Strength of Hydrogen Bonds: A Correlation Analysis between Atoms-in-Molecules Descriptors, Binding Energies, and Energy Components of Symmetry-Adapted Perturbation Theory. *J. Comput. Chem.* **2019**, *40* (32), 2868–2881. https://doi.org/10.1002/jcc.26068.
18. Scheibe, G. Über die Veränderlichkeit der Absorptionsspektren in Lösungen und die Nebenvalenzen als ihre Ursache. *Angew. Chem. Int. Ed* **1937**, *50* (11), 212–219. https://doi.org/10.1002/ange.19370501103.
19. Ma, S.; Du, S.; Pan, G.; Dai, S.; Xu, B.; Tian, W. Organic Molecular Aggregates: From Aggregation Structure to Emission Property. *Aggregate* **2021**, *2* (4). https://doi.org/10.1002/agt2.96.
20. Meher, N.; Panda, S.; Kumar, S.; Iyer, P. K. Aldehyde Group Driven Aggregation-Induced Enhanced Emission in Naphthalimides and Its Application for Ultradetection of Hydrazine on Multiple Platforms. *Chem. Sci.* **2018**, *9* (16), 3978–3985. https://doi.org/10.1039/c8sc00643a.
21. Meher, N.; Iyer, P. K. Pendant Chain Engineering to Fine-Tune the Nanomorphologies and Solid State Luminescence of Naphthalimide AIEEgens: Application to Phenolic Nitro-Explosive Detection in Water. *Nanoscale* **2017**, *9*

(22), 7674–7685. https://doi.org/10.1039/c7nr02174g.

22. Meher, N.; Bidkar, A. P.; Barman, D.; Ghosh, S. S.; Iyer, P. K. A Conformational Tweak for Enhanced Cellular Internalization, Photobleaching Resistance and Prolonged Imaging Efficacy. *Chem. Commun.* **2020**, *56* (94), 14861–14864. https://doi.org/10.1039/d0cc05557c.
23. Meher, N.; Iyer, P. K. Functional Group Engineering in Naphthalimides: A Conceptual Insight to Fine-Tune the Supramolecular Self-Assembly and Condensed State Luminescence. *Nanoscale* **2019**, *11* (28), 13233–13242. https://doi.org/10.1039/c9nr04593g.
24. Becke, A. D. Density-Functional Thermochemistry. I. The Effect of the Exchange-Only Gradient Correction. *J. Chem. Phys.* **1992**, *96* (3), 2155–2160. https://doi.org/10.1063/1.462066.
25. Frisch, M. J.; Trucks, G. W.; Schlegel, H. B.; Scuseria, G. E.; Robb, M. A.; Cheeseman, J. R.; Scalmani, G.; Barone, V.; Petersson, G. A.; Nakatsuji, H.; Li, X.; Caricato, M.; Marenich, A. V.; Bloino, J.; Janesko, B. G.; Gomperts, R.; Mennucci, B.; Hratchian, H. P.; Ortiz, J. V.; Izmaylov, A. F.; Sonnenberg, J. L.; Williams-Young, D.; Ding, F.; Lipparini, F.; Egidi, F.; Goings, J.; Peng, B.; Petrone, A.; Henderson, T.; Ranasinghe, D.; Zakrzewski, V. G.; Gao, J.; Rega, N.; Zheng, G.; Liang, W.; Hada, M.; Ehara, M.; Toyota, K.; Fukuda, R.; Hasegawa, J.; Ishida, M.; Nakajima, T.; Honda, Y.; Kitao, O.; Nakai, H.; Vreven, T.; Throssell, K.; Montgomery, J. A.; Peralta, J. E.; Ogliaro, F.; Bearpark R Kobayashi, M. J.; Normand, J.; Raghavachari, K.; Rendell, A. P.; Burant, J. C.; Iyengar, S. S.; Tomasi, J.; Cossi, M.; Millam, J. M.; Klene, M.; Adamo, C.; Cammi, R.; Ochterski, J. W.; Martin, R. L.; Morokuma, K.; Farkas, O.; Foresman, J. B.; Fox, D. J. Gaussian 16; Heyd, J. J., Brothers, E. N., Kudin, K. N., Staroverov, V. N., Keith, T. A., Eds.; Gaussian, Inc: Wallingford CT, 2016.
26. Hussain, S.; Chen, X.; Wang, C.; Hao, Y.; Tian, X.; He, Y.; Li, J.; Shahid, M.; Iyer, P. K.; Gao, R. Aggregation and Binding-Directed FRET Modulation of Conjugated Polymer Materials for Selective and Point-of-Care Monitoring of Serum Albumins. *Anal. Chem.* **2022**, *94* (30), 10685–10694. https://doi.org/10.1021/acs.analchem.2c00984.
27. Tanwar, A. S.; Iyer, P. K. Fluorescence “Turn-on” Indicator Displacement Assay-Based Sensing of Nitroexplosive 2,4,6-Trinitrophenol in Aqueous Media via a Polyelectrolyte and Dye Complex. *ACS Omega* **2017**, *2* (8), 4424–4430.

https://doi.org/10.1021/acsomega.7b00765.

28. Canfield, P. J.; Blake, I. M.; Cai, Z.-L.; Luck, I. J.; Krausz, E.; Kobayashi, R.; Reimers, J. R.; Crossley, M. J. Publisher Correction: A New Fundamental Type of Conformational Isomerism. *Nat. Chem.* **2018**, *10* (9), 989–989. https://doi.org/10.1038/s41557-018-0117-5.
29. Lawson, C. J.; Rees, D. A. An Enzyme for the Metabolic Control of Polysaccharide Conformation and Function. *Nature* **1970**, *227* (5256), 392–393. https://doi.org/10.1038/227392a0.
30. Bastiansen, O.; Hassel, O.; Sillén, L. G.; Linnasalmi, A.; Laukkanen, P. A New Isomer of Hexachloro-Cyclohexane with Zero Dipole Moment. *Preliminary Communication. Acta Chem. Scand.* **1947**, *1*, 683–683. https://doi.org/10.3891/acta.chem.scand.01-0683b.
31. Tang, C.; Tang, Y.; Ye, Y.; Yan, Z.; Chen, Z.; Chen, L.; Zhang, L.; Liu, J.; Shi, J.; Xia, H.; Hong, W. Identifying the Conformational Isomers of Single-Molecule Cyclohexane at Room Temperature. *Chem* **2020**, *6* (10), 2770–2781. https://doi.org/10.1016/j.chempr.2020.07.024.
32. Zhao, L.; Ren, X.; Yan, X. Assembly Induced Super-Large Red-Shifted Absorption: The Burgeoning Field of Organic near-Infrared *Materials. CCS Chem.* **2021**, *3* (5), 678–693. https://doi.org/10.31635/ccschem.021.202100771.
33. Meher, N.; Iyer, P. K. Spontaneously Self-Assembled Naphthalimide Nanosheets: Aggregation-Induced Emission and Unveiling a-PET for Sensitive Detection of Organic Volatile Contaminants in Water. *Angew. Chem. Int. Ed* **2018**, *57* (28), 8488–8492. https://doi.org/10.1002/anie.201802842.
34. Ai, K.; Liu, Y.; Lu, L. Hydrogen-Bonding Recognition-Induced Color Change of Gold Nanoparticles for Visual Detection of Melamine in Raw Milk and Infant Formula. *J. Am. Chem. Soc.* **2009**, *131* (27), 9496–9497. https://doi.org/10.1021/ja9037017.
35. Niu, C.; Liu, Q.; Shang, Z.; Zhao, L.; Ouyang, J. Dual-Emission Fluorescent Sensor Based on AIE Organic Nanoparticles and Au Nanoclusters for the Detection of Mercury and Melamine. *Nanoscale* **2015**, *7* (18), 8457–8465. https://doi.org/10.1039/c5nr00554j.
36. Rajpoot, M.; Bhattacharya, R.; Sharma, S.; Gupta, S.; Sharma, V.; Sharma, A. K. Melamine Contamination and Associated Health Risks: Gut Microbiota Does Make a Difference. *Biotechnol. Appl. Biochem.* **2021**, *68* (6), 1271–1280.

https://doi.org/10.1002/bab.2050.

37. Zhu, H.; Zhang, S.; Li, M.; Shao, Y.; Zhu, Z. Electrochemical Sensor for Melamine Based on Its Copper Complex. *Chem. Commun.* **2010**, *46* (13), 2259–2261. https://doi.org/10.1039/b924355k.
38. Zhang, X.-F.; Zou, M.-Q.; Qi, X.-H.; Liu, F.; Zhu, X.-H.; Zhao, B.-H. Detection of Melamine in Liquid Milk Using Surface-Enhanced Raman Scattering Spectroscopy: Detection of Melamine in Liquid Milk Using SERS. *J. Raman Spectrosc.* **2010**, *41* (12), 1655–1660. https://doi.org/10.1002/jrs.2629.
39. Sanji, T.; Nakamura, M.; Kawamata, S.; Tanaka, M.; Itagaki, S.; Gunji, T. Fluorescence "Turn-on" Detection of Melamine with Aggregation-Induced-Emission-Active Tetraphenylethene. *Chemistry* **2012**, *18* (48), 15254–15257. https://doi.org/10.1002/chem.201203081.
40. Wang, J.; Liu, X.; Huang, L.; Jin, J.; Jiang, C.; Li, D.; Wen, H.; Hu, J. Controllable and Robust Dual-Emissive Quantum Dot Nanohybrids as Inner Filter-Based Ratiometric Probes for Visualizable Melamine Detection. *Nanoscale* **2020**, *12* (7), 4562–4572. https://doi.org/10.1039/c9nr08849k.
41. Han, X.; Qin, Z.; Zhao, M.; Song, J.; Qu, F.; Qu, F.; Kong, R.-M. Convenient and Sensitive Colorimetric Detection of Melamine in Dairy Products Based on Cu(Ii)-H2O2-3,3′,5,5′-Tetramethylbenzidine System. *RSC Adv.* **2018**, *8* (61), 34877–34882. https://doi.org/10.1039/c8ra07167e.
42. Zhu, H.; Wang, N.; Xu, Y.; Chen, S.; Willander, M.; Cao, X.; Wang, Z. L. Triboelectric Nanogenerators Based on Melamine and Self-Powered High-Sensitive Sensors for Melamine Detection. *Adv. Funct. Mater.* **2016**, *26* (18), 3029–3035. https://doi.org/10.1002/adfm.201504505.
43. Chen, L.; Huang, Y.; Xing, T. T.; Ge, L.; Yang, T.; Chen, B.; Huang, C. Z. A Portable Multi-Channel Sensing Device Using Au Nano-Urchins as Probes for Melamine Detection in Milk. *J. Mater. Chem. C Mater.* **2017**, *5* (31), 7806–7812. https://doi.org/10.1039/c7tc01384a.
44. Zhang, Y.; Li, B.; Ma, H.; Zhang, L.; Jiang, H.; Song, H.; Zhang, L.; Luo, Y. A Nanoscaled Lanthanide Metal–Organic Framework as a Colorimetric Fluorescence Sensor for Dipicolinic Acid Based on Modulating Energy Transfer. *J. Mater. Chem. C.* **2016**, *4* (30), 7294–7301. https://doi.org/10.1039/c6tc01022a.
45. Zhu, C.; Liu, L.; Yang, Q.; Lv, F.; Wang, S. Water-Soluble Conjugated Polymers for Imaging, Diagnosis, and Therapy. *Chem. Rev.* **2012**, *112* (8), 4687–4735.

https://doi.org/10.1021/cr200263w.

46. Zhang, C.-J.; Gao, Z.-Y.; Wang, Q.-B.; Zhang, X.; Yao, J.-S.; Qiao, C.; Liu, Q.-Z. Highly Sensitive Detection of Melamine Based on the Fluorescence Resonance Energy Transfer between Conjugated Polymer Nanoparticles and Gold Nanoparticles. *Polymers* **2018**, *10* (8). https://doi.org/10.3390/polym10080873.
47. Feng, L.; Zhu, C.; Yuan, H.; Liu, L.; Lv, F.; Wang, S. Conjugated Polymer Nanoparticles: Preparation, Properties, Functionalization and Biological Applications. *Chem. Soc. Rev.* **2013**, *42* (16), 6620–6633. https://doi.org/10.1039/c3cs60036j.
48. Li, Y.; Xu, J.; Sun, C. Chemical Sensors and Biosensors for the Detection of Melamine. *RSC Adv.* **2015**, *5* (2), 1125–1147. https://doi.org/10.1039/c4ra13080d.
49. Huang, X.; Song, J.; Yung, B. C.; Huang, X.; Xiong, Y.; Chen, X. Ratiometric Optical Nanoprobes Enable Accurate Molecular Detection and Imaging. *Chem. Soc. Rev.* **2018**, *47* (8), 2873–2920. https://doi.org/10.1039/c7cs00612h.
50. Li, L.; Wu, G.; Hong, T.; Yin, Z.; Sun, D.; Abdel-Halim, E. S.; Zhu, J.-J. Graphene Quantum Dots as Fluorescence Probes for Turn-off Sensing of Melamine in the Presence of Hg^{2+}. *ACS Appl. Mater. Interfaces* **2014**, *6* (4), 2858–2864. https://doi.org/10.1021/am405305r.
51. Lakowicz, J. R. Principles of Fluorescence Spectroscopy; Lakowicz, J. R., Ed.; Springer: New York, NY, 2017.
52. Hussain, S.; Chen, X.; Wang, C.; Hao, Y.; Tian, X.; He, Y.; Li, J.; Shahid, M.; Iyer, P. K.; Gao, R. Aggregation and Binding-Directed FRET Modulation of Conjugated Polymer Materials for Selective and Point-of-Care Monitoring of Serum Albumins. *Anal. Chem.* **2022**, *94* (30), 10685–10694. https://doi.org/10.1021/acs.analchem.2c00984.

Appendix

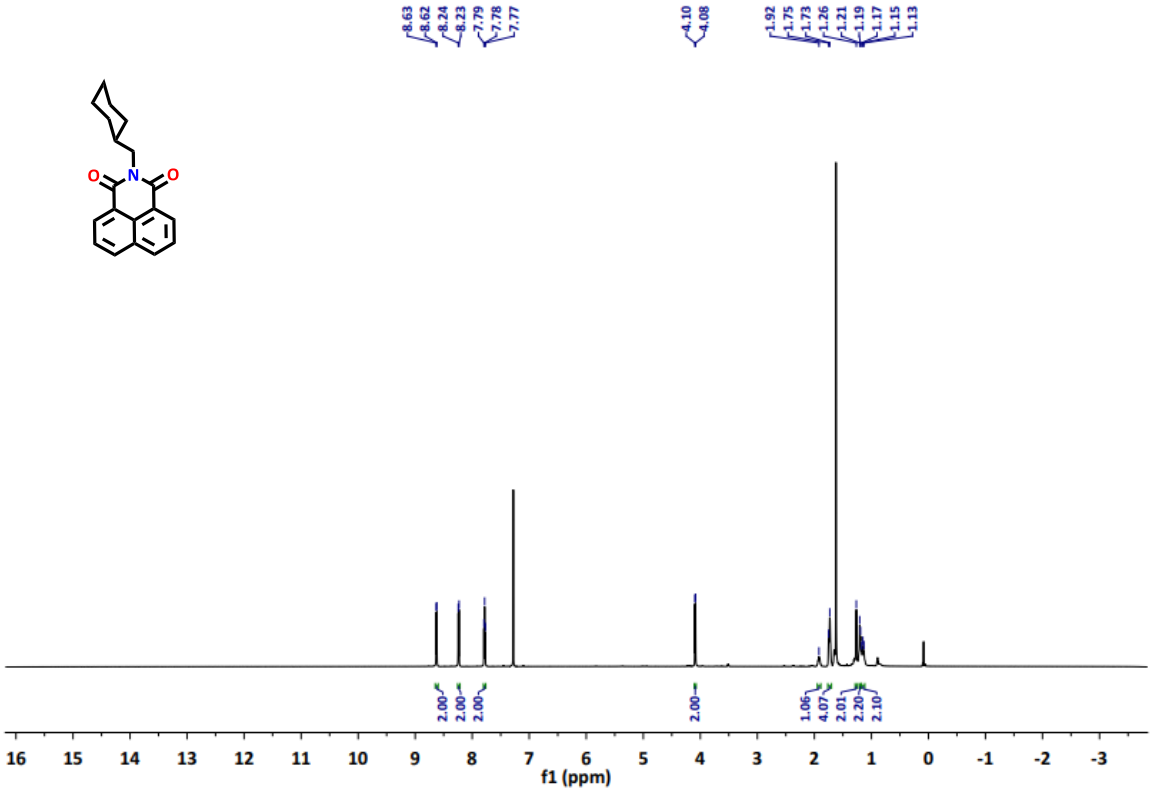

Figure A2.1.1 Proton NMR spectra of NMICY.

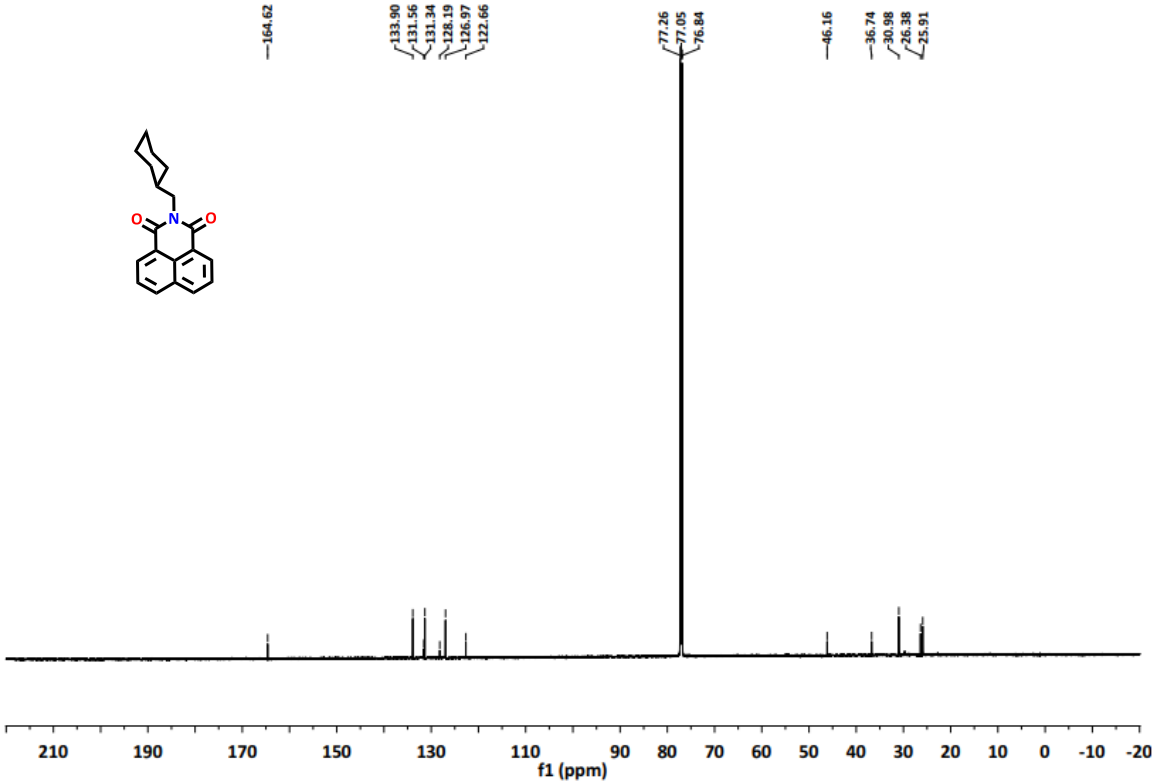

Figure A2.1.2 ^{13}C NMR spectra of NMICY.

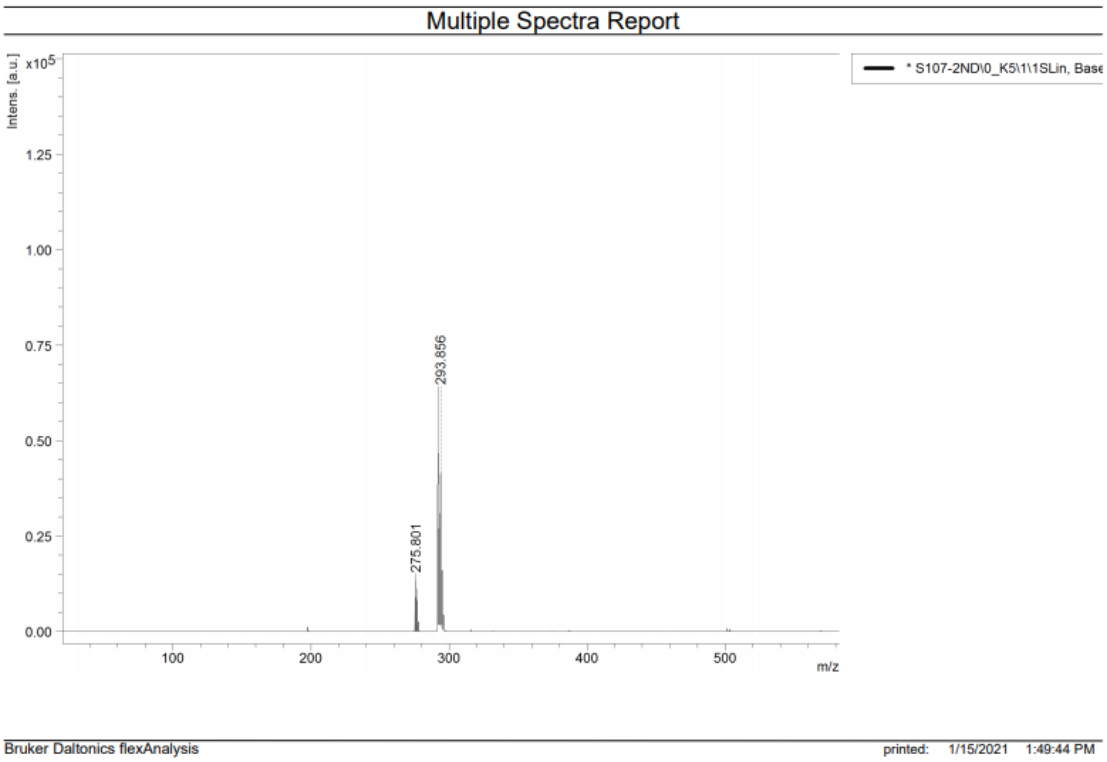

Figure A2.1.3 MALDI spectra of NMICY.

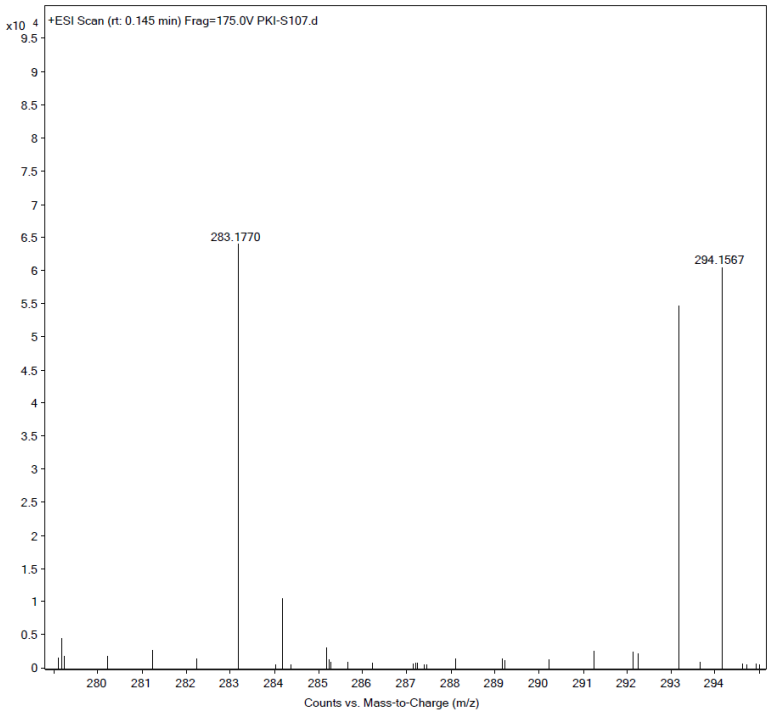

Figure A2.1.4 MALDI spectra of NMICY.

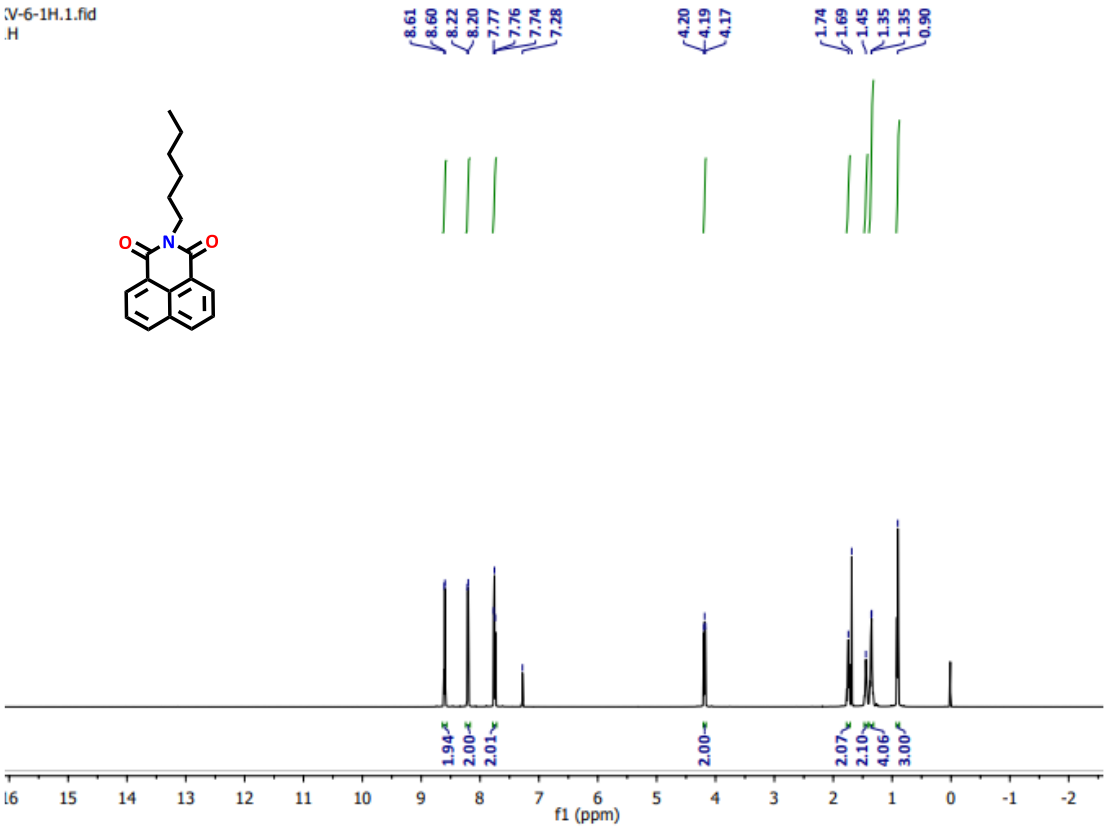

Figure A2.1.5 Proton NMR spectra of NMIH.

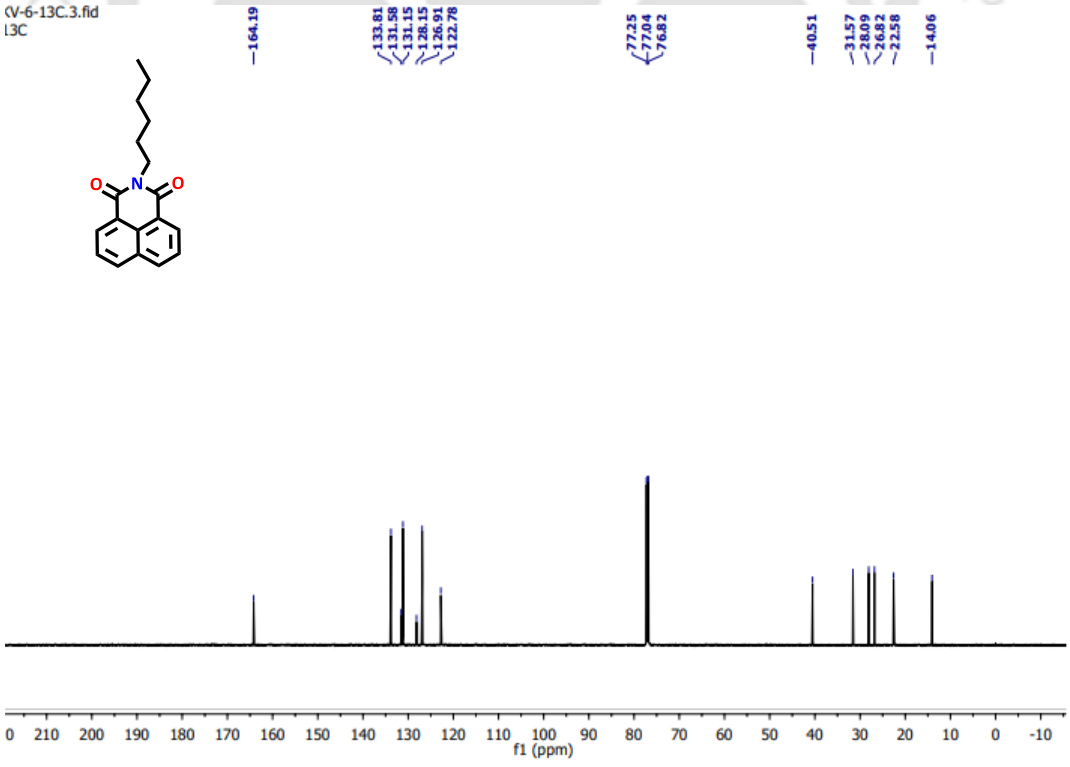

Figure A2.1.6 ^{13}C NMR spectrum of NMIH.

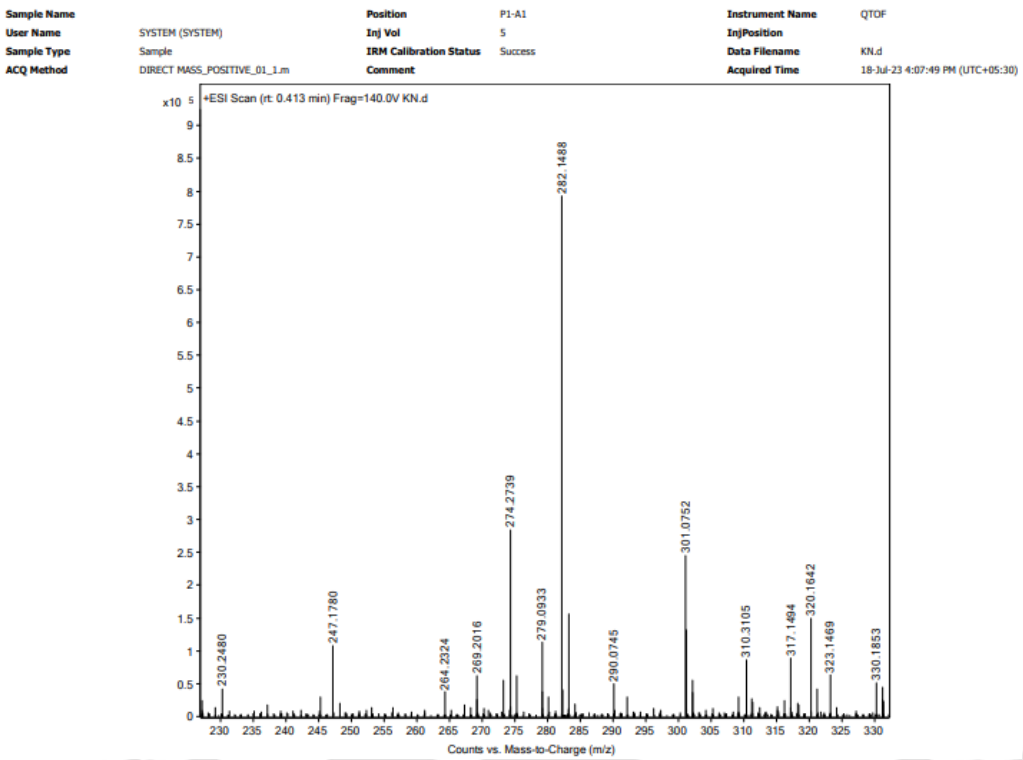

Figure A2.1.7 MALDI spectrum of NMIH.

Melamine sensing in milk powder

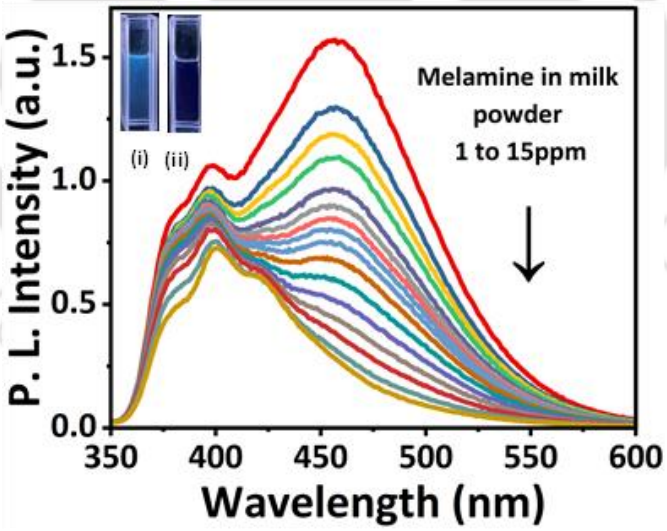

Figure A2.1.8 Fluorescence intensity vs wavelength plot while the increasing concentration of melamine (in milk powder). Inset: PL image of NMICY (20 µM, f_w = 99.9%) before and after addition of melamine sample.

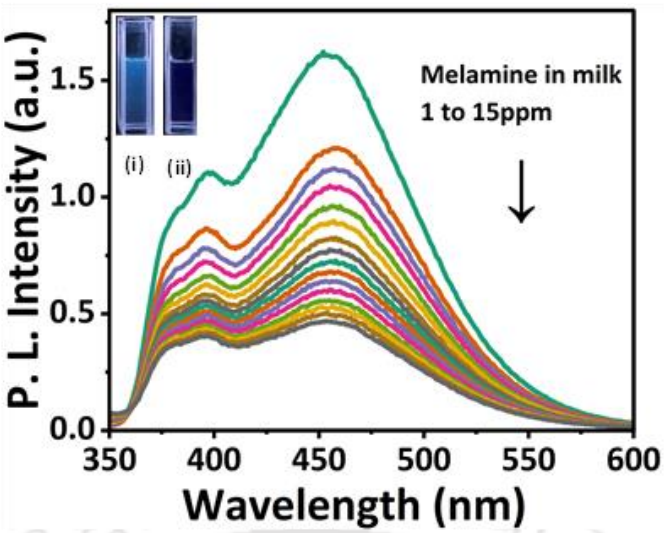

Figure A2.1.9 Fluorescence intensity vs wavelength plot while increasing concentration of melamine (in milk). Inset: PL image of NMICY (20 µM, f_w = 99.9%) before and after addition of melamine sample.

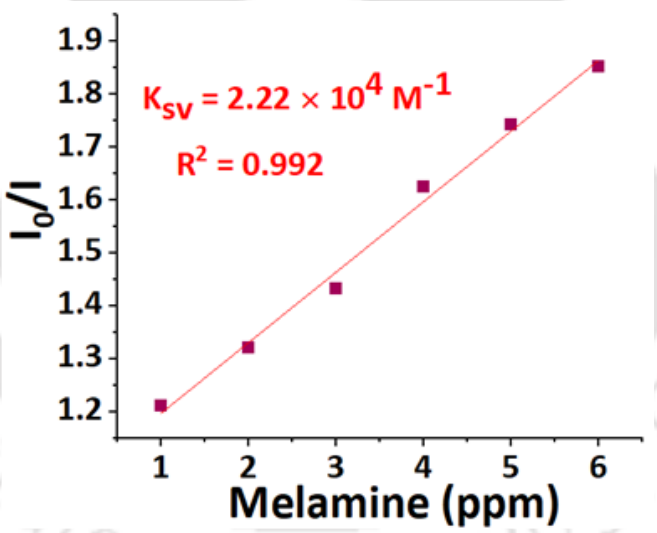

Figure A2.2.0 Change in the fluorescence intensity of NMICY (20 µM) with addition of melamine (in milk powder) from 0 to 6 ppm.

Calculation of Stern-Volmer plot and limit of detection (LOD)

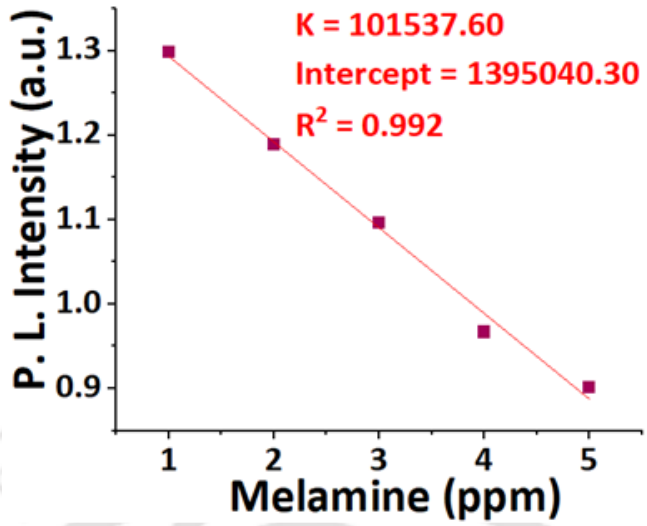

Figure A2.2.1 Emission intensity maxima of NMICY nano-cubes vs. melamine in milk powder at different concentrations.

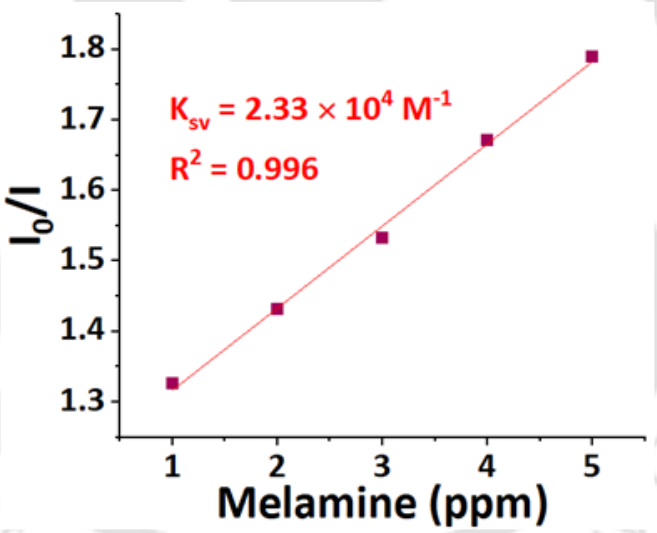

Figure A2.2.2 Change in the fluorescence intensity of NMICY (20 µM) with addition of melamine (in milk powder) from 0 to 6 ppm.

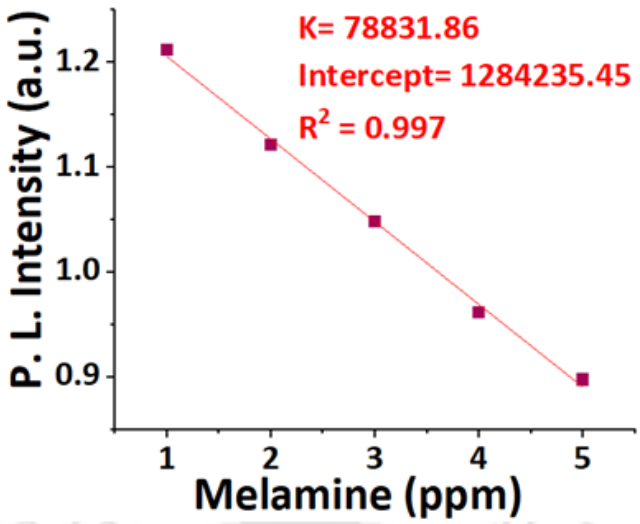

Figure A2.2.3 Emission intensity maxima of **NMICY** nano-cubes vs melamine in milk at different concentrations.

Table A2.1: Comparison Table of Melamine Detection

Sr. No.	Analyte	Analytical probe	Analytical principle	Analytical sample	LOD (limit of detection)	References
1.	*Melamine*	*Organic supramolecular self-assembled Nano-sensors*	*Turn-off fluorescence via a-PET mechanism*	*Raw milk and milk powder*	*0.804 µg/L, 0.101ppm (Milk Powder) 1.46 µg/L, 0.184 ppm (Milk)*	*This work*
2.	Melamine	Nanocomposite composed of Quantum Dots	Mini-emulsion polymerization	Milk samples	0.14 ppm	R. Üzek, E. Sari and A.Denizli, *ChemistrySelect*, 2021, **6**, 2149–2155.
3.	Melamine	Metal-organic framework (MOF)	ratiometric fluorescence	Milk powder sample	90 nM	C. Lin, C. Zhong, Y. Song and L. Wang, *Microchem. J.*, 2021, **162**, 105837.
4.	Melamine	Quantum dot Nanohybrid	Inner filter effect-based ratiometric probe	Raw milk and milk powder	7 nM	J. Wang, X. Liu, L. Huang, J. Jin, C. Jiang, D. Li, H. Wen and J. Hu, *Nanoscale*, 2020, **12**, 4562–4572.

5.	Melamine	DNA functional phosphorescent QDs	phosphorescence	Raw milk	0.0016 mM	Y. Miao, R. Wang, X. Sun and G. Yan, *RSC Adv.*, 2019, **9**, 21147–21154.
6.	Melamine	Ag Nano-particles	colorimetry	Melamine	0.38 mM	A. D. Ardianrama, Y. N. Wijaya, S. H. Hur, H.-C. Woo and M. H. Kim, *J. Colloid Interface Sci.*, 2019, **552**, 485–493.
7.	Melamine	Au Nano-urchin	Au-Nitrogen (of melamine) recognition	Milk samples	18 nM	L. Chen, Y. Huang, T. T. Xing, L. Ge, T. Yang, B. Chen and C. Z. Huang, *J. Mater. Chem. C* 2017, **5**, 7806–7812.
8.	Melamine	Ag Nano-clusters	Hydrogen bonding recognition	Milk samples	4 nM	H. Ren, M. Li, Y. Fu and L. Jin, *J. Mater. Chem. C* 2016, **4**, 6104–6109
10.	Melamine	Fluorescent AIE organic nanoparticles + Au Nanoparticles	Radiometric-Fluorescence turn-on	Raw milk and tap water	680 nM	C. Niu, Q. Liu, Z. Shang, L. Zhao and J. Ouyang, *Nanoscale*, 2015, **7**, 8457–8465.
11.	Melamine	H_2O_2-Au nanoparticles	colorimetry	Raw milk and milk powder	0.4 µM	M. Yin, L. Zhao, Q. Wei and H. Li, *RSC Adv.*, 2015, **5**, 32897–32901
12.	Melamine	Graphene Quantum Dots with Hg^{2+}	Fluorescence "turn-off"	Melamine and Raw milk	0.12 µM (15 ppb)	A. Venkateswararao, K. R. J. Thomas, C.-P. Lee, C.-T. Li and K.-C. Ho, *ACS Appl. Mater. Interfaces*, 2014, **6**, 2528–2539.
13.	Melamine	Zn-Se Quantum dots	Fluorescence turn-on via the Inner filter effect	Raw milk and egg sample	0.11 µg/L	X. Cao, F. Shen, M. Zhang and C. Sun, *Sens. Actuators B Chem.*, 2014, **202**, 1175–1182.
14.	Melamine	Au-Nanofinger chips	Surface enhanced Raman Scattering (SERS)	Water and infant formula	120 ppt (water) 100 ppb (infant formula)	A. Kim, S. J. Barcelo, R. S. Williams and Z. Li, *Anal. Chem.*, 2012, **84**, 9303–9309.
15.	Melamine	Polydiacetylene lysosomes	Calorimetry and fluorescence "turn-on"	Melamine	1 ppm (calorimetry) and 0.5	J. Lee, E. Jeong Jeong and J. Kim, *Chem. Commun.*, 2011, **47**, 358–360.

					ppm (fluor. "turn-on")	
16.	Melamine	Copper salt	Electrochemical response of copper-melamine	Melamine	0.25 ppb	H. Zhu, S. Zhang, M. Li, Y. Shao and Z. Zhu, *Chem. Commun.*, 2010, **46**, 2259–2261.
17.	Melamine	Au Nanoparticles	Hydrogen bonding recognition	Melamine in an aqueous medium	20 nM	H. Zhu, S. Zhang, M. Li, Y. Shao and Z. Zhu, *Chem. Commun.*, 2010, **46**, 2259–2261.
18.	Melamine	Riboflavin stabilized Au Nano-particles	Hydrogen bonding recognition	Melamine	7.5 µM	B. Roy, A. Saha and A. K. Nandi, *Analyst*, 2011, **136**, 67–70.
19.	Melamine	Au Nanoparticles	Hydrogen bonding recognition	Raw milk and milk powder	0.025 ppb	P. Ni, H. Dai, Y. Wang, Y. Sun, Y. Shi, J. Hu and Z. Li, *Biosens. Bioelectron.*, 2014, **60**, 286–291
20.	Melamine	Au nanoparticles	Hydrogen bonding recognition (calorimetric detection)	Raw milk and milk powder	2.5 ppb	K. Ai, Y. Liu and L. Lu, *J. Am. Chem. Soc.*, 2009, **131**, 9496–9497.

Table A2.2: Limit of detection of NMICY in melamine in milk and melamine in milk powder sample.

Sample	S. D. (σ)	K	LOD (limit of detection
Melamine in milk powder	27235.98763	101537.6	0.80471 µg/L or 0.101 ppm
Melamine in milk	38565.23506	78831.86	1.4676 µg/L or 0.184 ppm

HOMO-LUMO comparison NMICY and various analytes used in the sensing:

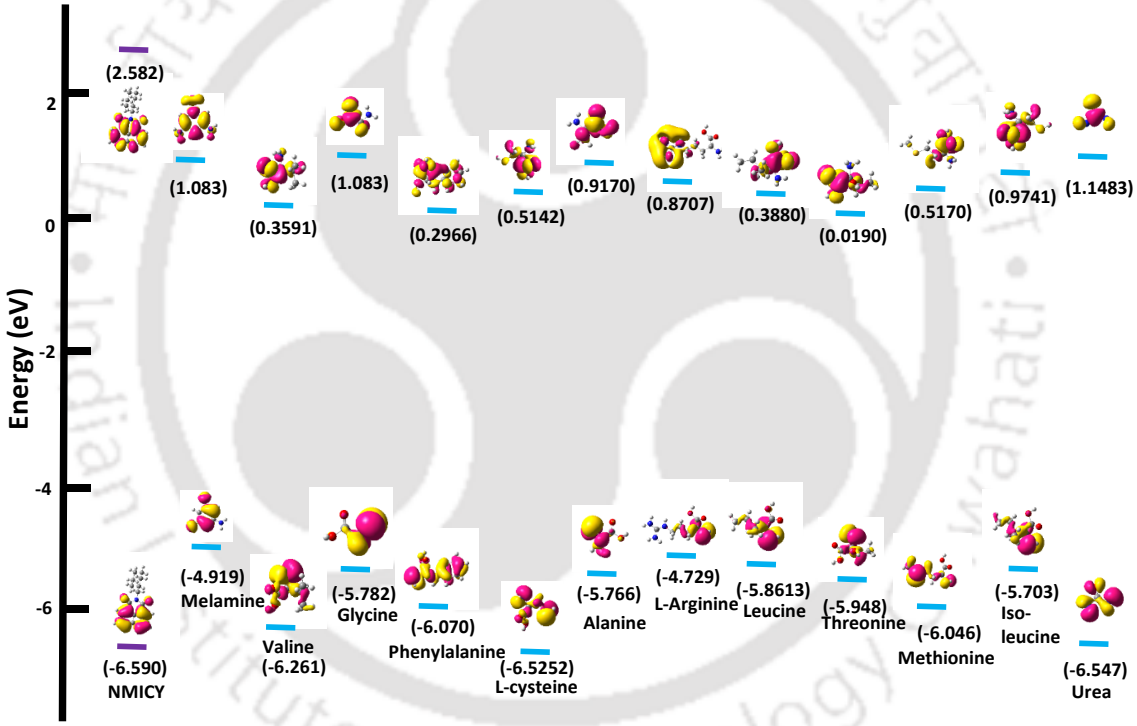

Chapter 3

Mechanistic insights on the impact of long alkyl chain and bromine substitution on the molecular packing and phosphorescence behaviour in naphthalimides

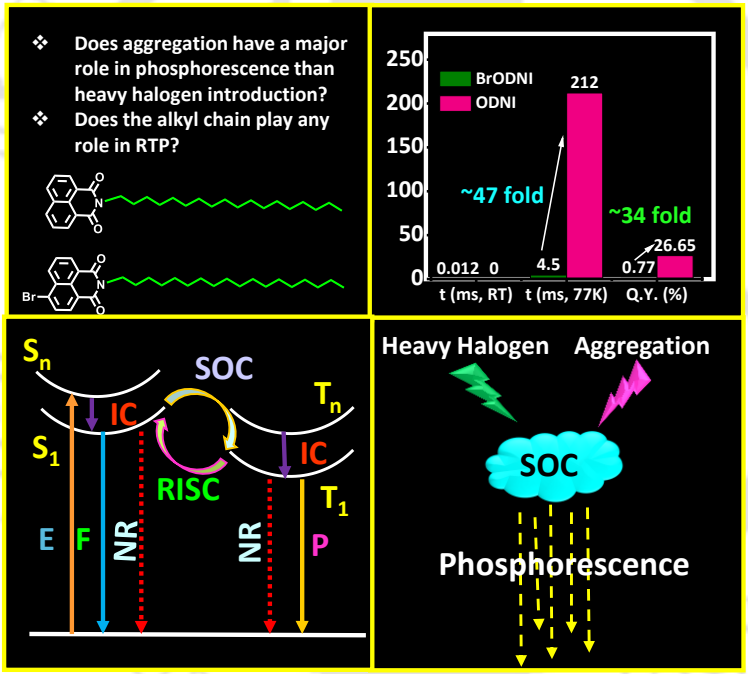

Narang, K.; Garain, S.; Iyer, P. K. Mechanistic insights on the impact of long alkyl chain and bromine substitution on the molecular packing and phosphorescence behavior in naphthalimides *(manuscript communicated)*

.

Abstract

This chapter investigates the realm of organic room-temperature phosphorescence (RTP) materials, identifying them as promising candidates for future applications. The conventional strategy of integrating heavy halogen atoms is acknowledged for its effectiveness in enhancing singlet-to-triplet processes and intersystem crossing, thus influencing the design of RTP materials. Conversely, the modification of alkyl chains has typically been regarded as adjusting the physical properties of luminogens. This study systematically examines the influence of incorporating heavy halogen atoms on RTP and conducts a comparative analysis of the effects of alkyl chain modifications, drawing insights from existing literature. Innovatively designed and synthesized two luminogens, ODNI and BrODNI, subsequently analysing their luminescent properties. Remarkably, at a temperature of 77K, ODNI exhibits a noteworthy phosphorescence lifetime of approximately ~212 milliseconds in the absence of heavy halogen atoms, whereas BrODNI demonstrates a significantly shorter lifetime of about 4.5 milliseconds. The investigation extends to the crystal structure analysis of ODNI, countered with detailed theoretical calculations for both ODNI and BrODNI. These comprehensive analyses aim to elucidate the intricate roles played by alkyl chains and heavy halogen atoms in shaping the luminescent behaviour of the materials. The findings presented in this study provide valuable insights into the ongoing discourse about the design and optimization of organic RTP materials for sustainable energy applications. This chapter contributes to the advancement of knowledge in this field, facilitating the development of innovative materials with enhanced luminescent properties for diverse technological applications.

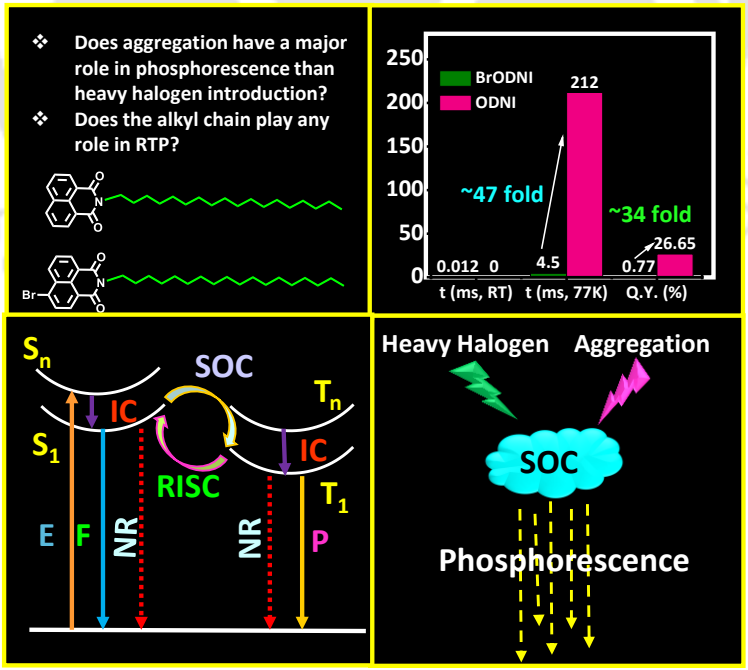

Figure 3.1 Graphical illustration of the presented work. {E = energy, S = singlet, T = triplet, F = fluorescence, P = phosphorescence. IC = internal conversion, NR = non-radiative decay, RISC = reverse inter-system crossing, SOC = spin orbit coupling}.

3.1 Introduction

Room temperature phosphorescence (RTP) in pure organic luminophores has undergone significant advancements in the past two decades, driven by their multifaceted applications in organic electronics,[1] data security,[2] sensing,[3] bio-imaging,[4] and their inherent biocompatibility,[5] and environmental friendliness compared to their inorganic counterparts.[6] Organic RTP materials, devoid of metals, have conventionally faced challenges due to the relatively low spin-orbit coupling (SOC), resulting in fewer spin-forbidden S1 to T1 intersystem crossovers compared to the spin-allowed S_1 to S_0 fluorescence. Additionally, radiative decay from the triplet state (T_1) to the singlet ground state (S_0) is typically slower than non-radiative decay.[7]

Currently, there are two primary strategies to enhance RTP efficiency: first, by accelerating singlet-to-triplet intersystem crossing (ISC) through merging singlets and triplets with various molecular orbital configurations (El-Sayed rule), such as aromatic carbonyls,[8] and second, by lowering the singlet-triplet splitting energy (ΔE_{st}) through intramolecular charge transfer (ICT) interactions,[9] another approach involves leveraging the heavy atom effect.[10] The other route is to prevent non-radiative decay of the excited triplet state, by crystallization,[11] or aggregation,[12] effective intra and intermolecular interactions,[13] proper molecular packing,[14] and functional unit clustering are also key factors in realizing efficient RTP. Many strategies, including CIP,[15] H-aggregation,[16] n-π* transition,[17] co-crystal,[18] and host-guest systems,[19] have been employed to populate triplet state and develop efficient organic RTP materials. The incorporation of heavy halogen atoms into organic π-conjugated systems has been extensively explored to exploit the SOC effect generated by these atoms.[20] Due to the acceleration of the SOC effect generated by heavy atoms, organic luminogens that defy the heavy atom effect remain a challange.[21]

Significant RTP and AIE luminophores have been documented in the naphthalimide core due to the two carbonyl groups having an n-π* transition and the possibility of substitutions.[22] In 2018, Zhang et al. systematically investigated that when the N-substituted naphthalimides (NNIs) are chemically changed with an electron donor, the model systems of NNI can bridge the comparatively wide energy gap between the aromatic ring's ^{1}π-π* and ^{3}π-π* states by generating intramolecular charge transfer (CT) states.[23] In the same year, the first liquid state paintable phosphorescence was reported in the NNI core, and it was suggested that the alkyl chain merely alters the physical state of phosphor molecules and has no discernible impact on phosphorescence.[24] However, recent reports

suggest that molecular packing has a huge impact on the exciton behaviour of luminogens, yet more details and strategies need to be explored.[25]

Recently it was reported that introducing long alkyl chain can reduce the π-π interaction between two NI cores and generate the elusive AIE property.[26] Compared to hexyl chains containing HNI, octadecyl chain constituted ODNI diminished π-π interaction between two NI cores.[26] Herein, heavy halogen bromine was introduced in ODNI molecule to explore the effect of bromine in phosphorescence, and compared it with the reported literature on NI molecules with different alkyl chain lengths with and without bromine substitution.

3.2 Experimental

3.2.1 Materials and measurements: All starting material reagents, i.e. 4-Bromo 1,8-naphthalic anhydride, 1,8-naphthalic anhydride, octadecyl-amine, and solvents (Dimethyl formamide (DMF) and Ethanol), were purchased from Sigma Aldrich (India) and were reagent grade.

NMR Measurements: A Bruker Avance 600 MHz Fourier transformation spectrometer was used to record the Proton NMR spectrum at 600 MHz and the ^{13}C NMR spectrum at 200 MHz. All Proton and ^{13}C spectra solutions were obtained using the residual solvent signal as an internal reference. The chemical shifts are reported in parts per million (ppm) with respect to TMS. The short notations used are s for singlet, d for doublet, t for triplet, q for quartet, and m for multiplet.

Matrix-Assisted Laser Desorption Ionization: MALDI was performed on Bruckner model auto-flex speeds using a MALDI TOF system spectrometer.

Optical Measurements: Solution state studies: Electronic absorption spectra of luminophores in solution state were recorded on a Perkin-Elmer Model Lambda-750 spectrophotometer. PL emission spectra were recorded on the Horiba Fluromax-4 spectrofluorometer. Optical measurements were performed using 4 mm quartz cuvettes at 298 K. **Crystal state studies:** Electronic absorption spectra were recorded on a Perkin Elmer Model Lambda-750 spectrophotometer. Emission spectra were recorded on the FLS1000 spectrometer, an Edinburg instrument.

Lifetime and quantum yield measurements: Fluorescence lifetime experiments were performed on the Horiba Delta Flex time-correlated single photon counting (TCSPC) instrument. A 373 nm Laser diode with a pulse repetition rate of 1 MHz was used as the light source. Phosphorescence lifetime ($\lambda_{exc.}$ = 450 nm and 540 nm) and gated emission were measured on an FLS1000 spectrometer from Edinburgh Instruments equipped with a

micro-flash-lamp (μ F2) set-up. Quantum yield was measured using an integrating sphere in the same instrument.

3.2.2 Theoretical studies:

The ground states of ODNI and BrODNI monomers were optimized using density functional theory (DFT) with B3LYP hybrid functions and 631G+d basis sets in Gaussian 16 software. Excited state calculations for both ODNI and BrODNI were performed with the same parameters in Gaussian 16 software. The spin-orbit matrix element (SOCME) is calculated using ORCA software using B3LYP hybrid functions and 631G+d basis sets.[27,28]

3.2.3 Synthetic procedure

3.2.3a Synthesis of 2-octadecyl-1H-benzo[de]isoquinoline-1,3(2H)-dione (ODNI):

To prepare ODNI, 1, 8 naphthalic anhydride (554.14 mg, 2 mmol) was taken in ethanol (20 mL), and octadecyl amine (592.92 mg, 2.2 mmol) was added in a 50 mL round bottom flask at room temperature. The suspension was refluxed with vigorous stirring for 12 hours. The reaction was monitored thoroughly with TLC. After the completion of the reaction, the reaction mixture was cooled at room temperature for 2 hours. The solvent was filtered out, and the crude material was dried in a vacuum oven at 27°C for 5 hours. The crude was followed by column chromatography separation with 5% chloroform/hexane. By column separation, a green-colored powder was obtained. (950 mg, 95% yield) The powder was further characterized with Proton NMR, ^{13}C NMR, and MALDI characterizations. A similar synthetic procedure was followed to prepare ODNI to obtain a white, shiny powder. (895 mg, 89% yield).[29]

Characterization data of ODNI: Proton NMR: ^{1}H NMR (600 MHz, $CDCl_3$, δ ppm) 8.61 (d, 2H), 8.21 (d,2H), 7.76 (t, 2H), 4.18 (m, 2H), 1.73 (s, 2H), 1.42 (s, 2H), 1.35 (s, 2H), 1.25 (s, 26H), 0.88 (t, 3H)

^{13}C NMR: (150 MHz, $CDCl_3$, ppm) 164.22, 133.82, 131.59, 131.17, 128.17, 126.92, 122.79, 40.53, 29.70, 29.68, 29.67, 29.66, 29.37, 14.13 MALDI: $C_{30}H_{43}NO_2$ molecular weight: 449.68, mass found: 450.0950.

3.2.3b Synthesis of 6-bromo-2-octadecyl-1H-benzo[de]isoquinoline-1,3(2H)-dione, (BrODNI): To prepare BrODNI, 4 Bromo 1, 8 naphthalic anhydride (554.14 mg, 2 mmol) was taken in ethanol (20 mL), and octadecyl amine (592.92 mg, 2.2 mmol) was added in a 50 mL round bottom flask at room temperature. The suspension was refluxed with vigorous stirring for 12 hours. The reaction was monitored thoroughly with TLC. After the

completion of the reaction, the reaction mixture was cooled at room temperature for 2 hours. The solvent was filtered out, and the crude material was dried in a vacuum oven at 27°C for 5 hours. The crude was followed by column chromatography separation with 5% chloroform/hexane. By column separation, a green-coloured powder was obtained. (900 mg, 92% yield) The powder was further characterized with Proton NMR, ^{13}C NMR, and MALDI characterizations. A similar synthetic procedure was followed to prepare ODNI to obtain a white, shiny powder. (840 mg, 93% yield).[29]

Characterization data of BrODNI: Proton NMR: ^{1}H NMR (600 MHz, $CDCl_3$, δ ppm) 8.66 (d, 1H), 8.58 (d, 1H), 8.42 (d, 1H), 8.05 (d, 1H), 7.85 (t, 1H), 4.16 (m, 2H), 2.17 (s, 4H), 1.72 (s, 2H), 1.41 (s, 2H), 1.35 (s, 2H), 1.25 (d,22H), 0.88 (t, 3H)
^{13}C NMR: (150 MHz, $CDCl_3$, ppm) 1.63, 133.23, 132.02, 131.22, 131.10, 130.66, 130.19, 129.05, 128.08, 123.20, 122.34, 40.65, 29.70, 29.67, 29.65, 29.61, 29.37, 14.13 MALDI: $C_{30}H_{42}BrNO_2$ molecular weight: 528.58, mass found: 528.231.

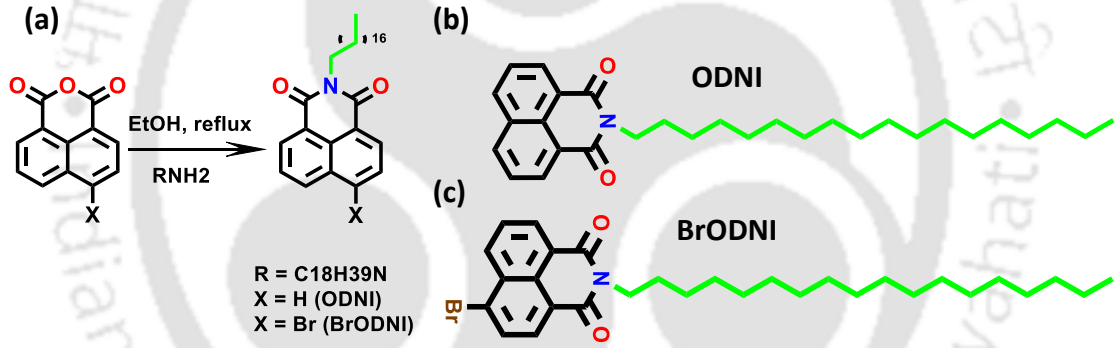

Scheme 3.1: (a) Synthetic Procedure of ODNI and BrODNI (b) Molecular structure of ODNI (c) Molecular structure of BrODNI

3.2.4 FETEM: Field emission transmission electron microscopy (FETEM) images were obtained on the JOEL 2100F field emission transmission electron microscope (FETEM).

3.2.5 Preparation of FETEM samples: A very dilute solution of BrODNI (f_w = 99.9%.) was drop cast over an ultra-cleaned glass substrate and dried at room temperature overnight before analysis.

3.2.6 Preparation of Samples for photophysical studies: 1. Stock solutions of 1 millimolar ODNI and BrODNI were made in HPLC DMF for solution state photophysical studies, Further dilution and procedures were followed according to the experiments

mentioned. 2. To study phosphorescence, crystals, and crystalline solid of ODNI and BrODNI, respectively, were used.

3.3 Result and discussion

3.3.1 Synthesis and photophysical properties of ODNI and BrODNI

ODNI and BrODNI **(Scheme 3.1)** were synthesized following established protocol[29] and characterized via NMR, MALDI, and SC-XRD. ODNI and BrODNI absorbance studies reveal nearly two identical peaks in monomeric (20 µM, 100% DMF) and aggregated state (20 µM, f_w = 99.9%, f_w = water fraction), characteristics of 0-1 and 0-2 transitions for π-π and C=O…π interactions, respectively. **(Figure 3.2a)** BrODNI exhibited a 3 nm redshifted absorbance compared to ODNI. **(Figure 3.3a)** Consistent with prior findings,[26] an increase in chain length from HNI to ODNI enhanced the fluorescence emission and improved the AIE characteristics (DMF/Water). **(Figure 3.2b, 3.2c)** Interestingly, despite possessing an octadecyl chain BrODNI displayed Aggregation-Caused Quenching (ACQ). This phenomenon might be attributed to two reasons: (a) bromine partially quenches the fluorescence due to enhanced spin-orbit coupling (SOC), and (b) steric effect of bromine influences the aggregation pattern. **(Figure 3.3b, 3.3c)**

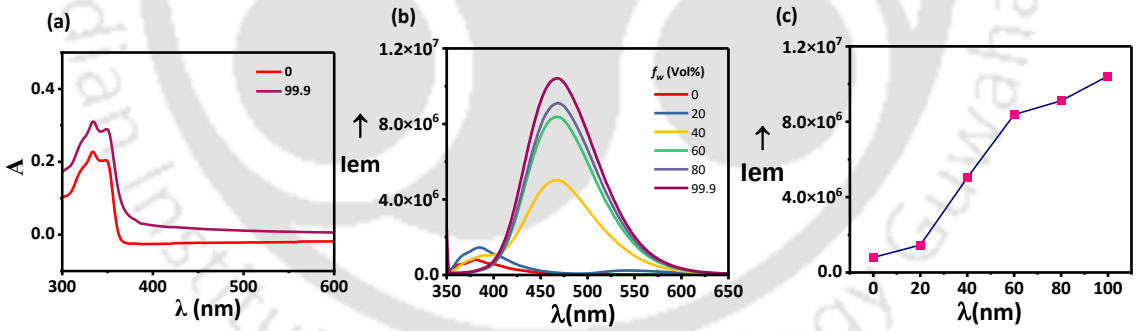

Figure 3.2 (a) Absorbance spectra of ODNI in pure DMF (Conc.-20 µM, 1 mM stock in DMF, f_w = 0%) (b) Fluorescence spectra of ODNI with increasing water fraction. (Conc. 20 µM, 1 mM stock in DMF, f_w = 0% to 99.9%) (f_w = water fraction).

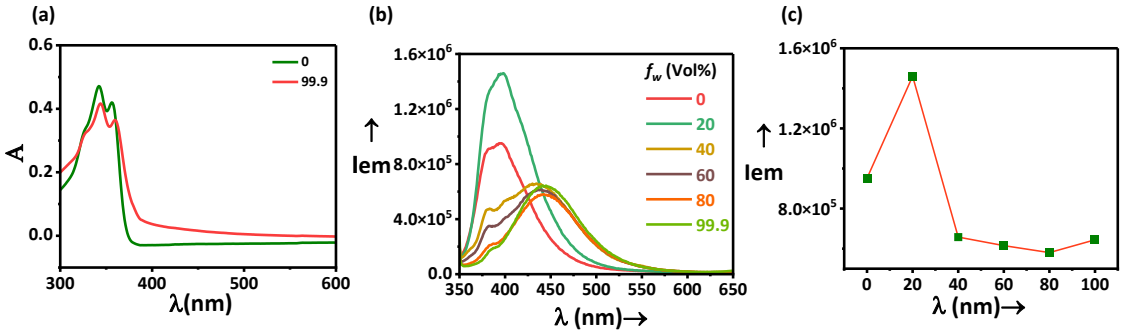

Figure 3.3 (a) Absorbance spectra of BrODNI in pure DMF (Conc. 20 µM, 1 mM stock in DMF, f_w = 0%) (b) Fluorescence spectra of BrODNI with increasing water fraction. (Conc. 20 µM, 1 mM stock in DMF, f_w = 0% to 99.9%) (f_w = water fraction).

3.3.2 Phosphorescence study of ODNI and BrODNI

The photophysical data of ODNI and BrODNI are listed in **Table 3.1 to 3.4** The PL emission maxima (λ_{max}) of ODNI (crystals) at 450 nm, while BrODNI (crystalline solid) had two emission maxima (λ_{max}); i.e., at 395 nm (monomeric emission) **(Figure 3.3, f_w = 0%)** and at 485 nm, which is ~35 nm bathochromic shifted than ODNI (450 nm), attributed to the Intramolecular charge transfer (ICT) feature, which is favourable for RTP properties. Nevertheless, PL emission intensity was significantly lower for BrODNI compared to ODNI. **(Figure 3.4a)** These results clearly depicted that the introduction of bromine changed the aggregation pattern in BrODNI compared to ODNI, resulting in a monomer peak, and the aggregation peak shifted the emission to a longer wavelength, possibly due to Br…Br and[30] Br…C interactions,[31] and ICT that are responsible for bathochromic shift of second emission peak at 485 nm. At room temperature, ODNI did not exhibit phosphorescence emission **(Figure 3.5a, 3.5b)** however, BrODNI showed phosphorescence-gated emission at 540 nm (0.5 ms steady state delay) which is due to triplet state emission with a 12 µs lifetime. **(Figure 3.4b, 3.4c)** The PL spectra of BrODNI depicted fluorescence emission at 395 nm and 490 nm. **(Figure 3.5c, 3.5d)** When phosphorescence measurements were performed at 77 K, both ODNI and BrODNI showed gated emission (0.5 ms delay) with an emission maxima at 540 nm, 590 nm, and 640 nm. **(Figure 3.4c)** The phosphorescence lifetime of BrODNI at 77 K was only ~4.5 ms **(Figure 3.1d)**, while ODNI exhibited emission maxima at 570 nm and 640 nm. **(Figure 3.4c)** Phosphorescence lifetime of ~212 ms was obtained for ODNI at 540 nm. **(Figure 3.4e)** The introduction of bromine in luminogen can enhance SOC and, consequently, intersystem

crossing. Previous studies have reported that intermolecular halogen bonding is beneficial to minimize non-radiative decay. Both factors, with the requisite molecular design, can facilitate phosphorescence. However, ODNI without the heavy atom effect has shown 48 times higher phosphorescence at 77 K, **(Figure 3.4e)** hence, it is crucial to find out the key concept operational here.

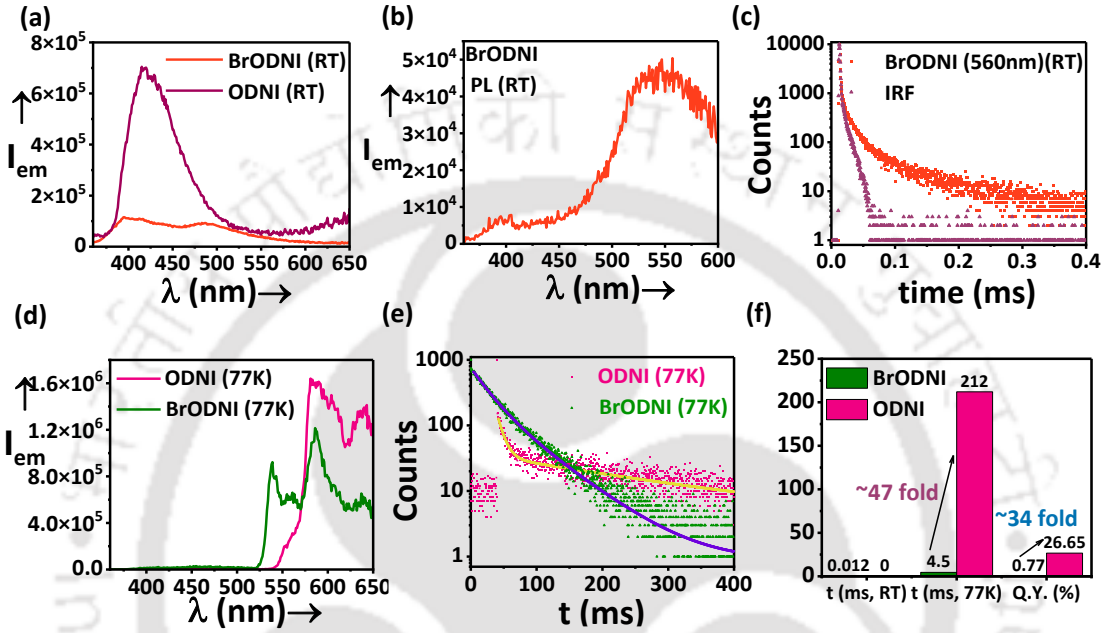

Figure 3.4 Photophysical studies of ODNI (crystals), BrODNI (Crystalline solid). a. Phosphorescence emission of ODNI (crystals), BrODNI (Crystalline solid) at room temperature. b. The steady state phosphorescence emission of BrODNI (Crystals) at RT. c. Phosphorescence lifetime decay profile of BrODNI (Crystals) emission at 540 nm at RT d. Steady state phosphorescence emission (0.5 ms gated delay) of ODNI and BrODNI at 77 K e. Phosphorescence lifetime decay profile of ODNI (crystal) and BrODNI (crystalline solid) at 77 K. f. Statistics of Phosphorescence at RT, 77 K and phosphorescence quantum yield of ODNI (crystal) and BrODNI (crystalline solid) at 77 K.

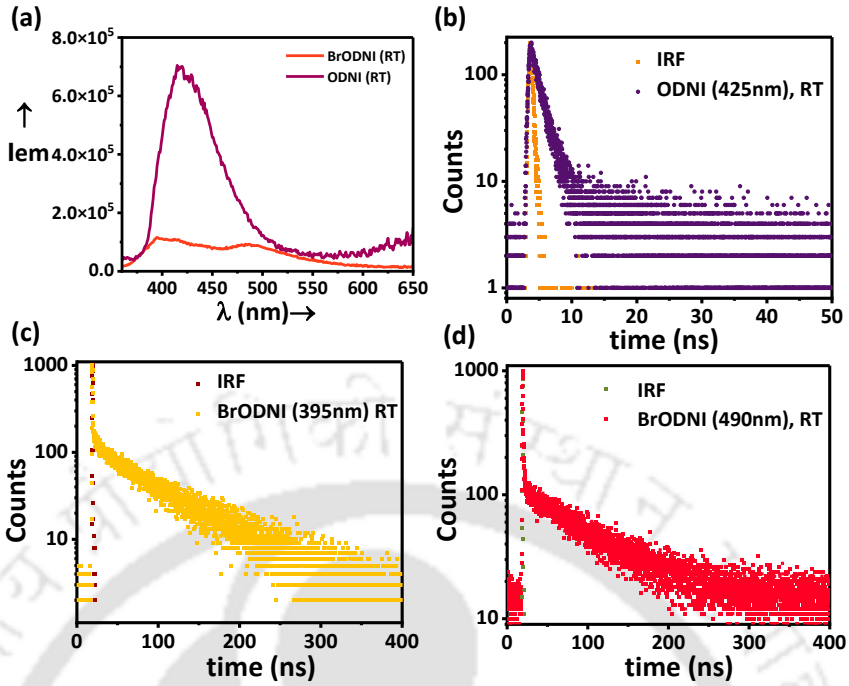

Figure 3.5 (a) PL emission of ODNI (crystals), BrODNI (crystalline solid). (b) Fluorescence lifetime decay profile of ODNI at 425 nm (λ_{ext} = 340 nm). (c) Fluorescence lifetime decay profile of BrODNI at 395 nm (λ_{ext} = 340nm). (d) Fluorescence lifetime decay profile of ODNI at 490 nm (λ_{ext} = 340nm).

Table 3.1 Summary of phosphorescence of BrODNI (crystalline solid) at room temperature.

Luminogen	**Absorbance (99.9% f_w) ($\lambda_{abs.}$)**	**Emission (PL,RT) ($\lambda_{max.}$)**	**Steady state emission ($\lambda_{max.}$) RT**	**Steady state emission ($\lambda_{max.}$) 77 K**	**Phosphorescence lifetime (τ_P, RT)**	**Phosphorescence lifetime (τ_P, 77 K)**	**Phosphorescence Quantum yield (%, 77 K)**
ODNI	340 nm, 352 nm	425 nm	-	600 nm	-	~212 ms	26.65
BrODNI	340 nm, 352 nm	395 nm, 490 nm	560 nm	600 nm	12 µs	~4.5 ms	0.77

Table 3.2 Summary of fluorescence decay of ODNI (crystal) and BrODNI (crystalline solid)

Luminogen	**(*λabs.*)**	**(*λmax.*) Monitered**	**t_1 (ns)**	**t_2 (ns)**	**t_3 (ns)**	**<$t_{avg..}$> (ns)**
ODNI	340 nm	425 nm	1.532	19.657	-	4.364
BrODNI	340 nm	395 nm	0.312 (36.257%)	11.602 (4.842%)	82.638 (58.902%)	49.350
BrODNI	340 nm	490 nm	0.249 (8.783%)	0.983 (4.509%)	81.973 (86.708%)	71.140

Table 3.3 Summary of phosphorescence decay of BrODNI (crystalline solid) at room temperature.

Luminogen	**(*λabs.*)**	**Steady state (*λmax.*) Monitered**	**t_1 (µs)**	**t_2 (µs)**	**t_3 (µs)**	**<$t_{avg..}$> (µs)**
BrODNI	340 nm	560 nm	1.164 (39.47%)	10.57 (48.31%)	52.85 (12.22%)	12.024 µs

Table 3.4 Summary of phosphorescence decay of BrODNI (crystalline solid) at room temperature.

Luminogen	**(*λabs.*)**	**Steady state (*λmax.*) Monitered**	**t_1 (ms)**	**t_2 (ms)**	**t_3 (ms)**	**<$t_{avg..}$> (ms)**
ODNI	340 nm	600 nm	9.201 (11.38%)	238 (88.62%)	-	~212 ms
BrODNI	340 nm	600 nm	2.491 (42.51%)	5.944 (57.49%)	-	~4.5 ms

3.3.3 SC-XRD study of ODNI

A comprehensive analysis of the Single Crystal X-Ray Diffraction (SC-XRD) data for ODNI **(Table 3.5)** were conducted, providing valuable insights of its molecular structure. Inopportunely, attempts to solve the single crystal structure of BrODNI were unsuccessful. Nonetheless, SC-XRD analysis revealed intriguing structural features of ODNI. In a single unit cell of ODNI containing a long alkyl chain, **(Figure 3.6a)** four molecules were arranged in a head-to-head and tail-to-tail manner. Each pair of chromophores exhibited a distance of 4.973 Å, and a bond angle of 69.9°, indicative of H-aggregation (≥ 54.7° = J-aggregation, ≤ = 54.7° = H-aggregation).[32] **(Figure 3.6b, 3.6c, 3.7a, 3.7b)** Strong intermolecular interactions between these H-aggregates of NMI-C11=O….H-C'1 (alkyl chain)-NMI' of 2.603 Å, NMI-C1…C9-NMI' of 3.392 Å were present. **(Figure 3.7c)** Additionally, another set of aggregates with a head-to-tail arrangement displayed intermolecular interactions, including two alkyl-C'6-H'….C7-NMI at 2.831Å. Furthermore, two lateral chromophores exhibited interactions such as two NMI-C11=O…H'-C9'-NMI' at 2.345 Å **(Figure 3.7d)** and two NMI-C1=O….H'-C2'-NMI' at 2.561 Å, along with NMI-C2-H…H'-C2'-NMI' of 2.200 Å. **(Figure 3.7e, 3.7f)** These detailed analyses provide valuable insights into the intermolecular interactions and structural arrangement of ODNI, laying the foundation for further investigations into its optical and photophysical properties.[33,34]

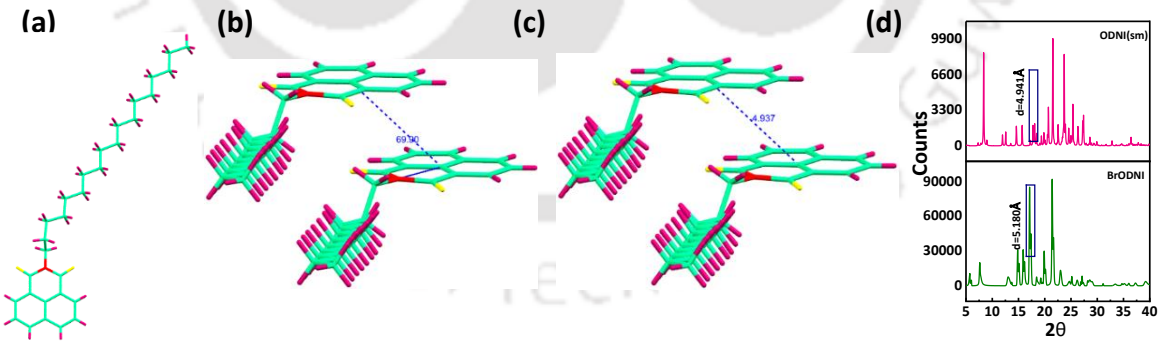

Figure 3.6 SC-XRD study (a) ODNI chromophore (b) H-aggregates of ODNI chromophores. The angle between two chromophores is 69.9°. (c) The distance between two H-Aggregates is 4.937Å. (d) Powder XRD pattern of ODNI (simulated) from single crystal XRD and BrODNI.

Additionally, the SC-XRD analysis unveiled a remarkable degree of molecular packing in ODNI, with the alkyl chain contributing significantly to the overall organization of the

crystal lattice.[35] Notably, the alkyl chain exhibited well defined confirmations, facilitating close packing of the chromophores within the crystal structure.[36] Furthermore, the presence of more intermolecular interactions, including hydrogen bonding and π-π stacking, further stabilize the molecular arrangement and influence the optical properties of ODNI.[37] These findings underscore the intricate interplay between molecular structure, packing motifs and intermolecular interactions in dictating the solid-state behaviour of organic luminogens.[38]

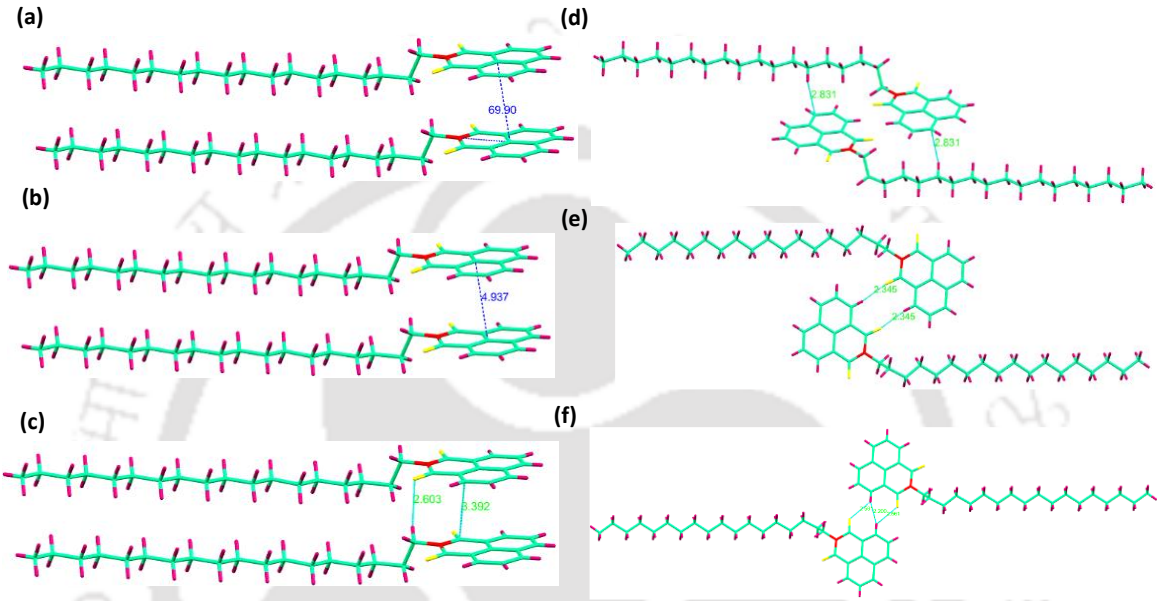

Figure 3.7 SC-XRD study (a) ODNI chromophore H-aggregates of ODNI chromophores. The angle between two chromophores is 69.9°. (b) The distance between two H-Aggregates is 4.937 Å. (c) intermolecular interaction between two aggregates NMI-C11=O….H-C'1(alkyl chain)-NMI' of 2.603 Å, NMI-C1…C9-NMI' of 3.392 Å. (d) two Alkyl-C'6-H'….C7-NMI of 2.831 Å between two aggregates in a head-to-tail orientation. (e) Two sidewise chromophores with two NMI-C11=O…C9'H'-NMI' 0f 2.345 Å (f) Two sidewise chromophores with two NMI-C1=O….H-C2'-NMI' of 2.561 Å, NMI-C2-H…H'-C2'-NMI' of 2.200 Å.

A bathochromic shift is evident in the photophysical analysis of absorbance and photoluminescence (PL) for ODNI, indicating the presence of head-to-head oriented chromophores throughout the molecular assembly, However, these observations do not classify ODNI as pure H-aggregates.[39,40] AIE molecules, constrained in intramolecular rotation (RIR), exhibit myriad intermolecular interactions within their condensed state, impending a strict categorization into H or J- aggregation patterns. Nevertheless, H-

aggregates, renowned for their ability to stabilize triplet excitons and promote ultralong phosphorescence[16] though strong coupling, are facilitated by numerous intermolecular interactions in ODNI, thus enabling efficient intersystem crossing (ISC) cannels and subsequent phosphorescence.[41,42] **(Figure 3.8)**

Furthermore, careful analysis reveals the presence of several non-covalent short-contact interactions involving the lateral molecular core (naphthalimide) of ODNI. Prior studies have indicated that such intermolecular interactions between dimers could amplify the number of ISC channels, consequently augmenting the spin orbit coupling (SOC) of the molecule.[43] To elucidate the aggregation patterns of BrODNI, the powder X-ray diffraction (XRD) patterns of ODNI (sm), simulated from single crystal XRD, is compared with that of the BrODNI crystalline solid.[44] **(Figure 3.6d)** Multiple Braggs Diffraction peaks for ODNI are observed sharply between 18 and 28, 2θ values, whereas for BrODNI, sharp diffractions are noted between 15 and 22, 2θ values.

The comparison of all d-spacing values for ODNI and BrODNI reveals that at 17.93 (2θ value), the d-spacing in ODNI is approximately ~4.94 Å, closely resembling the π-π core distance in the ODNI single crystal. **(Figure 3.6c)** Interestingly, a singular sharp peak for BrODNI is observed at 17.10 (2θ value), corresponding to a d-spacing value of approximately ~5.18 Å. A closer π-π core interaction facilitates efficient exciton transfer from the ground state to the excited state. This elucidates that the introduction of bromine increases the distance between π-π cores in BrODNI compared to ODNI, and the consequent low photoluminescence quantum yield (PLQY) of BrODNI is correlated with augmented SOC.

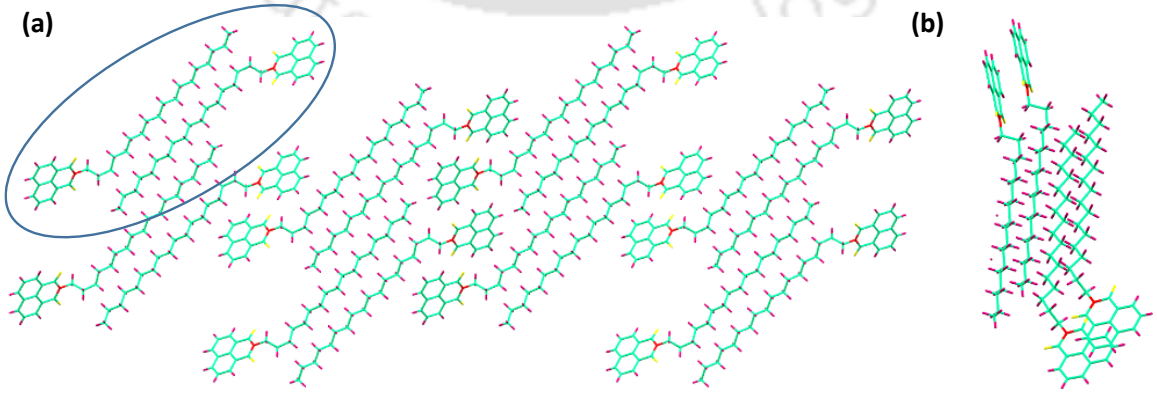

Figure 3.8 (a) molecular packing in ODNI (b) one-unit cell of ODNI

Moreover, the structural analysis of BrODNI reveals a slight alternation in the packing motif compared to ODNI, evident from the distinctive XRD patterns and d-spacing values.[45] The expanded distance between π-π cores induced by bromine substitution suggests a modulation in the molecular arrangement, potentially influencing the excited state dynamics and intermolecular interactions.[46] This deviation in packing arrangement may lead to a perturbation in the electronic coupling between chromophores, thereby affecting the efficiency of exciton migration and subsequent processes.[47,48]

Furthermore, the comparison of XRD patterns highlights subtle variations in crystal lattice parameters between ODNI and BrODNI, indicative of differences in molecular packing and intermolecular interactions. These findings underscore the intricate relationship between molecular structure, packing motifs and photophysical properties, elucidating the role of subtle structural modification in dictating the optoelectronic behavior of organic materials.

3.3.4 Theoretical Analysis of ODNI and BrODNI

To elucidate the influence of bromine substitution and aggregation patterns on the phosphorescence behaviour of ODNI and BrODNI, comprehensive theoretical investigations were conducted using time-dependent density functional theory (TD-DFT) implemented in Gaussian 16, employing the B3LYP functional and 6-31G basis sets. **(Figure 3.9, 3.10)** Remarkably, analysis revealed that both molecules exhibited triplet states (T1 to T4) energetically lower than the singlet state (S1), indicative of significant spin-orbit coupling (SOC) propensity, even in ODNI devoid of heavy halogen atoms.[49,50]

Adhering to El-Sayed's rule, which delineates the influence of ISC on the radiative decay pathways, transitions between similar electronic states (e.g., $^1(\pi\text{-}\pi^*)$ to $^3(\pi\text{-}\pi^*)$ or $^1(\text{n-}\pi^*)$ to $^3(\text{n-}\pi^*)$, typically exhibit diminished phosphorescence efficiency due to lower SOC.[8,51] Interestingly, our investigations unveiled a common feature of (n-π*) transitions in the singlet state (S1) for both ODNI and BrODNI, with the triplet state (T1) primarily originating from $^1(\pi\text{-}\pi^*)$ transitions. This hybrid transition nature favours heightened SOC values (ξ), thereby enhancing the probability of efficient ISC and subsequent phosphorescence emission.

Furthermore, Natural Transition Orbital (NTO) analyses were conducted for ODNI and BrODNI, **(Figure A 3.2.4, A3.2.5)** revealing that singlet states (S_1, S_2) predominantly

involve $^{1}(n\text{-}\pi^*)$ transitions, while triplets primarily consist of $^{3}(\pi\text{-}\pi^*)$ NTOs. This delineation of distinct transition types underscores the favourable conditions for efficient phosphorescence emission. Notably, the computed high probabilities of intersystem crossing from the singlet (S_1) to the triplet (T_1) state **(Figure 3.10)** further affirm the propensity for efficient phosphorescence in both ODNI and BrODNI systems.

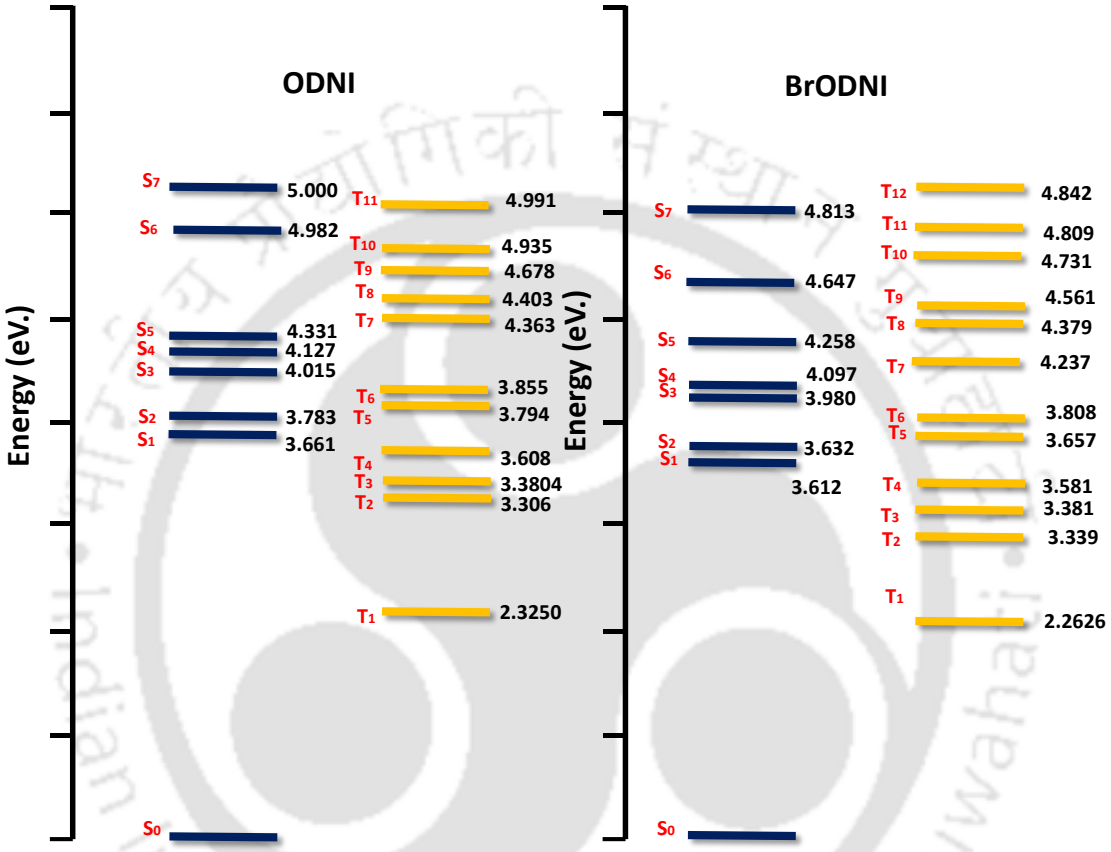

Figure 3.8 Calculated excited state energies of ODNI and BrODNI based on ground state geometry obtained from TD-DFT calculations using B3LYP and 631G (d) sets.

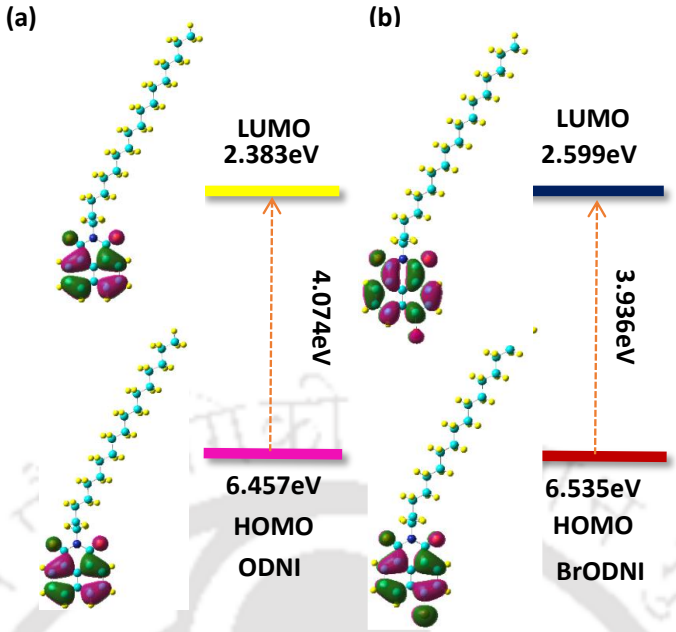

Figure A3.9 HOMO, LUMO molecular orbitals and band gap values of ODNI and BrODNI.

In general, a greater ξ (S_1, T_n) value signifies an increased likelihood of the intersystem crossing (ISC) process from the singlet (S_1) to triplet (T_n) state. To delve into the molecular exciton behavior in ODNI and BrODNI, calculations of the spin-orbit coupling matrix elements (SOCME) were conducting using ORCA **(Figure 3.10a, 3.10b)**. The computed ξ (S_1, T_1) for ODNI is 8.265 cm^{-1}, marginally lower than that of BrODNI, at 10.47 cm^{-1}, suggesting comparable SOC strength between the two. Similarly, the ξ (S_1, T_4) values for ODNI and BrODNI were 5.110 cm^{-1} and 2.525 cm^{-1}, respectively, exhibiting minimal discrepancy. These findings indicate that the aggregation pattern induced by the octadecyl chain exerted more pronounced influence on the SOC and ISC than the presence of heavy halogen atom (bromine).

Moreover, a larger ξ (S_0, T_1) typically promotes nonradiative decay of triplet exciton to the ground state (T_1 to S_0)[52] Remarkably, the computed ξ (S_0, T_1) for ODNI was 0.419 cm^{-1} approximately half that of BrODNI (S_0, T_1) at (1.112 cm^{-1}). Since the T_1 state predominantly contributes to the exciton population in both molecules, a greater proportion of excitons transition from T_1 to S_0 for BrODNI, predominantly via phosphorescence at room temperature. Conversely, although ODNI harbours a higher population of excitons in the T_1 state, they predominantly dissipate through nonradiative pathways. Thus, the

introduction of bromine in BrODNI proves more advantageous in mitigating nonradiative decay than merely augmenting SOC.

Considering the temperature dependent dynamics, the slower approach of exciton population to the ground state at room temperature reduces the nonradiative decay of ODNI, leading to longer phosphorescence lifetime at 77 K. This effect is evidenced by RTP lifetime of ~4.5 ms for BrODNI (77 K) and a notably prolonged ~212 ms for ODNI at 77 K, highlighting the nuanced interplay between molecular structure, temperature, and exciton dynamics in dictating phosphorescence properties.

The variation in SOCME values underscore molecular architecture's role in modulating spin forbidden transitions. ODNI exhibits slightly lower ξ (S_0, T_1), suggesting differences in electronic coupling, while distinct ξ (S_0, T_1) values indicate varying non radiative decay propensities between ODNI and BrODNI due to bromine substitution. Temperature dependent dynamics highlight temperature's influence on radiative decay pathways offering potential for controlled luminescence manipulation. Overall, the analysis provides insights into molecular structure's interplay with spin dynamics and environmental factors in ODNI and BrODNI photophysical properties.

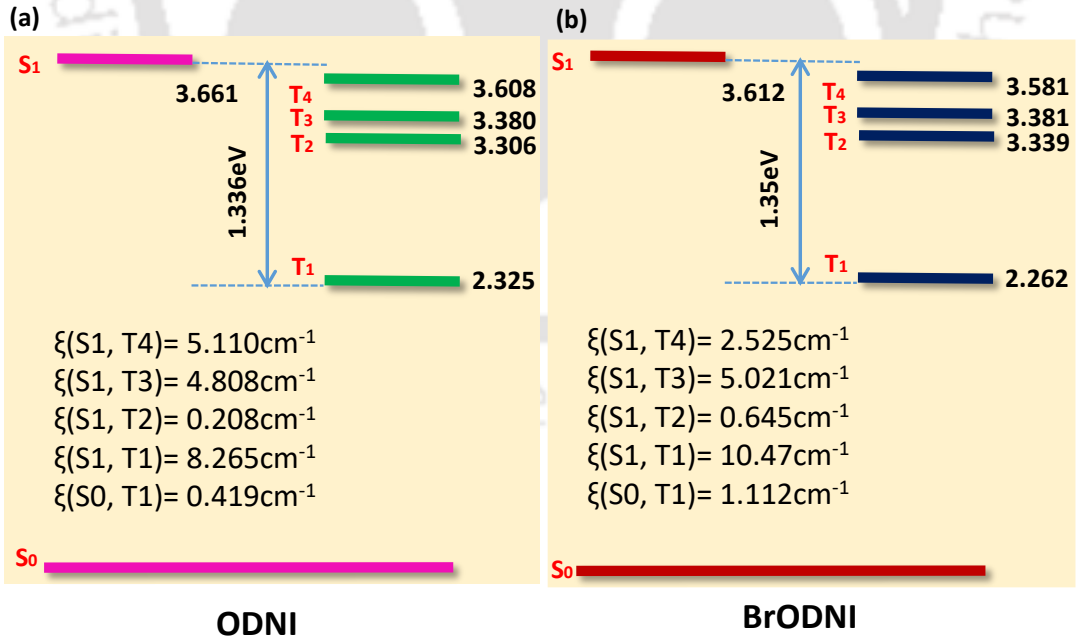

Figure 3.10 Calculated energy level diagram and spin-orbit coupling matrix element (SOCME) of ODNI and BrODNI

3.3.5. Mechanism:

Heavy halogen atoms like bromine can enhance SOC to improve phosphorescence, but excess HAE can be destructive due to the intrinsic competition between phosphorescence lifetime and quantum yield.[53] The synergistic impact of HAE and halogen bonding, which is crucial for balancing τ and ϕ, allows for the modification of RTP characteristics when halogen atoms are added.[54] H-aggregates in ODNI have a strong coupling effect that has stabilized the triplet excitons, and excess non-radiative decay could be minimized at 77 K; thus, ODNI exhibited a 48-fold greater phosphorescence lifetime than BrODNI (~212 ms). The introduction of bromine enhanced the SOC; however, it altered the molecular packing and aggregation pattern (visible in the redshift in absorbance, which indicates J-aggregation), which affected the overall molecular phosphorescence emission.[55] H aggregates have been known to boost phosphorescence and J aggregation for fluorescence enhancement, and HAE introduces competition between τ and ϕ. Interestingly, bromine also did not boost the ϕ in BrODNI either. By directly comparing HAE and H aggregation strategies, it was proven that molecular packing plays greater role in phosphorescence than HAE. Recent studies on polymorphs have demonstrated that variable molecular packings give variable RTP lifetimes, thereby highlighting the significant influence of molecular packing in luminescence.[56] **(Figure 3.11)**

The observed redshift in absorbance, indicating J-aggregation in BrODNI, highlights alternation in intermolecular interactions and electronic coupling, influencing phosphorescence efficiency.[57] Despite SOC enhancement, BrODNI shows no significant improvement in quantum yield ϕ, suggesting complex molecular packing effects comparing HAE and H aggregation strategies emphasizes molecular packing's predominant role in luminescence.[58,59] Recent studies on polymorphs underscore variable RTP lifetimes linked to distinct molecular arrangements, emphasizing the crucial role of molecular packing in luminescence phenomenon. Further investigations are reasonable to unravel the intricate relationship for material design.[60,61]

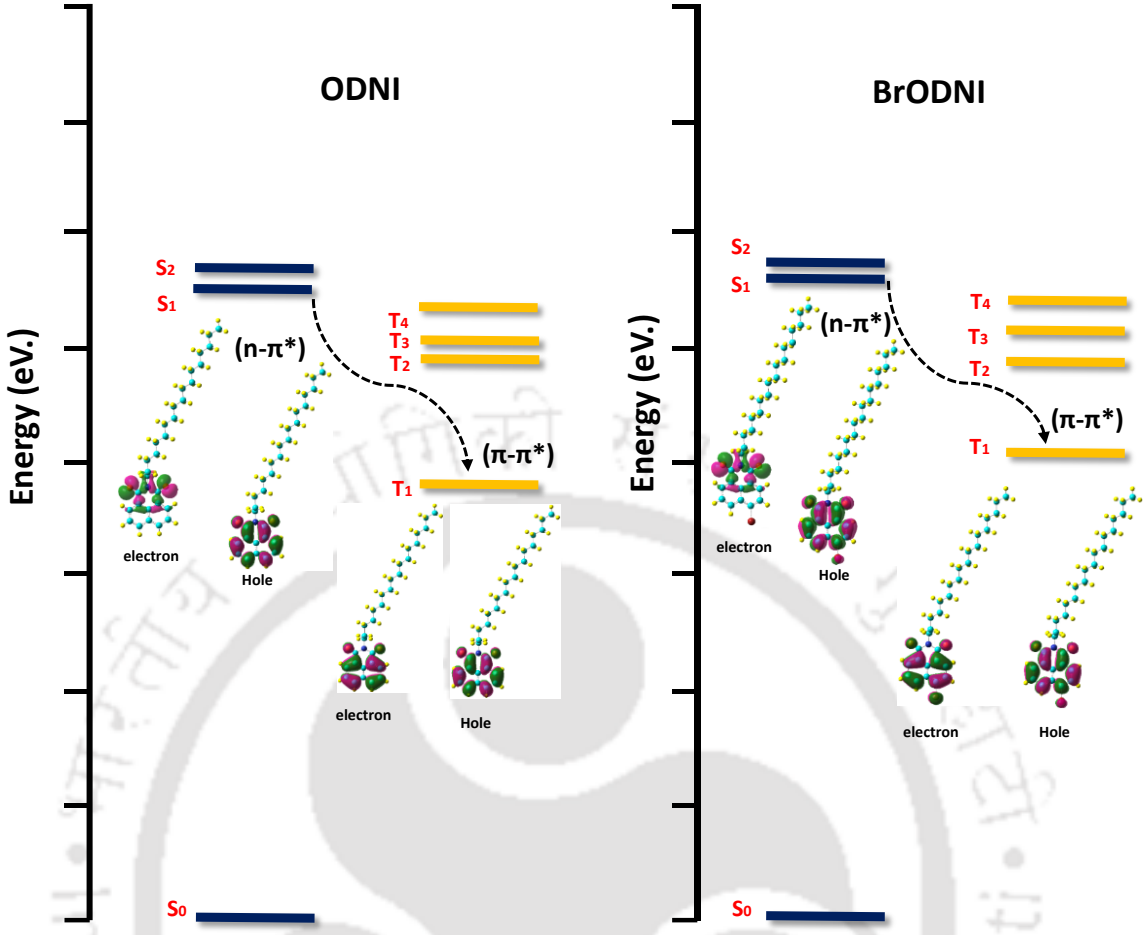

Figure 3.11 Theoretical calculations and Natural transition orbitals of ODNI and BrODNI. S_1 state of ODNI and BrODNI has (n-π*) type of hole electron natural transition orbitals are involved and in T_1 state (π-π*) type of hole electron natural transition orbitals are present.

3.3.6 Role of alkyl chain in organic material phosphorescence

Comparing prior studies on naphthalimide compounds with varying alkyl chain lengths, a distinct correlation emerged between the physical state of the luminophore and the length of the alkyl chain. Specifically, shorter chain luminophores were observed to adopt a crystalline state, while longer chain counterparts exhibited a liquid state, as evidenced by experimental data presented in **(Table A3.6)**

This observation has significant implications, particularly in the context of developing paintable (RTP) systems. Notably, the phosphorescence lifetime and quantum yield (Q. Y.) were found to modulated by altering the length of the alkyl chain. The ability to tailor

these luminescence properties through alkyl chain length variations underscores the pivotal role of molecular packaging in influencing phosphorescence behaviour.[62]

In essence, these findings highlight the importance of molecular structure and organizations in dictating the photophysical properties of luminophores. By elucidating the impact of alkyl chain length on the physical state and luminescence characteristics of naphthalimide compounds, our study contributes valuable insights towards the rational design and optimization of luminescent materials for various applications.[63]

3.4 Conclusion

In conclusion, this chapter has systematically explored the multifaceted influences of long alkyl chains, heavy halogen atom bromine, aggregation, and molecular packing on room-temperature phosphorescence (RTP) in naphthalimide core materials. These findings shed light on the intricate dynamics governing the phosphorescent behaviour of luminogens, challenging certain conventional assumptions in the field. Contrary to expectations, our investigation revealed that the introduction of heavy halogen atoms, particularly bromine, does not universally guarantee the enhancement of phosphorescence lifetime at both room temperature (RT) and 77 K. While bromine, as a heavy halogen atom, enhances spin-orbit coupling, its impact on phosphorescence is nuanced, with molecular packing emerging as a decisive factor in tuning the exciton properties of luminogens. This departure from conventional understanding underscores the complexity of triplet state harvesting rules, necessitating a deeper exploration of the factors governing these processes. Crucially, our research underscores the significant role played by molecular packing in influencing room-temperature phosphorescence. The molecular arrangement within the material proves to be a pivotal determinant, surpassing the influence of heavy halogen atoms in shaping the phosphorescent properties. This insight challenges preconceived notions about the sole efficacy of heavy halogen atom introduction in enhancing phosphorescence, emphasizing the need for a more nuanced understanding of molecular interactions within these materials. Moreover, our study highlights the intricate nature of triplet state harvesting rules, which are revealed to be far more complex than presently known. This complexity necessitates a re-evaluation of existing paradigms and a deeper exploration of the underlying mechanisms governing phosphorescent processes. We advocate for a more comprehensive understanding of the interplay between molecular structure, heavy halogen atoms, and

molecular packing to advance the design and optimization of room-temperature phosphorescent materials for diverse applications. In the realm of alkyl chain modulation, our research emphasizes that tuning the alkyl chain length plays a pivotal role in facilitating room temperature phosphorescence. This role extends beyond merely modulating the physical state of phosphors; rather, it emerges as a critical factor in fine-tuning the excitonic properties, providing an avenue for precise control over phosphorescent behaviour. In essence, our study contributes valuable insights to the evolving landscape of room-temperature phosphorescence research, challenging established notions and paving the way for more sophisticated and targeted design strategies for sustainable energy materials. As the field progresses, a holistic understanding of the interplay between heavy halogen atoms, alkyl chain length, aggregation, and molecular packing will undoubtedly propel the development of innovative and efficient phosphorescent materials for future applications.

References

1. Ostroverkhova, O. Organic Optoelectronic Materials: Mechanisms and Applications. *Chem. Rev.* **2016**, *116* (22), 13279–13412. https://doi.org/10.1021/acs.chemrev.6b00127.
2. Liu, X. W.; Zhao, W.; Wu, Y.; Meng, Z.; He, Z.; Qi, X.; Ren, Y.; Yu, Z.-Q.; Tang, B. Z. Photo-Thermo-Induced Room-Temperature Phosphorescence through Solid-State Molecular Motion. *Nat. Commun.* **2022**, *13* (1), 3887. https://doi.org/10.1038/s41467-022-31481-3.
3. Su, Y.; Phua, S. Z. F.; Li, Y.; Zhou, X.; Jana, D.; Liu, G.; Lim, W. Q.; Ong, W. K.; Yang, C.; Zhao, Y. Ultralong Room Temperature Phosphorescence from Amorphous Organic Materials toward Confidential Information Encryption and Decryption. *Sci. Adv.* **2018**, *4* (5), eaas9732. https://doi.org/10.1126/sciadv.aas9732.
4. Cui, M.; Dai, P.; Ding, J.; Li, M.; Sun, R.; Jiang, X.; Wu, M.; Pang, X.; Liu, M.; Zhao, Q.; Song, B.; He, Y. Millisecond-Range Time-Resolved Bioimaging Enabled through Ultralong Aqueous Phosphorescence Probes. *Angew. Chem. Int. Ed* **2022**, *61* (14), e202200172. https://doi.org/10.1002/anie.202200172.
5. Nicol, A.; Kwok, R. T. K.; Chen, C.; Zhao, W.; Chen, M.; Qu, J.; Tang, B. Z. Ultrafast Delivery of Aggregation-Induced Emission Nanoparticles and Pure Organic Phosphorescent Nanocrystals by Saponin Encapsulation. *J. Am. Chem. Soc.* **2017**, *139* (41), 14792 https://doi.org/10.1021/jacs.7b08710.
6. Kenry; Chen, C.; Liu, B. Enhancing the Performance of Pure Organic Room-Temperature Phosphorescent Luminophores. *Nat. Commun.* **2019**, *10* (1), 2111. https://doi.org/10.1038/s41467-019-10033-2.–14799.
7. Bolton, O.; Lee, K.; Kim, H.-J.; Lin, K. Y.; Kim, J. Activating Efficient Phosphorescence from Purely Organic Materials by Crystal Design. *Nat. Chem.* **2011**, *3* (5), 415–415. https://doi.org/10.1038/nchem.1027.
8. Zhao, W.; He, Z.; Lam, J. W. Y.; Peng, Q.; Ma, H.; Shuai, Z.; Bai, G.; Hao, J.; Tang, B. Z. Rational Molecular Design for Achieving Persistent and Efficient Pure Organic Room-Temperature Phosphorescence. *Chem* **2016**, *1* (4), 592–602. https://doi.org/10.1016/j.chempr.2016.08.010.
9. Li, F.; Guo, S.; Qin, Y.; Shi, Y.; Han, M.; An, Z.; Liu, S.; Zhao, Q.; Huang, W. Achieving Dual Persistent Room-temperature Phosphorescence from Polycyclic

Luminophores via Inter-/Intramolecular Charge Transfer. *Adv. Opt. Mater.* **2019**, *7* (19), 1900511. https://doi.org/10.1002/adom.201900511.

10. Zhou, J.; Stojanović, L.; Berezin, A. A.; Battisti, T.; Gill, A.; Kariuki, B. M.; Bonifazi, D.; Crespo-Otero, R.; Wasielewski, M. R.; Wu, Y.-L. Organic Room-Temperature Phosphorescence from Halogen-Bonded Organic Frameworks: Hidden Electronic Effects in Rigidified Chromophores. *Chem. Sci.* **2020**, *12* (2), 767–773. https://doi.org/10.1039/d0sc04646a.
11. Yuan, W. Z.; Shen, X. Y.; Zhao, H.; Lam, J. W. Y.; Tang, L.; Lu, P.; Wang, C.; Liu, Y.; Wang, Z.; Zheng, Q.; Sun, J. Z.; Ma, Y.; Tang, B. Z. Crystallization-Induced Phosphorescence of Pure Organic Luminogens at Room Temperature. *J. Phys. Chem. C* **2010**, *114* (13), 6090–6099. https://doi.org/10.1021/jp909388y.
12. Wang, T.; Su, X.; Zhang, X.; Nie, X.; Huang, L.; Zhang, X.; Sun, X.; Luo, Y.; Zhang, G. Aggregation-Induced Dual-Phosphorescence from Organic Molecules for Nondoped Light-Emitting Diodes. *Adv. Mater.* **2019**, *31* (51), e1904273. https://doi.org/10.1002/adma.201904273.
13. Zhang, Q.-S.; Wang, S.-C.; Xiong, X.-H.; Fu, P.-Y.; Zhang, X.-D.; Fan, Y.-N.; Pan, M. High-Temperature and Dynamic RGB (Red-Green-Blue) Long-Persistent Luminescence in an Anti-Kasha Organic Compound. *Angew. Chem. Int. Ed* **2022**, *61* (32), e202205556. https://doi.org/10.1002/anie.202205556.
14. Yang, J.; Zhen, X.; Wang, B.; Gao, X.; Ren, Z.; Wang, J.; Xie, Y.; Li, J.; Peng, Q.; Pu, K.; Li, Z. The Influence of the Molecular Packing on the Room Temperature Phosphorescence of Purely Organic Luminogens. *Nat. Commun.* **2018**, *9* (1). https://doi.org/10.1038/s41467-018-03236-6.
15. Shen, Q. J.; Pang, X.; Zhao, X. R.; Gao, H. Y.; Sun, H.-L.; Jin, W. J. Phosphorescent Cocrystals Constructed by 1,4-Diiodotetrafluorobenzene and Polyaromatic Hydrocarbons Based on C–I···π Halogen Bonding and Other Assisting Weak Interactions. *CrystEngComm* **2012**, *14* (15), 5027. https://doi.org/10.1039/c2ce25338k.
16. An, Z.; Zheng, C.; Tao, Y.; Chen, R.; Shi, H.; Chen, T.; Wang, Z.; Li, H.; Deng, R.; Liu, X.; Huang, W. Stabilizing Triplet Excited States for Ultralong Organic Phosphorescence. *Nat. Mater.* **2015**, *14* (7), 685–690. https://doi.org/10.1038/nmat4259.

17. Garain, S.; Wagalgave, S. M.; Kongasseri, A. A.; Garain, B. C.; Ansari, S. N.; Sardar, G.; Kabra, D.; Pati, S. K.; George, S. J. Anion-π-Induced Room Temperature Phosphorescence from Emissive Charge-Transfer States. *J. Am. Chem. Soc.* **2022**, *144* (24), 10854–10861. https://doi.org/10.1021/jacs.2c02678.
18. Zhou, B.; Zhao, Q.; Tang, L.; Yan, D. Tunable Room Temperature Phosphorescence and Energy Transfer in Ratiometric Co-Crystals. *Chem. Commun.* **2020**, *56* (56), 7698–7701. https://doi.org/10.1039/d0cc02730h.
19. Lei, Y.; Yang, J.; Dai, W.; Lan, Y.; Yang, J.; Zheng, X.; Shi, J.; Tong, B.; Cai, Z.; Dong, Y. Efficient and Organic Host-Guest Room-Temperature Phosphorescence: Tunable Triplet-Singlet Crossing and Theoretical Calculations for Molecular Packing. *Chem. Sci.* **2021**, *12* (19), 6518–6525. https://doi.org/10.1039/d1sc01175h.
20. Hamzehpoor, E.; Ruchlin, C.; Tao, Y.; Liu, C.-H.; Titi, H. M.; Perepichka, D. F. Efficient Room-Temperature Phosphorescence of Covalent Organic Frameworks through Covalent Halogen Doping. *Nat. Chem.* **2022**. https://doi.org/10.1038/s41557-022-01070-4.
21. Cai, X.; Xiong, Z.; Zhan, J.; Ping, X.; Zhu, Y.; Zuo, J.; Feng, H.; Qian, Z. Dramatic Emission Enhancement of Aggregation-Induced Emission Luminogens by Dynamic Metal Coordination Bonds and the Anti-Heavy-Atom Effect. *Chem. Commun.* **2022**, *58* (77), 10837–10840. https://doi.org/10.1039/d2cc03809a.
22. Wang, X.; Wang, Z.; Feng, H.; Lin, C.; Shi, H.; An, Z.; Su, Z.-M.; Liang, F.-S. Activating Room-Temperature Phosphorescence of 1,8-Naphthalimide by Doping into Aromatic Dicarboxylic Acids. *Chem. Commun.* **2022**, *58* (22), 3641–3644. https://doi.org/10.1039/d2cc00474g.
23. Chen, X.; Xu, C.; Wang, T.; Zhou, C.; Du, J.; Wang, Z.; Xu, H.; Xie, T.; Bi, G.; Jiang, J.; Zhang, X.; Demas, J. N.; Trindle, C. O.; Luo, Y.; Zhang, G. Versatile Room-Temperature-Phosphorescent Materials Prepared from N-Substituted Naphthalimides: Emission Enhancement and Chemical Conjugation. *Angew. Chem. Int. Ed* **2016**, *55* (34), 9872–9876. https://doi.org/10.1002/anie.201601252.
24. Goudappagouda; Manthanath, A.; Wakchaure, V. C.; Ranjeesh, K. C.; Das, T.; Vanka, K.; Nakanishi, T.; Babu, S. S. Paintable Room-Temperature

Phosphorescent Liquid Formulations of Alkylated Bromonaphthalimide. *Angew. Chem. Int. Ed* **2019**, *58* (8), 2284–2288. https://doi.org/10.1002/anie.201811834.

25. Sasikumar, D.; John, A. T.; Sunny, J.; Hariharan, M. Access to the Triplet Excited States of Organic Chromophores. *Chem. Soc. Rev.* **2020**, *49* (17), 6122–6140. https://doi.org/10.1039/d0cs00484g.
26. Meher, N.; Iyer, P. K. Spontaneously Self-Assembled Naphthalimide Nanosheets: Aggregation-Induced Emission and Unveiling a-PET for Sensitive Detection of Organic Volatile Contaminants in Water. *Angew. Chem. Int. Ed* **2018**, *57* (28), 8488–8492. https://doi.org/10.1002/anie.201802842.
27. Becke, A. D. Density-Functional Thermochemistry. I. The Effect of the Exchange-Only Gradient Correction. *J. Chem. Phys.* **1992**, *96* (3), 2155–2160. https://doi.org/10.1063/1.462066.
28. Frisch, M. J.; Trucks, G. W.; Schlegel, H. B.; Scuseria, G. E.; Robb, M. A.; Cheeseman, J. R.; Scalmani, G.; Barone, V.; Petersson, G. A.; Nakatsuji, H.; Li, X.; Caricato, M.; Marenich, A. V.; Bloino, J.; Janesko, B. G.; Gomperts, R.; Mennucci, B.; Hratchian, H. P.; Ortiz, J. V.; Izmaylov, A. F.; Sonnenberg, J. L.; Williams-Young, D.; Ding, F.; Lipparini, F.; Egidi, F.; Goings, J.; Peng, B.; Petrone, A.; Henderson, T.; Ranasinghe, D.; Zakrzewski, V. G.; Gao, J.; Rega, N.; Zheng, G.; Liang, W.; Hada, M.; Ehara, M.; Toyota, K.; Fukuda, R.; Hasegawa, J.; Ishida, M.; Nakajima, T.; Honda, Y.; Kitao, O.; Nakai, H.; Vreven, T.; Throssell, K.; Montgomery, J. A.; Peralta, J. E.; Ogliaro, F.; Bearpark R Kobayashi, M. J.; Normand, J.; Raghavachari, K.; Rendell, A. P.; Burant, J. C.; Iyengar, S. S.; Tomasi, J.; Cossi, M.; Millam, J. M.; Klene, M.; Adamo, C.; Cammi, R.; Ochterski, J. W.; Martin, R. L.; Morokuma, K.; Farkas, O.; Foresman, J. B.; Fox, D. J. Gaussian 16; Heyd, J. J., Brothers, E. N., Kudin, K. N., Staroverov, V. N., Keith, T. A., Eds.; Gaussian, Inc: Wallingford CT, 2016.
29. Meher, N.; Iyer, P. K. Pendant Chain Engineering to Fine-Tune the Nanomorphologies and Solid State Luminescence of Naphthalimide AIEEgens: Application to Phenolic Nitro-Explosive Detection in Water. *Nanoscale* **2017**, *9* (22), 7674–7685. https://doi.org/10.1039/c7nr02174g.
30. Wang, J.; Wang, C.; Gong, Y.; Liao, Q.; Han, M.; Jiang, T.; Dang, Q.; Li, Y.; Li, Q.; Li, Z. Bromine-Substituted Fluorene: Molecular Structure, Br-Br Interactions, Room-Temperature Phosphorescence, and Tricolor Triboluminescence. *Angew.*

Chem. Int. Ed **2018**, *57* (51), 16821–16826. https://doi.org/10.1002/anie.201811660.

31. Cai, S.; Shi, H.; Tian, D.; Ma, H.; Cheng, Z.; Wu, Q.; Gu, M.; Huang, L.; An, Z.; Peng, Q.; Huang, W. Enhancing Ultralong Organic Phosphorescence by Effective π-Type Halogen Bonding. *Adv. Funct. Mater*. **2018**, *28* (9), 1705045. https://doi.org/10.1002/adfm.201705045.
32. Hestand, N. J.; Spano, F. C. Expanded Theory of H- and J-Molecular Aggregates: The Effects of Vibronic Coupling and Intermolecular Charge Transfer. *Chem. Rev*. **2018**, *118* (15), 7069–7163. https://doi.org/10.1021/acs.chemrev.7b00581.
33. Wen, Y.; Liu, H.; Zhang, S.; Gao, Y.; Yan, Y.; Yang, B. One-Dimensional π–π Stacking Induces Highly Efficient Pure Organic Room-Temperature Phosphorescence and Ternary-Emission Single-Molecule White Light. *J. Mater. Chem. C Mater*. **2019**, *7* (40), 12502–12508. https://doi.org/10.1039/c9tc04580e.
34. Wen, Y.; Liu, H.; Zhang, S.; Gao, Y.; Yan, Y.; Yang, B. One-Dimensional π–π Stacking Induces Highly Efficient Pure Organic Room-Temperature Phosphorescence and Ternary-Emission Single-Molecule White Light. *J. Mater. Chem. C* **2019**, *7* (40), 12502–12508. https://doi.org/10.1039/c9tc04580e.
35. Yang, J.; Zhen, X.; Wang, B.; Gao, X.; Ren, Z.; Wang, J.; Xie, Y.; Li, J.; Peng, Q.; Pu, K.; Li, Z. The Influence of the Molecular Packing on the Room Temperature Phosphorescence of Purely Organic Luminogens. *Nat. Commun.* **2018**, *9* (1). https://doi.org/10.1038/s41467-018-03236-6.
36. Xie, Y.; Ge, Y.; Peng, Q.; Li, C.; Li, Q.; Li, Z. How the Molecular Packing Affects the Room Temperature Phosphorescence in Pure Organic Compounds: Ingenious Molecular Design, Detailed Crystal Analysis, and Rational Theoretical Calculations. *Adv. Mater.* **2017**, *29* (17). https://doi.org/10.1002/adma.201606829.
37. Lei, Y.; Yang, J.; Dai, W.; Lan, Y.; Yang, J.; Zheng, X.; Shi, J.; Tong, B.; Cai, Z.; Dong, Y. Efficient and Organic Host–Guest Room-Temperature Phosphorescence: Tunable Triplet–Singlet Crossing and Theoretical Calculations for Molecular Packing. *Chem. Sci.* **2021**, *12* (19), 6518–6525. https://doi.org/10.1039/d1sc01175h.
38. Yang, J.; Gao, X.; Xie, Z.; Gong, Y.; Fang, M.; Peng, Q.; Chi, Z.; Li, Z. Elucidating the Excited State of Mechanoluminescence in Organic Luminogens

with Room-temperature Phosphorescence. *Angew. Chem. Int. Ed* **2017**, *129* (48), 15501–15505. https://doi.org/10.1002/ange.201708119.

39. Lucenti, E.; Forni, A.; Botta, C.; Carlucci, L.; Giannini, C.; Marinotto, D.; Previtali, A.; Righetto, S.; Cariati, E. H-Aggregates Granting Crystallization-Induced Emissive Behavior and Ultralong Phosphorescence from a Pure Organic Molecule. *J. Phys. Chem. Lett.* **2017**, *8* (8), 1894–1898. https://doi.org/10.1021/acs.jpclett.7b00503.
40. Kenry; Chen, C.; Liu, B. Enhancing the Performance of Pure Organic Room-Temperature Phosphorescent Luminophores. *Nat. Commun.* **2019**, *10* (1). https://doi.org/10.1038/s41467-019-10033-2.
41. Ma, H.; Peng, Q.; An, Z.; Huang, W.; Shuai, Z. Efficient and Long-Lived Room-Temperature Organic Phosphorescence: Theoretical Descriptors for Molecular Designs. *J. Am. Chem. Soc.* **2019**, *141* (2), 1010–1015. https://doi.org/10.1021/jacs.8b11224.
42. Guo, J.; Yang, C.; Zhao, Y. Long-Lived Organic Room-Temperature Phosphorescence from Amorphous Polymer Systems. *Acc. Chem. Res.* **2022**, *55* (8), 1160–1170. https://doi.org/10.1021/acs.accounts.2c00038.
43. Garain, S.; Kuila, S.; Garain, B. C.; Kataria, M.; Borah, A.; Pati, S. K.; George, S. J. Arylene Diimide Phosphors: Aggregation Modulated Twin Room Temperature Phosphorescence from Pyromellitic Diimides. *Angew. Chem. Int. Ed* **2021**, *60* (22), 12323–12327. https://doi.org/10.1002/anie.202101538.
44. Tao, Y.; Chen, R.; Li, H.; Yuan, J.; Wan, Y.; Jiang, H.; Chen, C.; Si, Y.; Zheng, C.; Yang, B.; Xing, G.; Huang, W. Resonance-activated Spin-flipping for Efficient Organic Ultralong Room-temperature Phosphorescence. *Adv. Mater.* **2018**, *30* (44). https://doi.org/10.1002/adma.201803856.
45. Li, Q.; Tang, Y.; Hu, W.; Li, Z. Fluorescence of Nonaromatic Organic Systems and Room Temperature Phosphorescence of Organic Luminogens: The Intrinsic Principle and Recent Progress. *Small* **2018**, *14* (38). https://doi.org/10.1002/smll.201801560.
46. Ren, J.; Wang, Y.; Tian, Y.; Liu, Z.; Xiao, X.; Yang, J.; Fang, M.; Li, Z. Force-induced Turn-on Persistent Room-temperature Phosphorescence in Purely Organic Luminogen. *Angew. Chem. Int. Ed* **2021**, *133* (22), 12443–12448. https://doi.org/10.1002/ange.202101994.

47. Ma, X.; Wang, J.; Tian, H. Assembling-Induced Emission: An Efficient Approach for Amorphous Metal-Free Organic Emitting Materials with Room-Temperature Phosphorescence. *Acc. Chem. Res.* **2019**, *52* (3), 738–748. https://doi.org/10.1021/acs.accounts.8b00620.
48. He, Z.; Gao, H.; Zhang, S.; Zheng, S.; Wang, Y.; Zhao, Z.; Ding, D.; Yang, B.; Zhang, Y.; Yuan, W. Z. Achieving Persistent, Efficient, and Robust Room-temperature Phosphorescence from Pure Organics for Versatile Applications. *Adv. Mater.* **2019**, *31* (18). https://doi.org/10.1002/adma.201807222.
49. Li, J.; Li, X.; Wang, G.; Wang, X.; Wu, M.; Liu, J.; Zhang, K. A Direct Observation of Up-Converted Room-Temperature Phosphorescence in an Anti-Kasha Dopant-Matrix System. *Nat. Commun.* **2023**, *14* (1). https://doi.org/10.1038/s41467-023-37662-y.
50. Jovaišaitė, J.; Kirschner, S.; Raišys, S.; Kreiza, G.; Baronas, P.; Juršėnas, S.; Wagner, M. Diboraanthracene-doped Polymer Systems for Colour-tuneable Room-temperature Organic Afterglow. *Angew. Chem. Int. Ed* **2023**, *62* (4). https://doi.org/10.1002/anie.202215071.
51. Wu, B.; Su, H.; Cheng, A.; Zhang, X.; Wang, T.; Zhang, G. The El-Sayed's Rule Analogy Enables Long-Lived Room Temperature Phosphorescence in Twisted Biphenyls. *Cell Rep. Phys. Sci.* **2023**, *4* (2), 101245. https://doi.org/10.1016/j.xcrp.2022.101245.
52. Li, Q.; Li, Z. Molecular Packing: Another Key Point for the Performance of Organic and Polymeric Optoelectronic Materials. *Acc. Chem. Res.* **2020**, *53* (4), 962–973. https://doi.org/10.1021/acs.accounts.0c00060.
53. Lai, L.; Fang, B.; Fan, M.; Cheng, W.; Yin, M. Modulating Room-Temperature Phosphorescence through the Synergistic Effect of Heavy-Atom Effect and Halogen Bonding. *J. Phys. Chem. C Nanomater. Interfaces* **2021**, *125* (29), 16350–16357. https://doi.org/10.1021/acs.jpcc.1c04989.
54. Xu, L.; Zhou, K.; Ma, H.; Lv, A.; Pei, D.; Li, G.; Zhang, Y.; An, Z.; Li, A.; He, G. Ultralong Organic Phosphorescent Nanocrystals with Long-Lived Triplet Excited States for Afterglow Imaging and Photodynamic Therapy. *ACS Appl. Mater. Interfaces* **2020**, *12* (16), 18385–18394. https://doi.org/10.1021/acsami.0c04005.

55. Li, B.; Gong, Y.; Wang, L.; Lin, H.; Li, Q.; Guo, F.; Li, Z.; Peng, Q.; Shuai, Z.; Zhao, L.; Zhang, Y. Highly Efficient Organic Room-Temperature Phosphorescent Luminophores through Tuning Triplet States and Spin–Orbit Coupling with Incorporation of a Secondary Group. *J. Phys. Chem. Lett.* **2019**, *10* (22), 7141–7147. https://doi.org/10.1021/acs.jpclett.9b02885.

56. Barman, D.; Annadhasan, M.; Chandrasekar, R.; Iyer, P. K. Hot-Exciton Harvesting via through-Space Single-Molecule Based White-Light Emission and Optical Waveguides. *Chem. Sci.* **2022**, *13* (31), 9004–9015. https://doi.org/10.1039/d2sc02172b.

57. Shao, W.; Hao, J.; Jiang, H.; Zimmerman, P. M.; Kim, J. Metal-free Organic Triplet Emitters with on–off Switchable Excited State Intramolecular Proton Transfer. *Adv. Funct. Mater.* **2022**, *32* (29). https://doi.org/10.1002/adfm.202201256.

58. Farias, G.; Salla, C. A. M.; Aydemir, M.; Sturm, L.; Dechambenoit, P.; Durola, F.; de Souza, B.; Bock, H.; Monkman, A. P.; Bechtold, I. H. Halogenation of a Twisted Non-Polar π-System as a Tool to Modulate Phosphorescence at Room Temperature. *Chem. Sci.* **2021**, *12* (45), 15116–15127. https://doi.org/10.1039/d1sc04936d.

59. Farias, G.; Salla, C. A. M.; Aydemir, M.; Sturm, L.; Dechambenoit, P.; Durola, F.; de Souza, B.; Bock, H.; Monkman, A. P.; Bechtold, I. H. Halogenation of a Twisted Non-Polar π-System as a Tool to Modulate Phosphorescence at Room Temperature. *Chem. Sci.* **2021**, *12* (45), 15116–15127. https://doi.org/10.1039/d1sc04936d.

60. Zhao, W.; Cheung, T. S.; Jiang, N.; Huang, W.; Lam, J. W. Y.; Zhang, X.; He, Z.; Tang, B. Z. Boosting the Efficiency of Organic Persistent Room-Temperature Phosphorescence by Intramolecular Triplet-Triplet Energy Transfer. *Nat. Commun.* **2019**, *10* (1), 1595. https://doi.org/10.1038/s41467-019-09561-8.

61. Zhang, X.; Du, L.; Zhao, W.; Zhao, Z.; Xiong, Y.; He, X.; Gao, P. F.; Alam, P.; Wang, C.; Li, Z.; Leng, J.; Liu, J.; Zhou, C.; Lam, J. W. Y.; Phillips, D. L.; Zhang, G.; Tang, B. Z. Ultralong UV/Mechano-Excited Room Temperature Phosphorescence from Purely Organic Cluster Excitons. *Nat. Commun.* **2019**, *10* (1). https://doi.org/10.1038/s41467-019-13048-x.

62. Tu, L.; Che, W.; Li, S.; Li, X.; Xie, Y.; Li, Z. Alkyl Chain Regulation: Distinctive Odd–Even Effects of Mechano-Luminescence and Room-Temperature Phosphorescence in Alkyl Substituted Carbazole Amide Derivatives. *J. Mater. Chem. C Mater. Opt. Electron. Devices* **2021**, *9* (36), 12124–12132. https://doi.org/10.1039/d1tc02742e.

63. Yang, J.; Gao, H.; Wang, Y.; Yu, Y.; Gong, Y.; Fang, M.; Ding, D.; Hu, W.; Tang, B. Z.; Li, Z. The Odd–Even Effect of Alkyl Chain in Organic Room Temperature Phosphorescence Luminogens and the Corresponding in Vivo Imaging. *Mater. Chem. Front.* **2019**, *3* (7), 1391–1397. https://doi.org/10.1039/c9qm00108e.

Appendix

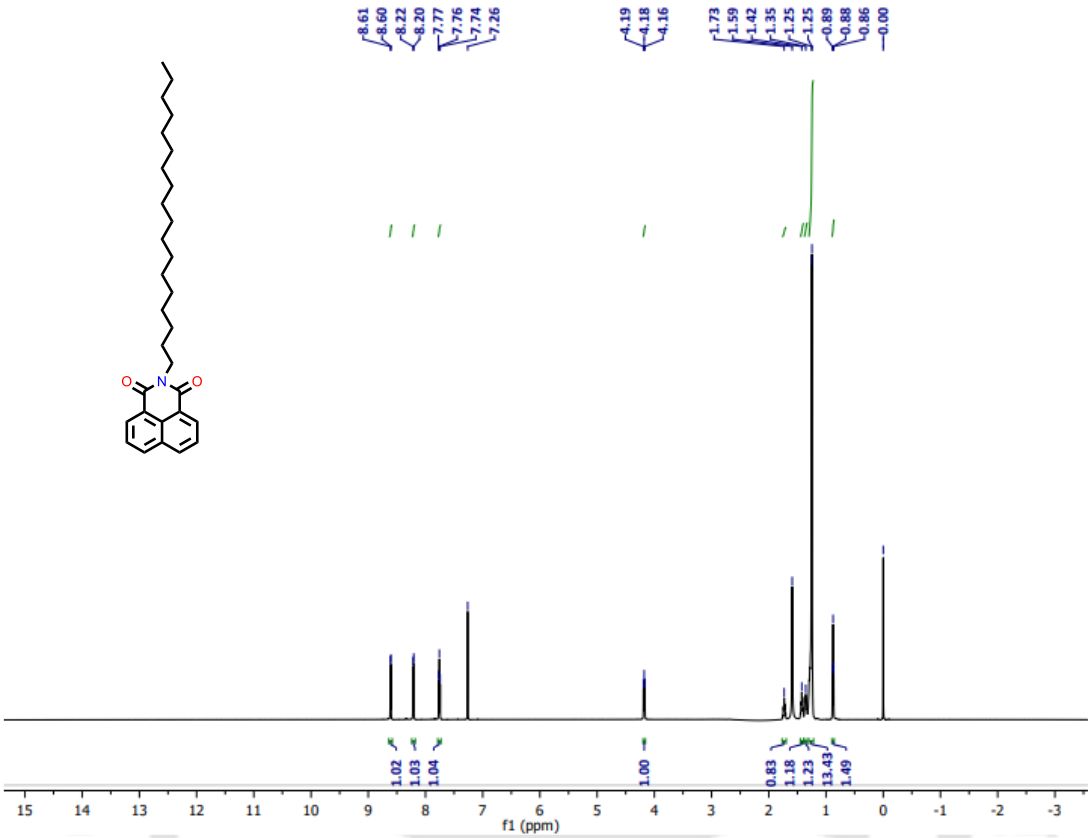

Figure A3.1.1 ^{1}H NMR spectra of ODNI.

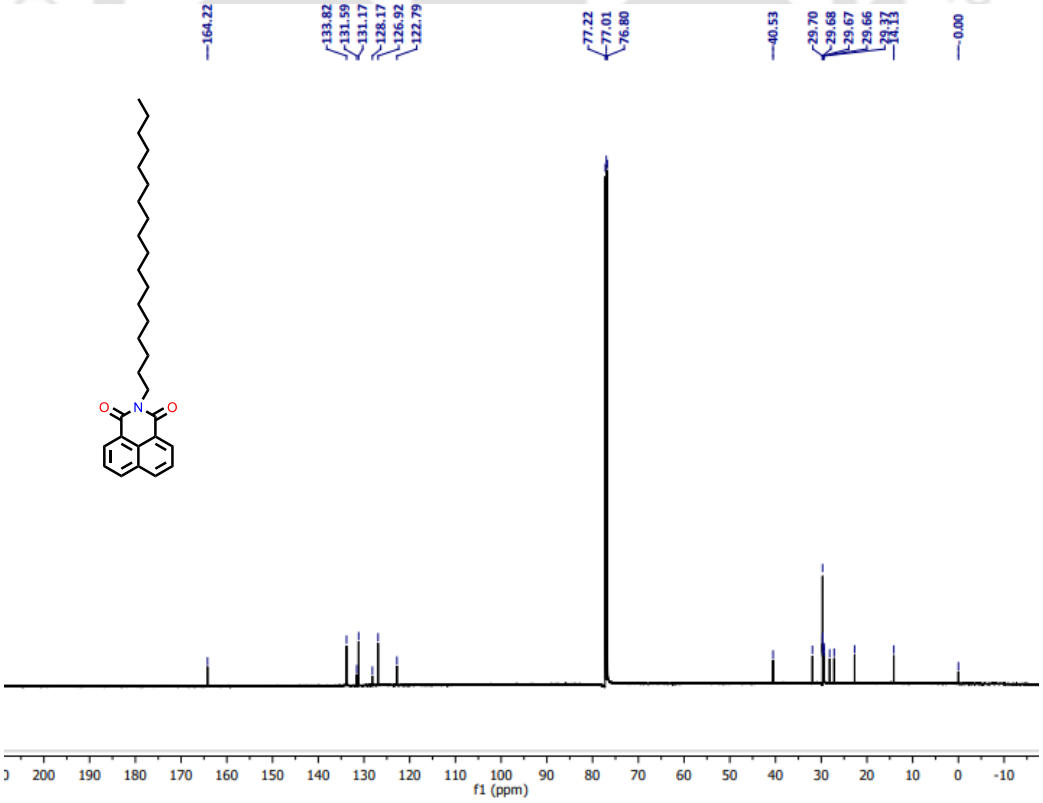

Figure A3.1.2 ^{13}C NMR spectra of ODNI.

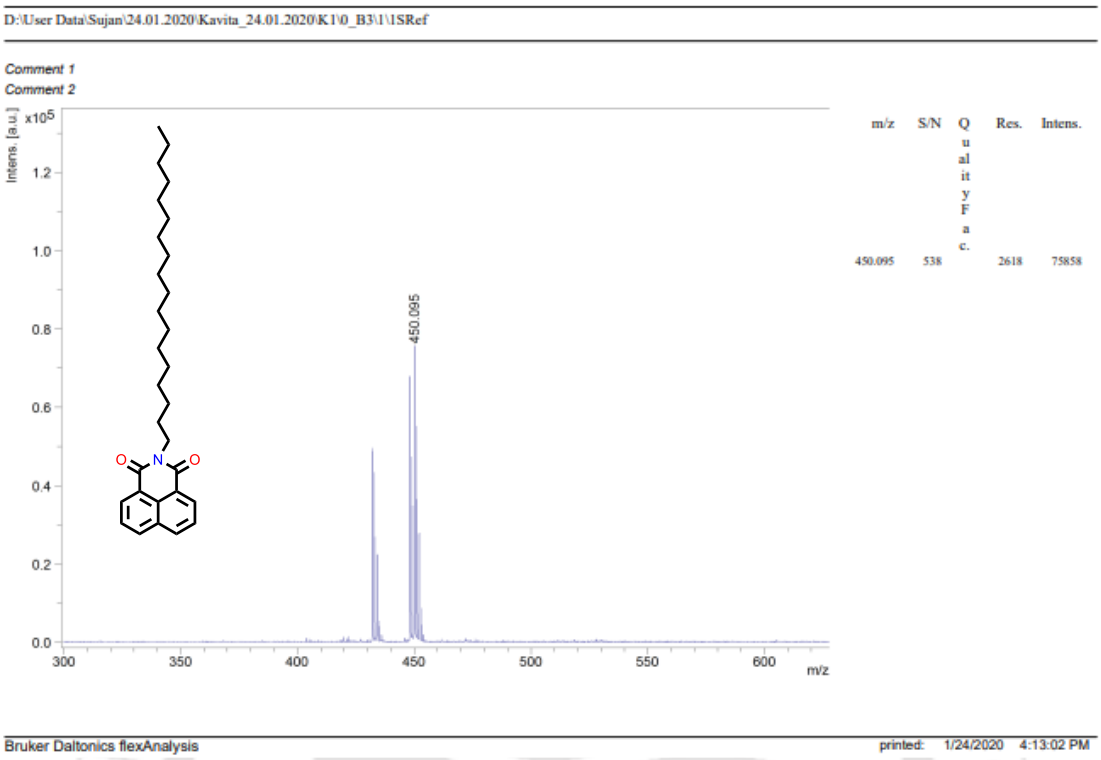

Figure A3.1.3 MALDI spectra of ODNI.

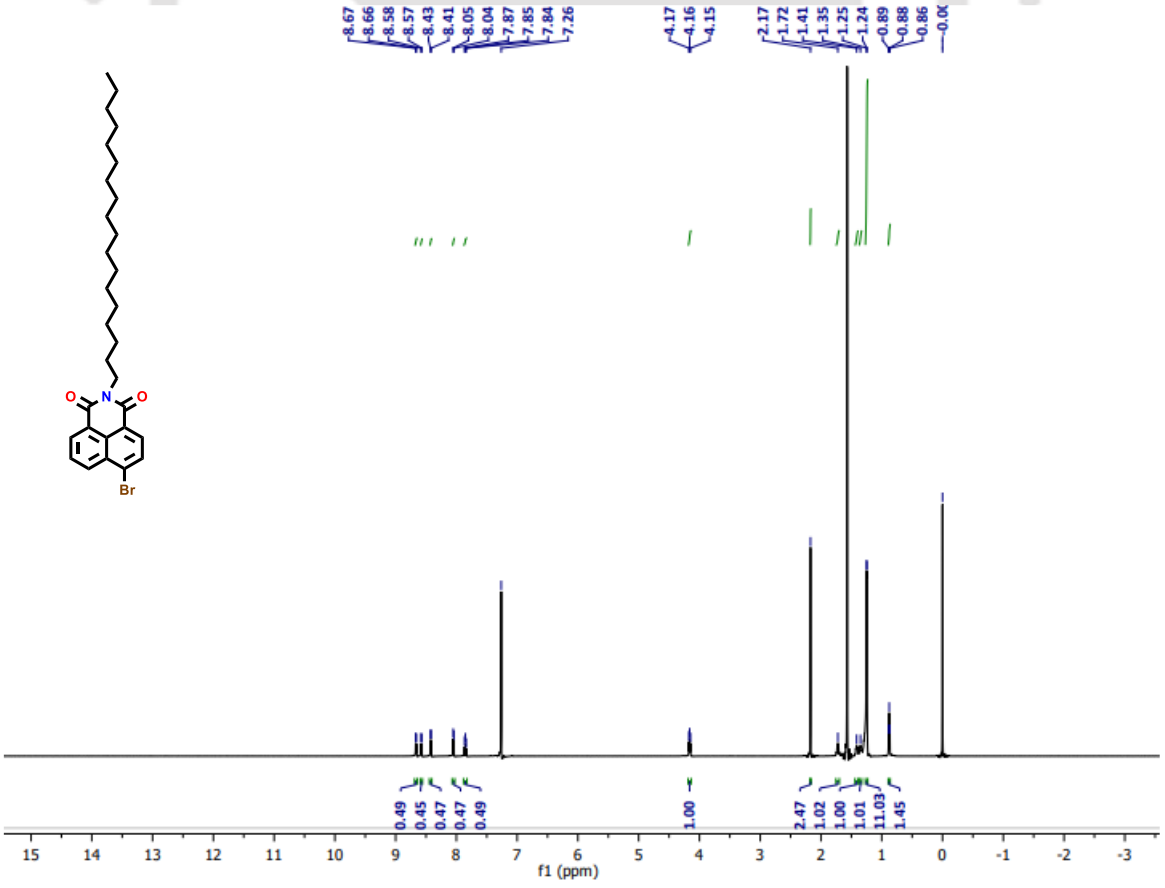

Figure A3.1.4 ^{1}H NMR spectrum of BrODNI.

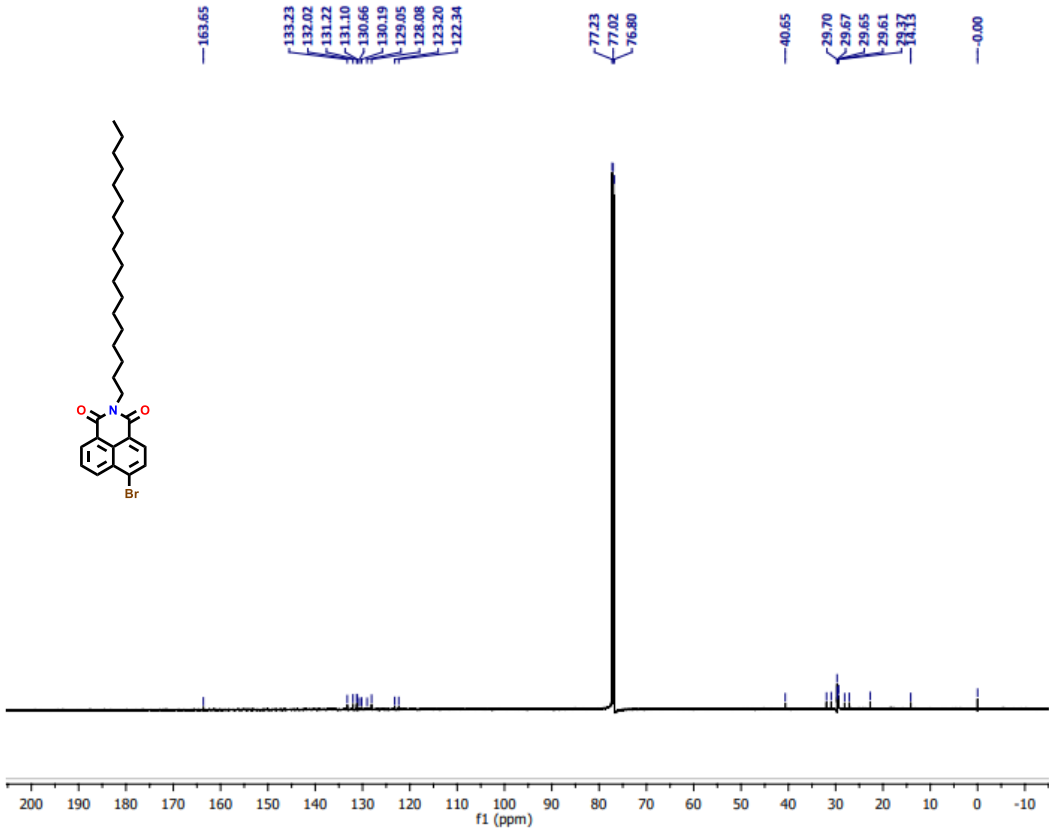

Figure A3.1.5 ^{13}C NMR spectra of BrODNI.

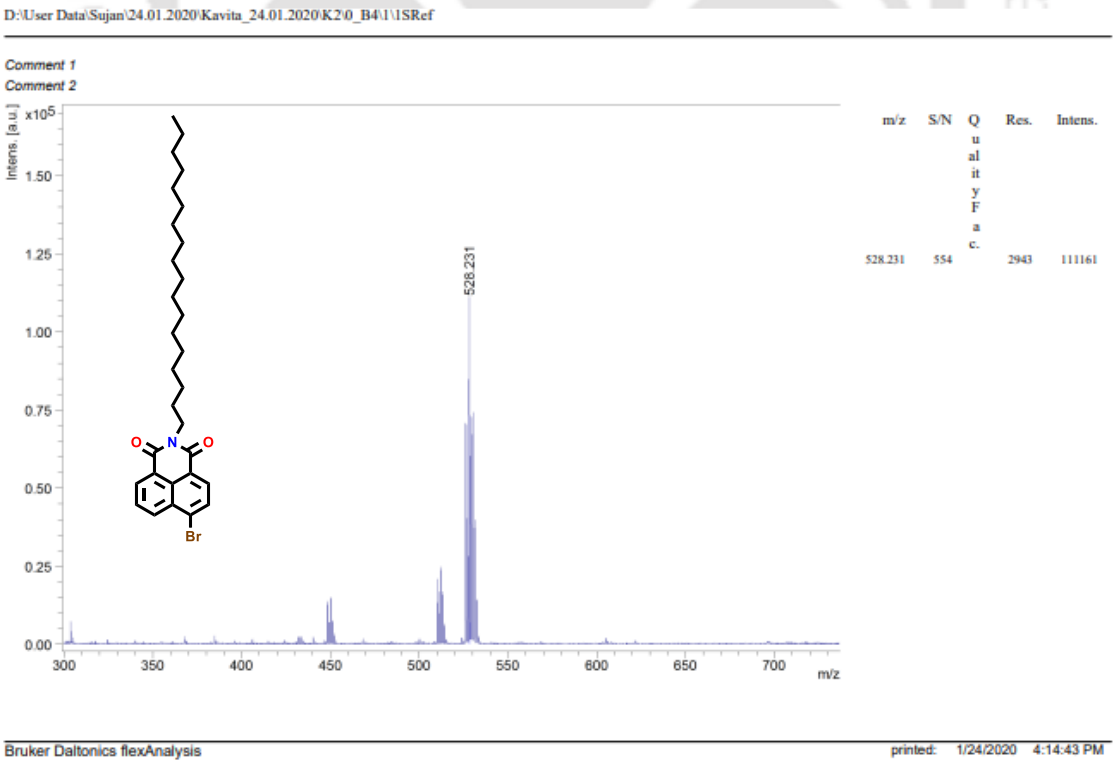

Figure A3.1.6 MALDI spectra of BrODNI.

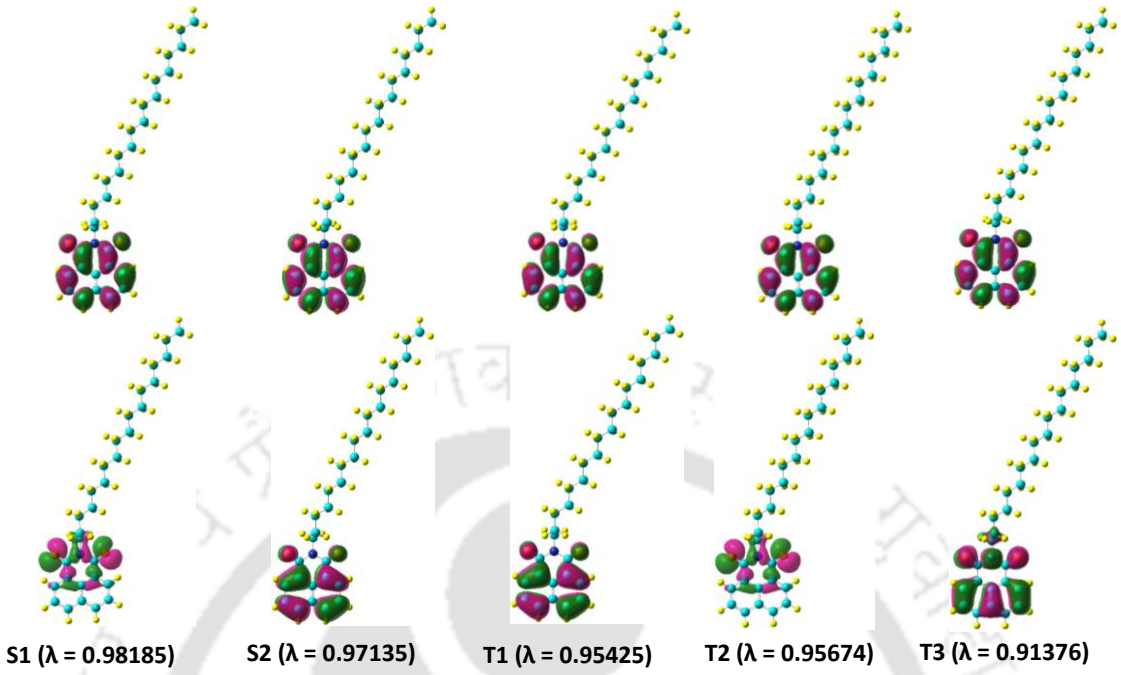

Figure A3.3.4 Natural transition orbitals (NTOs) of ODNI calculated with B3LYP and 631G (d) level of theory in Gaussian 09.

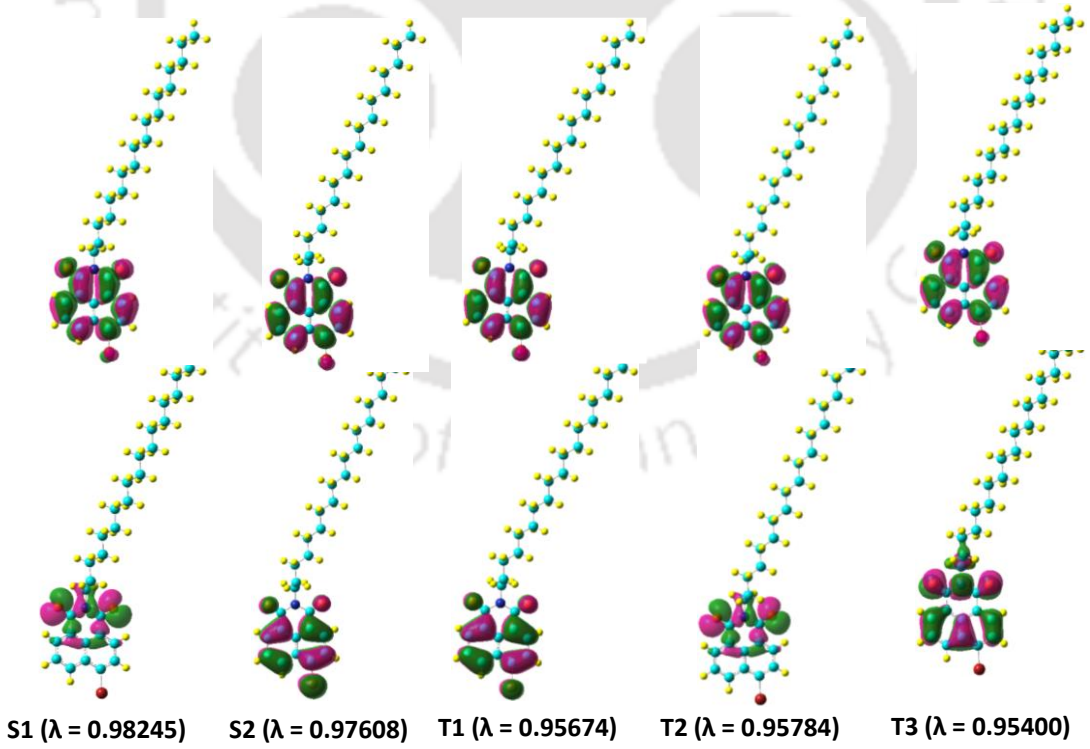

Figure A3.3.5 Natural transition orbitals (NTOs) of BrODNI calculated with B3LYP and 631G (d) level of theory in Gaussian 09.

Table 3.5: Single Crystal Data and parameters of ODNI crystals

Compound Name	**ODNI**
CCDC	1985599
Empirical Formula	C_{30} H_{43} N O_2
Formula weight	449.68
Temperature	115 K
Wavelength	0.71073
Crystal System	Monoclinic
Space Group	P21/n
Unit Cell Dimension	a 12.2380(12) b 4.9366(4) c 42.586(4), α 90 β 97.469(3) γ 90
Volume	2550.97
Z	4
Absorption Coefficient	0.072
Theta range for data collection	2.75 to 27.02
Reflection collected/Unique	0.8569
Goodness of Fit on F^2	1.032
Largest diffraction peak and hole (e $Å^{-3}$)	0.224, -0.219

Table A3.6 Alkyl chain substituent Naphthalimide compounds and their luminescence data

Phosphorescence luminogens	Physical state	Phos. Lifetime (RT)	Phos. Lifetime (77K)	Phos. Q.Y.	Reference
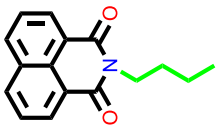	Crystals	-	-	-	*Angew. Chem. Int. Ed.*, 2016, **55**, 9872–9876. (Ref.23)
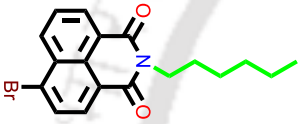	Crystals	5.1 ms	319 ms	-	*Angew. Chem. Int. Ed.*, 2019, **58**, 2284–2288. (Ref. 24)
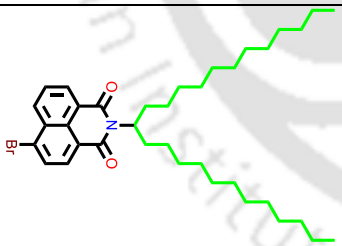	Liquide	6.2 (25 °C)	210 ms	-	*Angew. Chem. Int. Ed.*, 2019, **58**, 2284–2288. (Ref.24)
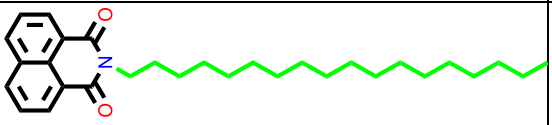	Crystals	-	~212 ms	26.65	*This work*
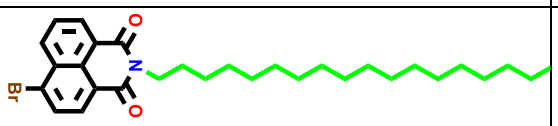	Crystalline solid	~12 µs	~4.5 ms	0.77	*This work*

Chapter 4

Beyond H and J aggregation in naphthalimide luminogens

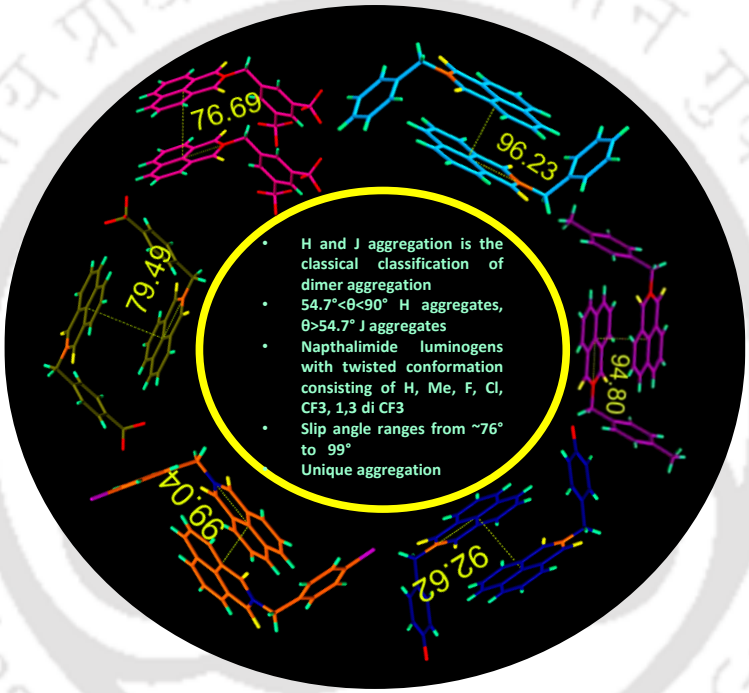

Narang, K.; Mehta, D.; Sarmah, T.; Iyer, Kumar, S.; P. K. Beyond H and J aggregation in naphthalimide luminogens. (*Manuscript prepared*)

Abstract

This thesis chapter investigates the supramolecular interactions of naphthalimide luminogens through a comprehensive analysis of their aggregation patterns utilizing single-crystal X-ray diffraction (XRD) and Field Emission Scanning Electron Microscopy (FESEM). The results reveal unique aggregation behaviours characterized by slip angles exceeding 90 degrees, challenging conventional categorization into H or J aggregates. This study enhances our understanding of the distinctive assembly patterns displayed by these luminogens, illuminating their intriguing structural complexities. Furthermore, the investigation extends to exploring the interactions between the naphthalimide luminogens and the NS1 protein, a critical component in the Japanese Encephalitis virus. Remarkably, the findings highlight exceptional luminescence quenching observed in a specific luminogen, (1,3 m-NPCF$_3$), upon interaction with the NS1 protein. This discovery suggests a promising avenue for developing innovative strategies to combat the Japanese Encephalitis virus, leveraging the unique properties of this luminogen. Thus, this thesis chapter provides valuable insights into the supramolecular behaviour of naphthalimide luminogens and their potential applications in targeted interactions with viral proteins, paving the way for future advancements in materials science and antiviral research.

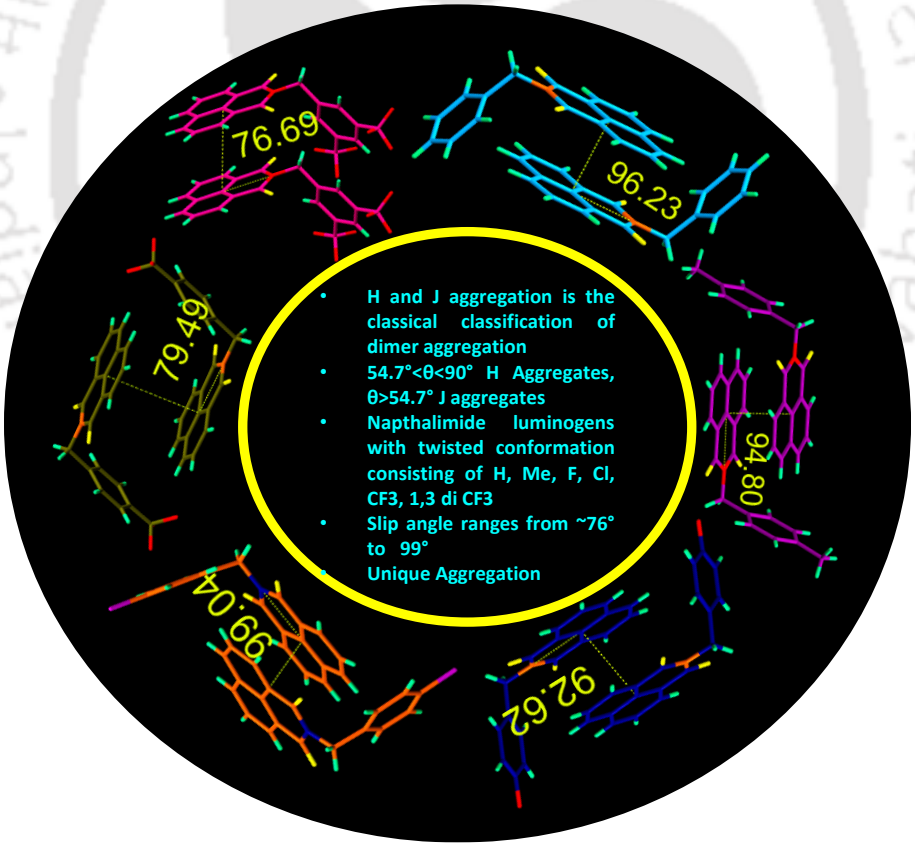

Figure 4.1 Proposed table of content of the present work.

4.1 Introduction

Organic-conjugated materials have garnered significant attention across diverse fields such as, optoelectronics,[1] sensing,[2] bio-medical applications[3] owing to their tuneability, cost-effectiveness and facile processibility.[4] A compressive understanding of the optical characteristics exhibited by conjugated materials necessitates meticulous analysis of their molecular configuration and aggregation behavior.[5,6] It is essential to recognize that the aggregated state characteristics of these materials may not necessarily represent their microscopic properties which primarily pertain to the molecular level. Consequently, there is a burgeoning interest in exploring molecular packing phenomena to gain deeper insights into the structure property relationships of these materials.[7,8]

Nearly six decades ago, Michael Kasha introduced one of the earliest theories to elucidate the impact of molecular aggregation on the photo-physical characteristics of chromophores.[9] By focusing on the coulomb coupling between adjacent chromophores, arising from the interaction between molecular transition dipole moments, Kasha proposed the "card-pack" model to describe linear molecular aggregation.[10] Building upon Kasha's work, McRae and Kasha, utilizing the exciton theory of Davydov, hypothesized that the coulomb coupling could be positive giving rise to H-aggregates, or negative, resulting in J aggregate or Scribe aggregate.[11] In H-aggregate, the singlet state monopolizes all the oscillator strength, leading to quenching of fluorescence from the lowest energy state, while phosphorescence is enhanced through intersystem crossing in most enstances.[12] In contrast to Kasha's research on molecular aggregation, halogen bonding represents a novel and intriguing avenue in the domain of noncovalent interactions for constructing supramolecular ensembles.[13,14] Compared to (single) hydrogen bonds, halogen bonds exhibit greater directionality and offer creative capabilities that are unmatched by other types of noncovalent interactions, thereby unveiling new prospects in the design of smart functional materials.[15,16]

Functional groups and those fragment's capable of free rotation can profoundly alter the electronic structure of luminogens, thereby highlighting the critical interplay between steric and electronic factors during the transition from solution to aggregated states.[17] The aggregation of organic luminogens in aqueous media gives rise to diverse nanostructures, imparting predictability, structural precision, surface functional group exposure. These phenomena have been extensively investigated across a spectrum of applications from organic electronics to biomaterials.[18,19] Naphthalimide, characterized by a planar electron-deficient core has garnered attention across diverse fields including Aggregation Induced Emission

(AIE),[20] Room Temperature Phosphorescence (RTP),[21,22] organic electronics,[23] sensors,[24] and medical applications[25,26] due to its versatile photo-physical properties. In our investigation, we incorporated a phenyl group with a sp^2 spacer into the naphthalimide core. This selection aimed to establish a molecular architecture with a folded structure, wherein two core molecules could evade π-π interactions sufficiently to mitigate exciton quenching and effectively constrain the molecular motion. Recent studies have demonstrated that such constrains, compared to twisted and restricted rotation (RIR) molecules, significantly enhance luminescence.[27] Furthermore, the folded π structure was anticipated to facilitate distinct charge separation, potentially imparting intriguing optical tuneability and self-assembly properties. Furthermore, the anticipated folded π structure is hypothesized to promote distinct charge separation dynamics, thereby potentially engendering intriguing optical tuneability and self-assembly phenomena.[28,29,30] In this study, six luminogens were synthesized employing straightforward condensation reactions, wherein two cores were linked via the sp^2 hybridized methyl group. Despite dissimilar core sizes, the resultant structures exhibit a consistent 2π fold conformation, as evidenced by our experimental observations.

The study was designed to synthesize a series of naphthalimide compounds via conjugation with benzyl substituents harbouring diverse functional groups, demonstrating both positive and negative inductive effects. Specifically, we introduced hydrogen, methyl, and halogen atoms like fluorine, chlorine, CF_3, and 1,3 m-CF_3. The Utilization of the methyl group as a spacer between the naphthalimide core and the benzyl moiety facilitated precise spatial distribution of molecular orbitals. Our investigation aimed at elucidating tuneable aggregation patterns, supramolecular interactions, and self-assembly inherent in these compounds. We meticulously examined the influence of various intermolecular interactions, including halogen bond, C-H bond, CH…π, and other weak intermolecular interactions on photo-physical properties, self-assembly, aggregation phenomena. Moreover, we aimed to leverage these findings to enable targeted interactions with the NS1 protein, a pivotal factor in the pathogenesis of Japanese Encephalitis (JE), thereby expanding the potential therapeutic applications of our synthesized compounds against this life-threatening disease.

All the naphthalimide luminogens NPH, NPMe, NPF, NPCl, $NPCF_3$, 1,3 m-$NPCF_3$ were synthesized using a simple condensation reaction. **(Scheme 4.1)** After purification by column chromatography (5% chloroform/hexane) all these lumino-gens were further characterized by NMR, MALDI, and SC-XRD.

4.2 Experimental

4.2.1 Materials and measurements: All starting material reagents, i.e. 1,8-naphthalic anhydride, Benzyl-methylamine, Benzylamine, 4-Methyl-Benzylamine, 4-Fluoro-Benzyl, 4-Chlorobenzyl, 4-Tri-Clorobenzyl and 1, 3 meta tri-Fluro-Benzyl and solvents (Dimethyl formamide (DMF) and Ethanol), were purchased from Sigma Aldrich (India) and were reagent grade.

NMR Measurements: A Bruker Avance 600 MHz Fourier transformation spectrometer was used to record the proton NMR spectrum at 600 MHz and the ^{13}C NMR spectrum at 200 MHz. All Proton and ^{13}C spectra solutions were obtained using the residual solvent signal as an internal reference. The chemical shifts are reported in parts per million (ppm) with respect to TMS. The short notations used are s for singlet, d for doublet, t for triplet, q for quartet, and m for multiplet.

Matrix-Assisted Laser Desorption Ionization: MALDI was performed on Bruckner model auto-flex speeds using a MALDI TOF system spectrometer.

Optical Measurements: Solution State Studies: Electronic absorption spectra of luminophores in solution state were recorded on a Perkin-Elmer Model Lambda-750 spectrophotometer. PL emission spectra were recorded on the Horiba Fluromax-4 spectrofluorometer. Optical measurements were performed using 4 mm quartz cuvettes at 298 K. **Crystal state studies:** Electronic absorption spectra were recorded on a Perkin Elmer Model Lambda-750 spectrophotometer. Emission spectra were recorded on the FLS1000 spectrometer, an Edinburg instrument.

Lifetime and measurements: Fluorescence lifetime experiments were performed on the Horiba Delta Flex time-correlated single photon counting (TCSPC) instrument. A 373 nm Laser diode with a pulse repetition rate of 1 MHz was used as the light source.

4.2.2 Synthetic procedure

4.2.2a Synthesis of 2-benzyl-1H-benzo[de]isoquinoline-1,3(2H)-dione, NPH:

In a 50 mL round bottom flask 0.5 g 1,8 Naphthalic anhydride was taken along with 10 mL pure ethanol. The reaction mixture was kept for stirring in a setup with condenser. 0.7 mL benzyl amine was added to the reaction mixture drop by drop. The reaction temperature kept at room temperature for 30 minutes, then gradually increased and maintained a reflux condition 12 hr. Completion of the reaction was monitored by TLC. After the reaction was completed, the whitish, muddy crude was then filtered through Whatman filter paper. The crude was further refined using column chromatography and 5% chloroform/hexane.[31] A white color solid

(NPH, 490 mg, yield 95%) was developed and characterized further using ^{1}H NMR, ^{13}C NMR, HRMS, MALDI, and SCXRD.

NPH: 1H NMR: (600MHz, $CDCl_3$, δ ppm) 8.60 (d, 2H), 8.19 (d, 2H), 7.74 (t,3H), 7.55 (d, 2H), 7.30 (t, 3H), 7.24 (dd, 4H), 5.39 (S, 1H) **13C NMR: (150MHz, CDCl3, ppm):** 164.22, 137.30, 134.03, 131.57, 131.42, 128.94, 128.43, 128.17, 127.46, 126.94, 122.63, 43.56. **Mass calculated for $C_{19}H_{13}NO_2$ = 288.32 [M]+, Found 294.15 [M+1]+**

4.2.2b Synthesis of 2-(4-methylbenzyl)-1H-benzo[de]isoquinoline-1,3(2H)-dione, NPMe: 0.5 g of 1,8-naphthalic anhydride and 10 mL of pure ethanol were added to a 50 mL round-bottom flask. The reaction mixture was set up in a setup equipped with a condenser for the purpose of stirring. Drop by drop, 0.7 mL of Methyl-Benzylamine was added to the reaction mixture. After 30 minutes at room temperature, the reaction temperature was progressively raised and the reflux condition was maintained for 12 hours. TLC was used to monitor the reaction's completion. The whitish, muddy crude was then filtered through Whatman filter paper after the reaction was completed, the crude was further refined using column chromatography and 5% chloroform/hexane. A light sea green colour solid (NPMe, 470 mg, Yield 93%) was developed and characterised further using ^{1}H NMR, ^{13}C NMR, HRMS, MALDI, and SCXRD.

NPMe: 1H NMR: (600 MHz, $CDCl_3$, δ ppm) 8.60 (dd, 2H), 8.18 (dd, 2H), 7.73 (m,3H), 7.45 (d, 2H), 7.11 (d, 3H), 7.24 (dd, 4H), 5.35 (s, 1H) 2.29 (s, 1H) **^{13}C NMR: (150 MHz, CDCl3, ppm):** 164.21, 137.13, 134.35, 133.97, 131.55, 131.38, 129.09, 128.98, 128.16, 126.91, 122.69, 43.30, 21.12 **Mass calculated for $C_{20}H_{15}NO_2$ = 301.35 [M]+, Found 301.259 [M+1]+**

4.2.2c Synthesis of 2-(4-fluorobenzyl)-1H-benzo[de]isoquinoline-1,3(2H)-dione, NPF: 0.5 grams of 1,8 Naphthalic anhydride was placed in a 50 mL round bottom flask, along with 10 mL of pure ethanol. In a condenser-equipped arrangement, the reaction mixture was stored for stirring. Drop by drop, 0.7 mL of 4-fluorobenzyl was added to the reaction mixture. After 30 minutes at room temperature, the reaction temperature was progressively raised, and the reflux condition was maintained for 12 hours. TLC was utilized to monitor the reaction's completion. The yellowish, murky crude was filtered through Whatman filter paper once the reaction was finished. Using column chromatography and 5% chloroform/hexane, the crude was further purified. A sea green colour solid (NPF, 420 mg, yield 87%) was developed and characterised further using ^{1}H NMR, ^{13}C NMR, HRMS, MALDI, and SCXRD.

NPF: 1H NMR: (600MHz, $CDCl_3$, δ ppm) 8.62 (dd, 2H), 8.21 (d, 2H), 7.76 (m,3H), 7.56 (d, 2H), 6.98 (m, 3H) **13C NMR: (150MHz, $CDCl_3$, ppm):** 164.22, 162.99, 161.36, 134.14, 133.13, 133.11, 131.61, 131.49, 130.99, 130.94, 128.19, 126.98, 122.57, 115.30, 115.16, 42.83 **Mass calculated for $C_{19}H_{12}FNO_2$ = 305.31 [M]+, Found 305.834 [M+1]+**

4.2.2d Synthesis of 2-(4-chlorobenzyl)-1H-benzo[de]isoquinoline-1,3(2H)-dione, NPCl: 0.5 grams of 1,8-naphthalic anhydride and 10 mL of pure ethanol were added in a 50-milliliter round-bottom flask. A setup with a condenser was used to keep the reaction mixture stirring. 0.7 mL of 4-chlorobenzyl was gradually added to the reaction mixture. After 30 minutes at room temperature, the reaction temperature was progressively raised, and a reflux condition was maintained for 12 hours. The progress of the reaction was observed using thin-layer chromatography (TLC). We used Whatman filter paper to filter the yellowish, murky crude once the reaction had been completed. We conducted additional purification of the crude substance using column chromatography with a 5% mixture of chloroform and hexane. A yellow green colour solid (NPCl, 390 mg, yield 79%) was developed and characterised further using ^{1}H NMR, ^{13}C NMR, HRMS, MALDI, and SCXRD.

NPCl: 1H NMR: (600 MHz, $CDCl_3$, δ ppm) 8.62 (dd, 2H), 8.23 (m, 2H), 7.76 (m,3H), 7.50 (d, 2H), 7.28 (s, 1H) 5.35 (s, 1H) **13C NMR: (150 MHz, $CDCl_3$, ppm):** 164.2, 135.78, 134.20, 133.34, 131.63, 131.54, 130.50, 128.58, 128.21, 127.0, 122.53, 42.92 **Mass calculated for $C_{19}H_{12}FNO_2$ = 321.76 [M]+, Found 321.846 [M+1]+**

4.2.2e Synthesis of 2-(4-(trifluoromethyl)benzyl)-1H-benzo[de]isoquinoline-1,3(2H)-dione, $NPCF_3$: In a 50 mL round bottom flask, 0.5 grams of 1,8 Naphthalic anhydride were combined with 10 mL of pure ethanol. In a condenser-equipped arrangement, the reaction mixture was stored for stirring. Drop by drop, 0.7 mL of tri-Fluro-Benzyl was added to the reaction mixture. The reaction temperature was initially maintained at ambient temperature for a duration of 30 minutes, after which it was gradually raised and maintained under reflux conditions for a period of 12 hours. The progress of the reaction was observed using thin-layer chromatography (TLC). Once the reaction was finished, the pale, turbid crude substance was subsequently passed through a filter made of Whatman filter paper. The crude substance underwent additional purification using column chromatography with a mixture of 5% chloroform and hexane. A yellow colour solid (NPCF3, 320 mg, yield 74%) was developed and characterised further using ^{1}H NMR, ^{13}C NMR, HRMS, MALDI, and SCXRD.

NPCF3: ^{1}H NMR: (600MHz, $CDCl_3$, δ ppm) 8.63 (dd, 2H), 8.24 (dd, 2H), 7.78 (m,3H), 7.65 (d, 2H), 7.56 (d, 1H) 5.35 (s, 1H) **^{13}C NMR: (150MHz, CDCl3, ppm):** 164.22, 141.18, 134.32, 131.63, 129.14, 128.24, 127.04, 125.44, 125.41, 122.42, 43.16 **Mass calculated for $C_{20}H_{12}F_3NO_2$ = 355.32 [M]+, Found 355.975 [M+1]+**

4.2.2f Synthesis of 2-(3,5-bis(trifluoromethyl)benzyl)-1H-benzo[de]isoquinoline-1,3(2H)-dione, 1,3 m-NPCF$_3$: 0.5 grams of 1,8 Naphthalic anhydride were added in a 50 mL round bottom flask, together with 10 mL of pure ethanol. The reaction mixture was stirred in a setup with a condenser, and 0.9 mL of 1, 3 meta tri-Fluro-Benzyl was gradually added to the reaction mixture. After maintaining a reflux state for 12 hours, the reaction temperature was progressively raised after being kept at room temperature for 30 minutes. TLC was used to monitor the reaction's completion. The yellowish, murky crude was filtered through Whatman filter paper once the reaction was finished. The crude was further refined using column chromatography and 5% chloroform/hexane. A white colour solid (1,3 m-NPCF$_3$, 300 mg, yield 71%) was developed and characterised further using ^{1}H NMR, ^{13}C NMR, HRMS, MALDI, and SCXRD.

1,3 m-NPCF3: ^{1}H NMR: (600 MHz, $CDCl_3$, δ ppm) 8.65 (dd, 2H), 8.26 (dd, 2H), 8.02 (s,3H), 7.79 (m, 2H), 5.47 (s, 1H) **^{13}C NMR: (150MHz, $CDCl_3$, ppm):** 164.18, 139.64, 134.52, 131.83, 131.69, 131.62, 129.45, 128.27, 127.08, 124.14, 122.33, 122.22, 121.66, 42.84 **Mass calculated for $C_{21}H_{11}F_6NO_2$ = 423.31 [M]+, Found 424.064 [M+1]+**

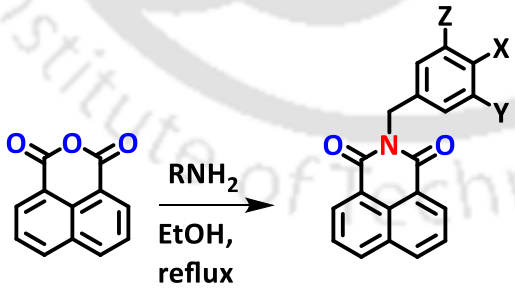

X = H, Y = H, Z = H (NPH)
X = Me, Y = H, Z = H (NPMe)
X = F, Y = H, Z = H (NPF)
X = Cl, Y = H, Z = H (NPCl)
X = CF_3, Y = H, Z = H (NPCF$_3$)
X = H, Y = CF_3, Z = CF_3 (1, 3 m-NPCF$_3$)

Scheme 4.1: Synthetic scheme for the NPH, NPMe, NPF, NPCl, NPCF$_3$, 1,3 m-NPCF$_3$

4.2.3 Preparation of SC-XRD sample: Following synthesis and column chromatography purification, luminogens in powder state were dissolved in HPLC methanol/chloroform mixture and stored at room temperature in the dark. NMICY crystals were discovered in white, transparent, and glossy form within 24 to 48 hours. To undertake SCXRD analysis, it was put over a glass slide.

4.2.4 Preparation of FESEM sample: For all Naphthalimide luminogens (20 µM, 1 mL, 99.9% f_w) one mL sample was drop cast over clean FTO substrate and was dried overnight at room temperature before analysis in an ultra-clean environment.

4.2.5 Theoretical Calculations: The ground state optimization and excited state TD-DFT of NPH, NPMe, NPF, NPCl, $NPCF_3$ and 1,3 m-$NPCF_3$ using a single crystal CIF file was calculated by using the Gaussian-16 package. B3LYP hybrid functional with 631G+d basis sets were used during the entire calculation.[32,33]

4.2.6 Production of NS1 protein: Japanese encephalitis virus vaccine strain (SA-14-14-2) was selected, and RNA was isolated using Trizol following manufacturer protocol.[34] (Takara, Japan). NS1 gene was amplified from viral genomic RNA in RT-PCR using gene specific primers with restriction site for cloning purposes.[35] Amplified product was then purified by gel extraction. Purified NS1 was digested with restriction enzymes EcoR1 and Nhe1. The NS1 insert was ligated to the pET- 28a (+) vector. The recombinant plasmid was transformed into E. coli BL21 DE3 competent cells. The transformed colonies were confirmed by restriction digestion. For bulk production of NS1 protein, the starter culture was prepared by inoculating transformed colonies in nutrient broth with appropriate antibiotics and incubated overnight. The transformation reactions were operated at 180 rpm and at 37°C.[36] Further, 1% of the overnight culture was inoculated in fresh nutrient broth containing antibiotics. Isopropyl β-d-1-thiogalactopyranoside (IPTG) of varying concentrations from 0.25 to 1 mM concentration was added to log phase culture (O.D. 0.5-0.6) and incubated for different time points at 37°C. Culture aliquot was collected at hourly intervals to study the expression kinetics of NS1 gene by SDS-PAGE. The recombinant 6×histidine tagged NS1 protein was purified by affinity chromatography containing Ni-NTA (BioRad, USA). In brief, the harvested cells containing proteins were solubilized in lysis buffer (300 mM NaCl, 50 mM Tris base, 2 mM Imidazole, 100 mM PMSF, pH 8.8) by vortex followed by incubation at room temperature for 1 hr. The suspension was centrifuged at 10,000 rpm for 20 min at 4 °C and the supernatant containing crude protein lysate was allowed to bind to Ni-charged resin (Bio Rad, USA) for 2-3 hr. The

protein was eluted by passing lysis buffer (pH 8.8) containing imidazole in increasing concentration through the column. Lysis buffer with 20 mM imidazole (10 mL) was passed through the column followed by subsequent passing of 6-10 mL each of buffer containing 40 mM, 80 mM, 100 mM, 200 mM, and 400 mM imidazole. The purified recombinant protein was dialyzed sequentially in decreasing concentrations of imidazole in lysis buffer. The concentration of purified antigen was measured using Bradford reagent (HiMedia, India) and stored at −80 °C for subsequent use.[37]

4.2.7 Purification of NS1 protein:

The protein was purified by 6X/Ni-NTA affinity chromatography. The NS1 protein, expressed with a 6XHis tag, exhibited a size of 48 kDa. The protein was expressed in the insoluble fraction.[38] Maximum expression was observed when induced a concentration of 1 mM IPTG. Study of hourly kinetics of IPTG-induced clones revealed that protein expression was maximum at 4 h post-induction, after which it was almost constant. The SDS-PAGE analysis revealed that protein started appearing with the first elute of 50 mM imidazole elute and increased steadily thereafter with maximum concentration in the 100 mM elute followed by a gradual decline in subsequent.[39] The elutes with visible high concentration protein on SDS were pooled and dialyzed. Purity of the recombinant protein was confirmed by a single band in SDS PAGE and western blot analysis. Protein concentration was found to be 100ug/ml by Bradford's protein estimation assay.[40,41]

4.3 Result and discussion

4.3.1 Synthesis and characterization of NPHA, NPHB, NPMeA, NPMeB

All the Naphthalimide luminogens NPH, NPMe, NPF, NPCl, $NPCF_3$, 1,3 m-$NPCF_3$ were synthesized using a simple condensation reaction. Illustrated in **Scheme 4.1** Following purification via column chromatography (using 5% chloroform/hexane), NPH, NPMe, NPF, NPCl, $NPCF_3$, 1,3 m-$NPCF_3$ were characterized using NMR, MALDI, and single-crystal X-ray diffraction (SC-XRD). The UV/Visible absorbance profiles of naphthalimide lumino-gens were investigated in DMF (dimethylformamide) solution with varying water fractions (f_w = 0%, f_w = water fraction). Stock solutions of the luminogens were prepared in DMF at a concentration of 1 mM. Under condition of 0% water fraction (f_w = 0%, 100% DMF), all the luminogens exhibited distinct absorption peaks near 342 nm and 352 nm, corresponding to π-π* transition of C=O bond and n-π* transition respectively. At 99% water fraction, evident aggregation phenomena were observed for all luminogens except for 1,3 m-$NPCF_3$. Notably,

NPH, NPMe, NPF and NPCl manifested a bathochromic shift in absorbance, indicative of J-aggregation in their condensed state. Conversely, $NPCF_3$ displayed a flat absorption line with an elevated baseline, while 1,3 m-$NPCF_3$ exhibited a slight red shift in absorbance. **(Figure 4.2a to 4.2f)** These findings underscore the diverse aggregation behaviour influenced by both the intrinsic chemical structure of the luminogens and the presence of water within the solvent system, delineating critical insights into their photophysical properties and self-assembly dynamics. All six naphthalimide luminogens exhibit notable aggregation-induced emission (AIE) properties. Upon increasing water fraction distinct fluorescence patterns were observed between the luminogens, albeit with slight variations. However, at a water fraction of 99.9% (f_w = 99.9%), the highest emission intensity was consistently recorded for all luminogens thereby confirming their robust AIE properties.

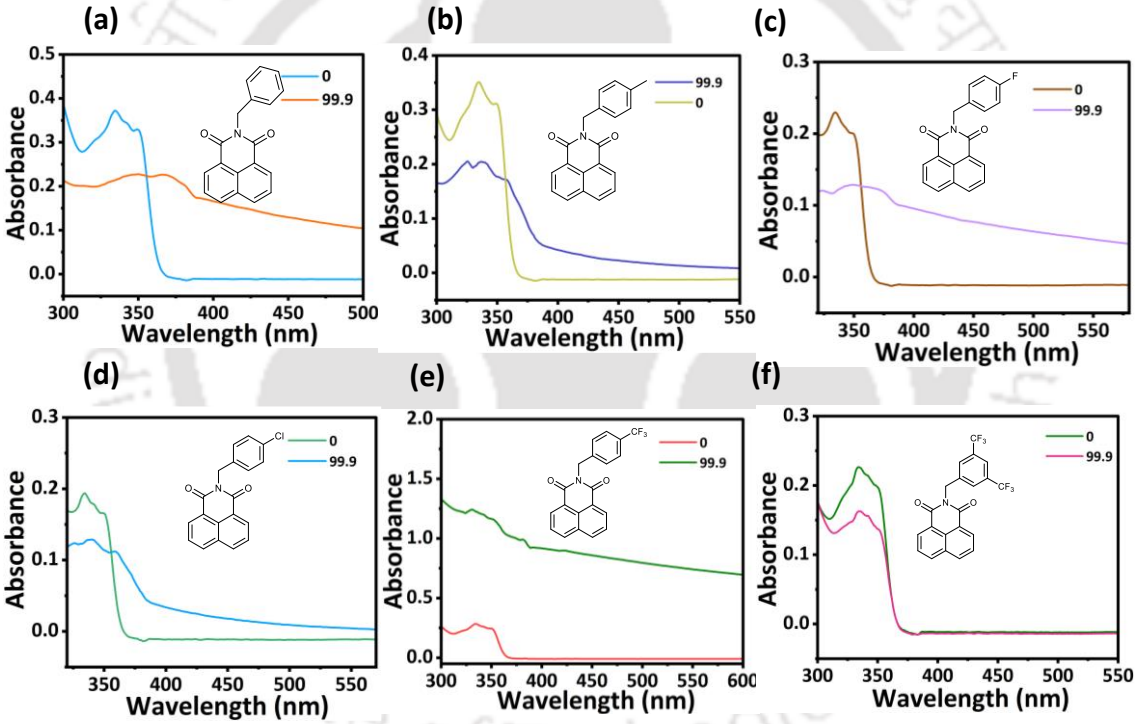

Figure 4.2 Absorbance spectra of naphtahlimide luminogens (a) NPH, (b) NPMe, (c) NPF, (d) NPCl, (e) $NPCF_3$, (f) 1,3 m-$NPCF_3$ in DMF f_w = 0% and f_w = 99.9% (water fraction = f_w).

Furthermore, all luminogens, demonstrated a significant red shift in emission from their monomeric state. The incorporation of phenyl and substituted phenyl groups effectively mitigated π-π interactions between adjacent naphthalimide cores. Plotting the emission spectra in their condensed state revealed a progressive increase in emission intensity from $NPCF_3$, NPH, NPCl, and NPF to 1,3 m-$NPCF_3$, with a substantial red shift of 31 nm observed from $NPCF_3$ to 1,3 m-$NPCF_3$. These findings elucidate the nuanced effects of molecular structure

on the photophysical properties and aggregation induced emission behaviour of naphthalimide luminogen, providing valuable in-sights for their potential applications in diverse optoelectronic and biotechnological applications. Fluorescence spectra of all Naphthalimide luminogens in both crystalline and aggregated state was investigated. **(Figure 4.3a to 4.3f)** (aggregated state f_w = 99.9%). Remarkably, 1,3 m-NPCF$_3$ exhibited the most significant hypochromic shift in emission, ($\lambda_{max.}$ = 395 nm) and NPH and NPMe have nearly same red shifted emission maxima ($\lambda_{max.}$ = 466 nm). The observed trend in emission maxima followed the order: 1,3 m-NPCF3 < NPCF3 < NPCl < NPF < NPMe < NPH as depicted in **(Table 4.1)**. These findings underscore the distinct photophysical behaviour exhibited by each naphthalimide luminogen, elucidating the influence of molecular structure on their emission characteristics in both crystalline and aggregated states.

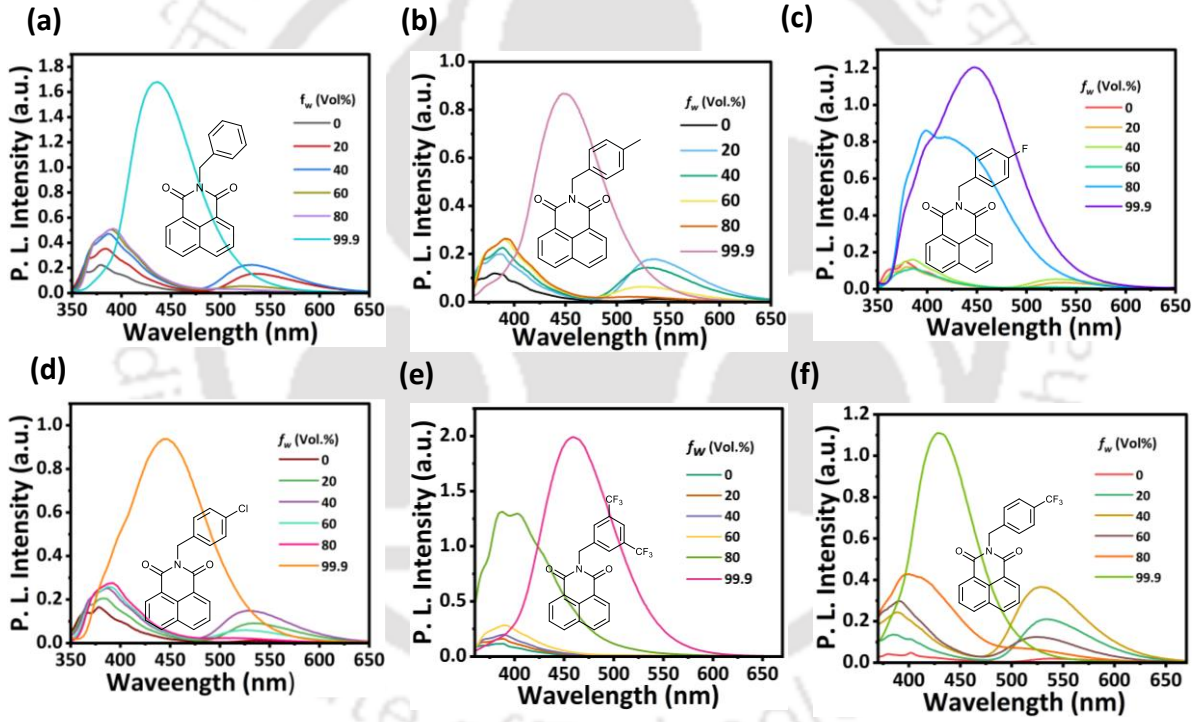

Figure 4.3 Fluorescence spectra of Naphthalimide luminogens by increasing water fraction f_w in DMF/ Water solvent system.

In the aggregated state (f_w = 99.9%), a markedly distinct trend was observed, potentially attributed to interactions between water molecule and the fluorine atoms present. The emission maxima exhibited a trend from blue to red shift as follows: NPCF$_3$ < NPH < NPCl < NPMe < NPF < 1,3 m-NPCF$_3$. This phenomenon prompts an essential inquiry into the nature of interaction between fluorine and water molecules. Notably, NPCF$_3$ displays most pronounced, blue shifted emission, while 1,3 m-NPCF$_3$ exhibits the most significant, red shifted emission,

contrary to their respective emission characteristics in the crystalline state. This intriguing discrepancy in emission maxima suggest a potential correlation with the observed aggregation patterns among these luminogens, highlighting the complex interplay between molecular interactions and photo-physical properties.[42]

Moreover, the distinct emission behaviour observed in the aggregated state (f_w = 99.9%) underscores the intricate interplay between molecular architecture and solvent effects, particularly the role of water molecules in modulating the photophysical properties of naphthalimide luminogens. The observed, blue-shifted emission in $NPCF_3$ suggests a potential interaction between the fluorine atoms and water molecules, possibly resulting in a perturbation of the electronic structure and subsequent alteration in the emission wavelength. Conversely, the pronounced, red-shifted emission in 1,3 m-$NPCF_3$ may indicate a different mode of interaction with water molecules, leading to a stabilization of the excited state and a longer emission wavelength.

These findings highlight the dynamic nature of molecular interactions within the aggregated state, where subtle variations in chemical structure can lead to significant changes in photophysical behaviour.[43] The observed discrepancies in emission maxima among the naphthalimide luminogens underscore the complexity of their aggregation-induced emission phenomena, necessitating a detailed investigation into the underlying mechanisms at play. Further studies exploring the specific nature of fluorine-water interactions and their influence on the photophysical properties of these luminogens are essential for unravelling the intricacies of their behaviour in complex environments.[44,45]

Understanding the fundamental principles governing the aggregation-induced emission of naphthalimide luminogens is pivotal for the rational design of novel materials with tailored optical properties.[46] By elucidating the relationship between molecular structure, solvent interactions, and emission behaviour, this research contributes to the broader understanding of AIE mechanisms and paves the way for the development of advanced functional materials for diverse applications in optoelectronics, sensing, and biomedical imaging.[47,48]

Table 4.1 fluorescence spectra of all naphthalimide luminogens in crystal state and aggregated state.

Luminogen	**NPH**	**NPMe**	**NPF**	**NPCl**	**$NPCF_3$**	**1,3 m-$NPCF_3$**
$\lambda_{max.}$ **(Crystals) (nm)**	466	466	412	405	438	395
$\lambda_{max.}$ **(f_w =99.9) (nm)**	435	448	449	445	429	460

4.3.2 TRPL: The fluorescence emission characteristics of all the naphthalimide luminogens in both their crystalline and aggregated state are detailed in **Table 4.2** (aggregated state f_w = 99.9%). Notably, in the crystalline state NPMe, exhibited the longest fluorescence lifetime (35.62 ns), followed by NPH (17.55 ns) and 1,3 $NPCF_3$ displayed shortest lifetime (3.51 ns). The fluorescence lifetime followed an ascending order: 1,3 $NPCF_3$ < $NPCF_3$~ NPCl < NPF < NPH < NPMe. The trend appears to correlate with the electron donating ability of the substituents and blue to red shifted emission observed across of all the luminogens. These findings underscore the intricate interplay between molecular structure, electronic properties, and photo-physical behaviour, elucidating key insights into the fluorescence dynamics of naphthalimide luminogens in diverse environmental contexts.[49]

As discussed earlier, the fluorescence emission maxima and fluorescence lifetime in aggregated state deviate from those observed in the crystalline state. Notably, NPCl exhibited the longest fluorescence lifetime at 22.89 ns, while 1,3 m-$NPCF_3$ displayed the shortest at 3.77 ns. The ascending order of fluorescence lifetime in the aggregated state is as follows: 1,3 m-$NPCF_3$ < $NPCF_3$ < NPH < NPMe < NPF < NPCl. Consequently, alongside the aggregation pattern, the interaction of water with hydrogen, methyl, fluorine, and chlorine moieties contributes to the irregular trend observed in the fluorescence lifetime of those luminogens in the aggregated state. To further elucidate the fluorescence lifetime characteristics, we analysed the single crystal XRD patterns of all the luminogens, aiming to gain deeper insights into their photophysical properties.[50]

Table 4.2. TRPL of all naphthalimide luminogens in crystal state and aggregated state.

Luminogen	**NPH**	**NPMe**	**NPF**	**NPCl**	**$NPCF_3$**	**1,3 m-$NPCF_3$**
τ_F (Crystals)(ns)	17.55	35.62	12.74	5.08	5.33	3.51
τ_F (f_w = 99.9) (ns)	9.07	18.71	19.16	22.89	5.45	3.77

4.3.3 H, J and X Aggregation: In organic conjugated materials, the aggregated structure and molecular stacking models exert a substantial in photoluminescence (PL) property primarily through the modulation of transition dipole interaction of adjacent molecules.[51] The molecular packing dictates the geometry of the emitters excited and ground state. Notably, alter-nations in packing arrangements significantly impact the dihedral angle within the donor acceptor (D-A) structure.[52,53] Consequently, the separation of the HOMO and LUMO significantly impacts the character of the Locally Excited State Charge Transfer (LMCT) state, while the extent of conjugation across the emitter affects excited state characteristics.[54] Kasha elucidated that that minimizing transition dipole interactions could enhance emissive characteristics by increasing the slippage of molecules from H to J- aggregate configurations (54.7° = J-aggregation, 54.7° = H-aggregation).[55,56]

The definition of the term "J-aggregate" has evolved over time. Wuerthner et al.[20] proposed a refined classification to differentiate classical J-aggregates characterized by predominant long-range coulomb coupling and charge transfer (CT) mediated or coupled J aggregates.[57] The latter's red shifts primarily arise from short range orbital interactions, a distinction informed by recent theoretical advancements in intermolecular interactions between slip stacked dyes.[58] Thus, categorizing J-aggregates merely based on the observed red-shift and slip angle can be deceptive. Traditional J-aggregates, renowned for their strong excitonic coupling enhancing solid state luminescence, do not fully elucidate the emission phenomenon observed in newly synthesized AIEgens, Intermolecular interaction within organic aggregates encompass a spectrum ranging from hydrogen bonds to cation or anion to cation interactions and dipole-

dipole interactions among others. These interactions undergo modification due to aggregation, flexible molecular conformation, the influence of excited state energy dissipation pathways and the electrical and geometric characteristics of the molecules.[59,60]

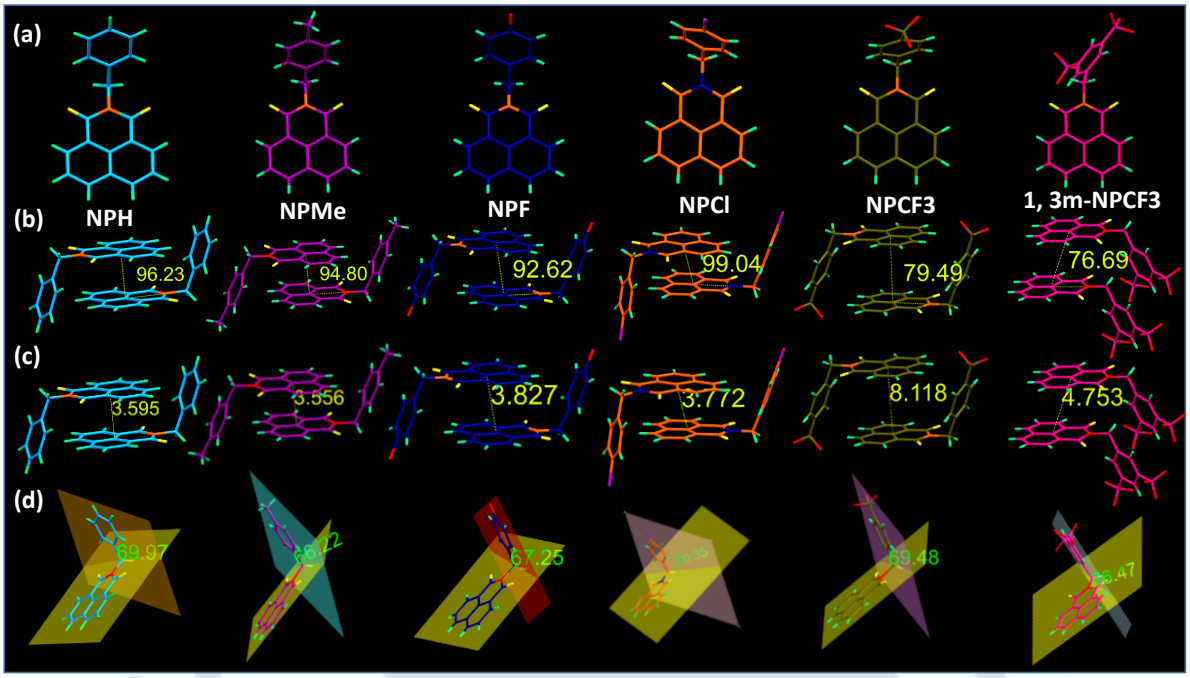

Figure 4.4 SC-XRD analysis summary of naphthalimide luminogens NPH, NPMe, NPF, NPCl, $NPCF_3$, 1,3 m-$NPCF_3$

4.3.4 SC-XRD study: To gain more insights of the aggregation pattern and supramolecular interactions which control the luminescence property and fluorescence emission lifetime, we have analysed the single crystal XRD pattern of all the naphthalimide luminogens NPH, NPMe, NPF, NPCl, $NPCF_3$, 1,3 m-$NPCF_3$. These luminogens featuring a naphthalimide moiety conjugated with a substituted benzyl core and various substituents, alongside a sp^2 spacer, induced a twisted conformation in each luminogen. However, the incorporation of different substituents induced nuanced alternations in both the relative orientations and the naphthalimide-Me-Benzyl angle across the luminogens. This investigation provides crucial insights into the structural dynamics underlaying their photo-physical behaviour, offering valuable insights into the mechanism governing their luminescence property. (NPH = 111.96°, NPMe = 112.72°, NPF = 112.10°, NPCl = 110.26°, NPCF3 = 111.92°, 1,3 m-NPCF3 = 112.77°) **(Figure 4.4a)**. The most important part of these crystal analysis is the observation of slip angle in all these luminogens. The slip angle between two adjacent chromophores are the following; NPH = 96.23°, NPMe = 94.80°, NPF = 92.62°, NPCl = 99.04°, NPCF3 = 79.49°, 1,3 m-NPCF3 = 76.69° and distance between those adjacent chromophores are d = 3.595Å

(NPH), d = 3.556 Å (NPMe), d = 3.827 Å (NPF), d = 3.772 Å (NPCl), d = 8.118 Å (NPCF3), d = 4.753 Å (1,3 m-NPCF$_3$). **(Figure 4.4b, 4.4c)** *Dihedral angle:* Dihedral angle of NPH (69.97°) is higher than NPMe (66.22°) and it was observed that increasing number of fluorine enhanced the dihedral angle which ranges from 67.25° for NPF, 69.48° for NPCl to 76.47° for 1,3 m-NPCF$_3$. All the luminogens consists of many intermolecular interactions. NPH (9) (two O…H = 2.631 Å, two O…H = 2.645 Å, two O...H = 2.648 Å, one C-H…H-C = 2.333 Å, two C-H...π = 2.895Å). NPMe (8) (two O…H = 2.631 Å, two O…H = 2.645 Å, two O...H = 2.648Å, one C-H…H-C = 2.333 Å, two C-H...π = 2.895 Å). NPF (4) (two C=O…H-C = 2.541 Å, two C-F…H-C = 2.477 Å). NPCl (9) (two C=O…H-C = 2.366 Å, π-π = 3.382 Å, two C=O…π = 2.528 Å, C-H… π = 2.877 Å, C=O… π = 3.125 Å, C=O…H-C = 2.587 Å, C-H…H-C = 2.262 Å). NPCF$_3$ (6) (two C=O….H-C = 2.683 Å, two C=O….C-H = 2.432 Å, two C-H…F-C = 2.670 Å). 1,3 m-NPCF$_3$ (6) (two C=O…C-H = 3.177 Å, two C-H….F-C = 2.535 Å, two C=O…H-C = 2.526 Å). **(Figure 4.4d)**

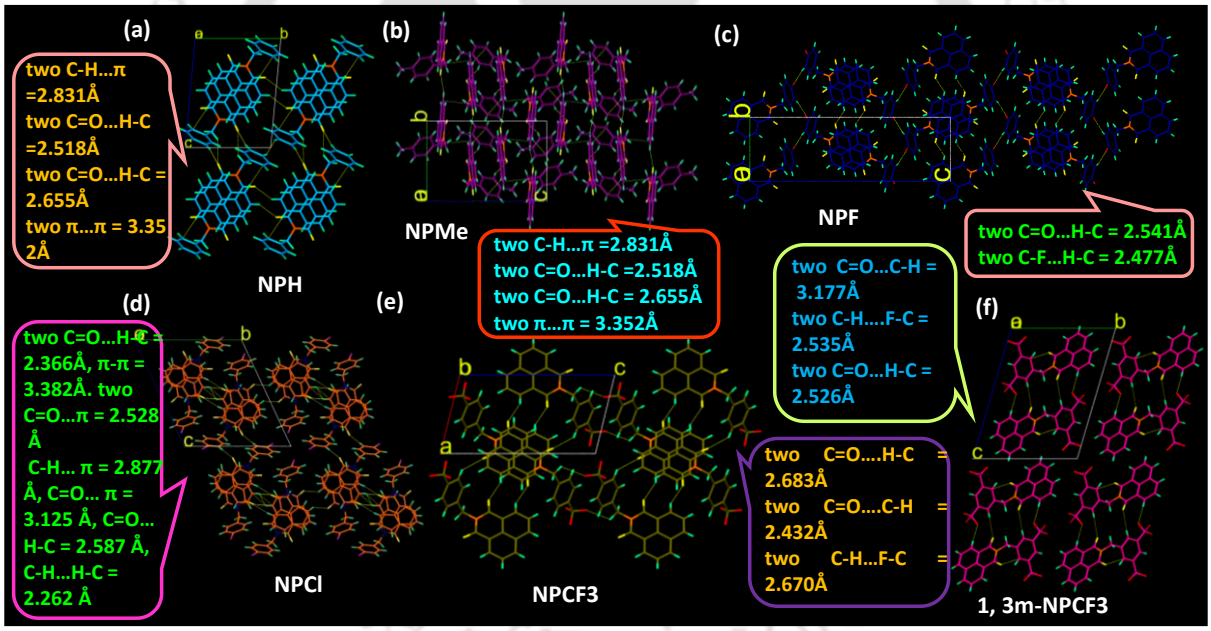

Figure 4.5 SC-XRD analysis summary of Naphthalimide Luminogens a. NPH b. NPMe c. NPF d. NPCl e. NPCF$_3$ f. 1,3 m-NPCF$_3$

We observed that NPH and NPMe have a greater number of intermolecular interactions, nine and eight respectively com-pared to NPF (4), NPCF$_3$ (6), 1,3 m-NPCF$_3$ (6). The redshift-ed emission can be related to number of intermolecular inter-actions that a greater number of intermolecular interactions facilitated more radiative decay channels in NPH and NPMe, but it could not explain that NPF has only four intermolecular interactions and NPCl has 8 which has redshifted emission than NPCF$_3$ and 1,3 m-NPCF$_3$ which has 6 intermolecular interactions.

Thus, it can be clear that a greater number of intermolecular interactions are responsible for redshifted emission. **(Figure 4.5a to 4.5f)**

4.3.4 Hirshfeld surface analysis: Hirschfeld surface analysis is a crucial tool in crystal engineering that helps delineate intermolecular interactions in organic luminogens. Understanding these interactions is essential for modulating photophysical properties and designing materials with tailored optoelectronic functionalities. This allows for precise manipulation of intermolecular contacts, enhancing performance and applicability in various optoelectronic devices. By performing Hirshfeld surface analysis, it was confirmed that similar interaction pattern observed in single crystal XRD analysis of all the luminogens. Hirshfeld surface analysis was utilized to get a statistical picture of the intermolecular interactions in the series of crystal packings. **(Figure 4.6a to 4.6f, and Table 4.3)** The calculations and fingerprint representations of Hirshfeld surfaces are implemented in the program CrystalExplorer.[61] The percentage contribution of various contacts to the total Hirshfeld surface comes from H-H interaction in NPH (47.8%), NPMe (50.5%), NPF (35.5%), NPCl (37.5%), and $NPCF_3$ (26.8%), and is significantly lower for 1,3 m-$NPCF_3$ (14.4%). After the introduction of F, Cl, CF_3, and 1,3m-CF_3 the contribution of H-H introduction reduces. Thus, a higher number of halogen atoms reduces the H-H interactions. Other interactions were also similar in all the naphthalimide luminogens. In NPF, $NPCF_3$, and 1,3 m-$NPCF_3$, as the number of fluorine atoms increases, the contribution of H-F and F-H increases. H-F percentage for NPF is 6.7%, $NPCF_3$ is 12.0%, 1,3 m-$NPCF_3$ is 15.1%, and H-F percentage is 7.2% for NPF, 12.9% for $NPCF_3$, and 16.1% for 1,3 m-$NPCF_3$. F-F interaction was also shown by $NPCF_3$ at 4.4% and a very high 10.6% in 1,3 m-$NPCF_3$ but was absent in NPF. NPCl has also exhibited H-Cl interaction at 5.4% and Cl-H interaction at 7.4%, and NPCl has also shown Cl-Cl interaction at 2.2%. In brief, Hirshfield surface analysis of naphthalimide luminogen shows that rationalization of any crystal structure requires various intermolecular interactions governing the crystal packing and crystallization as well. Hirschfeld surface analysis confirms consistent interaction patterns across luminogens, highlighting its reliability. The prevalence of specific intermolecular interactions, like hydrogen bonding or π-π stacking, reveals common structural motifs in organic luminogens. These insights deepen our understanding of solid-state luminescence principles and guide the design of next-generation materials with tailored optoelectronic properties.[62]

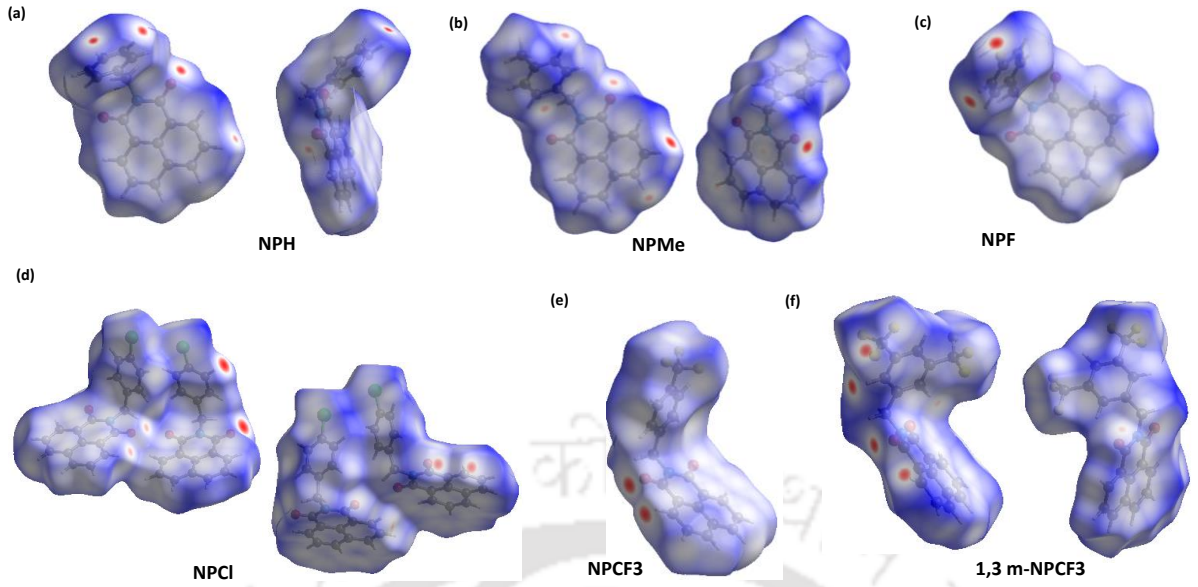

Figure 4.6 Hirshfield surface analysis of naphtalimide luminogens a) NPH (b) NPMe, (c) NPF, (d) NPCl, (e) $NPCF_3$, (f) 1,3 m-$NPCF_3$.

Table 4.3 Statistics of intermolecular interactions in Hirshfeld surface analysis of naphthalimide luminogens.

Luminogens	NPH	NPMe	NPF	NPCl	$NPCF_3$	1,3 m-$NPCF_3$
H-H	47.8%	50.4%	35.5%	37.5	26.8%	14.4%
C-H	10.6%	12.4%	12.0%	9.2%	10.4%	10.2%
O-H	8.4%	7.4%	7.3%	6.4%	5.9%	5.1%
C-O	0.4%	1%	1.1%	0.6%	1.3%	1.3%
C-C	15.1%	10.9%	12.1%	14.0%	9.8%	6.4%
H-F	-	-	6.7%	-	12.0%	15.1%
F-H	-	-	7.2%	-	12.9%	16.1%
F-F	-	-	0%	-	4.1%	10.6%
H-Cl	-	-	-	5.4%	-	-
Cl-H	-	-	-	7.4%	-	-
Cl-Cl	-	-	-	2.2%	-	-

4.3.4 Electrostatic maps analysis: Electrostatic map analysis is a computational technique that helps understand supramolecular interactions in organic luminogens by mapping electrostatic potential distributions within molecular structures. This understanding is crucial for adjusting solid-state properties like emission efficiency and colour tunability in organic luminogens, thereby enhancing their properties. Electrostatic map analysis helps identify key motifs like charge transfer pathways and electrostatic complementarity, influencing the spatial organization of molecules in the solid state. This approach allows precise control over molecular packing arrangements, enhancing luminogenic materials' performance and functionality for various optoelectronic applications. Electrostatic maps offer crucial insights into charge distribution within molecules, governing attraction, repulsion, and self-assembly in supramolecular interactions, contributing to the stability and properties of supramolecular networks.[63] An electrostatic surface potential (ESP) map was generated to visualize the charge distribution in naphthalimide crystals (**Figure 4.7a to 4.7f)**. The colour gradient from red to blue in ESP correlates to the varying intensities of the electrostatic potential energy values from negative to positive. A red region on the carbonyl oxygen indicates localized electron density, and the blue positive potential region represents electron deficient regions in naphthalimide derivatives. A significant difference in charge distribution in of the aromatic benzyl core is observed with the introduction of H, Me, F, Cl, CF_3 and 1,3 m-CF_3 in NPH, NPF, NPCl, NPCF_3 and 1,3 m-NPCF_3 respectively. It has played significant role in the electron distribution on this luminogen which consequently contributed to tuneable optical properties of these luminogens.

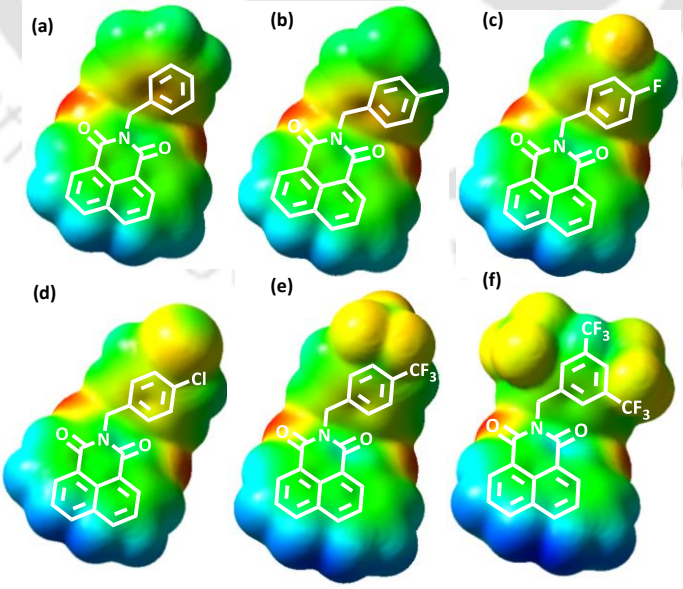

Figure 4.7 Electrostatic map analysis of naphtalimide luminogens a) NPH (b) NPMe, (c) NPF, (d) NPCl, (e) NPCF_3, (f) 1,3 m-NPCF_3.

4.3.4 Self-assembly: To investigate further into the morphological effect of different functional group and their self-assembly we studied the FESEM images of these naphthalimide luminogens in their aggregated state (f_w = 99.9%). We observed that the self-assembly of these morphologies change drastically. NPH exihibits rod like self-assembly, NPMe forms aggregated round shaped assembly, NPF, NPCl and $NPCF_3$ have some similarity in thin sticks like structures and NPCl and $NPCF_3$ demonstrate shown multiple growth contrasted to NPF The most notable leaf's self-assembly, demonstrated by 1,3 m-$NPCF_3$, has developed in two unique orientations, most likely due to the presence of two CF_3 groups in the meta locations of Benzyl group **(Figure 4.8a to 4.8f)**. The study reveals that the morphological diversity of naphthalimide luminogens is influenced by subtle structural variations. The self-assembly motifs, including rod-like, spherical, and stick-like structures, suggest intricate intermolecular interactions governed by factors like π-π stacking, hydrogen bonding, and van der Waals forces. This understanding of morphology-structure relationships enhances our understanding of molecular self-assembly and allows for targeted material property manipulation.[64,65]

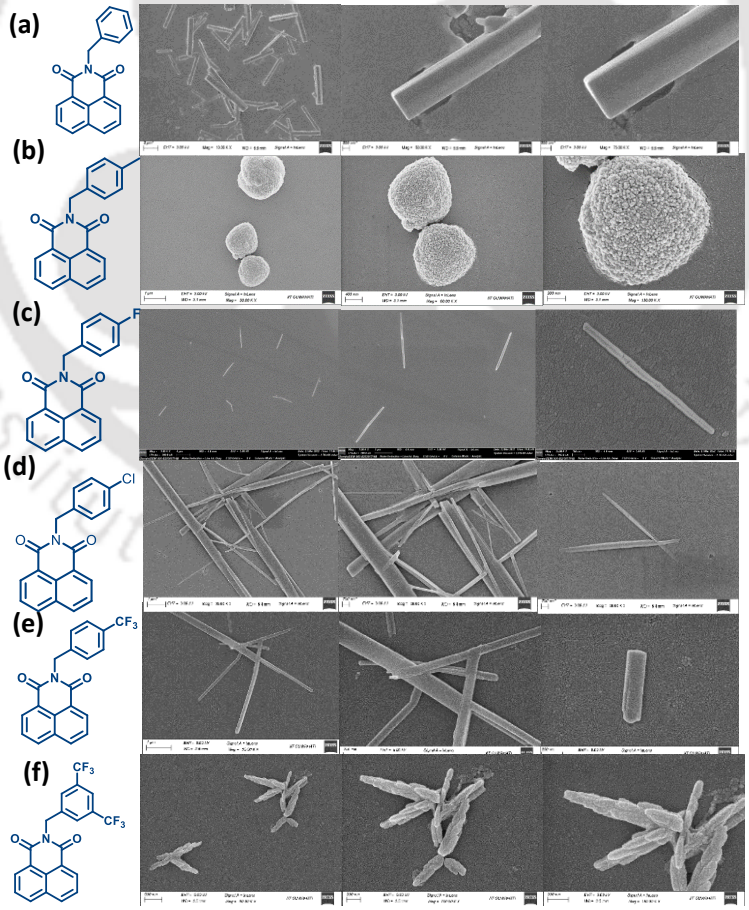

Figure 4.8 Molecular supramolecular self-assembly Macro-architecture of a) NPH (b) NPMe, (c) NPF, (d) NPCl, (e) $NPCF_3$, (f) 1,3 m-$NPCF_3$.

4.3.7 Theoretical Calculations: To gain more information about molecular orbital contribution in the overall luminescence and fluorescence lifetime and aggregation pattern we performed theoretical calculations TD-DFT in Gaussian 09 package.[32,33] Although benzyl is an electron donating core and naphthalimde is an electron accepting core, the electron donating and electron accepting properties of both cores are affected or influence by the functional groups including hydrogen, methyl, fluorine, chlorine, CF_3 and 1,3 m-CF_3. In compounds NPH, NPMe, NPF and NPCl, the naphthalimide core acts as an electron deficient core with the LUMO group located on it and benzyl group acts as an electron donating core with the HOMO or-bitals located on it. Both the $NPCF_3$ and 1,3 m-$NPCF_3$ exhibits HOMO and LUMO orbitals located solely on naphthalimide core. It indicates that benzyl core with CF_3 group and 1, 3 m-CF_3 group have become significantly electronegative preventing them to act as electron donating cores. This suggests that in NPH, NPMe, NPF, and NPCl there is TICT phenomenon due to clear separation of HOMO and LUMO due to sp^2 spacer group. Fluorescence emits from lowest singlet excited state, while performing TD-DFT we observed that from NPMe, NPF, NPCl, NPCF3, 1,3 m-$NPCF_3$, (except for NPH) S_1 state is going higher. it described the fluores-cence lifetime order which is highest for NPMe (35.62 ns) then decrease continuously to 1,3 m-$NPCF_3$.

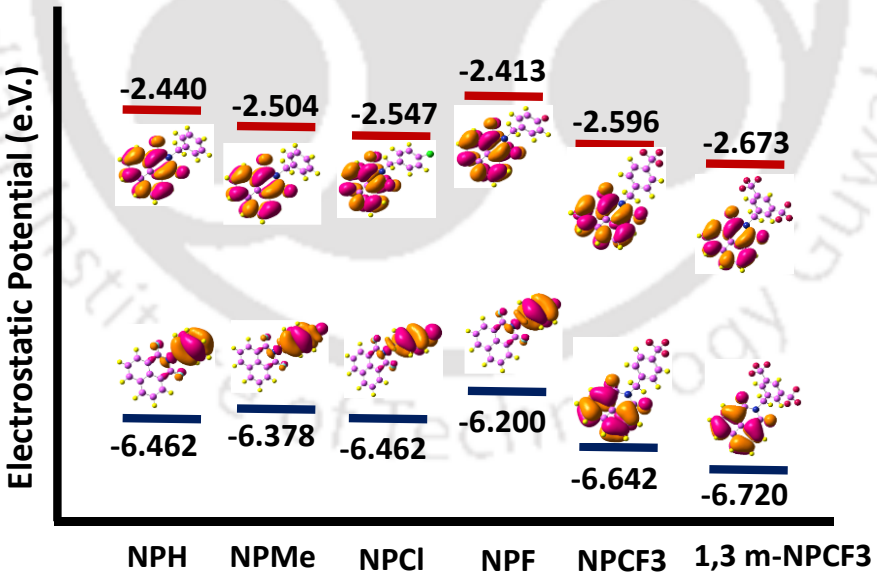

Figure 4.9 HOMO, LUMO values and molecular orbitals of a) NPH (b) NPMe, (c) NPF, (d) NPCl, (e) $NPCF_3$, (f) 1,3 m-$NPCF_3$.

4.4 Application

Supramolecular interactions in biological systems confer flexibility and are crucial for metabolic regulation. These interactions enable rapid and reversible association of molecules, facilitating diverse biochemical processes. The elucidation of these interactions between drugs and biomolecules remains an ongoing challenge, necessitating further exploration and refinement for better interpretation of recognition and binding. Supramolecular interactions are possible avenues for detecting viral and related biomolecules. By tailoring the self-assembly approach to the specific characteristics of virus proteins, researchers can design sophisticated detection platforms for applications in diagnostics, healthcare, and biosensing. The integration of microfluidics with molecular self-assembly yields advantages such as reduced sample volume, rapid analysis, and enhanced sensitivity.[66]

In the context of antiviral therapy, supramolecular nanomedicine has gained well reputation. Those nanomedicines exhibit characteristics like 'targeted delivery', improved bioavailability and reduced side effects. Viruses interact intricately with infected cells during replication. Supramolecular interactions can be exploiting those interaction and more efficient and safer antiviral agents can be developed. Functional supra-molecules can be designed to target various stages of viral infection including viral entry and replication. Supramolecules provide an avenue for developing drugs and combat infections.[67,68]

Japanese encephalitis (JE) is a resurging zoonotic disease, leading to high childhood mortality. It is a significant cause of endemic encephalitis in over 24 countries in the Western Pa-cific and Southeast Asia, resulting in 50,000 to 67,900 cases and 10,000 to 20,000 deaths annually, with a 30% fatality rate among affected individuals[69,70] This disease poses a major public health concern, affecting nearly half of the global popu-lation residing in endemic areas.[71] The worldwide burden of JE is estimated to be 709,000 disability-adjusted life years (DALYs),[72] leading to substantial economic losses due to the significant psychiatric and neurological complications that affect 30 to 50% of survivors.[73]

JEV falls under the family Flaviviridae. It is known that fla-viviruses cause many human diseases. JEV is an enveloped virus around 50 nm in diameter with a positive sense, single stranded RNA, and genome of around 11 kb in length.[74] The genome is having capsid made by capsid (C) protein which is enclosed by lipid bilayer derived from host. The genome pos-sesses an open reading frame (ORF) which encodes for a single polyprotein which upon enzymatic

cleavage by viral prote-ases divides into 3 structural proteins - capsid (C), membrane precursor (prM), envelope (E) and 7 non-structural proteins as NS1, NS2-A, NS2-B, NS3, NS4-A, NS4-B and NS5, post-translationally. The ORF on the margins is flanked by 50 and 30 non-coding regions, which act as cis acting elements for viral replication, transcription, and translation.[75] JEV RNA genome is capped by m7GpppAmp at 5'-terminal and absence of a poly (A) tail at 3'-terminal.[76]

Among non-structural proteins, NS1 is a highly conserved protein with a molecular weight ranging from 46 to 55 kDa, depending on the extent of glycosylation.[77] Glycosylation of NS1 is essential for efficient secretion, virulence, and viral replication.[78] In this study, we purified viral protein NS1 and allowed it to interact with naphthalimide luminogens. To deepen our understanding of NS1 protein, its self-assembly and interaction study is crucial to develop more accurate di-agnostic method, antiviral techniques and vaccines. We have studied the interaction of our six different naphthalimide luminogen with NS1 protein and found interesting results. Out of six luminogens only 1,3 m-NPCF$_3$ has showed interaction with the NS1 protein. Fluorescence response of 20 µM NPH, NPMe, NPF, NPCl, NPCF$_3$ and 1,3 m-NPCF$_3$ with addition of 1 µM (NS1) has been studied. It was observed that only 1,3 m-NPCF$_3$ has drastically quenched fluorescence and other luminogens has not shown any interactions. The results revealed significant observations, shedding light on the unique nature of this interaction between the protein and the luminogens. Further biological significance of the interaction is an area of active investigations. **(Figure 4.10a to 4.10c)**

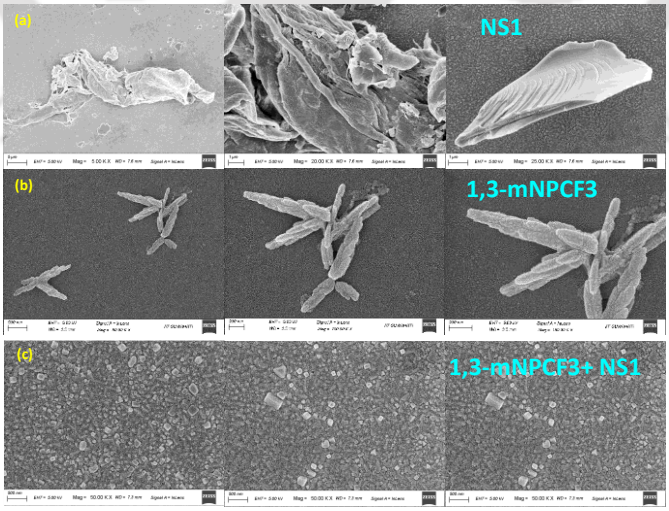

Figure 4.10 a) FESEM images of Molecular supramolecular self-assembly of a) NS1 protein (f_w = 99.9%) b) 1,3 m-NPCF3 (f_w = 99.9%) c) after NS1 and 1,3 m-NPCF$_3$ interaction. (f_w = 99.9%).

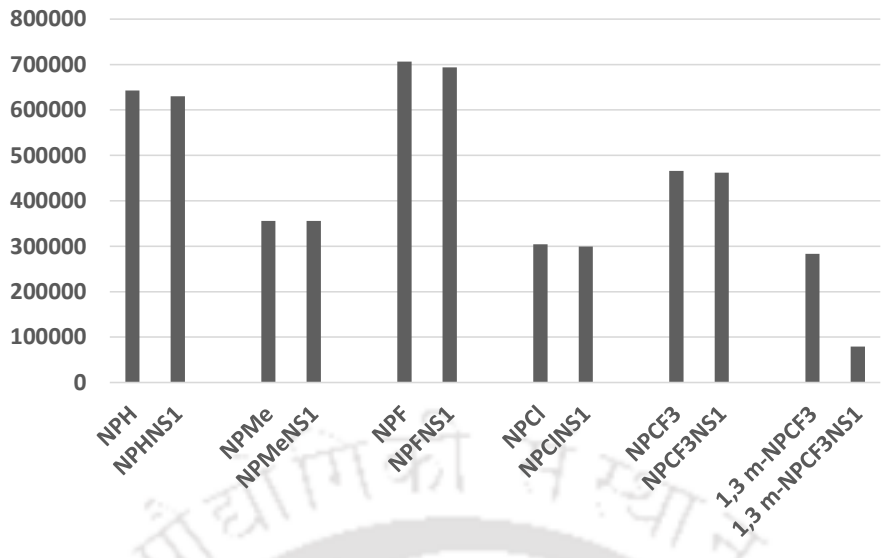

Figure 4.10 Fluorescence response of naphthalimide luminogens before and after the exposer of NS1 protein. X axis: PL intensity (a.u.) Y axis different luminogens before and after the exposer with NS1 protein.

4.5 Conclusion

In conclusion, this research has provided a comprehensive exploration of the supramolecular interactions of naphthalimide luminogens, emphasizing the significance of a detailed analysis of their aggregation patterns using single crystal X-ray diffraction (XRD). The study has successfully revealed unprecedented aggregation behaviours marked by slip angles exceeding 90 degrees, challenging traditional classifications into H or J aggregates. This advancement significantly enriches our understanding of the unique assembly patterns inherent in naphthalimide luminogens, offering valuable in-sights into their structural intricacies. Moreover, the extension of this investigation to probe the interactions between these luminogens and the NS1 protein, a pivotal component in the Japanese Encephalitis virus, has yielded noteworthy out-comes. The identification of exceptional luminescence quenching, particularly demonstrated by the luminogen 1,3 m-NPCF$_3$ upon interaction with NS1, suggests a promising avenue for developing innovative strategies to combat the Japanese Encephalitis virus. This discovery not only contributes to the field of materials science by elucidating the supramolecular behaviour of naphthalimide luminogens but also holds potential applications in targeted interactions with viral proteins, laying the groundwork for future advancements in antiviral research. In summary, this research bridges the gap between fundamental molecular

insights and practical applications, paving the way for a new era of advancements at the intersection of materials science and virology.

References

1. Forrest, S. R.; Thompson, M. E. Introduction: Organic Electronics and Optoelectronics. *Chem. Rev.* **2007**, *107* (4), 923–925. https://doi.org/10.1021/cr0501590.
2. Zhou, L.; Lv, F.; Liu, L.; Wang, S. Water-Soluble Conju-gated Organic Molecules as Optical and Electrochemical Materials for Interdisciplinary Biological Applications. *Acc. Chem. Res.* **2019**, *52* (11), 3211–3222. https://doi.org/10.1021/acs.accounts.9b00427.
3. Dong, S.; Li, Z. Recent Progress in Open-Shell Organic Conjugated Materials and Their Aggregated States. *J. Mater. Chem. C* **2022**, *10* (7), 2431–2449. https://doi.org/10.1039/d1tc04598a.
4. Li, Q.; Li, Z. Molecular Packing: Another Key Point for the Performance of Organic and Polymeric Optoelectronic Materials. *Acc. Chem. Res.* **2020**, *53* (4), 962–973. https://doi.org/10.1021/acs.accounts.0c00060.
5. Hestand, N. J.; Spano, F. C. Expanded Theory of H- and J-Molecular Aggregates: The Effects of Vibronic Coupling and Inter-molecular Charge Transfer. *Chem. Rev.* **2018**, *118* (15), 7069–7163. https://doi.org/10.1021/acs.chemrev.7b00581.
6. Yang, J.; Fang, M.; Li, Z. Organic Luminescent Materials: The Concentration on Aggregates from Aggregation-induced Emission. *Aggregate* **2020**, *1* (1), 6–18. https://doi.org/10.1002/agt2.2.
7. Kokado, K.; Sada, K. Consideration of Molecular Structure in the Excited State to Design New Luminogens with Aggregation-induced Emission. *Angew. Chem. Int. Ed* **2019**, *131* (26), 8724–8731. https://doi.org/10.1002/ange.201814462.
8. Liao, Q.; Li, Q.; Li, Z. The Key Role of Molecular Packing in Luminescence Property: From Adjacent Molecules to Molecular Aggregates. *Adv. Mater.* **2023**. https://doi.org/10.1002/adma.202306617.
9. Kasha, M.; Rawls, H. R.; Ashraf El-Bayoumi, M. The Exciton Model in Molecular Spectroscopy. *Pure Appl. Chem.* **1965**, *11* (3–4), 371–392. https://doi.org/10.1351/pac196511030371.
10. Kasha, M. Energy Transfer Mechanisms and the Molecular Exciton Model for Molecular Aggregates. *Radiat. Res.* **1963**, *20*, 55–70.

11. McRae, E. G.; Kasha, M. Enhancement of Phosphorescence Ability upon Aggregation of Dye Molecules. *J. Chem. Phys.* **1958**, *28* (4), 721–722. https://doi.org/10.1063/1.1744225.
12. Priimagi, A.; Cavallo, G.; Metrangolo, P.; Resnati, G. The Halogen Bond in the Design of Functional Supramolecular Materials: Recent Advances. *Acc. Chem. Res.* **2013**, *46* (11), 2686–2695. https://doi.org/10.1021/ar400103r.
13. Halogen Bonding: Fundamentals and Applications; Metran-golo, P., Resnati, G., Eds.; Springer: Berlin, Germany, 2010.
14. Priimagi, A.; Cavallo, G.; Metrangolo, P.; Resnati, G. The Halogen Bond in the Design of Functional Supramolecular Materials: Recent Advances. *Acc. Chem. Res.* **2013**, *46* (11), 2686–2695. https://doi.org/10.1021/ar400103r
15. Yoshida, Y.; Tanigaki, N.; Yase, K.; Hotta, S. Color-Tunable Highly Polarized Emissions from Uniaxially Aligned Thin Films of Thiophene/Phenylene Co-Oligomers. *Adv. Mater.* **2000**, *12* (21), 1587–1591. https://doi.org/10.1002/1521-4095(200011)12:21<1587::aid-adma1587>3.0.co;2-s
16. Tang, S.; Yang, T.; Zhao, Z.; Zhu, T.; Zhang, Q.; Hou, W.; Yuan, W. Z. Nonconventional Luminophores: Characteristics, Advancements and Perspectives. *Chem. Soc. Rev.* **2021**, *50* (22), 12616–12655. https://doi.org/10.1039/d0cs01087a.
17. Stupp, S. I.; Palmer, L. C. Supramolecular Chemistry and Self-Assembly in Organic Materials Design. *Chem. Mater.* **2014**, *26* (1), 507–518. https://doi.org/10.1021/cm403028b.
18. Wang, D.; Tang, B. Z. Aggregation-Induced Emission Luminogens for Activity-Based Sensing. *Acc. Chem. Res.* **2019**, *52* (9), 2559–2570. https://doi.org/10.1021/acs.accounts.9b00305.
19. Jiang, G.; Yu, J.; Wang, J.; Tang, B. Z. Ion−π Interactions for Constructing Organic Luminescent Materials: Special Issue: Emerging Investigators. *Aggregate* **2022**, *3* (6). https://doi.org/10.1002/agt2.285.
20. Song, N.; Zhang, Z.; Liu, P.; Yang, Y.-W.; Wang, L.; Wang, D.; Tang, B. Z. Nanomaterials with Supramolecular Assembly Based on AIE Luminogens for Theranostic Applications. *Adv. Mater.* **2020**, *32* (49). https://doi.org/10.1002/adma.202004208.
21. Zhao, W.; He, Z.; Tang, B. Z. Room-Temperature Phosphorescence from Organic Aggregates. *Nat. Rev. Mater.* **2020**, *5* (12), 869–885. https://doi.org/10.1038/s41578-020-0223-z.

22. Xu, W.; Yu, Y.; Ji, X.; Zhao, H.; Chen, J.; Fu, Y.; Cao, H.; He, Q.; Cheng, J. Self-stabilized Amorphous Organic Materials with Room-temperature Phosphorescence. *Angew. Chem. Int. Ed* **2019**, *131* (45), 16164–16168. https://doi.org/10.1002/ange.201906881.

23. Zhang, J.; Zhang, X.; Xiao, H.; Li, G.; Liu, Y.; Li, C.; Huang, H.; Chen, X.; Bo, Z. 1,8-Naphthalimide-Based Planar Small Molecular Acceptor for Organic Solar Cells. ACS *Appl. Mater. Inter-faces* **2016**, *8* (8), 5475–5483. https://doi.org/10.1021/acsami.5b10211.

24. Narang, K.; Iyer, P. K. Molecular Engineering of Naph-thalimide Methylcyclohexane Luminogen: Unraveling J*-Aggregation Pattern and Sensing Melamine in Aqueous Media. *CCS Chem* **2023**, 6, 1–9. https://doi.org/10.31635/ccschem.023.202303123.

25. Meher, N.; Bidkar, A. P.; Barman, D.; Ghosh, S. S.; Iyer, P. K. A Conformational Tweak for Enhanced Cellular Internalization, Photobleaching Resistance and Prolonged Imaging Efficacy. *Chem. Commun.* **2020**, *56* (94), 14861–14864. https://doi.org/10.1039/d0cc05557c.

26. Cai, Q.; Musiol, R.; Shubhra, Q. T. H. Advancing Fluorescence Imaging with Dual-Mode AIE Nanoparticles. *Chem* **2024**, *10* (2), 429–432. https://doi.org/10.1016/j.chempr.2024.01.010.

27. Xu, S.; Liu, B. High Exciton Utilization of 1D Molecular Column with High Packing Energy Formed by Folded π-Molecules. *J. Am. Chem. Soc.* **2022**, *144* (39), 17897–17904. https://doi.org/10.1021/jacs.2c06838.

28. Hecht, M.; Würthner, F. Supramolecularly Engineered J-Aggregates Based on Perylene Bisimide Dyes. *Acc. Chem. Res.* **2021**, *54* (3), 642–653. https://doi.org/10.1021/acs.accounts.0c00590.

29. Nitti, A.; Pasini, D. Aggregation-induced Circularly Polarized Luminescence: Chiral Organic Materials for Emerging Optical Technologies. *Adv. Mater.* **2020**, *32* (41). https://doi.org/10.1002/adma.201908021.

30. Xu, J.; Yang, C.; Bi, S.; Wang, W.; He, Y.; Wu, D.; Liang, Q.; Wang, X.; Zhang, F. Vinylene-linked Covalent Organic Frameworks (COFs) with Symmetry-tuned Polarity and Photocatalytic Activity. *Angew. Chem. Int. Ed* **2020**, *132* (52), 24053–24061. https://doi.org/10.1002/ange.202011852.

31. Meher, N.; Iyer, P. K. Pendant Chain Engineering to Fine-Tune the Nanomorphologies and Solid State Luminescence of Naphthalimide AIEEgens:

Application to Phenolic Nitro-Explosive Detection in Water. *Nanoscale* **2017**, *9* (22), 7674–7685. https://doi.org/10.1039/c7nr02174g.

32. Becke, A. D. Density-Functional Thermochemistry. I. The Effect of the Exchange-Only Gradient Correction. *J. Chem. Phys.* **1992**, *96* (3), 2155–2160. https://doi.org/10.1063/1.462066.
33. 31. Frisch, M. J.; Trucks, G. W.; Schlegel, H. B.; Scuseria, G. E.; Robb, M. A.; Cheeseman, J. R.; Scalmani, G.; Barone, V.; Petersson, G. A.; Nakatsuji, H.; Li, X.; Caricato, M.; Marenich, A. V.; Bloino, J.; Janesko, B. G.; Gomperts, R.; Mennucci, B.; Hratchian, H. P.; Ortiz, J. V.; Izmaylov, A. F.; Sonnenberg, J. L.; Williams-Young, D.; Ding, F.; Lipparini, F.; Egidi, F.; Goings, J.; Peng, B.; Petrone, A.; Henderson, T.; Ranasinghe, D.; Zakrzewski, V. G.; Gao, J.; Rega, N.; Zheng, G.; Liang, W.; Hada, M.; Ehara, M.; Toyota, K.; Fukuda, R.; Hasegawa, J.; Ishida, M.; Nakajima, T.; Honda, Y.; Kitao, O.; Nakai, H.; Vreven, T.; Throssell, K.; Montgomery, J. A.; Peralta, J. E.; Ogliaro, F.; Bearpark R Kobayashi, M. J.; Normand, J.; Raghavachari, K.; Rendell, A. P.; Burant, J. C.; Iyengar, S. S.; Tomasi, J.; Cossi, M.; Millam, J. M.; Klene, M.; Adamo, C.; Cammi, R.; Ochterski, J. W.; Martin, R. L.; Morokuma, K.; Farkas, O.; Foresman, J. B.; Fox, D. J. Gaussian 16; Heyd, J. J., Brothers, E. N., Kudin, K. N., Staroverov, V. N., Keith, T. A., Eds.; Gaussian, Inc: Wallingford CT, 2016.
34. Campbell, G.; Hills, S.; Fischer, M.; Jacobson, J.; Hoke, C.; Hombach, J.; Marfin, A.; Solomon, T.; Tsai, T.; Tsui, V.; Gins-burg, A. Estimated Global Incidence of Japanese Encephalitis: Bull. *World Health Organ.* **2011**, *89* (10), 766–774. https://doi.org/10.2471/blt.10.085233.
35. Zhang, T.; Chen, Z.; Xie, L.; Xu, R.; Chen, L.; Jia, T.; Shi, W.; Wang, Y.; Song, Y.; Han, Q.; Xia, X.; Yuan, T.; Zhang, J. A Fusion Protein of Vimentin with Fc Fragment Inhibits Japanese Encephalitis Virus Replication. *Front. Vet. Sci.* **2024**, *11*. https://doi.org/10.3389/fvets.2024.1368725.
36. Egorov, A.; Brandt, S.; Sereinig, S.; Romanova, J.; Ferko, B.; Katinger, D.; Grassauer, A.; Alexandrova, G.; Katinger, H.; Muster, T. Transfectant Influenza A Viruses with Long Deletions in the NS1 Protein Grow Efficiently in Vero Cells. *J. Virol.* **1998**, *72* (8), 6437–6441. https://doi.org/10.1128/jvi.72.8.6437-6441.1998.
37. Huang, J.-L.; Huang, J.-H.; Shyu, R.-H.; Teng, C.-W.; Lin, Y.-L.; Kuo, M.; Yao, C.-W.; Shaio, M.-F. High-level Expression of Recombinant Dengue Viral NS-1

Protein and Its Potential Use as a Diagnostic Antigen. *J. Med. Virol.* **2001**, *65* (3), 553–560. https://doi.org/10.1002/jmv.2072.abs.

38. Larentis, A. L.; Nicolau, J. F. M. Q.; Esteves, G. dos S.; Vareschini, D. T.; de Almeida, F. V. R.; dos Reis, M. G.; Galler, R.; Medeiros, M. A. Evaluation of Pre-Induction Temperature, Cell Growth at Induction and IPTG Concentration on the Expression of a Leptospiral Protein in E. Coli Using Shaking Flasks and Microbioreactor. *BMC Res. Notes* **2014**, *7* (1). https://doi.org/10.1186/1756-0500-7-671.
39. Teng, A. C. T.; Tavassoli, M.; Shrestha, S.; Marks, R. M.; McFadden, M. J.; Evagelou, S. L.; Lindsay, K.; Vandenbelt, A.; Li, W.; Ivakine, E.; Cohn, R.; Santerre, J. P.; Gramolini, A. O. An Efficient and Cost-Effective Purification Protocol for Staphylococcus Aureus Cas9 Nuclease. *STAR Protoc.* **2023**, *4* (1), 101933. https://doi.org/10.1016/j.xpro.2022.101933.
40. Wolff, T.; O'Neill, R. E.; Palese, P. NS1-Binding Protein (NS1-BP): A Novel Human Protein That Interacts with the Influenza A Virus Nonstructural NS1 Protein Is Relocalized in the Nuclei of Infected Cells. *J. Virol.* **1998**, *72* (9), 7170–7180. https://doi.org/10.1128/jvi.72.9.7170-7180.1998.
41. Nemeroff, M. E.; Qian, X.-Y.; Krug, R. M. The Influenza Virus NS1 Protein Forms Multimers in Vitro and in Vivo. *Virology* **1995**, *212* (2), 422–428. https://doi.org/10.1006/viro.1995.1499.
42. Segura, C.; Ormazabal-Toledo, R.; García-Beltrán, O.; Squeo, B. M.; Bachmann, C.; Flores, C.; Osorio-Román, I. O. Photophysical Analysis of aggregation-Induced Emission (AIE) Luminogens Based on Triphenylamine and Thiophene: Insights into Emission Behavior in Solution and PMMA Films. *Chemistry* **2024**, *30* (10). https://doi.org/10.1002/chem.202302940.
43. Wang, K.; Xie, Y.; Liu, M.; Tao, W.; Zhang, H.; Huang, M.; You, J.; Liu, Y.; Li, Y.; Li, Z.; Dong, Y. Q. High-contrast Polymorphic Luminogen Formed through Effect of Tiny Differences in Intermolecular Interactions on the Intramolecular Charge Transfer Process. *Adv. Opt. Mater.* **2020**, *8* (16). https://doi.org/10.1002/adom.202000436.
44. Ma, S.; Du, S.; Pan, G.; Dai, S.; Xu, B.; Tian, W. Organic Molecular Aggregates: From Aggregation Structure to Emission Property. *Aggregate* **2021**, *2* (4). https://doi.org/10.1002/agt2.96.

45. Liu, W.; Li, S.; Xie, Z.; Huang, K.; Yan, K.; Zhao, Y.; Redshaw, C.; Feng, X.; Tang, B. Z. Molecular Engineering toward Broad Color-tunable Emission of Pyrene-based Aggregation-induced Emission Luminogens. *Adv. Opt. Mater.* **2024**. https://doi.org/10.1002/adom.202400301.

46. Feng, X.; Wang, X.; Redshaw, C.; Tang, B. Z. Aggregation Behaviour of Pyrene-Based Luminescent Materials, from Molecular Design and Optical Properties to Application. *Chem. Soc. Rev.* **2023**, *52* (19), 6715–6753. https://doi.org/10.1039/d3cs00251a.

47. Yu, M.; Huang, R.; Guo, J.; Zhao, Z.; Tang, B. Z. Promising Applications of Aggregation-Induced Emission Luminogens in Organic Optoelectronic Devices. *Photonix* **2020**, *1* (1). https://doi.org/10.1186/s43074-020-00012-y.

48. Zhang, X.; Liu, H.; Zhuang, G.; Yang, S.; Du, P. An Unexpected Dual-Emissive Luminogen with Tunable Aggregation-Induced Emission and Enhanced Chiroptical Property. *Nat. Commun.* **2022**, *13* (1). https://doi.org/10.1038/s41467-022-31281-9.

49. Geng, J.; Zhu, Z.; Qin, W.; Ma, L.; Hu, Y.; Gurzadyan, G. G.; Tang, B. Z.; Liu, B. Near-Infrared Fluorescence Amplified Organic Nanoparticles with Aggregation-Induced Emission Characteristics for in Vivo Imaging. *Nanoscale* **2014**, *6* (2), 939–945. https://doi.org/10.1039/c3nr04243j.

50. Chen, B.; Huang, W.; Su, H.; Miao, H.; Zhang, X.; Zhang, G. An Unexpected Chromophore–Solvent Reaction Leads to Bicomponent Aggregation-induced Phosphorescence. *Angew. Chem. Int. Ed.* **2020**, *59* (25), 10023–10026. https://doi.org/10.1002/anie.202000865.

51. Eder, T.; Vogelsang, J.; Bange, S.; Remmerssen, K.; Schmitz, D.; Jester, S.-S.; Keller, T. J.; Höger, S.; Lupton, J. M. Interplay between J- and H-type Coupling in Aggregates of Π-conjugated Polymers: A Single-molecule Perspective. *Angew. Chem. Int. Ed.* **2019**, *58* (52), 18898–18902. https://doi.org/10.1002/anie.201912374.

52. Li, H.; Lv, L.; Yuan, K.; Pan, S.; Li, Z. Understanding H-Aggregates Crystallization Induced Emissive Behavior: Insights from Theory. *Sci. Rep.* **2023**, *13* (1). https://doi.org/10.1038/s41598-023-39605-5.

53. Cao, Z.; Tolba, S. A.; Li, Z.; Mason, G. T.; Wang, Y.; Do, C.; Rondeau-Gagné, S.; Xia, W.; Gu, X. Molecular Structure and Conformational Design of Donor-acceptor

Conjugated Polymers to Enable Predictable Optoelectronic Property. *Adv. Mater.* **2023**, *35* (41). https://doi.org/10.1002/adma.202302178.

54. Xu, J.; Huang, M.; Pang, H.; Weng, Z.; Hu, G.; Zhang, S.; Yang, Q.; Wu, Q. C─H···π Interaction Induced H-aggregates for Wide Range Water Content Detection in Organic Solvents. *Aggregate* **2024**. https://doi.org/10.1002/agt2.546.
55. Eder, T.; Stangl, T.; Gmelch, M.; Remmerssen, K.; Laux, D.; Höger, S.; Lupton, J. M.; Vogelsang, J. Switching between H- and J-Type Electronic Coupling in Single Conjugated Polymer Aggregates. *Nat. Commun.* **2017**, *8* (1). https://doi.org/10.1038/s41467-017-01773-0.
56. Zuo, Y.; Liu, J.; Li, P.; Li, K.; Lam, J. W. Y.; Wu, D.; Tang, B. Z. Full-Color-Tunable AIE Luminogens for 4D Code, Security Patterns, and Multicolor LEDs. *Cell Rep. Phys. Sci.* **2023**, *4* (1), 101202. https://doi.org/10.1016/j.xcrp.2022.101202.
57. Hestand, N. J.; Spano, F. C. Molecular Aggregate Photophysics beyond the Kasha Model: Novel Design Principles for Organic Materials. *Acc. Chem. Res.* **2017**, *50* (2), 341–350. https://doi.org/10.1021/acs.accounts.6b00576.
58. Deng, X.; Yu, X.; Xiao, J.; Zhang, Q. Our Research Progress in Heteroaggregation and Homoaggregation of Organic Π-conjugated Systems. *Aggregate* **2021**, *2* (3). https://doi.org/10.1002/agt2.35.
59. Cai, K.; Xie, J.; Zhang, D.; Shi, W.; Yan, Q.; Zhao, D. Concurrent Cooperative J-Aggregates and Anticooperative H-Aggregates. *J. Am. Chem. Soc.* **2018**, *140* (17), 5764–5773. https://doi.org/10.1021/jacs.8b01463.
60. Li, H.; Lv, L.; Yuan, K.; Pan, S.; Li, Z. Understanding H-Aggregates Crystallization Induced Emissive Behavior: Insights from Theory. *Sci. Rep.* **2023**, *13* (1). https://doi.org/10.1038/s41598-023-39605-5.
61. Spackman, P. R.; Turner, M. J.; McKinnon, J. J.; Wolff, S. K.; Grimwood, D. J.; Jayatilaka, D.; Spackman, M. A. CrystalExplorer: A Program for Hirshfeld Surface Analysis, Visualization and Quantitative Analysis of Molecular Crystals. *J. Appl. Crystallogr.* **2021**, *54* (3), 1006–1011. https://doi.org/10.1107/s1600576721002910.
62. Mukherjee, S.; Thilagar, P. Fine-Tuning Solid-State Luminescence in NPIs (1,8-Naphthalimides): Impact of the Molecular Environment and Cumulative Interactions. *Phys. Chem. Chem. Phys.* **2014**, *16* (38), 20866–20877. https://doi.org/10.1039/c4cp02071e.

63. John, A. T.; Narayanasamy, A.; Sudhakaran, K. P.; Hariharan, M. Resonance-Assisted Hydrogen Bonding and π–π Stacking Modulates the Charge Transfer Coupling in Crystalline Naphthothiazoles. *Cryst. Growth Des.* **2022**, *22* (9), 5686–5693. https://doi.org/10.1021/acs.cgd.2c00798.

64. Li, J.; Wang, J.; Li, H.; Song, N.; Wang, D.; Tang, B. Z. Supramolecular Materials Based on AIE Luminogens (AIEgens): Construction and Applications. *Chem. Soc. Rev.* **2020**, *49* (4), 1144–1172. https://doi.org/10.1039/c9cs00495e.

65. Huang, Z.; Ma, X. Tailoring Tunable Luminescence via Supramolecular Assembly Strategies. *Cell Rep. Phys. Sci.* **2020**, *1* (8), 100167. https://doi.org/10.1016/j.xcrp.2020.100167.

66. Lehn, J.-M. Perspectives in Supramolecular Chemistry—from Molecular Recognition towards Molecular Information Processing and Self-organization. *Angew. Chem., Int. Ed.* **1990**, *29* (11), 1304–1319. https://doi.org/10.1002/anie.199013041.

67. Ma, X.; Zhao, Y. Biomedical Applications of Supramolecular Systems Based on Host–Guest Interactions. *Chem. Rev.* **2015**, *115* (15), 7794–7839. https://doi.org/10.1021/cr500392w.

68. Barman, D.; Narang, K.; Parui, R.; Zehra, N.; Khatun, M. N.; Adil, L. R.; Iyer, P. K. Review on Recent Trends and Prospects in Π-conjugated Luminescent Aggregates for Biomedical Applications. *Aggregate* **2022**, *3* (5). https://doi.org/10.1002/agt2.172.

69. Campbell, G.; Hills, S.; Fischer, M.; Jacobson, J.; Hoke, C.; Hombach, J.; Marfin, A.; Solomon, T.; Tsai, T.; Tsui, V.; Ginsburg, A. Estimated Global Incidence of Japanese Encephalitis: *Bull. World Health Organ.* **2011**, *89* (10), 766–774. https://doi.org/10.2471/blt.10.085233.

70. Kulkarni, R.; Sapkal, G. N.; Kaushal, H.; Mourya, D. T. Japanese Encephalitis: A Brief Review on Indian Perspectives. *Open Virol. J.* **2018**, *12* (1), 121–130. https://doi.org/10.2174/1874357901812010121.

71. Ghosh, D.; Basu, A. Japanese Encephalitis—A Pathological and Clinical Perspective. *PLoS Negl. Trop. Dis.* **2009**, *3* (9), e437. https://doi.org/10.1371/journal.pntd.0000437.

72. Mathers, C. D.; Ezzati, M.; Lopez, A. D. Measuring the Burden of Neglected Tropical Diseases: The Global Burden of Disease Framework. *PLoS Negl. Trop. Dis.* **2007**, *1* (2), e114. https://doi.org/10.1371/journal.pntd.0000114.

73. Fischer, M.; Hills, S.; Staples, E.; Johnson, B.; Yaich, M.; Solomon, T. Japanese Encephalitis Prevention and Control: Advances, Challenges, and New Initiatives. In Emerging Infections 8; ASM Press: Washington, DC, USA, 2014; pp 93–124.

74. Unni, S. K.; Růžek, D.; Chhatbar, C.; Mishra, R.; Johri, M. K.; Singh, S. K. Japanese Encephalitis Virus: From Genome to Infec-tome. *Microbes Infect.* **2011**, *13* (4), 312–321. https://doi.org/10.1016/j.micinf.2011.01.002.

75. Winkler, G.; Randolph, V. B.; Cleaves, G. R.; Ryan, T. E.; Stollar, V. Evidence That the Mature Form of the Flavivirus Non-structural Protein NS1 Is a Dimer. *Virology* **1988**, *162* (1), 187–196. https://doi.org/10.1016/0042-6822(88)90408-4.

76. Pryor, M. J.; Wright, P. J. Glycosylation Mutants of Den-gue Virus NS1 Protein. *J. Gen. Virol.* **1994**, *75* (5), 1183–1187. https://doi.org/10.1099/0022-1317-75-5-1183.

77. Hills, S. L.; Walter, E. B.; Atmar, R. L.; Fischer, M.; Wal-ter, E., Jr; Atmar, R. L.; Barnett, E.; Barrett, A.; Bocchini, J. A.; Chen, L.; Deussing, E.; Fink, D.; Holbrook, M.; Levin, M.; Marfin, A.; Meissner, C.; Schechter, R.; Shlim, D.; Wilson, M.; Fischer, M.; Staples, J. E.; Waterman, S.; Gershman, M.; Hyde, T.; McNeil, M. M.; Hills, S. L.; ACIP Japanese Encephalitis Vaccine Work Group. Japanese Encephalitis Vaccine: Recommendations of the Advisory Committee on Immunization Practices. *MMWR Recomm. Rep.* **2019**, *68* (2), 1–33. https://doi.org/10.15585/mmwr.rr6802a1.

78. Rastogi, M.; Sharma, N.; Singh, S. K. Flavivirus NS1: A Multifaceted Enigmatic Viral Protein. *Virol. J.* **2016**, *13* (1). https://doi.org/10.1186/s12985-016-0590-7.

Appendix

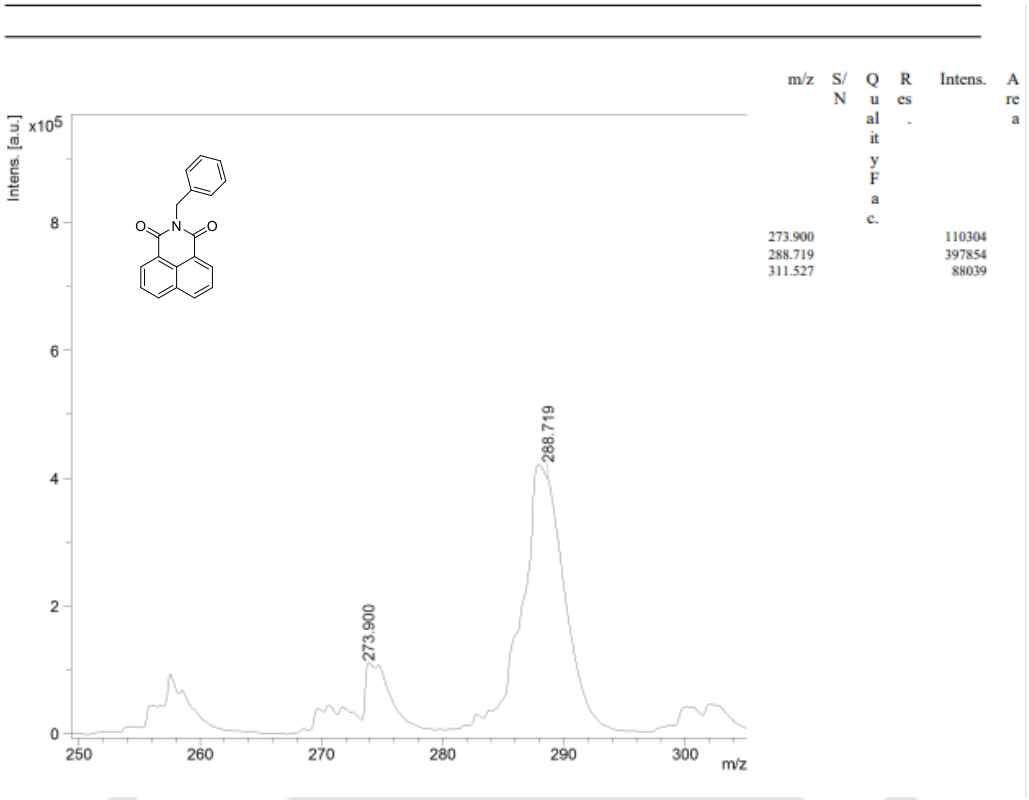

Figure A4.1 MALDI spectra of NPH.

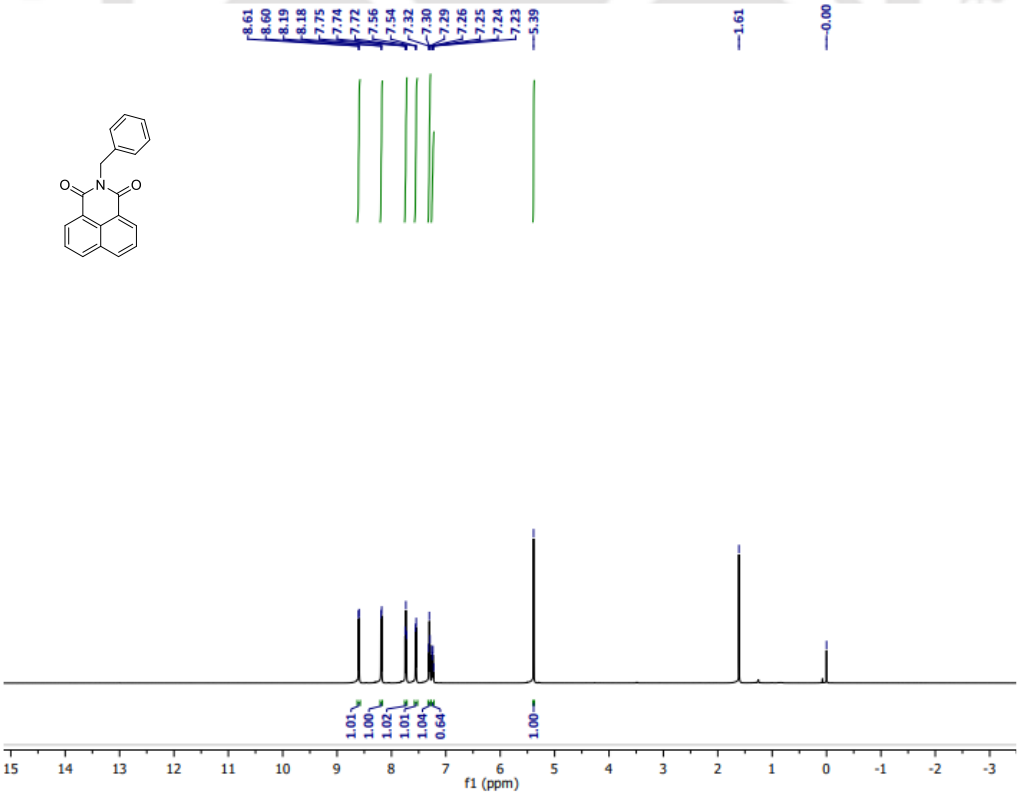

Figure A4.2 Proton NMR spectra of NPH.

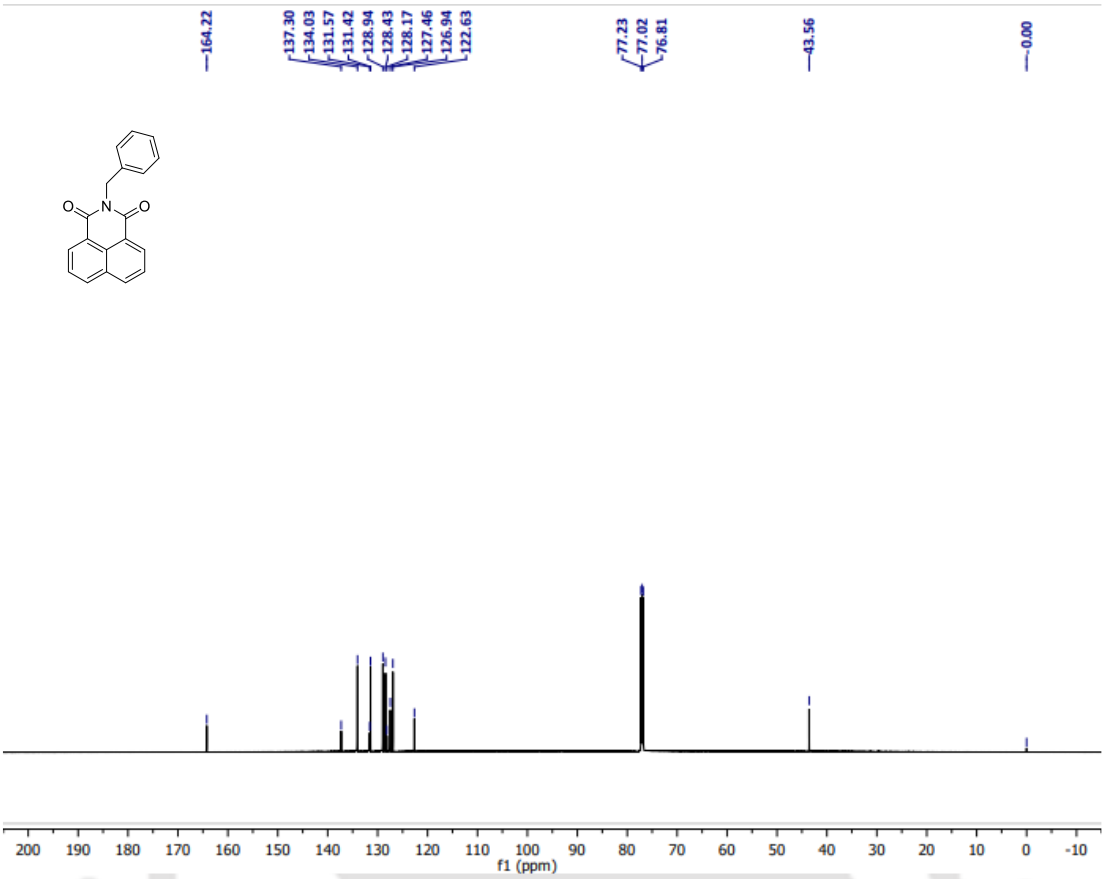

Figure A4.3 ^{13}C NMR spectra of NPH.

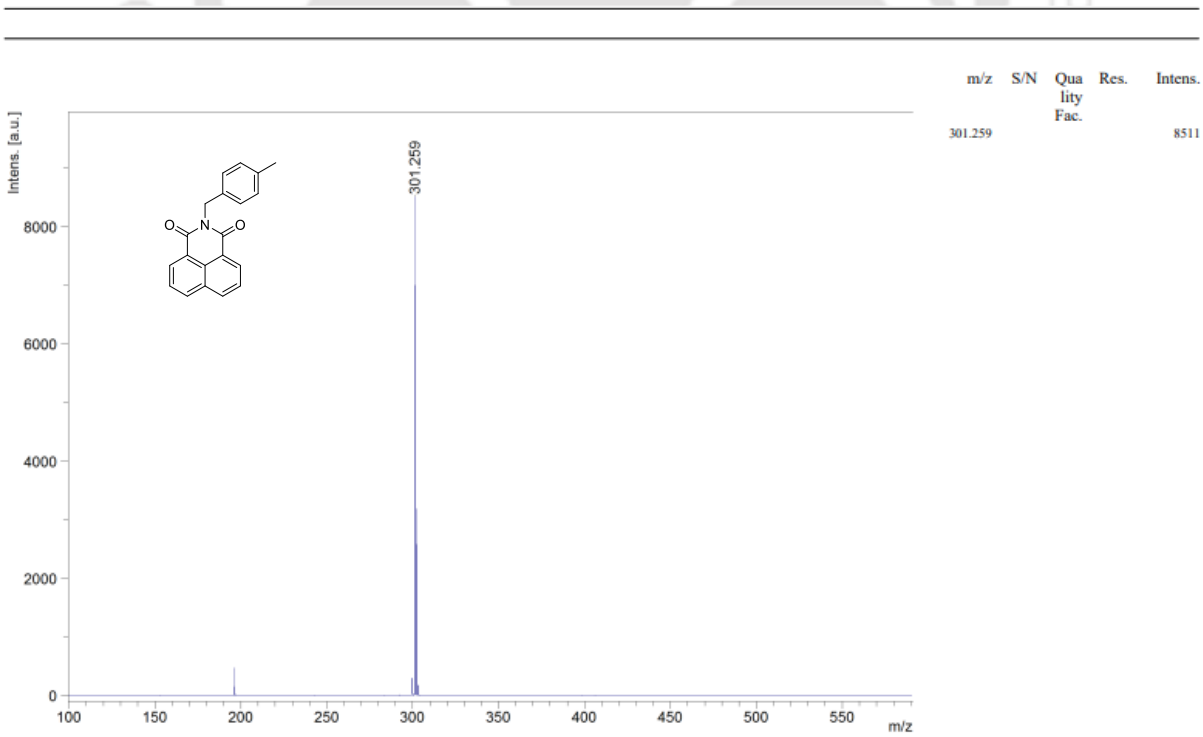

Figure A4.4 MALDI spectra of NPMe.

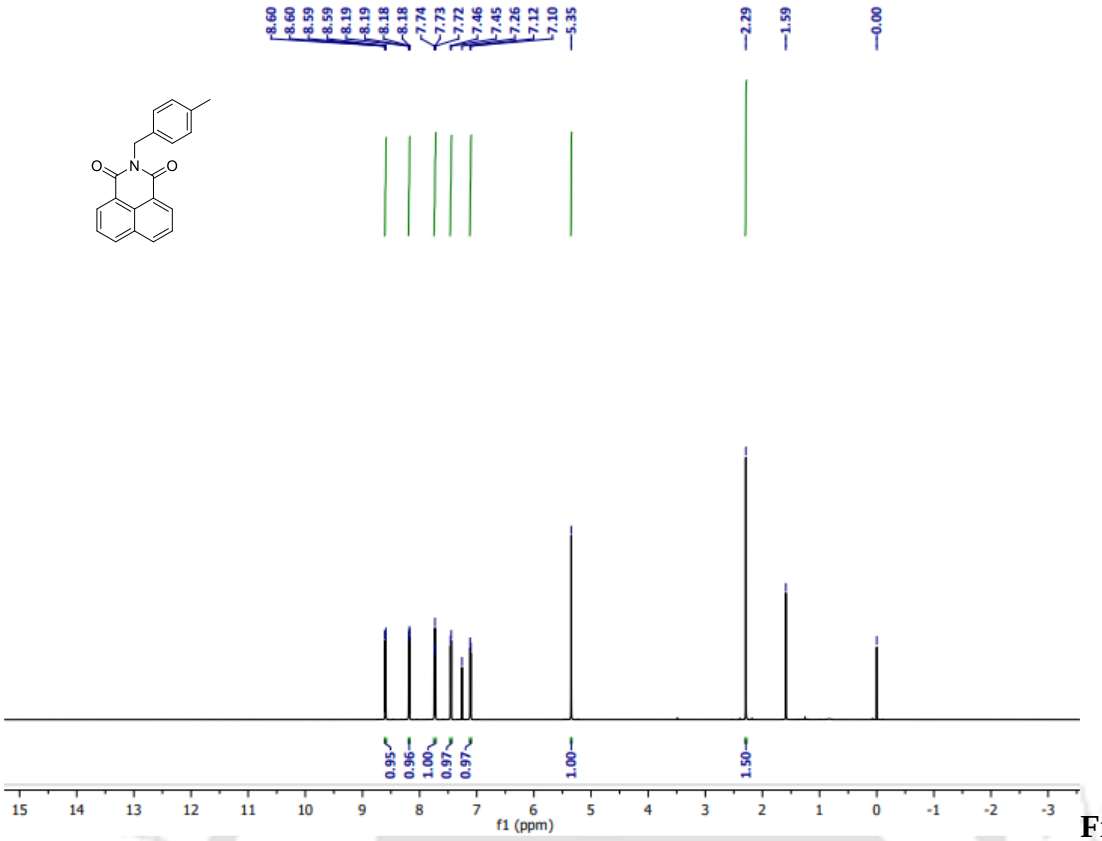

Figure A4.5 Proton NMR spectra of NPMe

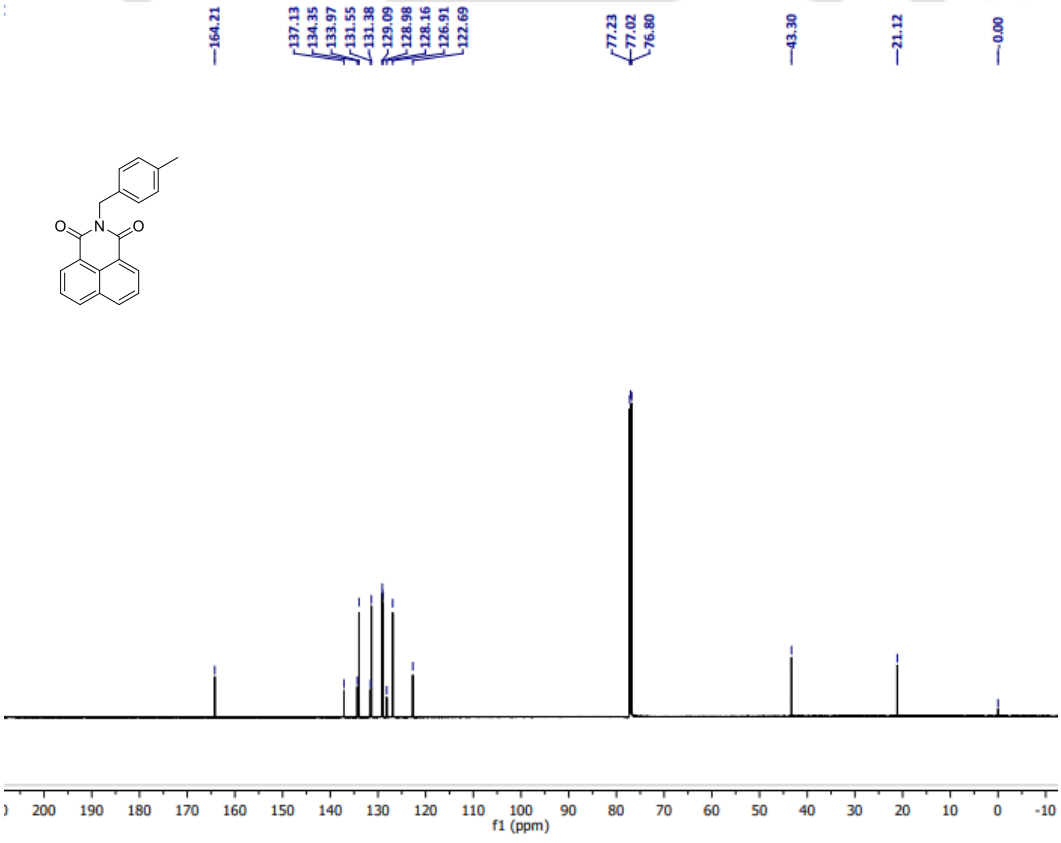

Figure A4.6 ^{13}C NMR spectra of NPMe.

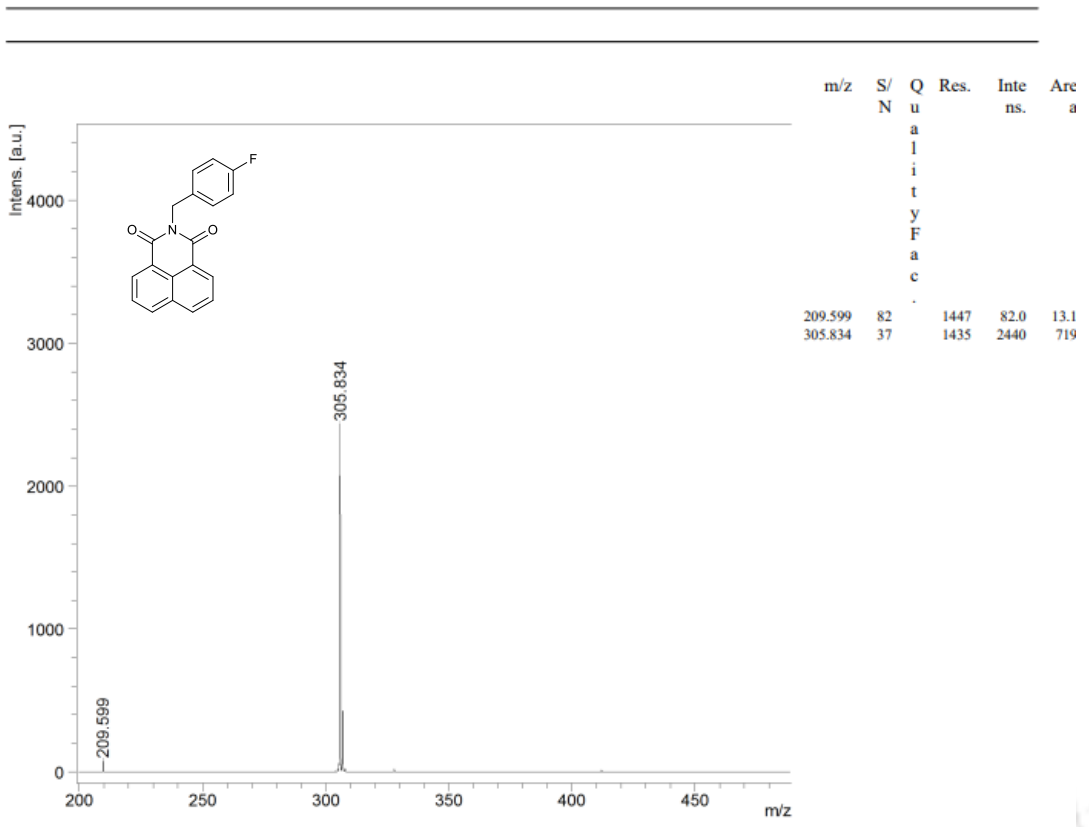

Figure A4.7 MALDI spectra of NPF.

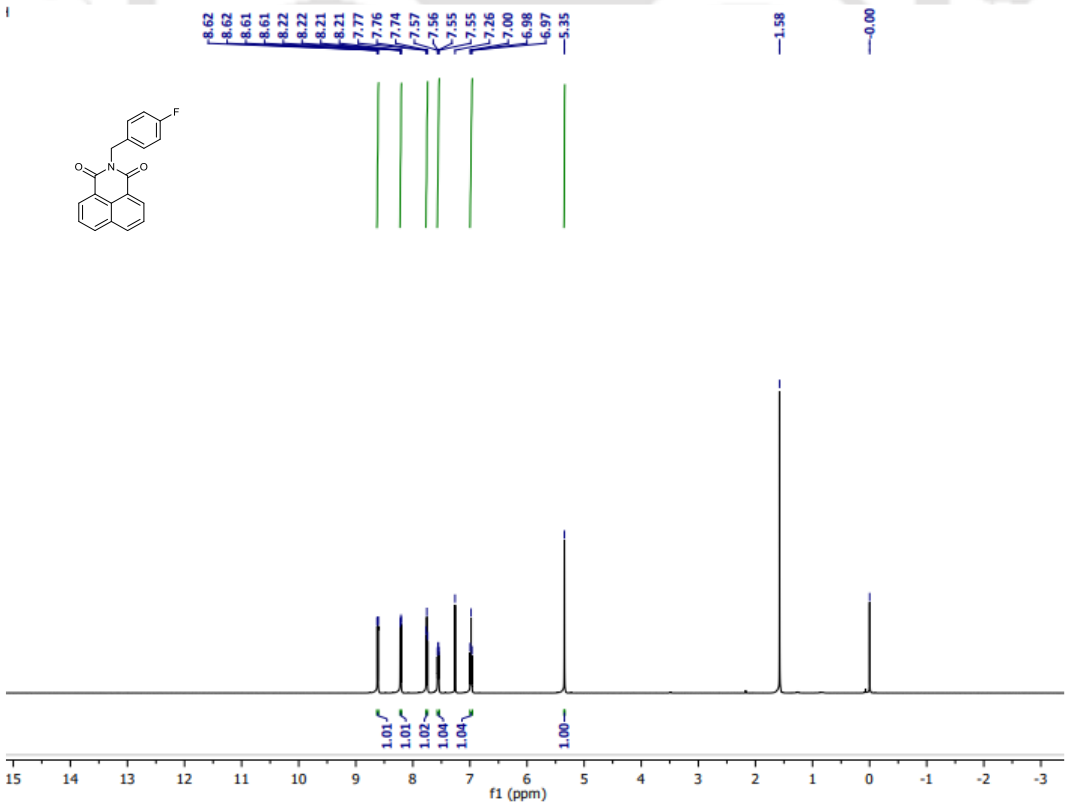

Figure A4.8 Proton NMR spectra of NPMe

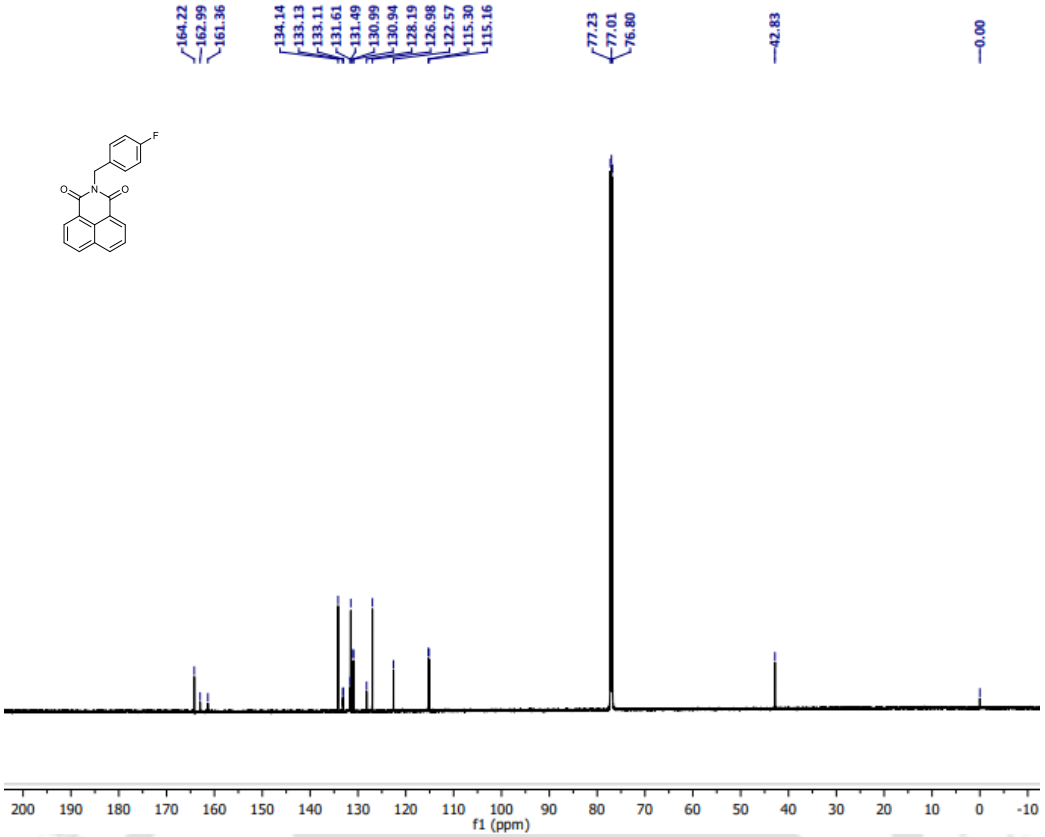

Figure A4.9 ^{13}C NMR spectra of NPF.

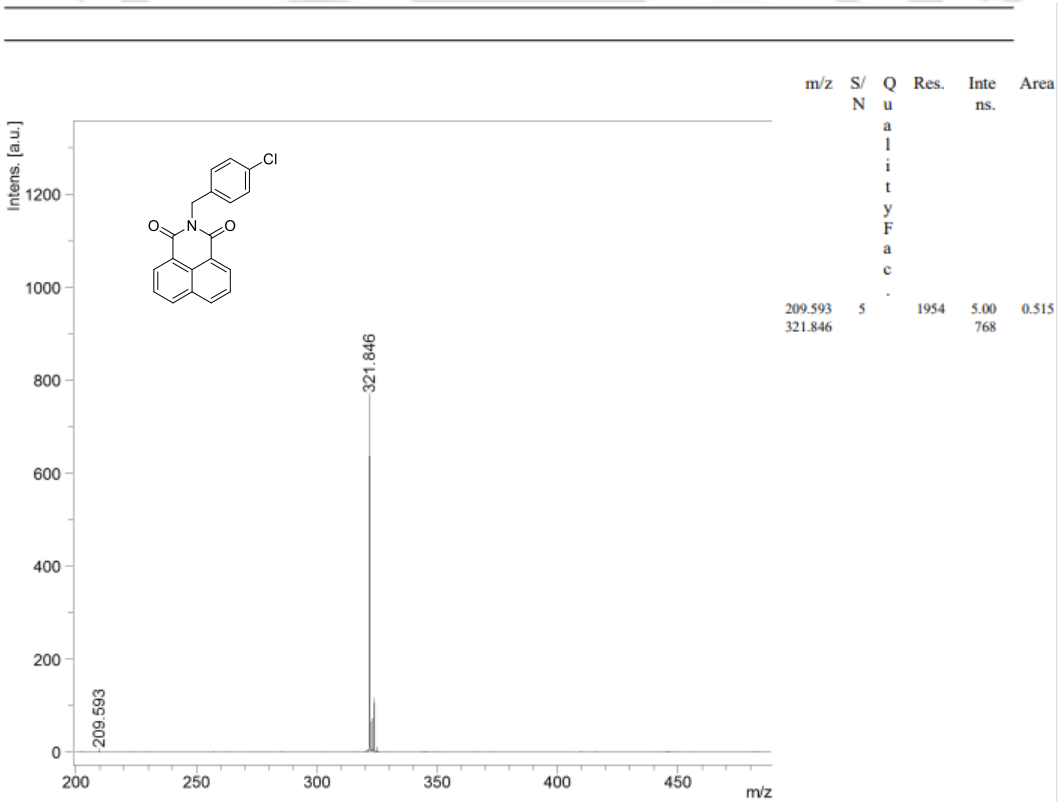

Figure A4.10 MALDI spectra of NPCl.

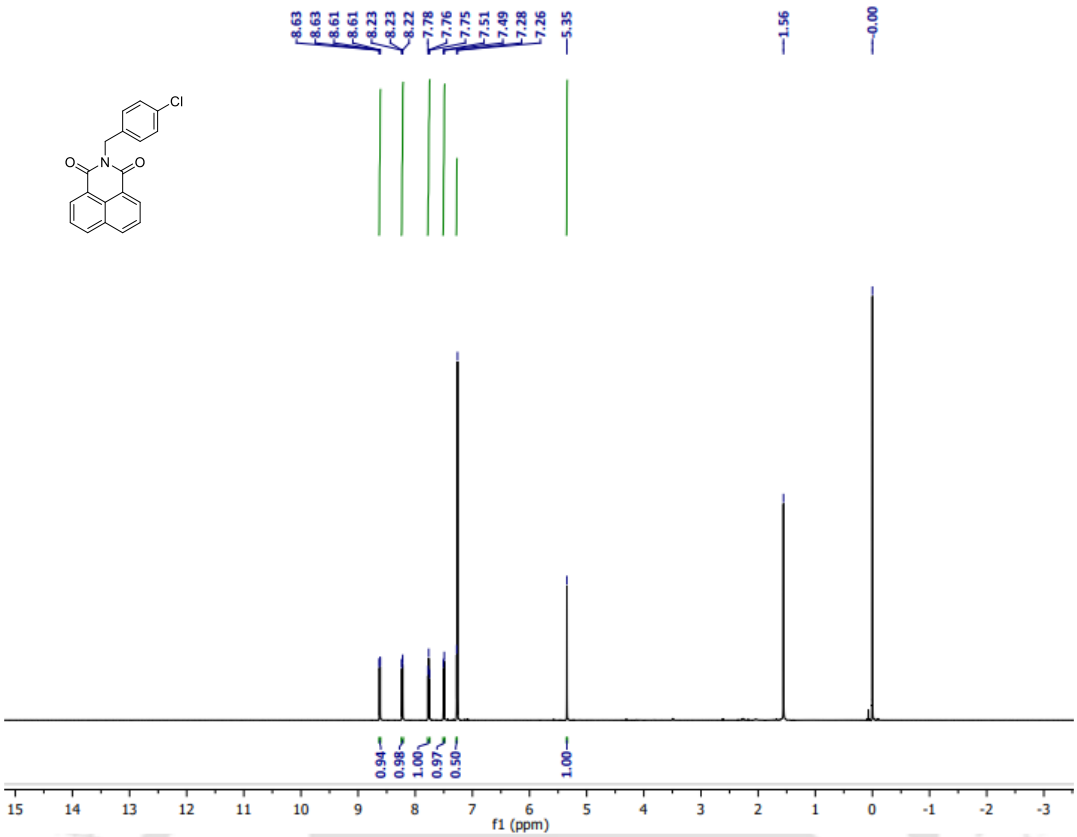

Figure A4.10 Proton NMR spectra of NPCl

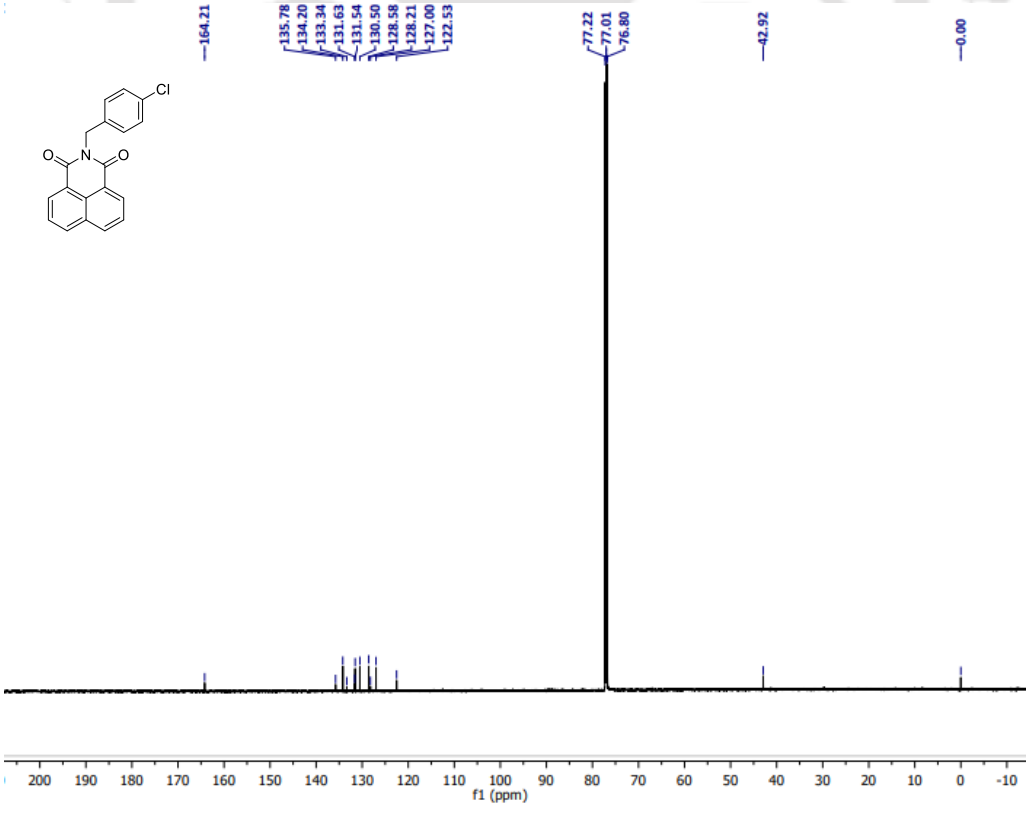

Figure A4.11 ^{13}C NMR spectra of NPCl.

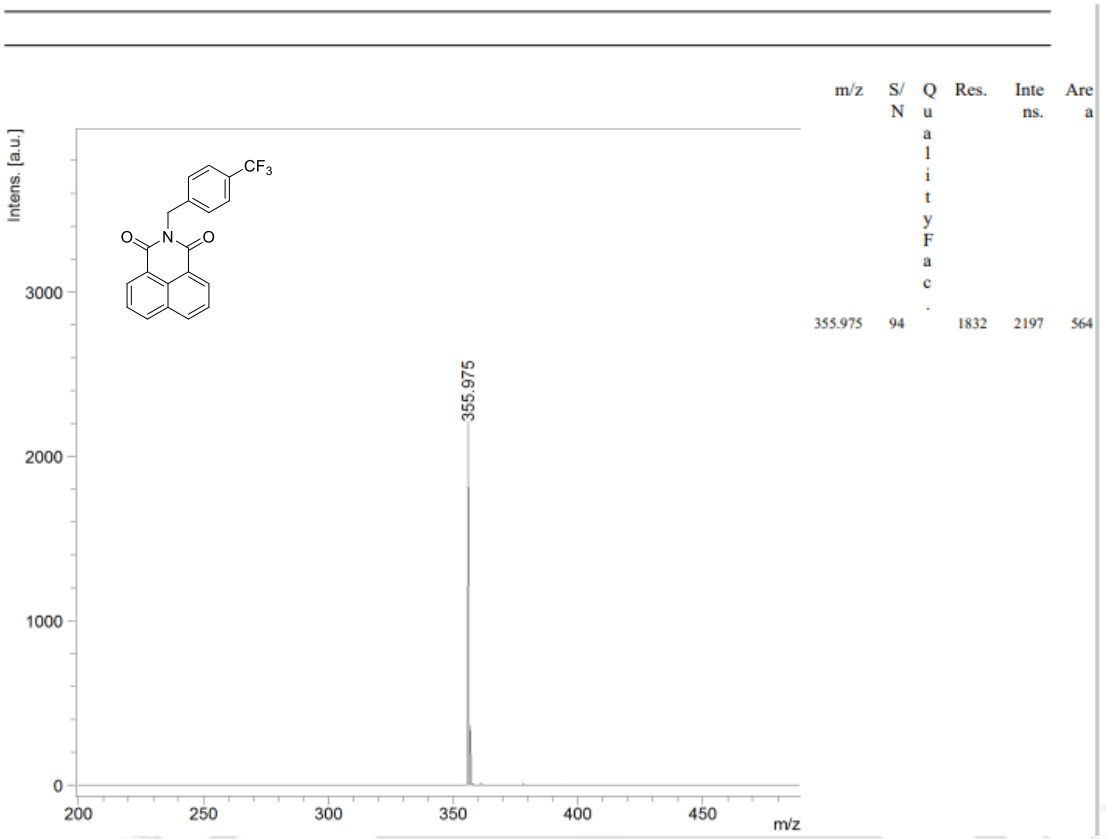

Figure A4.12 MALDI spectra of $NPCF_3$.

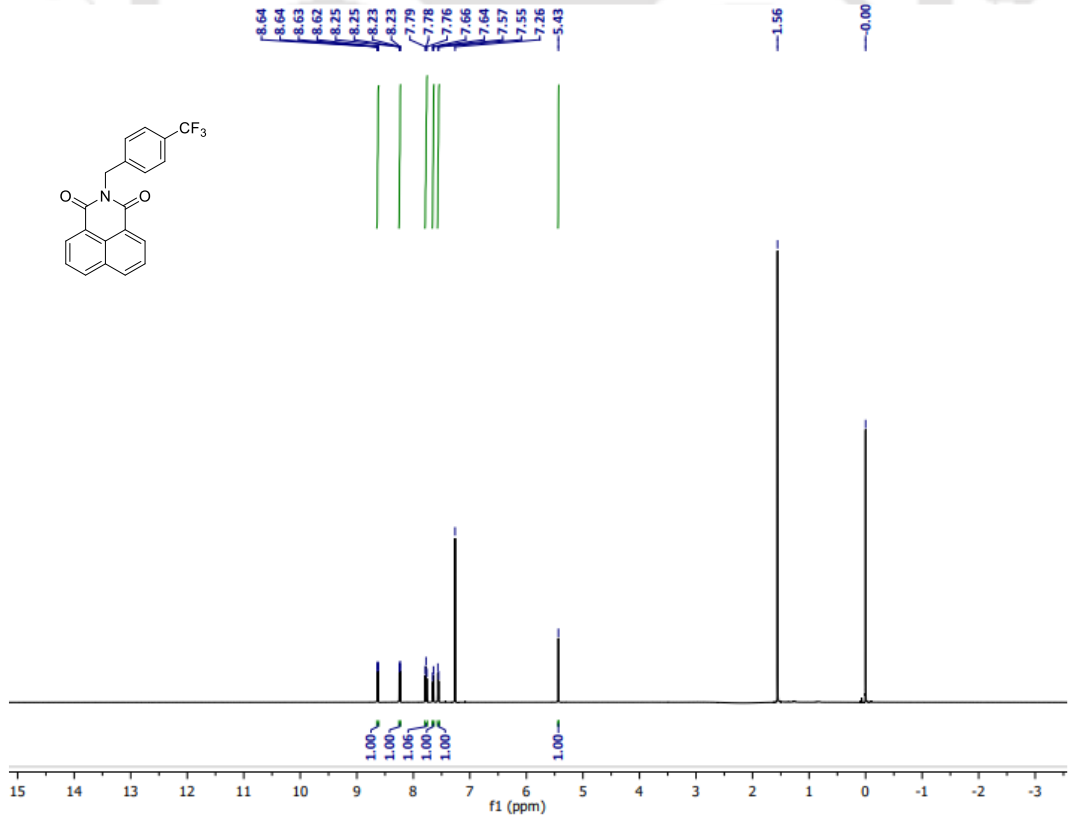

Figure A4.13 Proton NMR spectra of $NPCF_3$.

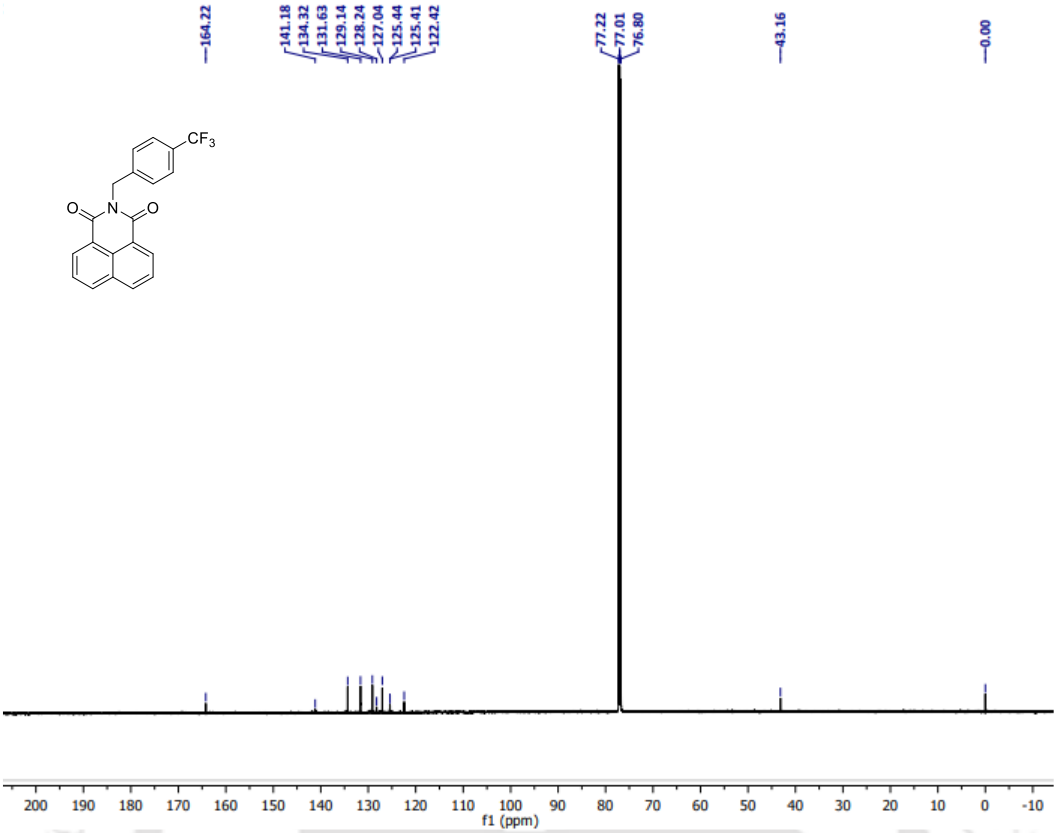

Figure A4.14 ^{13}C NMR spectra of $NPCF_3$.

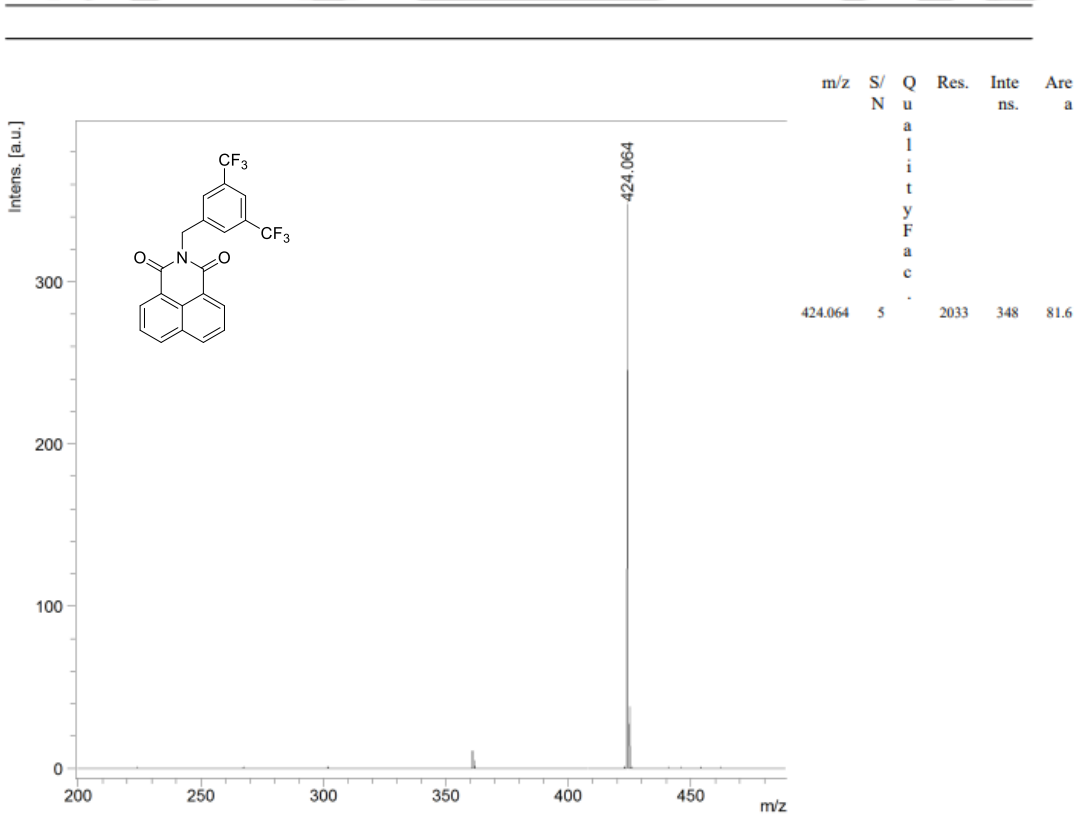

Figure A4.15 MALDI spectra of 1,3 m-$NPCF_3$.

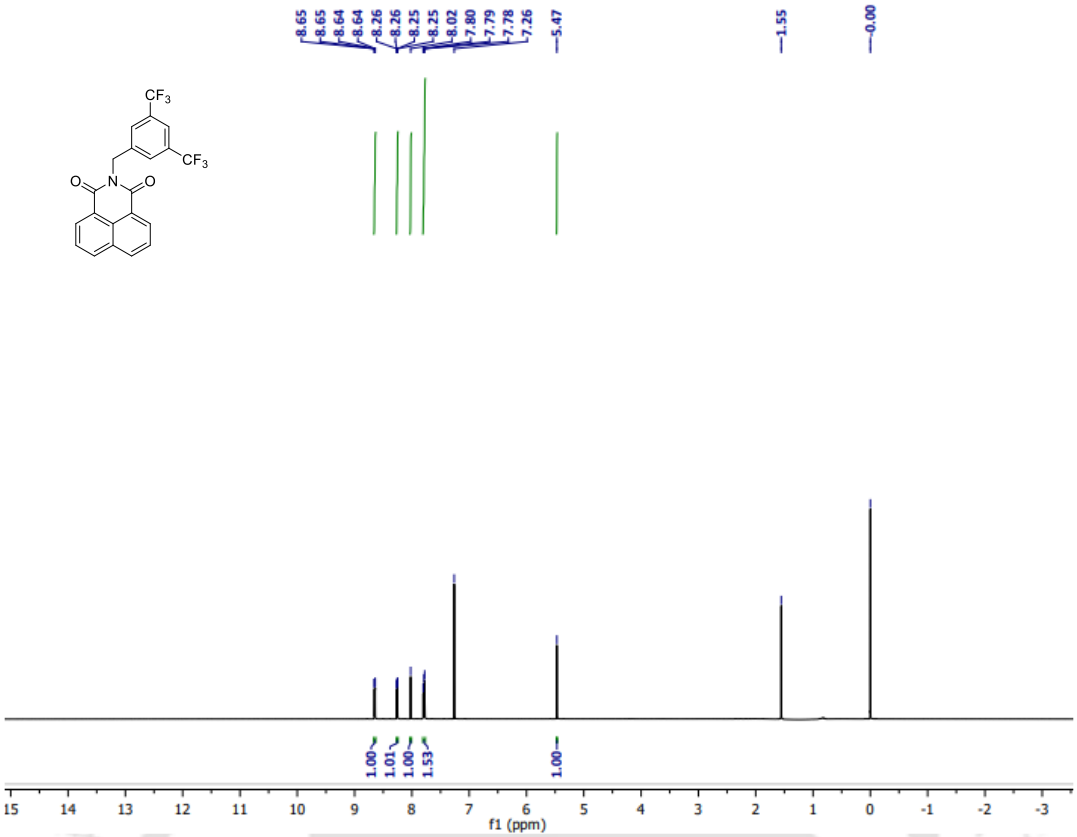

Figure A4.16 Proton NMR spectra of 1,3 m-NPCF$_3$.

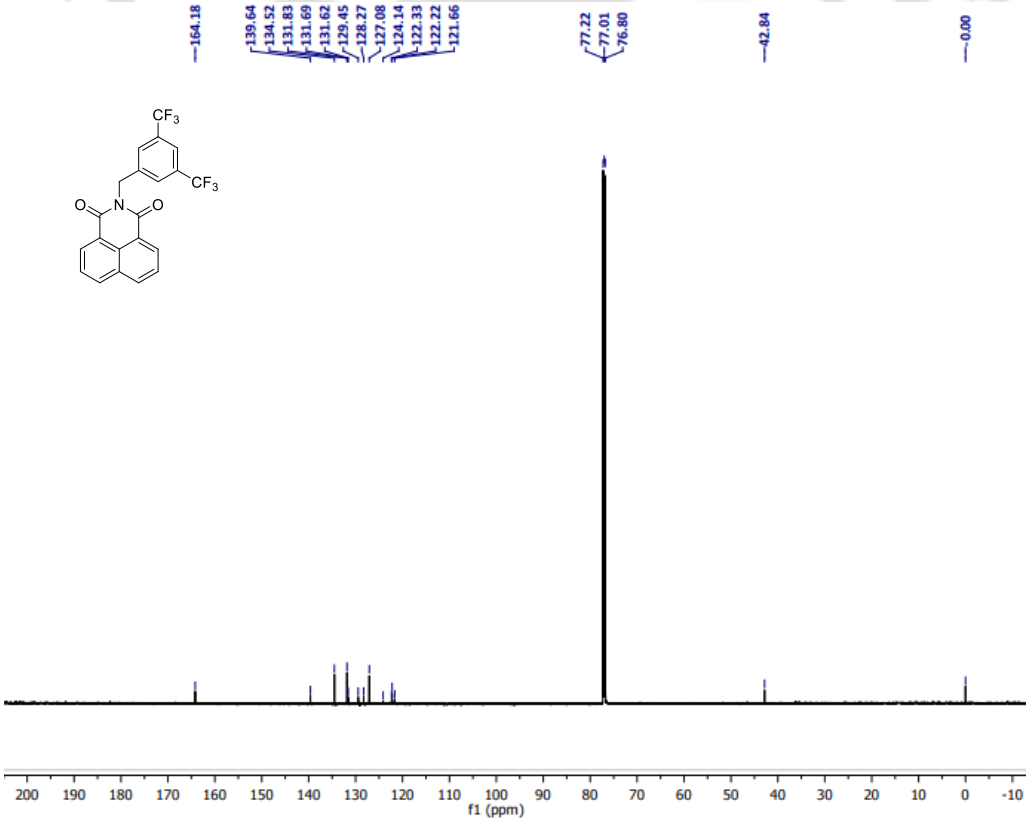

Figure A4.17 ^{13}C NMR spectra of 1,3 m-NPCF$_3$.

.

Chapter 5

Molecular Packing Dictates Optical Destiny: Polymorphism and Mechanoluminescence in Naphthaliimide Luminogens.

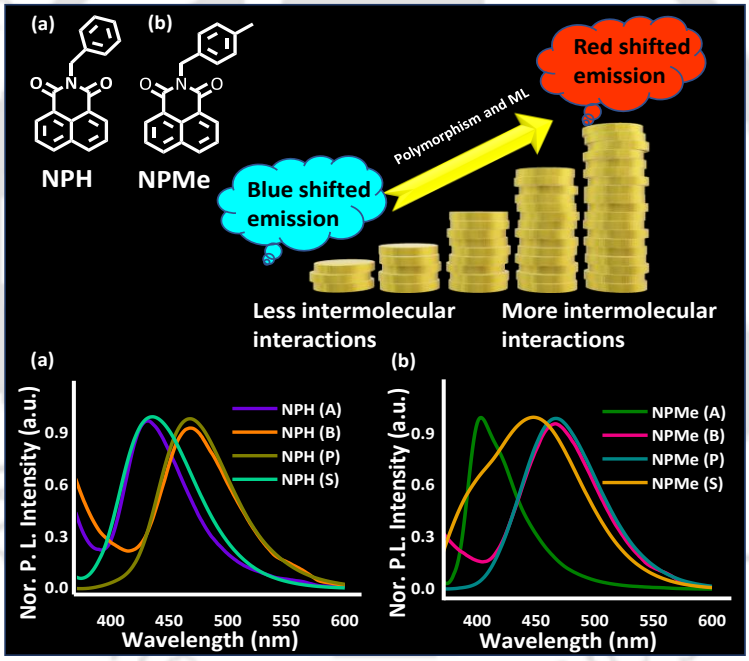

Narang, K.; Saramah, T.; Iyer, P. K. Molecular Packing Dictates Optical Destiny: Polymorphism and Mechanoluminescence in Naphthaliimide Luminogens (*Manuscript communicated*).

Abstract

This thesis chapter investigates the polymorphic behaviour and mechanoluminescent properties of the naphthalimide luminogens NPH and NPMe, aiming to elucidate their optical characteristics and potential applications. Through meticulous analysis of the X-ray diffraction pattern, we unveil the polymorphic forms of these luminogens. These structural variations provide insights into the intermolecular interactions and packing motifs governing their photophysical properties. Densely packed configurations observed in NPHB and NPMeB variants manifest a distinct red shift in the emission spectrum coupled with heightened fluorescence intensity. On the other hand, structures that are loosely packed, like NPHA and NPMeA, have an emission spectrum that is blue shifted and has less fluorescence intensity. Furthermore, we investigate the mechanoluminescent properties of NPH and NPMe, shedding light on their responses to mechanical stimuli. Theoretical insights via DFT add clarity to the results of the experiments and give us a better understanding of how the molecular packing arrangements, electronic structure, and optical behaviour of naphthalimide luminogens are closely related. Understanding the intricate relationship between molecular packing arrangements and optical characteristics is critical for maximising the utility of these luminogens in a variety of fields, including optoelectronics and material science.

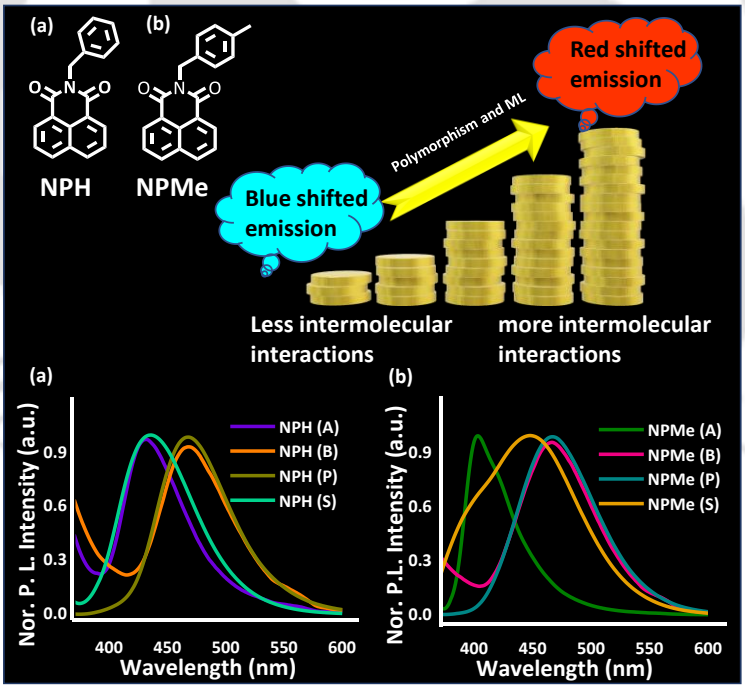

Figure 5.1 Proposed table of content of the present work.

5.1 Introduction

Organic π-conjugated molecules have garnered significant attention for their potential applications across various domains such as organic electronics,[1] sensing,[2] memory storage,[3] bioimaging,[4] information encryption,[5] security,[6] and more.[7] Besides the electronic characteristics of their molecular structure, the arrangement of molecules in the solid state, known as molecular packing, plays a crucial role in determining their optical properties, especially as these molecules are predominantly utilized in practical applications in solid form.[8] Smart luminescent materials represent a class of materials that exhibit remarkable changes in their luminescence properties when subjected to external stimuli such as light, electricity, temperature, pressure, or solvent. These materials hold immense potential for applications in sensors,[9] information storage,[10] biomedical,[11] photoelectric devices[12] and mechanoluminescence (ML) materials, which emit light in response to mechanical stress, are particularly intriguing due to their ability to provide real-time detection with environmentally friendly excitation mechanisms.[13,14,15] The design of organic ML materials has seen considerable progress since 2015,[16] when a pioneering technique integrating aggregation-induced emission (AIE)[17] and ML[18] characteristics into a single molecule was introduced, leading to the development of vibrant ML materials. However, despite these advancements, the lack of predictable design methods and a comprehensive understanding of excited-state processes continues to pose challenges in the development of ML materials.[19] Addressing these challenges requires meticulous consideration of both the chemical structures of luminogens and their molecular packing arrangements to achieve optimal ML performance. Polymorphism serves as a practical means to adjust the emission properties of organic solids based on a single component, offering a convenient approach to the production of optoelectronic materials.[20] Thus, establishing the link between the emission characteristics of organic solids and their molecular conformation or arrangement is crucial.[21] Extensive theoretical and experimental investigations have been undertaken to explore this relationship.[22] However, the H and J aggregation patterns in naphthalimide compounds have been relatively underexplored.[23] Given the significance of naphthalimide compounds in various applications such as optoelectronics,[24] sensors,[25] and room temperature phosphorescence materials,[26] there is a pressing need for fundamental studies to elucidate the structure-property relationship and photophysical properties in this context.

Naphthalimide, known for its electron-deficient core, typically serves as an acceptor when conjugated with a donor molecule.[27] In our study, we introduced a phenyl group with a sp^2

spacer into the naphthalimide core. This spacer was chosen to impart a molecular framework with a folded structure in which two core molecules could avoid π-π interaction sufficiently enough to avoid exciton quenching and effectively restrict the molecular motion, which has recently been demonstrated to enhance luminescence significantly compared to twisted and restriction in rotation (RIR) molecules.[28] Moreover, the folded π-structure was anticipated to facilitate clear charge separation, potentially leading to interesting properties of mechanoluminescence (ML) and optical tuneability. NPH and NPMe were synthesized via condensation reactions between 1,8-naphthalic anhydride, benzylamine, and benzyl methylamine, respectively. **(Scheme 5.1a, 5.1b)**. Following purification via column chromatography (using 5% chloroform/hexane), NPH and NPMe were characterized using NMR, MALDI, and single-crystal X-ray diffraction (SC-XRD).

5.2 Experimental

5.2.1 Materials and measurements: All starting material reagents, i.e., 1,8-naphthalic anhydride, benzyl-methylamine, benzylamine, and solvents (dimethyl formamide (DMF) and ethanol), were purchased from Sigma Aldrich (India) and were reagent grade.

NMR Measurements: A Bruker Avance 600 MHz Fourier transformation spectrometer was used to record the proton NMR spectrum at 600 MHz and the ^{13}C NMR spectrum at 200 MHz All proton and ^{13}C spectra solutions were obtained using the residual solvent signal as an internal reference. The chemical shifts are reported in parts per million (ppm) with respect to TMS. The short notations used are s for singlet, d for doublet, t for triplet, q for quartet, and m for multiplet.

Matrix-Assisted Laser Desorption Ionization: MALDI was performed on Brucker model auto-flex speeds using a MALDI TOF system spectrometer.

Optical Measurements: Solution state studies: Electronic absorption spectra of luminophores in solution state were recorded on a Perkin-Elmer Model Lambda-750 spectrophotometer. PL emission spectra were recorded on the Horiba Fluromax-4 spectrofluorometer. Optical measurements were performed using 4 mm quartz cuvettes at 298 K.

Crystal state studies: Electronic absorption spectra were recorded on a Perkin Elmer Model Lambda-750 spectrophotometer. Emission spectra were recorded on the FLS1000 spectrometer, an Edinburg instrument.

Lifetime and measurements: Fluorescence lifetime experiments were performed on the Horiba Delta Flex time-correlated single photon counting (TCSPC) instrument. A 373 nm laser diode with a pulse repetition rate of 1 MHz was used as the light source.

5.2.2 Synthetic procedure

5.2.2a Synthesis of 2-benzyl-1H-benzo[de]isoquinoline-1,3(2H)-dione, NPH:

In a 50 mL round bottom flask, 0.5 g of 1,8 naphthalic anhydride was taken along with 10 mL of pure ethanol. The reaction mixture was kept for stirring in a setup with condenser. 0.7 mL of benzyl amine was added to the reaction mixture drop by drop. The reaction temperature was kept at room temperature for 30 minutes, then gradually increased and maintained a reflux condition for 12 hours. The completion of the reaction was monitored by TLC. After the reaction was completed, the whitish, muddy crude was then filtered through Whatman filter paper. The crude was further refined using column chromatography and 5% chloroform/hexane.[29] A white solid (NPH, 500 mg, yield 95%) was developed and characterized further using ^{1}H NMR, ^{13}C NMR, HRMS, MALDI, and SCXRD.

1H NMR: (600 MHz, $CDCl_3$, δ ppm) 8.60 (d, 2H), 8.19 (d, 2H), 7.74 (t,3H), 7.55 (d, 2H), 7.30 (t, 3H), 7.24 (dd, 4H), 5.39 (S, 1H) 13C NMR: (150 MHz, CDC_{l3}, ppm): 164.22, 137.30, 134.03, 131.57, 131.42, 128.94, 128.43, 128.17, 127.46, 126.94, 122.63, 43.56. Mass calculated for $C_{19}H_{13}NO_2$ = 288.32 [M]+, Found 294.15 $[M+1]^+$

5.2.2b Synthesis of 2-(4-methylbenzyl)-1H-benzo[de]isoquinoline-1,3(2H)-dione, NPMe:

0.5 g of 1,8-naphthalic anhydride and 10 mL of pure ethanol were mixed in a 50 mL round bottom flask. The reaction mixture was stirred in a setup equipped with a condenser. 0.7 mL of benzyl methylamine was added drop by drop. The reaction temperature was initially maintained at ambient temperature for a duration of 30 minutes, after which it was gradually raised and maintained under reflux conditions for a period of 12 hours. The progress of the reaction was observed using thin-layer chromatography (TLC). Once the reaction was finished, the pale, turbid crude substance was subsequently passed through Whatman filter paper. The crude substance underwent additional purification using column chromatography using a 5% mixture of chloroform and hexane.[29] A light sea green solid (NPMe, 460 mg, yield 92%) was developed and characterized further using ^{1}H NMR, ^{13}C NMR, HRMS, MALDI, and SCXRD.

NPMe: 1H NMR: (600 MHz, $CDCl_3$, δ ppm) 8.60 (dd, 2H), 8.18 (dd, 2H), 7.73 (m,3H), 7.45 (d, 2H), 7.11 (d, 3H), 7.24 (dd, 4H), 5.35 (s, 1H) 2.29 (s, 1H) 13C NMR: (150 MHz, $CDCl_3$, ppm): 164.21, 137.13, 134.35, 133.97, 131.55, 131.38, 129.09, 128.98, 128.16, 126.91, 122.69, 43.30, 21.12 Mass calculated for $C_{20}H_{15}NO_2$ = 301.35 $[M]^+$, Found 301.259 $[M+1]^+$

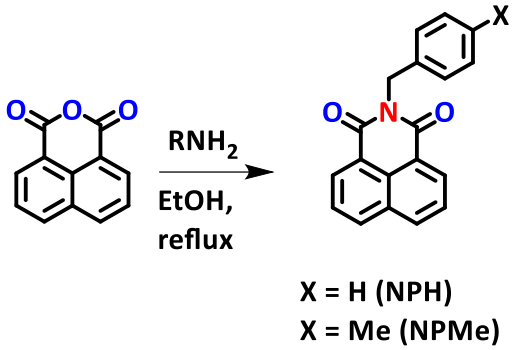

Scheme 5.1 Synthetic scheme for the NPH and NPMe

5.2.3 Preparation of SC-XRD sample: Following synthesis and column chromatography purification, NMICY powder was dissolved in HPLC methanol and stored at room temperature in the dark. NMICY crystals were discovered in white, transparent, and glossy form within 24 hours. To undertake SCXRD analysis, it was put over a glass slide.

5.2.4 Theoretical Calculations: The ground state optimization and excited state TD-DFT of NPHA, NPMHB, NPMeA, and NPMeB using a single crystal CIF file were calculated using the Gaussian-16 package. B3LYP hybrid functional with 631G+d basis sets were used during the entire calculation.[30,31]

5.3 Results and discussion

5.3.1 Synthesis and characterization of NPHA, NPHB, NPMeA, NPMeB

NPH and NPMe were synthesized via condensation reactions between 1,8-naphthalic anhydride, benzylamine, and benzyl methylamine, respectively. Illustrated in **Scheme 5.1.** Following purification via column chromatography (using 5% chloroform/hexane), NPH and NPMe were characterized using NMR, MALDI, and single-crystal X-ray diffraction (SC-XRD). Both NPH and NPMe exhibit absorbance peaks near 342 nm and 352 nm in their monomeric states, indicating carbonyl and π-π interactions.[32] In their condensed states (f_w = 99.9%, f_w = water fraction), both compounds display an increased baseline with a flat surface, indicating aggregation, making it challenging to observe sharp peaks of π-π or C=O interactions due to their complex molecular framework.[33] Fluorescence spectra were recorded by varying the water fraction of NPH (20 µM) and NPMe (20 µM) (both stocks at 1 mM in DMF). Monomeric emissions were observed at 375 nm for NPH and 385 nm for NPMe (f_w = 0%, DMF = 100%). As the water fraction increased, the emission intensity for both compounds also increased, though not in a similar pattern. The highest emission intensities were recorded at

450 nm for NPH and 455 nm for NPMe. This resulted in a 75 nm shift for NPH and an 80 nm shift for NPMe in their condensed states (f_w = 99.9%). Hence, there is a noticeable bathochromic shift, in the emission maxima along with increasing emission intensity for both NPH and NPMe with increasing polarity or water fraction. **(Figure 5.2)**

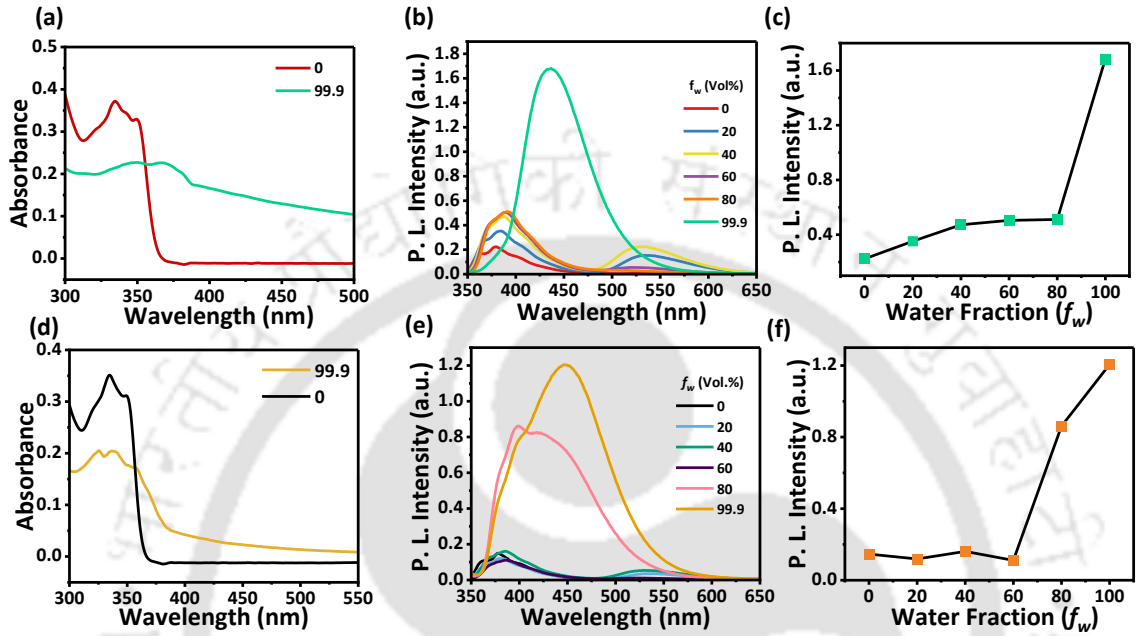

Figure 5.2 (a) NPH (20 µM in DMF) absorbance spectra in pure DMF (red) and in f_w = 99.9% (see green) (b) fluorescence emission intensity of NPH (20 µM in DMF) in different water fractions. (c) Respective plot of emission maxima vs water fraction. (d) NPMe (20 µM in DMF) absorbance spectra in pure DMF (Black) and in f_w = 99.9% (dark yellow) (e) fluorescence emission intensity of NPMe (20 µM in DMF) in different water fractions. (f) Respective plot of emission maxima vs water fraction.

5.3.2 Polymorphism: To investigate the impact of molecular packing[34] on the properties of pure organic luminogens, we grew single crystals of NPH in chloroform using a slow evaporation method,[35] resulting in green emissive crystals (NPHB). Additionally, a polymorph was developed in the MeOH solvent, exhibiting blue emission (NPHA).[36] Further exploration of molecular packing effects led to the development of two polymorphs of NPMe in chloroform through slow evaporation (NPMeB) and in MeOH using a fast-heating procedure (NPMeA).[37,38] **(Figure 5.3)**

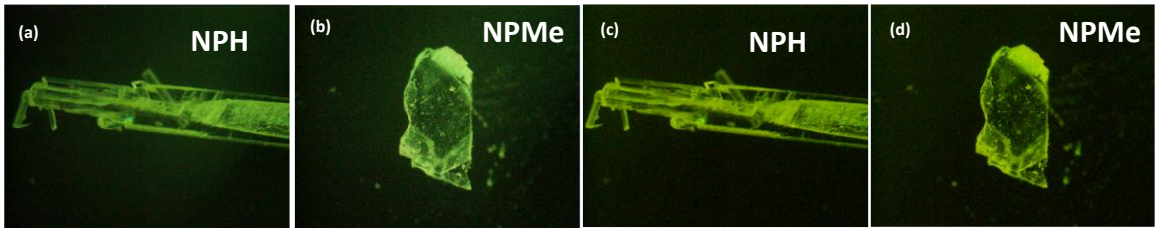

Figure 5.3 (a) NPH (b) NPMe under UV light (c) NPH and (d) NPMe under visible light.

5.3.3 Fluorescence study and Mechanochromism of Polymorphs:

In this study, we investigated the fluorescence emission of both polymorphs of NPH and NPMe in both their crystalline and condensed states (f_w = 99.9%). NPHA exhibited a fluorescence emission wavelength of 431 nm, while NPHB displayed a comparatively redshifted emission at 468 nm. Similarly, NPMeA demonstrated a fluorescence emission maximum at 402 nm, and NPMeB exhibited a redshifted emission at 466 nm. The notable redshift emission for the B set of polymorphs compared to the A set inspired a more in-depth examination of the aggregation patterns of these luminogens.[39,40] **(Figure 5.2, 5.4a, 5.4b)** To investigate the mechanochromism properties of NPH and NPMe polymorphs, mechanical force was applied, resulting in the conversion of NPHA into powdered NPH (P), which exhibits a similar emission at 467 nm to NPHB (468 nm). Additionally, grinding NPMeA led to its conversion into NPMe (P), which displayed emission at 467 nm similar to NPMeB (466 nm). However, grinding NPHB and NPMeB did not induce any fluorescence emission changes. This prompted further investigation into the mechanism underlying the mechanochromism property.[41]

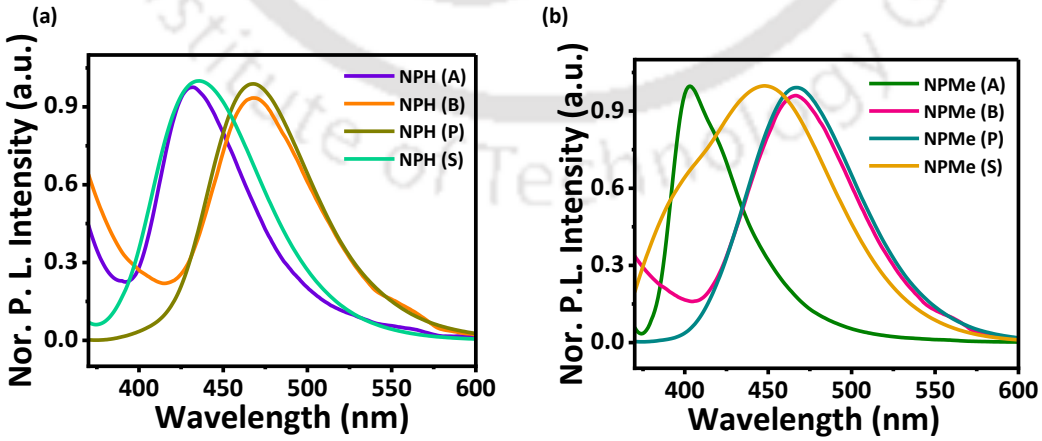

Figure 5.4 a) Normalized PL intensity of NPH(A) crystal, NPH(B) crystal, NPH(P)powder and NPH(S)solution (f_w = 99.9%). b) Normalized PL intensity of NPMe(A) crystal, NPMe(B)crystal, NPMe(P)powder and NPMe(S) solution (f_w = 99.9%).

5.3.4 Powder XRD study of Polymorphs:

In our investigation, we compared simulated X-ray diffraction (XRD) patterns of NPHASM and NPHBSM with NPH (P) powder, finding similar 2θ peaks, supporting analogous emission in NPH (P) and NPHB crystals. Grinding NPHA transformed it into microcrystals resembling NPHB, revealing NPHA's less stable or metastable nature. Further grinding converted the NPHA into a more stable powder state. Similarly, simulated powder XRD of NPMeA and NPMeB exhibited nearly identical 2θ peaks to NPMeB. Grinding NPMeA yielded NPMe(P), a more stable state **(Figure 5.5a, 5.5b)**. Fluorescence emission studies of NPH and NPMe in their aggregated states, NPH(S), and NPMe(S), revealed that NPH(S) emitted at 435 nm, alike NPHA, suggesting similar aggregation patterns.[42] In contrast, NPMe(S) emitted light at 448 nm between NPMeA (402 nm) and NPMeB (466 nm), attributed to methyl hydrogen interactions with water molecules causing a redshift from the expected NPMeA emission **(Figure 5.4a and 5.4b)**.

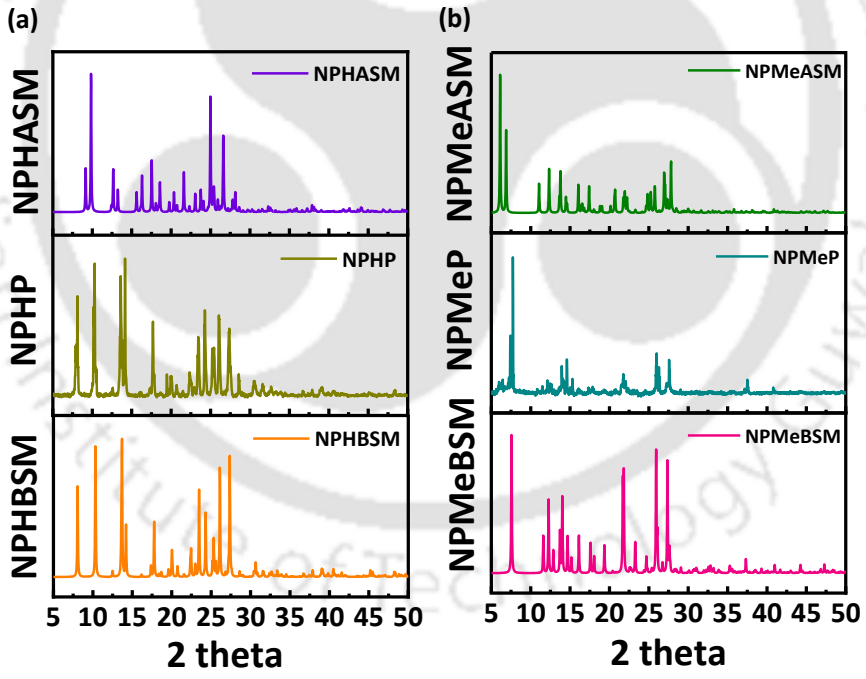

Figure 5.5 Powder XRD data (a) NPHASM (simulated), NPHP (powder), NPHBSM (simulated) (b) (a) NPMeASM (simulated), NPMeP (powder), NPMeBSM (simulated).

5.3.5 Single Crystal XRD study of Polymorphs:

The polymorphs of NPH (NPHA, NPHB) and NPMe (NPMeA, NPMeB) exhibited twisted structures.[43] **(Figure 5.6a)** Notably, the NMI(c)-Me-Bz angle varies among these structures, measuring 111.96° (NPHB), 112.81° (NPHA), 112.74° (NPMeB), and 110.11° (NPMeA). **(Figure 5.6b)** Interestingly, there appears to be an opposing trend in the NMI(c)-Me-Bz angle between the B and A sets of polymorphs for both NPH and NPMe.[44] All four polymorphs exhibit a head-to-tail arrangement, yet the slip angle and distance between two chromophores (d) differ for each set. For the NPH set of polymorphs, the slip angle between two chromophores is 96.23° (d = 3.595 Å) for NPHB and 88.93° (d = 4.208 Å) for NPHA, but the trend was exactly opposite for the NPMe set of polymorphs, and the slip angle for NPMeB is 94.80° (d = 3.595 Å) and NPMeA is 98.00° (d = 3.740 Å) **(Figures 5.6b, 5.6c, 5.7 to 5.10)**. Similarly, the dihedral angle is higher for NPHB (69.97°) than NPHA (67.77°), but NPMeA has a higher dihedral angle (77.34°) than NPMeA (66.22°) **(Figures 5.6d, 5.7 to 5.10)**.[45] In the NMI(C)-Me-Bz angle, slip angle, distance between chromophores, and dihedral angle, we could not find a trend between the redshifted long wavelength and higher fluorescence lifetime of NPHB and NPMeB and the shorter wavelength and low fluorescence lifetime of NPHA and NPMeA. **(Figure 5.11)**

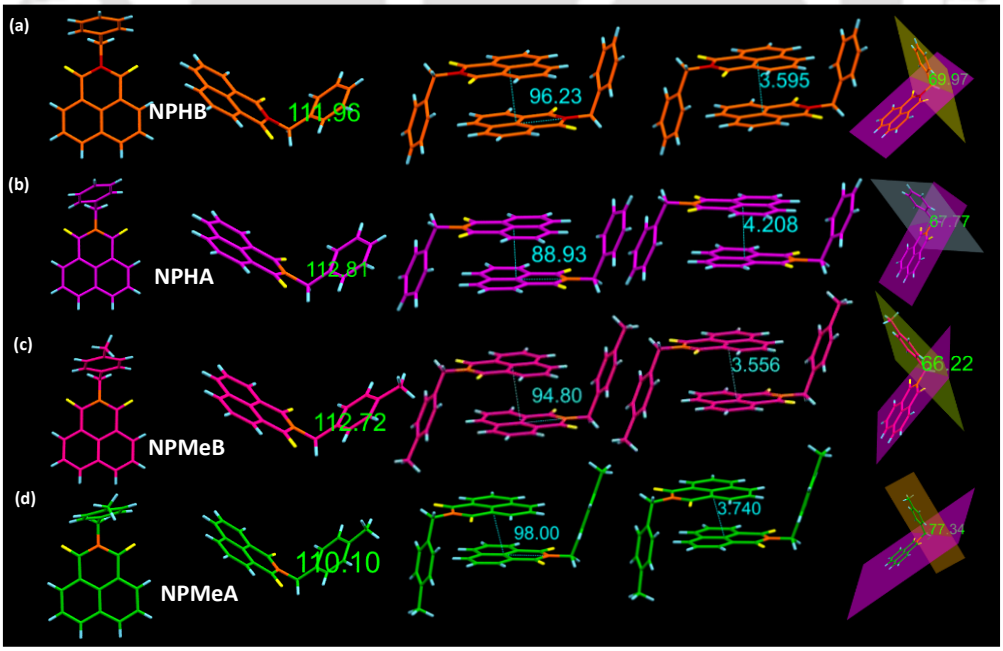

Figure 5.6 SC-XRD analysis summary of naphthalimide luminogens a) NPHB, b) NPHA, c) NPMeB, d) NPMeA

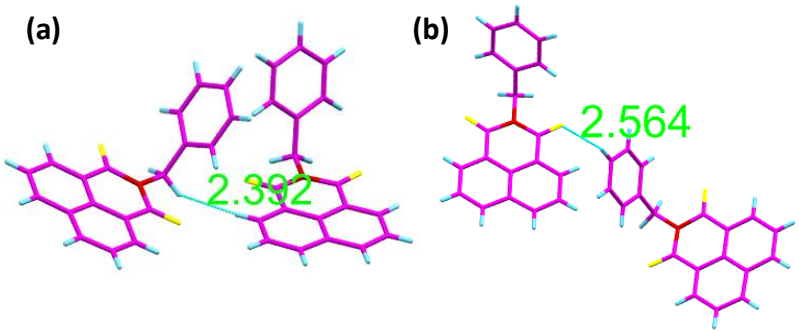

Figure 5.7 NPHA intermolecular interactions (a) Me-H….H-C9-NMI of 2.392Å. (b) Bz-C4-H..O=C11-NMI of 2.564 Å.

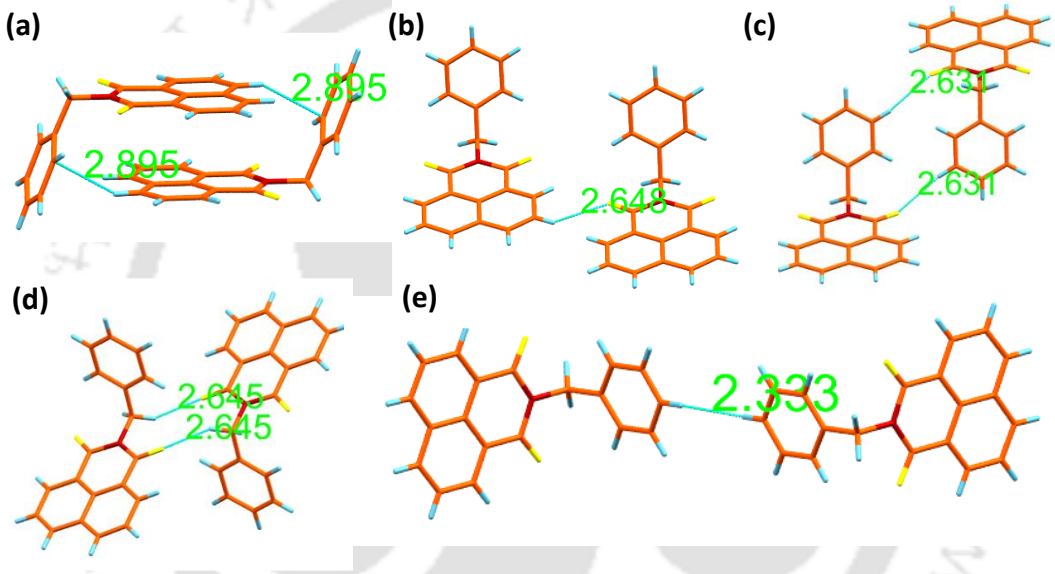

Figure 5.8 NPHB intermolecular interactions (a) two Bz-C2…H-C5-NMI of 2.805Å (b) two NMI-C4-H…O=C4-NMI 2.648Å. (c) Bz-C5-H…O=C1-NMI of 2.631Å. (c) two Me-H..O=C1-NMI of 2.645Å (e) Bz-C4-H…H…C4-Bz of 2.333Å.

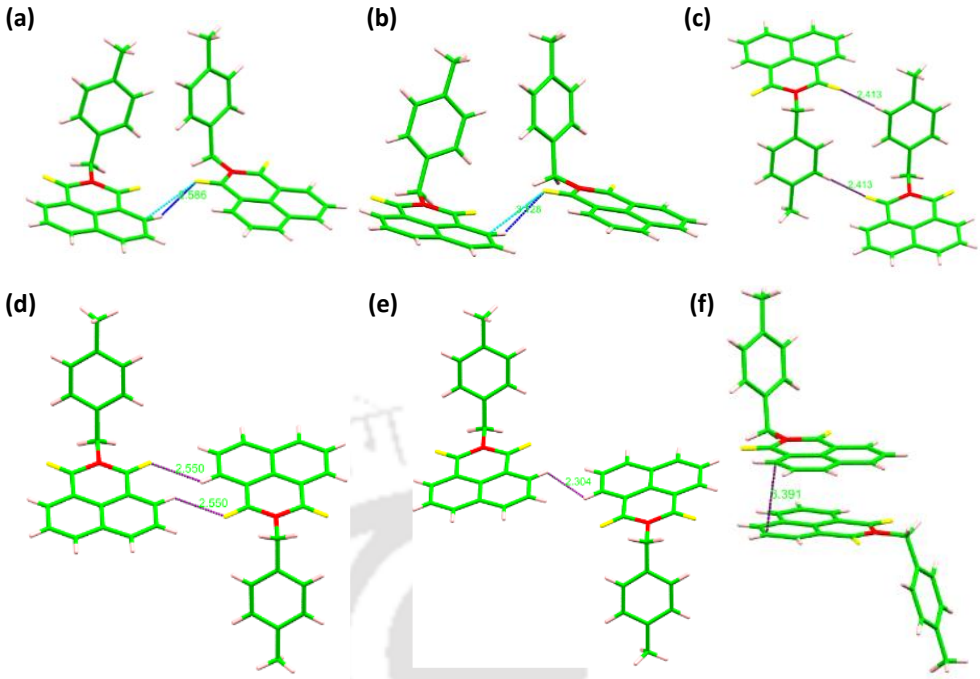

Figure 5.9 Intermolecular interactions in NPMeA. (a) NMI-C3H…O=C11-NMI of 2.586Å (b) NMI-C3…O=C11-NMI of 3.128Å (c) two NMI-C11=O…H-C3-Bz of 2.413Å (d) NMI-C1=O…H-C3-NMI' of 2.550 Å (e) NMI-C3-H…H-C3-NMI' of 2.304Å (f) NMI-C9…C9-NMI' of 3.391Å.

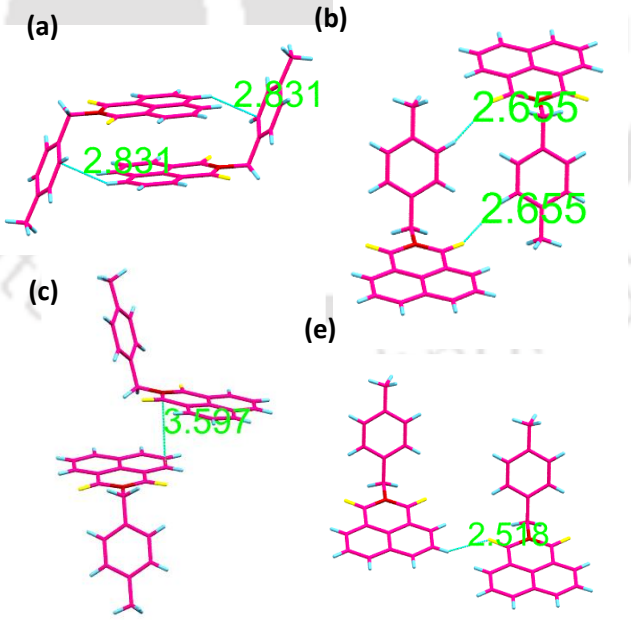

Figure 5.10 Intermolecular interaction: NPMe4B (a) two NMI-C5-H….C2-BZ of 2.831Å (b) NMI-C=O…H-C5-BZ of 2.655Å (c) NMI-C4…C1-NMI' of 3.352Å (d) NMI=C4-H…O=C11-NMI' of 2.516 Å.

5.3.5 Fluorescence lifetime analysis of Polymorphs:

A Detailed analysis of molecular packing has unveiled the explanation for the redshifted emission observed in the B set of polymorphs.[39,46] The fundamental answer for the nucleation process used to develop the A and B sets of polymorphs. NPHB and NPMeB were carefully grown in chloroform via slow evaporation, whereas NPHA and NPMeA were rapidly formed in methanol through fast evaporation. This discrepancy in the nucleation conditions highlights the significant role of molecular packing in determining their emission and fluorescence lifetime. **(Figure 5.11)**

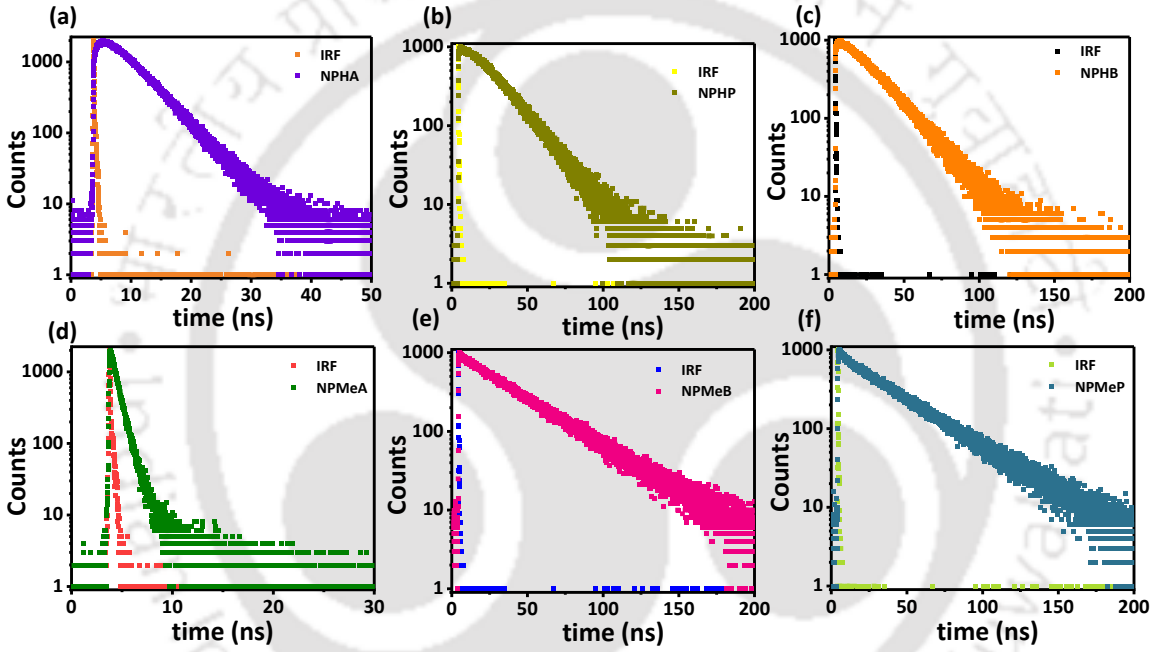

Figure 5.11 TRPL data of (a) NPHA (crystals), (b) NPHB (crystals), (c) NPHP, (d) NPMeA (e) NPMeB (f) NPMeP.

Table 5.1 Fluorescence lifetime of (a) NPHA, (b) NPH (powder) (c) NPHB (d) NPMeA (e) NPMeB (f) NPMeB

Luminogens	NPH (A)	NPH (B)	NPH (P)	NPMe (A)	NPMe (B)	NPMe (P)
τ_F (Crystals)(ns)	4.07	12.74	16.07	0.72	35.62	35.18

5.3.6 Molecular Packing analysis of Polymorphs:

Our analysis demonstrates that the NPHB and NPMeB polymorphs feature tighter packing compared to the looser packing observed in NPHA and NPMeA. **(Figure 5.12)** Additionally, NPHB exhibits a greater number of intermolecular interactions compared to NPHA, while NPMeB shows a lesser number of intermolecular interactions.[47] **(Figure 5.13)** The powder XRD pattern closely resembles the B group of crystals for both NPH and NPMe, indicating a synergistic effect of enhanced intermolecular interactions in NPH (B) compared to NPH (A), and NPMe (B) compared to NPMe (A). This enhancement in π-π interactions results in a shift of molecular emission towards longer wavelengths. Conversely, reduced intermolecular interactions and diminished π-π interactions lead to shorter wavelength emission.[48] **(Figure 5.13) Aggregation pattern:** *J, H, and X aggregation:* The slippage angle between two chromophores plays a crucial role in aggregation patterns.[40] A slip angle ranging from 0 to 54.6° results in a bathochromic shift in absorption and emission maxima, indicative of J aggregation. Between 54.6° and 84°, H aggregation is observed. Beyond this range, the limits of these aggregations become of interest. Both the B sets of molecules and powder patterns exhibit a bathochromic shift, with slip angles exceeding 90°, while the A sets show slip angles below 90°. Intriguingly, beyond 90°, there is a further increase in absorption and emission intensity.[49] **(Figure 5.6)**

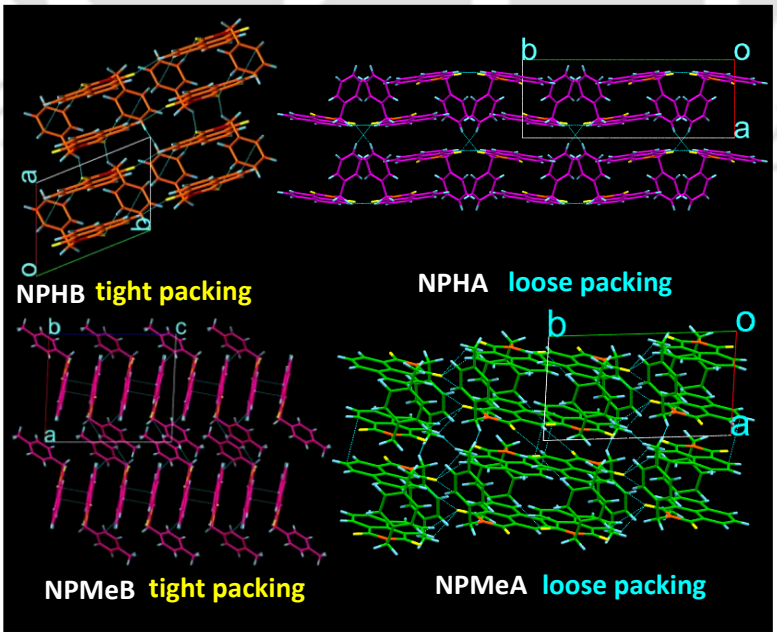

Figure 5.12 SC-XRD intermolecular interactions analysis summary of naphthalimide luminogens a) NPHB, b) NPHA, c) NPMeB, d) NPMeA.

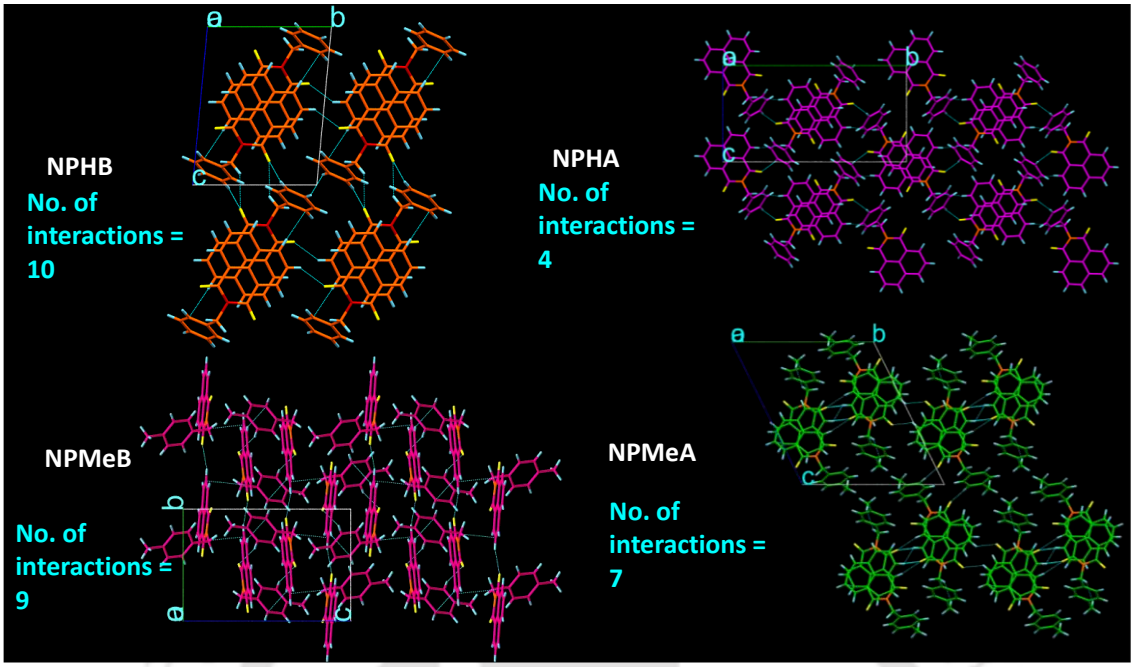

Figure 5.13 SC-XRD packing analysis summary of naphthalimide luminogens a) NPHB, b) NPHA, c) NPMeB, d) NPMeA

5.3.7 Hirshfeld Surface Analysis of Polymorphs

This study strategically used Hirshfeld surfaces, a common tool in crystallography, and 2D fingerprint analysis to quantitatively analyze intermolecular interactions within the crystal structures of the compounds under investigation. Using these sophisticated analytical techniques, we gained a detailed understanding of molecular arrangements and their subsequent impact on emission behaviour. **Figures 5.7 to 5.13** illustrate the results obtained through this analysis. Notably, the color shading in these figures represents the strength of various intermolecular interactions, with shades of red indicating stronger interactions. The hierarchy of interactions is systematically ordered, with H-H interactions being the strongest, followed by π-π interactions, C-H···π interactions, and so forth, including other non-covalent interactions. Hirshfeld surface analysis was utilized to get a statistical picture of the intermolecular interactions in the crystal packing of polymorphs. **Figures 5.14, 5.15,** and **Table 5.2** The calculations and and fingerprint representations of Hirshfeld surfaces are implemented in the program CrystalExplorer.[50] The percentage contribution of various contacts to the total Hirshfeld surface majorly comes from H-H interaction in NPHA (47.5%), NPHB (47.8%) NPMeA (53.4%), NPMeB (50.5%). C-H interaction was higher for NPHA 13.4% and 10.6% for NPHB, but it was same 12.4 % for both NPMeA and NPMeB. C-O interaction was almost

similar for both set of polymorphs. O-H interaction is higher for B sets of polymorphs, (8.4%) for NPHB, (7.5%) for NPHA, (7.4%) for NPMeB, (6.4%) for NPMeA. C-C interaction is (15.1%) for NPHB, (11.3%) for NPHA and (13.6%) for NPMeA and (10.9%) for NPMeA. Furthermore, it is observed that NPHB and NPMeB display more of these stronger interactions than NPHA and NPMeA, respectively, suggesting a more tightly packed arrangement in these crystal structures. This quantitative analysis provides valuable insights into the specific intermolecular forces governing the investigated compounds' crystal packing and emission properties.

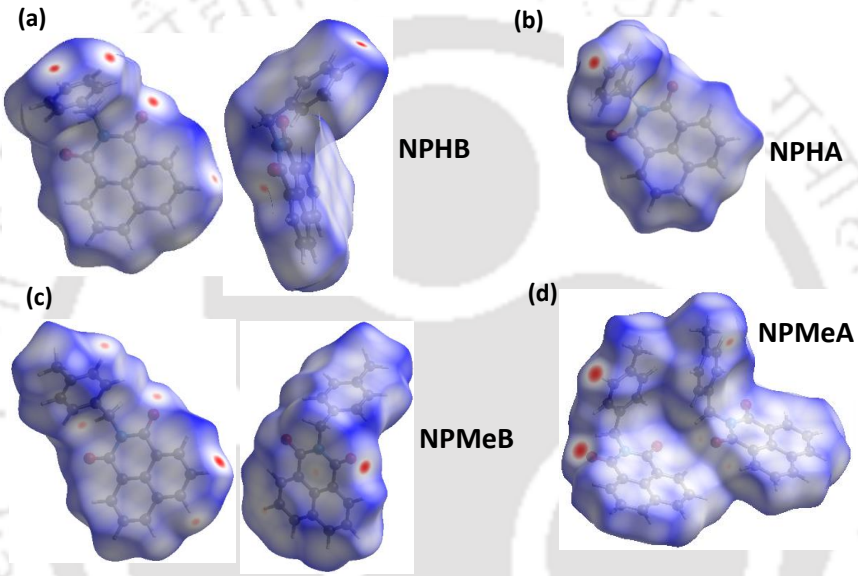

Figure 5.14 Hirshfield surface analysis of (a) NPHB, (b) NPHA (c) NPMeB (d) NPMeA

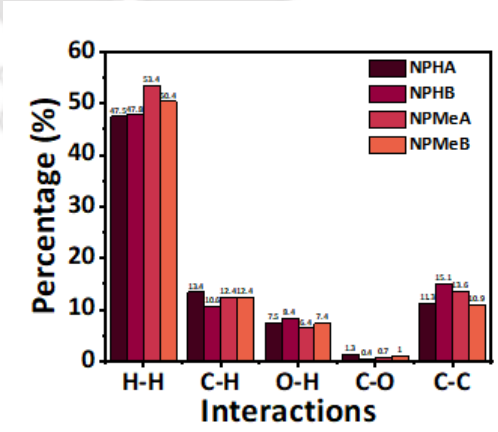

Figure 5.15 Histogram representing various intermolecular interactions present in NPHA, NPHB, NPMeA, and NPMeB.

Table 5.2 Statistics of intermolecular interactions in Hirshfeld surface analysis of polymorphs

Luminogens	NPHA	NPHB	NPMeA	NPMeB
H-H	47.5%	47.8%	53.4%	50.4%
C-H	13.4%	10.6%	12.4%	12.4%
O-H	7.5%	8.4%	6.4%	7.4%
C-O	1.3%	0.4%	0.7%	1%
C-C	11.3%	15.1%	13.6%	10.9%

5.3.8 Theoretical Calculations and ESP analysis of Polymorphs

To explore the intricate influence of molecular orbitals, including the highest occupied molecular orbital (HOMO), lowest unoccupied molecular orbital (LUMO), band gap, and charge distribution, rigorous theoretical optimization and TD-DFT (Time-Dependent Density Functional Theory) calculations were conducted using the Gaussian 16 computational package. The HOMO and LUMO energy levels serve as pivotal indicators of the electronic structure and reactivity of organic compounds. The band gap, representing the energy difference between these orbitals, crucially determines the material's conductivity and optical characteristics. Through theoretical optimization, the molecular structures of the polymorphs were refined to attain their most energetically favourable conformations. Subsequently, TD-DFT calculations provided predictive insights into the electronic excitation spectra and optical behaviour, facilitating an understanding of the compounds' absorption and emission properties. The computational analyses revealed consistency in the HOMO, LUMO, and band gap values across the diverse polymorphs of NPH and NPMe. This suggests that variations in molecular packing arrangements exert minimal influence on the electronic structure or optical properties of the compounds. Additionally, examination of the electrostatic potential distributions across the polymorphs unveiled subtle disparities in charge distribution patterns. Nonetheless, these differences were relatively minor, indicating that despite variations in molecular packing, the overall charge distribution within the molecules remains largely uniform across all studied polymorphs. The findings, presented in (**Figures 5.15 and 5.16)** and summarized in **Table 5.3**, offer valuable insights into the electronic structure and charge distribution of the NPH and NPMe polymorphs. This elucidation contributes to a deeper understanding of the intricate

interplay between molecular packing and electronic properties, fostering the comprehensive characterization of these materials for a myriad of applications spanning optoelectronics and beyond.

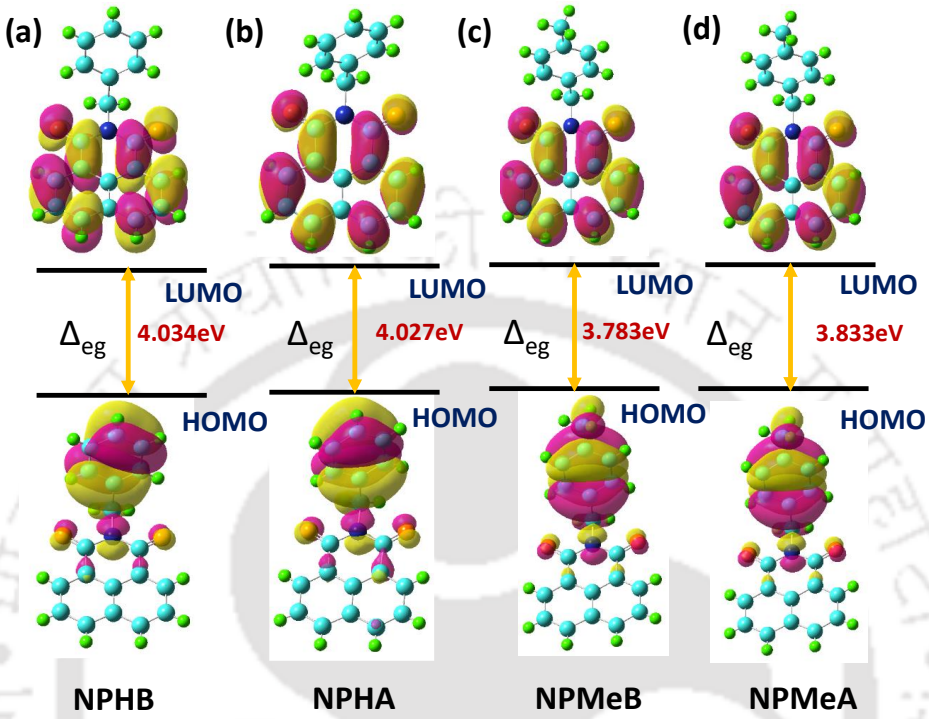

Figure 5.16 HOMO, LUMO and molecular orbitals of (a) NPHB, (b) NPHA (c) NPMeB (d) NPMeA.

Table 5.3 HOMO LUMO and band gap values (eV) of polymorphs

Polymorph	NPHB	NPHA	NPMeB	NPMeA
HOMO (eV)	6.458	6.445	6.189	6.222
LUMO (eV)	2.424	2.418	2.406	2.389
Band Gap (eV)	4.034	4.027	3.783	3.833

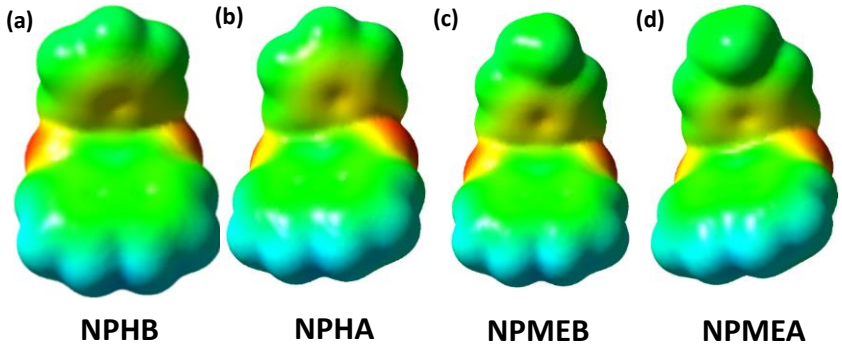

Figure 5.17 Electrostatic map analysis (ESP Analysis) of (a) NPHB, (b) NPHA (c) NPMeB (d) NPMeA.

5.3.9 Electrostatic map analysis

Electrostatic map analysis is a computational method used to visualize and analyze the distribution of electrostatic potential on a molecular surface. It helps in understanding how charges are distributed within a molecule and how these charge distributions influence molecular interactions. The correlation between supramolecular interactions and electrostatic map analysis lies in the fact that electrostatic interactions, particularly between charged or polar regions of molecules, often drive supramolecular assembly and binding processes. For example, hydrogen bonding involves the electrostatic interaction between a hydrogen atom with a partial positive charge and a more electronegative atom with a partial negative charge. Similarly, π-π interactions often involve electrostatic interactions between π electron clouds of aromatic rings. The electrostatic potential maps of molecules involved in supramolecular interactions can be analysed to gain insights into the strength and nature of these interactions. Strong electrostatic complementarity between interacting molecules typically indicates favourable binding interactions, while electrostatic repulsion may hinder binding. Therefore, electrostatic map analysis can provide valuable information for understanding the mechanisms and driving forces behind supramolecular interactions. An electrostatic surface potential (ESP) map was generated to visualize the charge distribution in naphthalimide crystals (**Figure 5.17a to 5.17d)**. The colour gradient from red to blue in ESP correlates to the varying intensities of the electrostatic potential energy values from negative to positive. A red region on the carbonyl oxygen indicates localized electron density, and the blue positive potential region represents electron deficient regions in naphthalimide derivatives. Here in ESP maps of all polymorphs have been analysed and discovered that there is not much difference in the ESP map of

polymorphs indicative of twisted angle and overall aggregation have played the major role for the luminescence tuneability in all polymorphs.

5.3.10 Mechanism of Polymorphism and Mechanochromism:

Polymorphism in NPH and NPMe arises from variations in molecular packing arrangements, which can be influenced by factors such as intermolecular interactions, steric hindrance, and molecular flexibility. In tightly packed structures (e.g., NPHB and NPMeB), the molecules are closely arranged with minimal intermolecular spaces. This arrangement promotes strong π-π interactions between adjacent molecules, leading to efficient energy transfer and enhanced fluorescence. The proximity of molecules restricts molecular motion, favouring a specific crystal structure with characteristic optical properties. Conversely, in loosely packed structures (e.g., NPHA, NPMeA), the molecules are more dispersed, with increased intermolecular distances. This arrangement weakens π-π interactions, resulting in diminished energy transfer and lower fluorescence. Molecular motion is less restricted, allowing for different packing arrangements and polymorphic forms to coexist. Mechanochromism in NPH and NPMe occurs due to the alteration of molecular packing induced by mechanical stress, leading to changes in the electronic structure and optical properties. The application of mechanical stress disrupts the equilibrium of molecular packing, causing molecular reorganization and deformation of the crystal lattice. Mechanical stress induces changes in molecular orientation, intermolecular distances, and π-π stacking interactions. This alteration in packing arrangement perturbs the electronic environment around the phthalimide core, affecting its absorption and emission properties. The changes in molecular packing result in shifts in absorption and emission spectra, leading to a change in the observed colour. This mechanochromic response enables real-time detection of mechanical stimuli and offers insights into the dynamic behaviour of these materials under external perturbation. Overall, the polymorphism and mechanochromism observed in NPH and NPMe compounds are governed by the delicate interplay between molecular structure, packing arrangements, and external stimuli, providing a basis for tailoring their optical properties for various applications.[51,52]

5.4 Conclusion

In conclusion, our investigation into the polymorphism and mechanoluminescence of naphthalimide luminogens, NPH and NPMe, has unveiled a profound connection between their structural intricacies and optical characteristics. Employing single-crystal X-ray diffraction

(XRD) analysis, we differentiated distinct outcomes arising from variations in molecular packing arrangements. Notably, loose molecular packing in NPHA and NPMeA resulted in a blue-shifted spectrum, reduced fluorescence, and lower quantum yield, contrasting sharply with the red-shifted spectrum and heightened fluorescence quantum yield observed in tightly packed structures. This stark dichotomy underscores the pivotal role of molecular packing in dictating the optical characteristics of these luminogens. Reflection upon these findings underscores the strategic importance of manipulating molecular packing arrangements to tailor the properties of NPH and NPMe luminogens. This comprehension not only enhances our understanding of their mechanoluminescent behaviour, but also unveils promising avenues for leveraging these materials across diverse applications, spanning from optoelectronics to emerging fields. In essence, our research significantly contributes to the broader discourse on the influence of molecular packing in shaping the properties of luminescent materials, thereby fostering opportunities for deliberate engineering of their functionalities. Looking ahead, continued exploration in this direction holds immense potential for developing advanced materials with meticulously tailored optical characteristics, propelling advancements in both scientific understanding and technological applications. In broader terms, this study enriches the ongoing discourse on the influence of molecular packing in delineating the properties of luminescent materials. The implications transcend the boundaries of this study, laying a solid foundation for further exploration and innovation. Ultimately, this work establishes the groundwork for developing advanced materials endowed with precisely engineered optical functionalities, thus catalysing progress in diverse scientific and technological domains.

References

1. Dou, L.; Liu, Y.; Hong, Z.; Li, G.; Yang, Y. Low-Bandgap near-IR Conjugated Polymers/Molecules for Organic Electronics. *Chem. Rev.* **2015**, *115* (23), 12633–12665. https://doi.org/10.1021/acs.chemrev.5b00165.
2. Meng, Z.; Mirica, K. A. Covalent Organic Frameworks as Multifunctional Materials for Chemical Detection. *Chem. Soc. Rev.* **2021**, *50* (24), 13498–13558. https://doi.org/10.1039/d1cs00600b.
3. Rössler, S. L.; Grob, N. M.; Buchwald, S. L.; Pentelute, B. L. Abiotic Peptides as Carriers of Information for the Encoding of Small-Molecule Library Synthesis. *Science* **2023**, *379* (6635), 939–945. https://doi.org/10.1126/science.adf1354.
4. Zhang, Y.; Li, H.; Yang, M.; Dai, W.; Shi, J.; Tong, B.; Cai, Z.; Wang, Z.; Dong, Y.; Yu, X. Organic Room-Temperature Phosphorescence Materials for Bioimaging. *Chem. Commun.* **2023**, *59* (36), 5329–5342. https://doi.org/10.1039/d3cc00923h.
5. Li, B.; Zhao, M.; Zhang, F. Rational Design of Near-Infrared-II Organic Molecular Dyes for Bioimaging and Biosensing. *ACS Mater. Lett.* **2020**, *2* (8), 905–917. https://doi.org/10.1021/acsmaterialslett.0c00157.
6. Barman, D.; Narang, K.; Parui, R.; Zehra, N.; Khatun, M. N.; Adil, L. R.; Iyer, P. K. Review on Recent Trends and Prospects in Π-conjugated Luminescent Aggregates for Biomedical Applications. *Aggregate* **2022**, *3* (5). https://doi.org/10.1002/agt2.172.
7. Sun, Y.; Lei, Z.; Ma, H. Twisted Aggregation-Induced Emission Luminogens (AIEgens) Contribute to Mechanochromism Materials: A Review. *J. Mater. Chem. C* **2022**, *10* (40), 14834–14867. https://doi.org/10.1039/d2tc02512d.
8. Haque, A.; Alenezi, K. M.; Khan, M. S.; Wong, W.-Y.; Raithby, P. R. Non-Covalent Interactions (NCIs) in π-Conjugated Functional Materials: Advances and Perspectives. *Chem. Soc. Rev.* **2023**, *52* (2), 454–472. https://doi.org/10.1039/d2cs00262k.
9. Li, Q.; Li, Z. Molecular Packing: Another Key Point for the Performance of Organic and Polymeric Optoelectronic Materials. *Acc. Chem. Res.* **2020**, *53* (4), 962–973. https://doi.org/10.1021/acs.accounts.0c00060.

10. Yu, H.; Alkhamis, O.; Canoura, J.; Liu, Y.; Xiao, Y. Advances and Challenges in Small-molecule DNA Aptamer Isolation, Characterization, and Sensor Development. *Angew. Chem. Int. Ed.* **2021**, *60* (31), 16800–16823. https://doi.org/10.1002/anie.202008663.
11. Yang, S.-Y.; Qu, Y.-K.; Liao, L.-S.; Jiang, Z.-Q.; Lee, S.-T. Research Progress of Intramolecular π-stacked Small Molecules for Device Applications. *Adv. Mater.* **2022**, *34* (22). https://doi.org/10.1002/adma.202104125.
12. Li, K.; Ren, T.-B.; Huan, S.; Yuan, L.; Zhang, X.-B. Progress and Perspective of Solid-State Organic Fluorophores for Biomedical Applications. *J. Am. Chem. Soc.* **2021**, *143* (50), 21143–21160. https://doi.org/10.1021/jacs.1c10925.
13. Murugan, P.; Hu, T.; Hu, X.; Chen, Y. Advancements in Organic Small Molecule Hole-Transporting Materials for Perovskite Solar Cells: Past and Future. *J. Mater. Chem. A* **2022**, *10* (10), 5044–5081. https://doi.org/10.1039/d1ta11039j.
14. Wang, Y.; Wu, H.; Hu, W.; Stoddart, J. F. Color-tunable Supramolecular Luminescent Materials. *Adv. Mater.* **2022**, *34* (22). https://doi.org/10.1002/adma.202105405.
15. Xie, Y.; Li, Z. The Development of Mechanoluminescence from Organic Compounds: Breakthrough and Deep Insight. *Mater. Chem. Front.* **2020**, *4* (2), 317–331. https://doi.org/10.1039/c9qm00580c.
16. Huang, Q.; Li, W.; Yang, Z.; Zhao, J.; Li, Y.; Mao, Z.; Yang, Z.; Liu, S.; Zhang, Y.; Chi, Z. Achieving Bright Mechanoluminescence in a Hydrogen-Bonded Organic Framework by Polar Molecular Rotor Incorporation. *CCS Chem* **2022**, *4* (5), 1643–1653. https://doi.org/10.31635/ccschem.021.202100968.
17. Xu, B.; He, J.; Mu, Y.; Zhu, Q.; Wu, S.; Wang, Y.; Zhang, Y.; Jin, C.; Lo, C.; Chi, Z.; Lien, A.; Liu, S.; Xu, J. Very Bright Mechanoluminescence and Remarkable Mechanochromism Using a Tetraphenylethene Derivative with Aggregation-Induced Emission. *Chem. Sci.* **2015**, *6* (5), 3236–3241. https://doi.org/10.1039/c5sc00466g.
18. Xu, B.; Li, W.; He, J.; Wu, S.; Zhu, Q.; Yang, Z.; Wu, Y.-C.; Zhang, Y.; Jin, C.; Lu, P.-Y.; Chi, Z.; Liu, S.; Xu, J.; Bryce, M. R. Achieving Very Bright Mechanoluminescence from Purely Organic Luminophores with Aggregation-Induced Emission by Crystal Design. *Chem. Sci.* **2016**, *7* (8), 5307–5312. https://doi.org/10.1039/c6sc01325b.

19. Song, Y.; Pan, G.; Zhang, C.; Wang, C.; Xu, B.; Tian, W. Organic Luminescent Crystals: Role of Packing Structures and Optical Properties. *Mater. Chem. Front.* **2023**, *7* (21), 5104–5119. https://doi.org/10.1039/d3qm00494e.
20. Cruz-Cabeza, A. J.; Reutzel-Edens, S. M.; Bernstein, J. Facts and Fictions about Polymorphism. *Chem. Soc. Rev.* **2015**, *44* (23), 8619–8635. https://doi.org/10.1039/c5cs00227c.
21. Chung, H.; Diao, Y. Polymorphism as an Emerging Design Strategy for High Performance Organic Electronics. *J. Mater. Chem. C* **2016**, *4* (18), 3915–3933. https://doi.org/10.1039/c5tc04390e.
22. Langenstroer, A.; Kartha, K. K.; Dorca, Y.; Droste, J.; Stepanenko, V.; Albuquerque, R. Q.; Hansen, M. R.; Sánchez, L.; Fernández, G. Unraveling Concomitant Packing Polymorphism in Metallosupramolecular Polymers. *J. Am. Chem. Soc.* **2019**, *141* (13), 5192–5200. https://doi.org/10.1021/jacs.8b11011.
23. Narang, K.; Iyer, P. K. Molecular Engineering of Naphthalimide Methylcyclohexane Luminogen: Unraveling J*-Aggregation Pattern and Sensing Melamine in Aqueous Media. *CCS Chem* **2023**, 1–9. https://doi.org/10.31635/ccschem.023.202303123.
24. Zhang, J.; Zhang, X.; Xiao, H.; Li, G.; Liu, Y.; Li, C.; Huang, H.; Chen, X.; Bo, Z. 1,8-Naphthalimide-Based Planar Small Molecular Acceptor for Organic Solar Cells. *ACS Appl. Mater. Interfaces* **2016**, *8* (8), 5475–5483. https://doi.org/10.1021/acsami.5b10211.
25. Dong, H.-Q.; Wei, T.-B.; Ma, X.-Q.; Yang, Q.-Y.; Zhang, Y.-F.; Sun, Y.-J.; Shi, B.-B.; Yao, H.; Zhang, Y.-M.; Lin, Q. 1,8-Naphthalimide-Based Fluorescent Chemosensors: Recent Advances and Perspectives. *J. Mater. Chem. C* **2020**, *8* (39), 13501–13529. https://doi.org/10.1039/d0tc03681a.
26. Barman, D.; Gogoi, R.; Narang, K.; Iyer, P. K. Recent Developments on Multi-Functional Metal-Free Mechanochromic Luminescence and Thermally Activated Delayed Fluorescence Organic Materials. *Front. Chem.* **2020**, *8*, 483. https://doi.org/10.3389/fchem.2020.00483.
27. Gopikrishna, P.; Meher, N.; Iyer, P. K. Functional 1,8-Naphthalimide AIE/AIEEgens: Recent Advances and Prospects. *ACS Appl. Mater. Interfaces* **2018**, *10* (15), 12081–12111. https://doi.org/10.1021/acsami.7b14473.

28. Xu, S.; Liu, B. High Exciton Utilization of 1D Molecular Column with High Packing Energy Formed by Folded π-Molecules. *J. Am. Chem. Soc.* **2022**, *144* (39), 17897–17904. https://doi.org/10.1021/jacs.2c06838.
29. Meher, N.; Iyer, P. K. Pendant Chain Engineering to Fine-Tune the Nanomorphologies and Solid State Luminescence of Naphthalimide AIEEgens: Application to Phenolic Nitro-Explosive Detection in Water. *Nanoscale* **2017**, *9* (22), 7674–7685. https://doi.org/10.1039/c7nr02174g.
30. Becke, A. D. Density-Functional Thermochemistry. I. The Effect of the Exchange-Only Gradient Correction. *J. Chem. Phys.* **1992**, *96* (3), 2155–2160. https://doi.org/10.1063/1.462066.
31. Frisch, M. J.; Trucks, G. W.; Schlegel, H. B.; Scuseria, G. E.; Robb, M. A.; Cheeseman, J. R.; Scalmani, G.; Barone, V.; Petersson, G. A.; Nakatsuji, H.; Li, X.; Caricato, M.; Marenich, A. V.; Bloino, J.; Janesko, B. G.; Gomperts, R.; Mennucci, B.; Hratchian, H. P.; Ortiz, J. V.; Izmaylov, A. F.; Sonnenberg, J. L.; Williams-Young, D.; Ding, F.; Lipparini, F.; Egidi, F.; Goings, J.; Peng, B.; Petrone, A.; Henderson, T.; Ranasinghe, D.; Zakrzewski, V. G.; Gao, J.; Rega, N.; Zheng, G.; Liang, W.; Hada, M.; Ehara, M.; Toyota, K.; Fukuda, R.; Hasegawa, J.; Ishida, M.; Nakajima, T.; Honda, Y.; Kitao, O.; Nakai, H.; Vreven, T.; Throssell, K.; Montgomery, J. A.; Peralta, J. E.; Ogliaro, F.; Bearpark R Kobayashi, M. J.; Normand, J.; Raghavachari, K.; Rendell, A. P.; Burant, J. C.; Iyengar, S. S.; Tomasi, J.; Cossi, M.; Millam, J. M.; Klene, M.; Adamo, C.; Cammi, R.; Ochterski, J. W.; Martin, R. L.; Morokuma, K.; Farkas, O.; Foresman, J. B.; Fox, D. J. Gaussian 16; Heyd, J. J., Brothers, E. N., Kudin, K. N., Staroverov, V. N., Keith, T. A., Eds.; Gaussian, Inc: Wallingford CT, 2016.
32. Zhang, W.; Ma, Y.; Song, H.; Miao, R.; Kong, J.; Zhou, M. Deciphering the Photophysical Properties of Naphthalimide Derivatives Using Ultrafast Spectroscopy. *Phys. Chem. Chem. Phys.* **2024**, *26* (5), 4607–4613. https://doi.org/10.1039/d3cp05654f.
33. Ma, S.; Liu, Y.; Zhang, J.; Xu, B.; Tian, W. Polymorphism-Dependent Enhanced Emission in Molecular Aggregates: J-Aggregate versus X-Aggregate. *J. Phys. Chem. Lett.* **2020**, *11* (24), 10504–10510. https://doi.org/10.1021/acs.jpclett.0c02917.
34. Wang, J.; Chai, Z.; Wang, J.; Wang, C.; Han, M.; Liao, Q.; Huang, A.; Lin, P.; Li, C.; Li, Q.; Li, Z. Mechanoluminescence or Room-temperature Phosphorescence:

Molecular Packing-dependent Emission Response. *Angew. Chem. Int. Ed.* **2019**, *131* (48), 17457–17462. https://doi.org/10.1002/ange.201911648

35. Tu, L.; Xie, Y.; Li, Z. Advances in Pure Organic Mechanoluminescence Materials. *J. Phys. Chem. Lett.* **2022**, *13* (24), 5605–5617. https://doi.org/10.1021/acs.jpclett.2c01283.
36. Xie, Z.; Zhang, X.; Xiao, Y.; Wang, H.; Shen, M.; Zhang, S.; Sun, H.; Huang, R.; Yu, T.; Huang, W. Realizing Photoswitchable Mechanoluminescence in Organic Crystals Based on Photochromism. *Adv. Mater.* **2023**, *35* (21). https://doi.org/10.1002/adma.202212273.
37. Yue, L.; Wang, Y.; Ma, J.; Yuan, S.; Xue, S.; Sun, Q.; Yang, W. Touch-Sensitive Yellow Organic Mechanophosphorescence and a Versatile Strategy for White Organic Mechanoluminescence. *Mater. Chem. Front.* **2021**, *5* (14), 5497–5502. https://doi.org/10.1039/d1qm00496d.
38. Zhang, K.; Sun, Q.; Zhang, Z.; Tang, L.; Xie, Z.; Chi, Z.; Xue, S.; Zhang, H.; Yang, W. Touch-Sensitive Mechanoluminescence Crystals Comprising a Simple Purely Organic Molecule Emit Bright Blue Fluorescence Regardless of Crystallization Methods. *Chem. Commun.* **2018**, *54* (41), 5225–5228. https://doi.org/10.1039/c8cc02513d.
39. Xiong, P.; Peng, M.; Yang, Z. Near-Infrared Mechanoluminescence Crystals: A Review. *iScience* **2021**, *24* (1), 101944. https://doi.org/10.1016/j.isci.2020.101944.
40. Yu, Y.; Wang, C.; Wei, Y.; Fan, Y.; Yang, J.; Wang, J.; Han, M.; Li, Q.; Li, Z. Halogen-containing TPA-based Luminogens: Different Molecular Packing and Different Mechanoluminescence. *Adv. Opt. Mater.* **2019**, *7* (18). https://doi.org/10.1002/adom.201900505.
41. Di, B.-H.; Chen, Y.-L. Recent Progress in Organic Mechanoluminescent Materials. *Chin. Chem. Lett.* **2018**, *29* (2), 245–251. https://doi.org/10.1016/j.cclet.2017.08.043.
42. Roy, B.; Reddy, M. C.; Panja, S. N.; Hazra, P. Strategy to Mechanical Activation of Centrosymmetrically Packed Organic Luminogens. *J. Phys. Chem. C* **2019**, *123* (6), 3848–3854. https://doi.org/10.1021/acs.jpcc.8b10696.
43. Sun, Y.; Lei, Z.; Ma, H. Twisted Aggregation-Induced Emission Luminogens (AIEgens) Contribute to Mechanochromism Materials: A Review. *J. Mater. Chem. C* **2022**, *10* (40), 14834–14867. https://doi.org/10.1039/d2tc02512d.

44. Khan, F.; Ekbote, A.; Singh, G.; Misra, R. Mechanochromic Luminogens with Hypsochromically Shifted Emission Switching Property: Recent Advances and Perspectives. *J. Mater. Chem. C* **2022**, *10* (13), 5024–5064. https://doi.org/10.1039/d1tc06140b.
45. Zhang, T.; Han, Y.; Huo, J.; Xue, P. Effect of Electron-Withdrawing Moieties on Mechanochromism of Phenothiazine Derivatives. *CrystEngComm* **2020**, *22* (31), 5137–5144. https://doi.org/10.1039/d0ce00770f.
46. Zhang, K.; Zhang, X.; Fan, J.; Song, Y.; Fan, J.; Wang, C.-K.; Lin, L. Novel Deep Red Thermally Activated Delayed Fluorescence Molecule with Aggregation-Induced Emission Enhancement: Theoretical Design and Experimental Validation. *J. Phys. Chem. Lett.* **2022**, *13* (21), 4711–4720. https://doi.org/10.1021/acs.jpclett.2c00779.
47. Wang, W.; Li, R.; Xiao, S.; Xing, Q.; Yan, X.; Zhang, J.; Zhang, X.; Lan, H.; Yi, T. Design of High-Contrast Mechanochromic Materials Based on Aggregation-Induced Emissive Pyran Derivatives Guided by Polymorph Predictions. *CCS Chem* **2022**, *4* (3), 899–909. https://doi.org/10.31635/ccschem.021.202100885.
48. Ekbote, A.; Mobin, S. M.; Misra, R. Stimuli-Responsive Phenothiazine-Based Donor–Acceptor Isomers: AIE, Mechanochromism and Polymorphism. *J. Mater. Chem. C* **2020**, *8* (10), 3589–3602. https://doi.org/10.1039/c9tc05192a.
49. Zhang, J.; Zhu, M.; Lu, Y.; Zhang, X.; Xiao, S.; Lan, H.; Yi, T. Design of Stimuli-responsive Phenothiazine Derivatives with Triplet-related Dual Emission and High-contrast Mechanochromism Guided by Polymorph Prediction. *Chemistry* **2022**, *28* (29). https://doi.org/10.1002/chem.202200458.
50. Ma, X.; Zhao, Y. Biomedical Applications of Supramolecular Systems Based on Host–Guest Interactions. *Chem. Rev.* **2015**, *115* (15), 7794–7839. https://doi.org/10.1021/cr500392w.
51. Tan, R.; Lin, Q.; Wen, Y.; Xiao, S.; Wang, S.; Zhang, R.; Yi, T. Polymorphism and Mechanochromic Luminescence of a Highly Solid-Emissive Quinoline-β-Ketone Boron Difluoride Dye. *CrystEngComm* **2015**, *17* (35), 6674–6680. https://doi.org/10.1039/c5ce01138h.
52. Qi, Q.; Zhang, J.; Xu, B.; Li, B.; Zhang, S. X.-A.; Tian, W. Mechanochromism and Polymorphism-Dependent Emission of Tetrakis(4-(Dimethylamino)Phenyl)Ethylene. *J. Phys. Chem. C* **2013**, *117* (47), 24997–25003. https://doi.org/10.1021/jp407965a.

Appendix

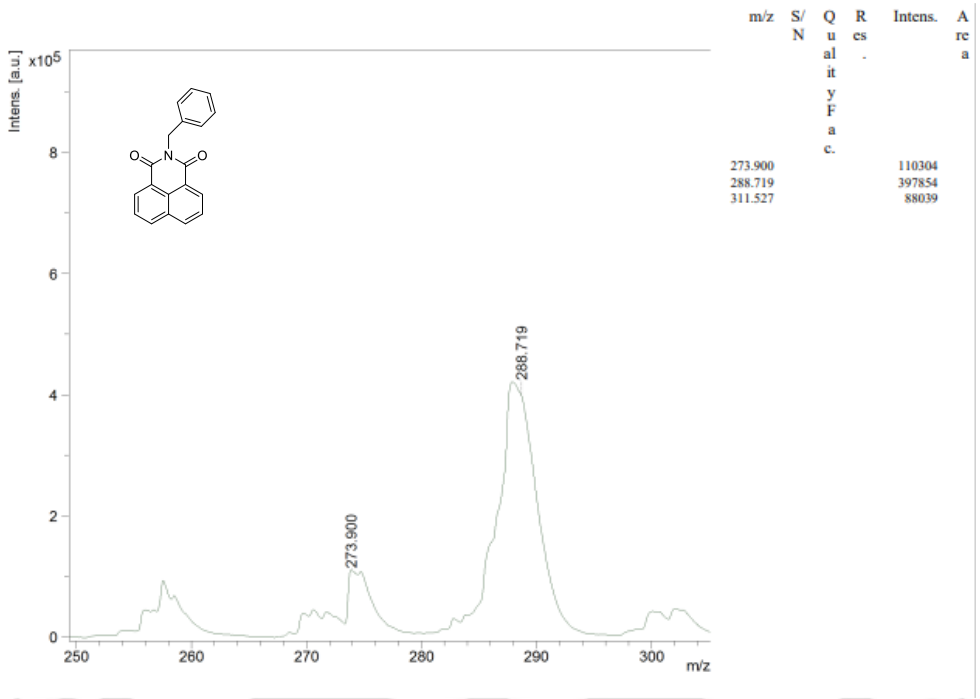

Figure A5.1 ^{1}H NMR spectra of NPH.

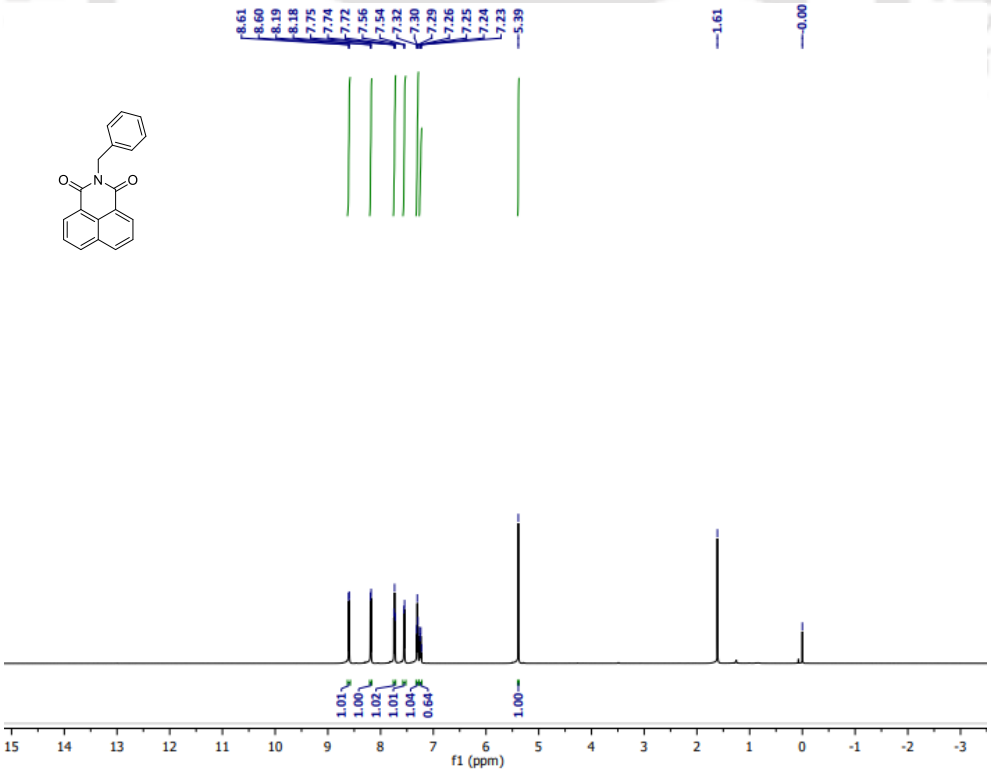

Figure A2.2 ^{13}C NMR spectra of NPH.

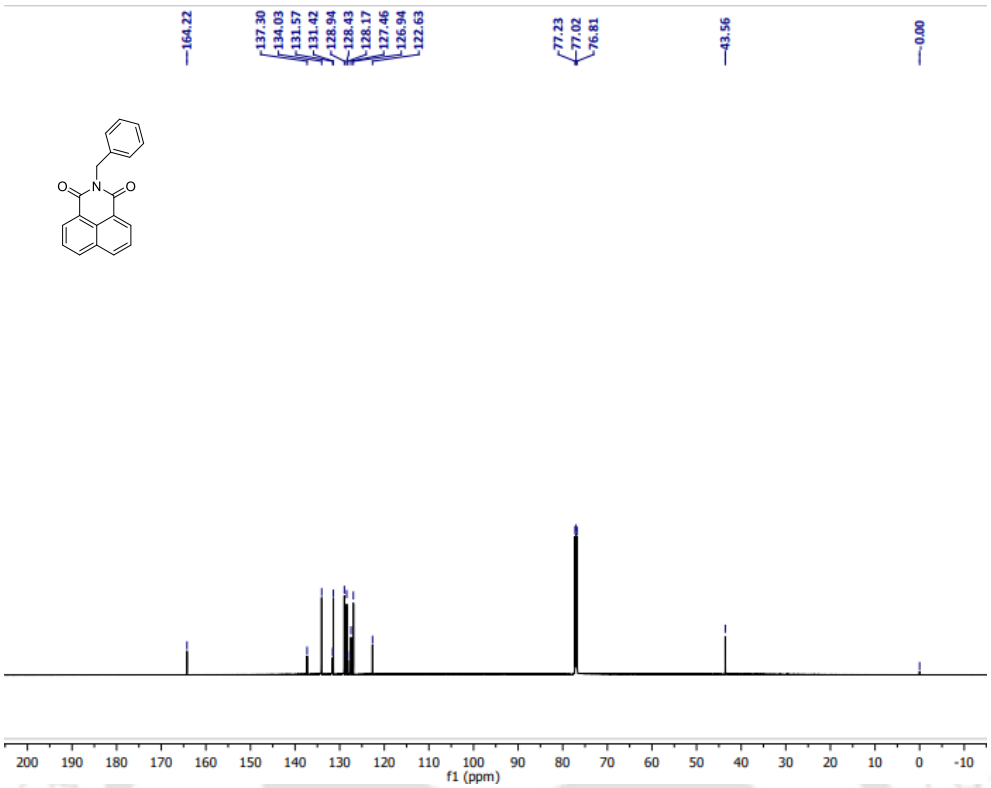

Figure A2.4 ^{13}C NMR spectrum of NPH.

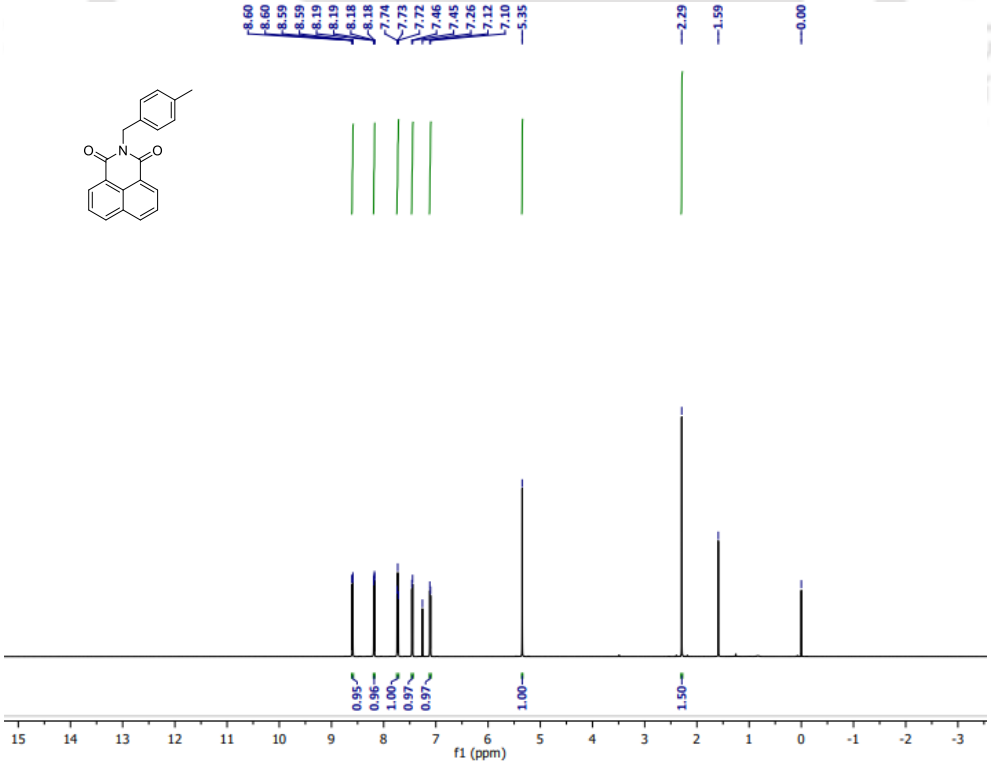

Figure A2.5 ^{1}H NMR spectra of NPMe.

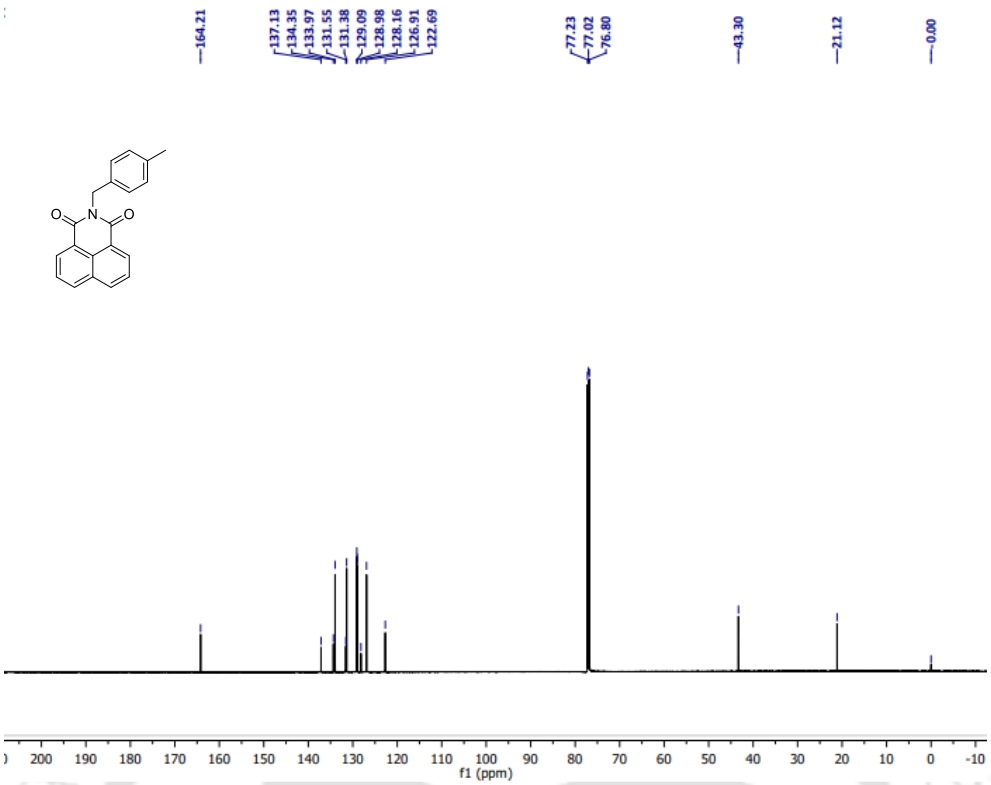

Figure A2.6 ^{1}H NMR spectrum of NPMe.

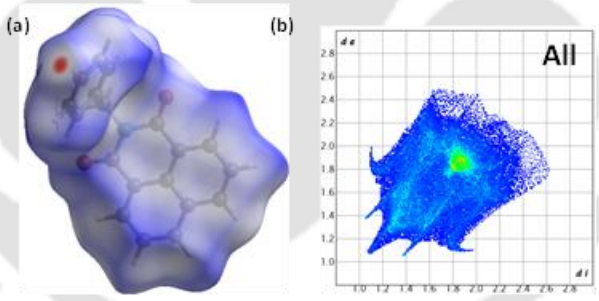

Figure A5.7 a) Hirshfield surface analysis of NPHA b) fingerprint analysis of all intermolecular interactions in NPHA.

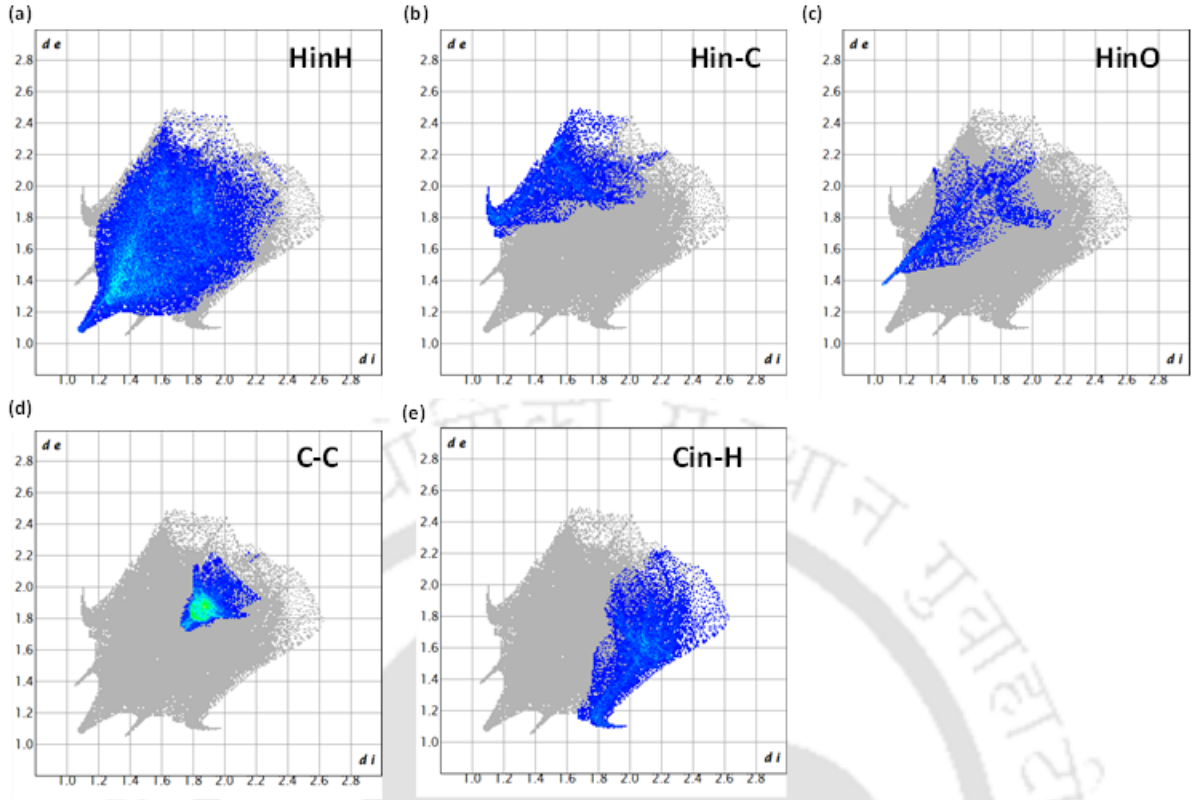

Figure A5.8 fingerprint analysis of all intermolecular interactions in NPHA. (a) Hydrogen…Hydrogen (b) Hydrogen…carbon (c) Hydrogen…Oxygen (d) Carbon…Carbon e) Carbon…Hydrogen.

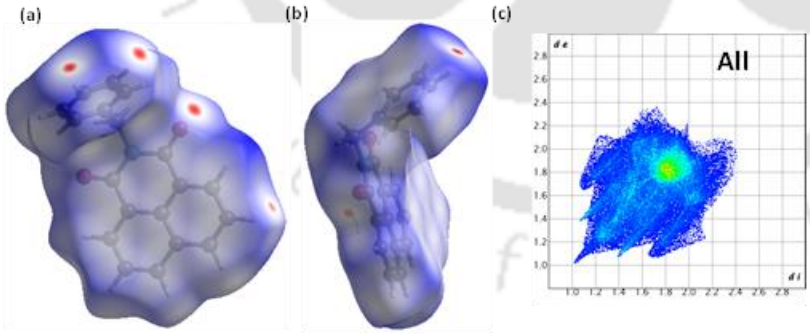

Figure A5.9 a) Hirshfield surface analysis of NPHB b) fingerprint analysis of all intermolecular interactions in NPHB.

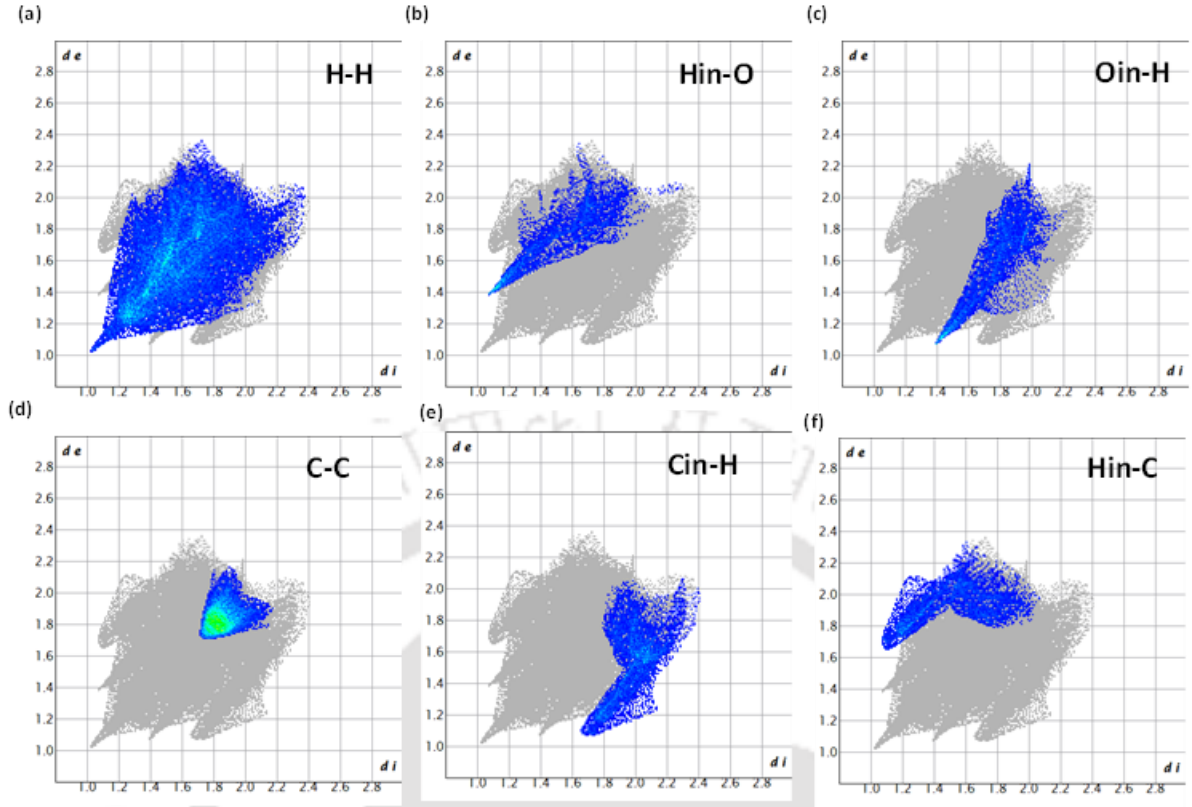

Figure A5.10 Fingerprint analysis of all intermolecular interactions in NPHA. (a) Hydrogen…Hydrogen (b) Hydrogen…Oxygen (c) Oxygen…Hydrogen (d) Carbon…Carbon e) Carbon…Hydrogen (f) Hydrogen…Carbon.

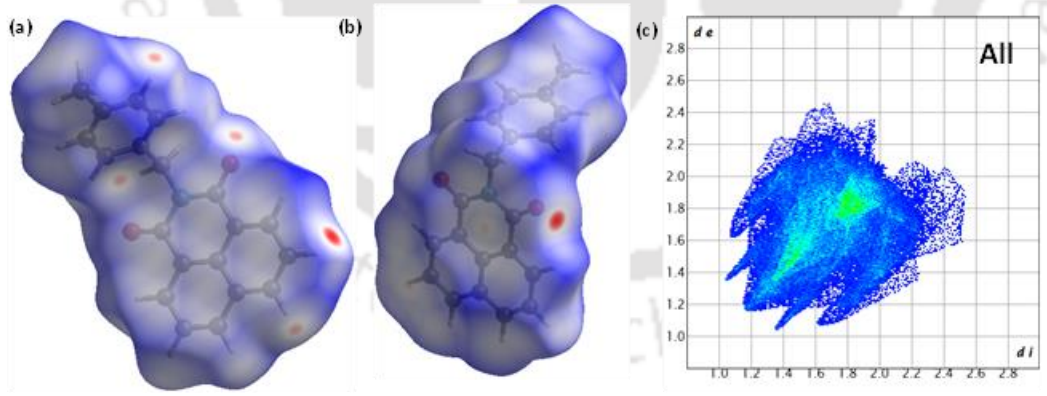

Figure A5.11 a) Hirshfield surface analysis of NPMeA b) fingerprint analysis of all intermolecular interactions in NPMeA.

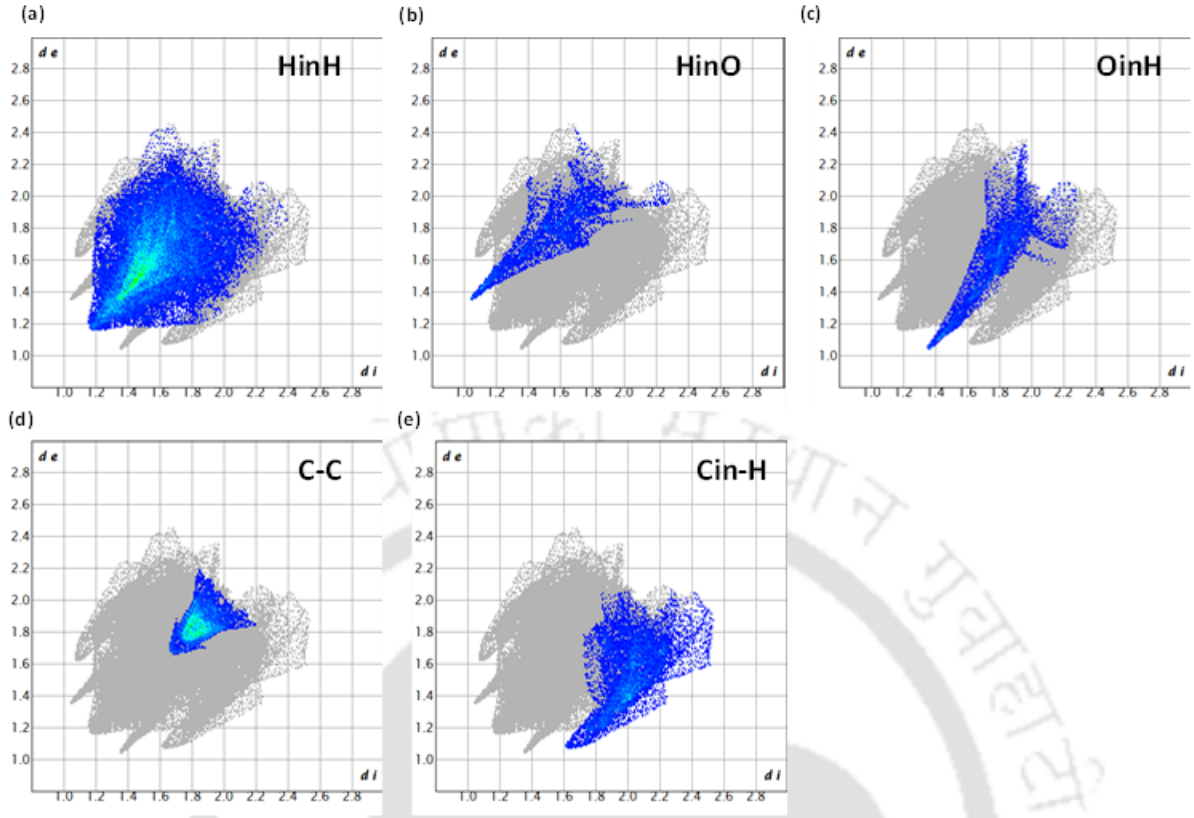

Figure 5.12 Fingerprint analysis of all intermolecular interactions in NPHA. (a) Hydrogen…Hydrogen (b) Hydrogen…Oxygen (c) Oxygen…Hydrogen (d) Carbon…Carbon e) Carbon…Hydrogen.

Thesis Overview and Future Perspective

The presented thesis represents a comprehensive endeavour to delve into the realm of pure organic luminogens and explore the intricate landscape of supramolecular chemistry. At its core, this work aims to unravel the fundamental principles governing the design, synthesis, and application of novel luminogens, while also shedding light on their supramolecular interactions and potential implications across diverse fields.

The thesis journey begins by laying the groundwork for understanding the structural intricacies and aggregation-induced emission (AIE) phenomenon of naphthalimide methylcyclohexane (NMICY), a promising luminogen with vast potential in chemical sensing applications. Through meticulous synthesis and characterization efforts, the primary objective of the initial research endeavour is to elucidate the molecular conformational effects on the aggregation behaviour and optical properties of NMICY. By unravelling the unique J*-aggregation pattern exhibited by NMICY, this study not only advances our understanding of supramolecular self-assembly but also paves the way for the development of efficient sensing platforms for detecting contaminants such as melamine in complex matrices like milk and milk powder solutions. The innovative use of smartphone-based sensing technologies underscores the practical implications of this research for addressing real-world challenges in food safety and quality assurance.

Building upon these foundational insights, the thesis further explores the fascinating realm of room temperature phosphorescence (RTP) materials, with a focus on elucidating the role of heavy halogen atom incorporation and alkyl chain modifications in enhancing RTP characteristics. Through a systematic investigation of luminogens such as ODNI and BrODNI, the study sheds light on the intricate interplay between molecular structure, spin-orbit coupling (SOC), and intersystem crossover (ISC) processes, which are crucial for achieving efficient RTP emission. The findings not only deepen our understanding of the underlying mechanisms governing RTP phenomena but also hold immense promise for advancing sustainable energy technologies through the design of novel RTP materials with enhanced efficiency and stability.

In parallel, the thesis journey ventures into uncharted territories of supramolecular behaviour and viral interactions, wherein the aggregation patterns and unique structural complexities of naphthalimide luminogens are thoroughly examined. By employing advanced techniques such as single crystal X-ray diffraction (XRD), the study unveils unprecedented insights into the supramolecular assembly patterns exhibited by these

luminogens, challenging traditional classification schemes and paving the way for innovative applications in targeted interactions with viral proteins. The remarkable luminescence dampening observed in the presence of the NS1 protein holds significant implications for antiviral research, offering new avenues for the development of therapeutic strategies and diagnostic tools against viral infections.

Furthermore, the thesis journey culminates in an exploration of the polymorphic behaviour and mechanoluminescent features of naphthalimide luminogens, providing a deeper understanding of the intricate relationship between molecular packing and optical properties. Through meticulous analysis of single crystal XRD patterns, the study elucidates the direct correlation between molecular arrangement and fluorescence behaviour, offering valuable insights for the customized design and control of luminogens with tailored optical characteristics. These findings not only broaden our fundamental understanding of molecular packing phenomena but also pave the way for the development of advanced materials with tailored properties for applications spanning optoelectronics, sensing, and beyond.

In summary, the thesis represents the culmination of interdisciplinary efforts aimed at unravelling the mysteries of pure organic luminogens and exploring their vast potential in supramolecular chemistry. By elucidating the fundamental principles governing their design, synthesis, and application, this work opens new vistas for innovation across diverse fields, from chemical sensing and energy technologies to antiviral research and materials science. As we embark on this journey of discovery, the insights gleaned from this thesis serve as a beacon of inspiration, guiding future endeavours in harnessing the transformative power of pure organic luminogens and supramolecular interactions for the betterment of society.

Future Directions

The culmination of this thesis work paves the way for promising avenues in both fundamental research and practical applications. The insights gained from the investigation of pure organic luminogens and their supramolecular interactions offer a foundation for future advancements in several key areas:

Chemical Sensing and Detection: The development of efficient sensing platforms, exemplified by the creation of the equatorial form of naphthalimide methylcyclohexane (NMICY), opens doors for rapid and reliable detection methods. The synthesis and

characterization of novel luminogens present opportunities for addressing emerging challenges in environmental monitoring, food safety, and healthcare diagnostics.

Room Temperature Phosphorescence (RTP) Materials: The study on heavy halogen atom incorporation and alkyl chain modifications provides valuable insights into enhancing the RTP characteristics of luminogens. These findings lay the groundwork for the design and development of next-generation RTP materials with enhanced efficiency and stability, holding promise for applications in optoelectronics and energy-related technologies.

Supramolecular interaction and Viral Interactions: The exploration of unique aggregation patterns and supramolecular interactions of naphthalimide luminogens sheds light on their potential applications in targeted interactions with viral proteins. These findings offer a platform for further research in antiviral strategies and biomaterial design, contributing to the development of novel therapeutic approaches and diagnostic tools.

Mechanoluminescence and Polymorphism Studies: The investigation into the polymorphic behaviour and mechanoluminescent features of naphthalimide luminogens provides fundamental insights into the relationship between molecular packing and optical properties. This understanding facilitates the tailored design of luminogens for specific applications in optoelectronics, materials science, and beyond.

In conclusion, the findings and methodologies outlined in this thesis not only advance our understanding of supramolecular chemistry but also hold immense potential for driving innovations across interdisciplinary fields. Moving forward, further exploration and collaboration will be instrumental in harnessing the full spectrum of possibilities offered by pure organic luminogens and their supramolecular interactions.

Publications

1. **Narang, K.;** Iyer, P. K. Molecular Engineering of Naphthalimide Methylcyclohexane Luminogen: Unraveling J*-Aggregation Pattern and Sensing Melamine in Aqueous Media. *CCS Chem* **2024**, *6* (4), 923–931. https://doi.org/10.31635/ccschem.023.202303123.
2. **Narang, K.;** Garain, S.; Iyer, P. K. Mechanistic Insights on the Impact of Long Alkyl Chain and Bromine Substitution on the Molecular Packing and Phosphorescence Behavior in Naphthalimides. *(manuscript communicated)*
3. Narang, K.; Mehta, D.; Sarmah, T.; Iyer, Kumar, S.; P. K. Beyond H and J Aggregation in Naphthalimide Luminogens. *(Manuscript communicated)*
4. **Narang, K.**; Saramah, T.; Iyer, P. K. Molecular Packing Dictates Optical Destiny: Polymorphism and Mechanoluminescence in Naphthaliimide Luminogens. *(Manuscript communicated).*
5. Ghosh, P.; **Narang, K.**; Iyer, P. K. Role of Amyloid Beta in Neurodegeneration and Therapeutic Strategies for Neuroprotection. In Neuroprotection; Springer US: New York, NY, 2024; pp 337–354. https://doi.org/10.1007/978-1-0716-3662-6_25
6. Barman, D.; **Narang, K.**; Parui, R.; Zehra, N.; Khatun, M. N.; Adil, L. R.; Iyer, P. K. Review on Recent Trends and Prospects in Π-conjugated Luminescent Aggregates for Biomedical Applications. *Aggregate* **2022**, *3* (5), e172. https://doi.org/10.1002/agt2.172.
7. Barman, D.; **Narang, K.**; Gogoi, R.; Barman, D.; Iyer, P. K. Exceptional Class of Thermally Activated Delayed Fluorescent Emitters That Display Pure Blue, near-IR, Circularly Polarized Luminescence and Multifunctional Behaviour for Highly Efficient and Stable OLEDs. *J. Mater. Chem. C* **2022**, *10* (22), 8536–8583. https://doi.org/10.1039/d1tc05906h.
8. Barman, D.; Parui, R.; **Narang, K.**; Gogoi, R.; Iyer, P. K. Aggregation Induced Bright Organic Luminogens: Design Strategies, Advanced Bio-Imaging and Theranostic Applications. In Progress in Molecular Biology and Translational Science; Elsevier, 2021; pp 75–112. https://doi.org/10.1016/bs.pmbts.2021.07.001
9. Barman, D.; Gogoi, R.; **Narang, K.**; Iyer, P. K. Recent Developments on Multi-Functional Metal-Free Mechanochromic Luminescence and Thermally Activated Delayed Fluorescence Organic Materials. *Front. Chem.* **2020**, *8*, 483. https://doi.org/10.3389/fchem.2020.00483.

Conferences & Seminars

1. Presented a Poster *at* 7th International Conference for Nanotechnology, organized by Centre for Nanotechnology, IIT Guwahati during 14th – 17th December 2021.
2. Participated in 6th International Conference on Advanced Nanomaterials and Nanotechnology**,** organized by Centre for Nanotechnology, IIT Guwahati during 18th – 21st December 2019.
3. Participated in Research Conclave'19, organized by Student Academic Board (SAB), IIT Guwahati during 14th –17th March 2019.
4. Participated 4th National Workshop on NEMS/MEMS and Theranostics Devices organized by Centre for Nanotechnology, held at IIT Guwahati from 21th – 23th February 2019.
5. Participated 5th International Conference for Nanotechnology, organized by Centre for Nanotechnology, IIT Guwahati from 18th –21th Dec 2017.
6. Attended the full agenda of RSC on Campus 2018 **(**An initiative Royal Society of Chemistry) at IIT Guwahati on 16 Jan 2018.